The investigation and modelling of the steel compression V-belt continuously variable transmission

Micklem, J. D.

Award date:
1994

Awarding institution:
University of Bath

The Investigation and Modelling of the Steel Compression V-Belt Continuously Variable Transmission

submitted by J.D.Micklem

for the degree of PhD

of the University of Bath

1994

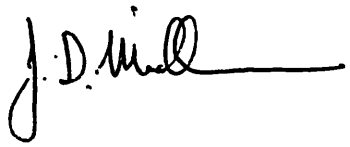

ProQuest LLC
789 East Eisenhower Parkway
P.O. Box 1346
Ann Arbor, MI 48106-1346

Acknowledgements

The author wishes to thank Professor Cliff Burrows for the opportunity to work on the transmission project and for his continued encouragement and interest as the work progressed.

Thanks are also due to Dr Robert Dorey who acted as supervisor for the first part of the project and to Dr Derek Longmore who took over after Dr Dorey left the University. Both gave considerable encouragement and advice.

The many discussions with Dr Markus Guebeli, who was working on a parallel project involving the control of the transmission, are appreciated, he was a friendly and stimulating colleague.

Thanks to the technicians who worked on the test rig, to Wilf Phillips who undertook the initial work and to Alan Jefferis who completed the installation and assisted with the testing, cheerfully dismantling and reassembling the transmission many times.

Finally, his thanks go to his wife, Pauline, who put up with his many absences to work on the project after she, following his retirement, had expected him to be at home.

Summary

This work investigates the steel, compression V-belt, a type of continuously variable transmission (CVT) currently commercially available for use in passenger automobiles. Papers on modelling the system are reviewed and it is shown that the use of Coulomb friction for the shear connection between the belt and the pulleys used in these papers cannot predict the measured slips. An alternative connection making use of elastohydrodynamic theory is proposed and a system model developed.

A test rig is described in which the transmission is operated in the same way as in normal automobile use. Results from measurements on the rig are presented which confirm that the elastohydrodynamic model is appropriate.

The problem of the effect of the total gap between the belt segments on the belt slip is resolved and it is shown that this gap has no effect on the slip.

The various losses in the transmission are determined and their magnitudes established. In particular three types of inherent loss are identified, the belt torque loss, the hydraulic pump loss and the loss due to slip. It is shown that although the standard transmission is operated close to the correct way for a CVT, that is with a higher engine torque and a lower engine speed than with a conventional transmission, the magnitude of the losses is such that there is no advantage in improved fuel economy. Proposals are made for reducing these losses, in particular by the use of an optimising control system which minimises the sum of the three inherent losses. It is shown that improvements in the City Cycle fuel economy of at least 15 per cent are obtainable.

CONTENTS

	Page
Summary	3
List of figures	11
Notation	17
Chapter 1 Introduction	21
1.1 The advantages to be gained from the use of a Continuously Variable Transmission (CVT)	21
1.2 The development position of CVTs and research needs	23
1.3 The Van Doorne CVTs	25
1.4 The performance of the Van Doorne CVT	26
1.5 The necessity for modelling and testing the Van Doorne CVT	27
1.6 The importance of the overall slip in the investigation	27
1.7 The objectives of the investigation	28
Chapter 2 Description of the steel, compression V-belt CVT	29
2.1 Introduction	29
2.2 The belt and pulley system	30
2.3 The epicyclic gear and clutch system	32
2.4 The primary and final drive reduction gears	33
2.5 The hydraulic pump and control unit	33
2.6 The behaviour of the belt when the transmission is running	37

Chapter 3 Consideration of the Coulomb friction model 38

3.1 Introduction 38

3.2 Review of papers proposing models of the transmission 39

3.3 The overall slip with a simple Coulomb friction model 43

3.4 Measurement of the stiffness in compression of the belt segments 48

3.5 Comparison of slip calculated from the simple model with Becker's values 50

3.6 The shear connection between segments and bands 52

3.7 Summary of conclusions 53

Chapter 4 Consideration of viscous shear models 54

4.1 Introduction 54

4.2 Choice of an elastohydrodynamic model 55

4.3 The central, Hertzian contact 56

4.4 The oil film thickness for a line contact 57

4.5 Radius of curvature of the pulley surface at radius R 59

4.6 Viscosity values for the central contact region 60

4.7 Asperity contact 61

4.8 The viscous model for the segment-pulley contact 62

4.9 Comparison of values from the viscous model with measured results 62

4.10 Consideration of an extension to the model to allow for asperity contact 64

4.11 The shear connections between the segment shoulders and the inner band and between neighbouring bands 71

4.12 Summary of the viscous shear models at the contacts 72

Chapter 5 The system model 73

5.1 Introduction 73

5.2 Assumptions made in the analysis of the transmission 73

5.3 Division of the belt into regions 74

5.4 The belt geometry 75

5.5 Speeds of the bands relative to the speed of the segments 77

5.6 The forces on a segment engaged with a pulley 79

5.7 Overall relationships for a pulley and a section of belt engaged with it 84

5.8 Relationships between the band tensions 87

5.9 The change in segment compression along the straight parts of the belt 90

5.10 The torque required to drive the oil pump 90

5.11 Inherent losses in the transmission system 91

Chapter 6 The test rig and the instrumentation 92

6.1 The design philosophy 92

6.2 The major components of the test rig 93

1. The test bed 93

2. The dynamometer 96

3. The flywheel 96

4. The transmission 104

5. The engine 108

6.3 The instrumentation 109

1. The quantities to be measured 109

2. Torque measurement 110

3. Speed measurements 111

4. Belt radius measurement 111

5. Pressure measurements 113

6. Engine throttle angle 113

7. Data collection 113

Chapter 7 Belt related torque loss 114

7.1 Introduction 114

7.2 Belt torque loss 115

7.3 Torque loss on no-load 116

7.4 Measurement of the torque loss on no-load 119

7.5 Torque loss when the transmission is delivering a torque 121

7.6 Comparison of calculated and measured torque losses on load 124

7.7 Inclusion of the torque loss in calculations on the transmission 126

7.8 The torque loss when the transmission is in an overdrive ratio 127

Chapter 8 The effect of gaps between the segments 129

8.1 Introduction 129

8.2 Extra overall slip caused by gaps between segments in the primary pulley 129

8.3 The possible positions of the gaps 131

8.4 Experimental determination of the position of the gaps 133

8.5 Theoretical verification of the effect of gaps on slip 136

Chapter 9 Use of the model to determine the conditions in the transmission 141

9.1 Introduction 141

9.2 Choice of the input parameters 142

9.3 A possible sequence of calculations 143

1. Specify the five operating parameters 143

2. Determine geometric relations 143

3. Determine the band speeds in terms of the segment speed 143

4. Determine the conditions at the secondary pulley 144

5. Evaluate the extra torques that must be transferred at the pulleys due to belt torque loss 144

6. Determine the slip speed between the segments and the pulley surface on the secondary pulley 145

7. Determine the speed of the segments and the band speeds and tensions 147

8. Determine the slip speed on the primary pulley 148

9. Determine the remaining properties required 149

10. Output of the properties determined 150

9.4 A simplified sequence of calculations 151

Chapter 10 Description of tests carried out and evaluation of results 153

10.1 Introduction 153

10.2 Checks on the instrumentation 155

1. Belt radius measurements 155

2. Speed measurements 157

3. The overall slip 158

10.3 The First set of tests 159

10.4 Validation of the viscous shear model using Test 2 168

10.5 The Second set of tests, steady state tests using the standard control system 174

10.6 The Third set of tests, steady state tests with fixed radii and using an external control system to supply the required pressures 180

10.7 Values of other quantities determined by use of the transmission model 186

10.8 The magnitude of losses in the transmission 190

Chapter 11 Discussion of results and conclusions 196

11.1 The test rig 196

11.2 The performance of the transmission with the standard control system 196

11.3 Validation of the viscous shear model 199

11.4 Validation of the transmission model 203

11.5 The effect of gaps between the segments 205

11.6 The belt related torque loss 206

11.7 The losses in the system 208

11.8 Conclusions 212

References 214

Appendix 1 Papers published with synopses 221

Appendix 2 A simplified system model 225

The simplified equations 226

Comparison with experimental results 230

Appendix 3 The computer programmes 231

Values of dimensions, etc, for the transmission 231

Listing of the final programme, BELTOP14 233

Typical print out of results 236

Appendix 4 Tables of results 237

List of Figures

		Page
Fig 1.1	An engine map typical of a petrol engine	22
Fig 2.1	A diagram of the Ford CTX transmission	30
Fig 2.2	The belt and pulley system	31
Fig 2.3	The pulley servo control system	34
Fig 2.4	The ratio diagram for the CTX control system	35
Fig 3.1	The simple model of the belt-pulley system	45
Fig 3.2	Free body diagram for an element in the active arc of the primary pulley	46
Fig 3.3	The support used for measuring the segment stiffness	49
Fig 3.4	Compressive load-strain curve for the belt segments	50
Fig 3.5	Overall slip-time curves from Becker with additions	51
Fig 3.6	Segment-band connection	52
Fig 4.1	Contact point A, radius *R*, on the surface of a pulley half	60
Fig 4.2	Variation of relative film thickness between segment and pulley surface with load and slip speed. From Collier and Goldsmith	63
Fig 4.3	Measured and calculated film thickness - 39.3 mm radius	65

Fig 4.4	Measured and calculated film thickness - 50.0 mm radius	65
Fig 4.5	Measured and calculated film thickness - 60.0 mm radius	66
Fig 4.6	Measured and calculated film thickness - 71.3 mm radius	66
Fig 4.7	Measured and calculated drag force on segment - 39.3 mm radius	67
Fig 4.8	Measured and calculated drag force on segment - 50.0 mm radius	67
Fig 4.9	Measured and calculated drag force on segment - 60.0 mm radius	68
Fig 4.10	Measured and calculated drag force on segment - 71.3 mm radius	68
Fig 4.11	Measured and calculated drag force on segment using the model which includes the effect of asperity contact - 50.0 mm radius	70
Fig 4.12	Summary of the viscous shear models	72
Fig 5.1	The four stations on the belt	75
Fig 5.2	The belt geometry	76
Fig 5.3	The shear stresses acting on band 10	77
Fig 5.4	Free body diagram for a segment engaged with a pulley	79
Fig 5.5	The contact between segment and pulley	81
Fig 5.6	An element of belt engaged with a pulley	85
Fig 5.7	The centre lines of bands n and $(n - 1)$	87
Fig 5.8	The shear stresses acting on band 1	88

Fig 6.1	Schematic diagram of the test rig	94
Fig 6.2	A photograph showing the test rig	95
Fig 6.3	Schematic diagram of the dynamometer hydraulic system	97
Fig 6.4	The dynamometer and flywheel on the rear of the test rig	98
Fig 6.5	Sectional drawing of the flywheel and additional rings	102
Fig 6.6	The transmission mounted on the test rig	104
Fig 6.7	The differential assembly and the replacement block	106
Fig 6.8	Belt radius probe	112
Fig 7.1	The line of the belt on no-load	116
Fig 7.2	The belt at outlet from the primary pulley	118
Fig 7.3	Measured and calculated belt torque loss on no-load	120
Fig 7.4	An ideal system delivering a torque T_s	122
Fig 7.5	System with torque loss	123
Fig 7.6	Measured and calculated torque losses - 32 N m input	125
Fig 7.7	Measured and calculated torque losses - 64 N m input	126
Fig 8.1	The possible positions of the gaps between the segments	133
Fig 8.2	Separation of segments by reverse bend in belt at outlet from secondary pulley	134
Fig 8.3	Slip measurements with two values of belt total gap	135
Fig 8.4	Slip measurements with two values of belt total gap	135
Fig 8.5	Slip measurements with large gap compared with standard	136
Fig 8.6	Measured and calculated slips for standard belt and belt	139

less one segment - primary radius 29 mm

Fig 10.1(a)Test 1. Results for a full throttle acceleration showing the starting sequence for the standard control system 160

Fig 10.1(b)Test 1. Results for a full throttle acceleration (continued) 161

Fig 10.2(a)Test 2. Results for a full throttle acceleration on a level road to near maximum speed 163

Fig 10.2(b)Test 2. Results for a full throttle acceleration (continued) 164

Fig 10.3 Test 3. Results for a closed throttle deceleration on a level road from near maximum speed 165

Fig 10.4 Test 4. Results for a full throttle acceleration from rest up a 10% incline 166

Fig 10.5 Test 5. Results for a closed throttle deceleration from maximum speed up a 10% incline 167

Fig 10.6 Test 2. Measured and calculated slips on the primary pulley 169

Fig 10.7 Test 2. Measured and calculated slips on the secondary pulley 170

Fig 10.8 Test 2. Measured and calculated overall slips 171

Fig 10.9 Test 2. Measured and calculated primary cylinder pressures 172

Fig 10.10 Test 2. Measured and calculated torque input 173

Fig 10.11 Test 2. Measured and calculated input shaft speeds 173

Fig 10.12 Measured and calculated steady state results with the standard control system, 16 N m input torque 176

Fig 10.13 Measured and calculated steady state results with the 176

standard control system, 32 N m input torque

Fig 10.14 Measured and calculated steady state results with the standard control system, 48 N m input torque 177

Fig 10.15 Measured and calculated steady state results with the standard control system, 64 N m input torque 177

Fig 10.16 Measured and calculated steady state results with the standard control system, maximum input torque 178

Fig 10.17 Measured and calculated input shaft speeds in steady state with the standard control system 179

Fig 10.18 Measured and calculated input shaft torques in steady state with the standard control system 179

Fig 10.19 Measured and calculated overall slips plotted against input torque. Primary radius 28.8 mm, input shaft speed 3100 rev/min 183

Fig 10.20 Measured and calculated overall slips plotted against input torque. Primary radius 39.2 mm, input shaft speed 2950 rev/min 183

Fig 10.21 Measured and calculated overall slips plotted against input torque. Primary radius 50.0 mm, input shaft speed 2900 rev/min 184

Fig 10.22 Measured and calculated overall slips plotted against input torque. Primary radius 70.1 mm, input shaft speed 4200 rev/min 184

Fig 10.23 Variation of input shaft loss with input speed, no belt or pump 185

Fig 10.24 Variation in some transmission properties with vehicle speed in steady state using the standard control system 189

Fig 10.25 Variation of transmission mechanical efficiency with 192

vehicle speed in steady state and the division of the input shaft torque into the useful torque and the various losses

Fig 10.26 Variations in the various input torque losses with vehicle speed in steady state 193

Fig 11.1 The engine map showing the steady state running lines for the transmission and for a car in fifth gear 198

Fig 11.2 The improvements in mechanical efficiency obtainable by the use of an optimising control system 210

Fig A2.1 Comparison of results from the simplified model with measured values from Test 2 230

NOTATION

Symbols that appear briefly in the text and are defined in that place are not listed.

a	half width of Hertzian contact
c	length of the pulley-segment contact
C	compressive force in the segments
C_L	compressive force in the segments between stations 1 and 2 due to belt torque loss on no-load
$\Delta C_{x\text{-}y}$	the change in C between stations x and y
D_{p1},D_{p2}	outer and inner diameters of the primary pulley cylinder
D_{s1},D_{s2}	outer and inner diameters of the secondary pulley cylinder
E	modulus of elasticity
F,F_p,F_s	axial clamping force on pulley, on primary pulley, on secondary
ΔF_{seg}	axial force on one segment
F_{sp}	force exerted by spring in secondary pulley cylinder
g_t	total gap between segments including effect of band tensions
G	component in radial plane and parallel to pulley surface of shear force produced by relative motion of segment over pulley
h	gap between segments on a section of the belt when the belt is running
h_o	film thickness in ehd contact
J	radial component of the two forces G

k_p,k_s	factors applied to pulley radii to allow for belt torque loss
K	constant used in determining k_p and k_s
L	length of belt at radius of rocking edge
L_c	length of contact between segment and pulley
L_g	length of belt section where gaps are situated
m	mass per unit length of one band
m_b	mass per unit length of belt
m_s	mass of a segment
n	number of a band, n = 1 to 10
n_i,n_o	speeds of input and output shafts
n_p,n_s	speeds of primary and secondary pulleys
N	normal force at segment-pulley contact
p_m	mean pressure in a contact
P_p,P_s	primary and secondary pulley cylinder pressures
Q	radial component of the two forces N
R_c	reduced radius at a contact
R_d	final drive speed ratio
R_p,R_s	radius of belt to line of rocking edges on primary, secondary pulley
s	thickness of a segment
S	inward radial force applied by the bands to a segment *or* segment stiffness in compression
S_l	overall slip
t	time
t_b	thickness of a band

t_c	oil film thickness in an ehd contact
t_f,t_{fl}	oil film thickness between bands and between inner band and segment shoulder
t_s,t_{sp},t_{ss}	oil film thickness between segment and pulley surface, on primary pulley and on secondary
t_{smin}	minimum value of t_s due to asperity contact
T,T_p,T_s	torque applied to a pulley, to primary pulley, to secondary
T_b	total band tension
T_g	torque required to drive the oil pump
T_i,T_o	input and output shaft torques
T_L,T_{Lx}	extra input shaft torque to overcome belt torque loss on no-load and when on load
T_{Lp},T_{Ls}	extra torque to be applied to primary/secondary pulley to overcome belt torque loss on that pulley
T_n,$T_{n,x}$	tension in band n, tension in band n at station x
$\Delta T_{n,x\text{-}y}$	change in T_n between stations x and y
T_{seg}	pulley torque contributed by a segment
v_n	speed of band n
v_{rel}	relative speed of one surface to another adjacent surface
v_R,v_{Rp},v_{Rs}	radial velocity of belt on a pulley, on primary pulley, on secondary
v_s	segment speed at the level of the rocking edges
v_{sl},v_{slp},v_{sls}	tangential slip speed of segment relative to pulley surface, on primary pulley, on secondary pulley
V	tangential force between inner band and segment due to relative motion

V_p	volumetric flow rate of oil through the pump
w	total width of the two band packs
W	tangential component of the shear force due to the relative motion of the segment over the pulley surface, $W/2$ each side
W_c	normal load on an ehd contact
x	distance of segment shoulder above the rocking edge
X	pulley centres distance *or* forces in 'peg and hole' connections between segments
y	distance of element of a segment-pulley contact below the rocking edge
$\overline{y}$	distance of line of action of W below the rocking edge
Y	quantity defined by equation 5.23
α	viscosity pressure coefficient
α_s	viscosity pressure coefficient in segment-pulley contact
β_p,β_s	angle of lap of the belt on primary/secondary pulley
δ_c	strain in segments due to compressive load C
Δ	total initial gap between segments
η_o	basic viscosity of the oil
η_{os}	basic viscosity of the oil in the segment-pulley contact
$\eta_s,\eta_{sp},\eta_{ss}$	viscosity of the oil in the segment-pulley contact, on primary pulley, on secondary pulley
$\eta_{md},\eta_{mo},\eta_{mp}$	mechanical efficiency of final drive, of transmission, of oil pump
θ	half the pulley wedge angle
μ	coefficient of friction
τ,τ_s	viscous shear stress, stress between segment and pulley surface

CHAPTER 1

Introduction

1.1 The advantages to be gained from the use of a Continuously Variable Transmission (CVT)

The fuel saving advantage to be gained from the use of a CVT has been known from the 1930s but interest has intensified in recent years because of the desire to reduce fuel consumption after the fuel supply and cost problems in the 1970s and, more recently, by the desire to reduce carbon dioxide emission because of the problem of global warming.

Use of a CVT offers the possibility of improved powertrain matching to the vehicle requirements. With a CVT fitted in a vehicle there is always the possibility , whatever the vehicle speed and provided that the CVT has a sufficiently large ratio range, of operating the engine at its most efficient operating point for the particular power requirement. For the mid range of speeds this involves running the engine in its most efficient region where the engine torque output is high, the engine speed is low and the engine friction and pumping losses are small. This region is not accessible to the alternative 4 or 5 ratio gearbox because the lowest ratio is fixed by the starting requirements of the car and, for good driveability, the ratios of adjacent gears must

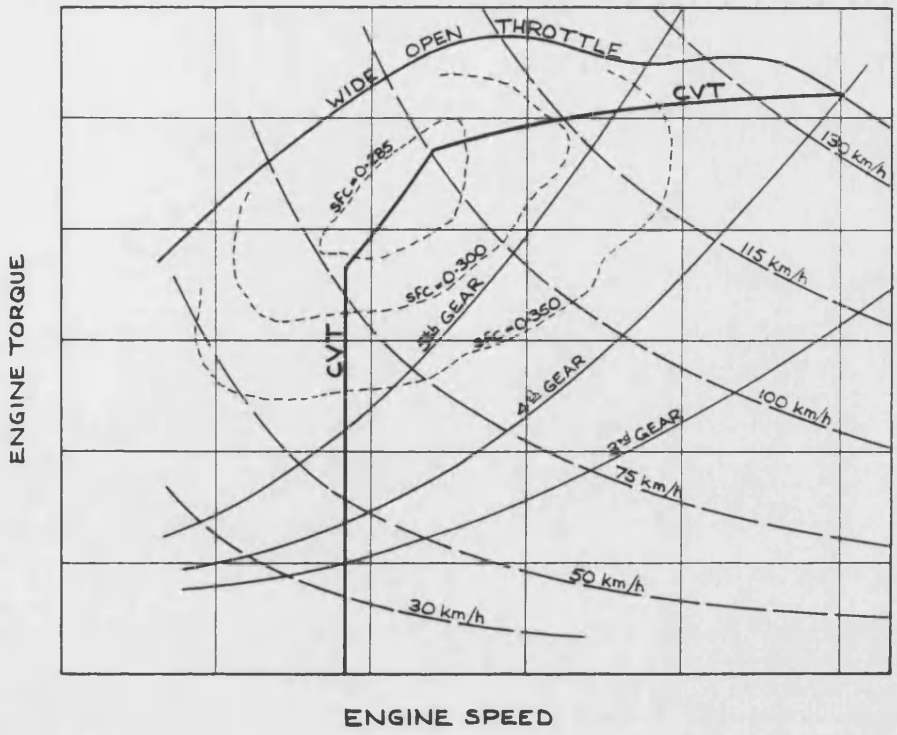

Figure 1.1 An engine map typical of a petrol engine

be reasonably close. Figure 1.1 shows an engine map, a diagram of engine torque output plotted against engine speed, typical of a petrol engine. On the engine map are shown lines typical of a small automobile of:-

Wide open throttle torque

A few lines of constant specific fuel consumption (sfc)

Constant power lines for particular speeds

Running lines for fixed ratio gears

A running line suitable for a CVT.

The vertical part of the CVT running line is at the minimum engine speed that will give comfortable engine operation, perhaps 1700 rev/min. It can be seen that for a wide range of medium speeds the CVT is able to run the engine in the region where the sfc values are low. An automobile with a conventional gearbox in fifth gear will

run the engine in regions where the sfc values are much greater.

One feature of CVT operation can be seen on the engine map. When the CVT is operating close to the maximum torque line for the engine there is little surplus torque available for an acceleration. The torque required is obtained by means of a rapid ratio change to increase the engine speed which, if the engine does not respond rapidly to the increased throttle opening, can result in a momentary check to the vehicle when the driver is calling for an acceleration.

The CVT also offers better acceleration performance than a conventional gearbox as it can allow the engine to operate at peak power throughout the acceleration and without any interruptions for gear changes.

Vehicle emissions can be more closely controlled when a CVT is used because the more restricted engine operating schedule made possible by the CVT enables the engine to be designed and calibrated for minimum emissions. However, the use of an emission control system is important with the CVT as operation of the engine in its most efficient region results in high peak cylinder temperatures which promote NO_x formation. Radtke et al [1.1] compared the fuel economies of a vehicle fitted with a CVT and one fitted with a conventional three speed automatic transmission when emission constraints were required. They found that, as the constraints were tightened, both fuel economies worsened but the relative advantage of the CVT improved.

1.2 The development position of CVTs and research needs

A paper published in 1980 by Cuypers [1.2] evaluated the potential torque capacities per unit volume of mechanical CVT drives relative to that of a standard gearset. He found that the CVT with the greatest potential was the metal, compression V-belt with

a torque capacity 68% of the value for gears. Other belts and chains achieved lower values while traction drives were very poor at under 10%.The criterion for the limiting condition in the compression V-belt was the tensile stress in the bands including the effect of bending around a pulley. The criterion for traction drives was the stress in the contact region. However, his analysis for traction drives has proved to be inadequate as a compact toroidal traction drive CVT has been successfully tested in a Rover 820 automobile fitted with a 2 litre engine, Smith et al [1.3].

A further paper, Cuypers [1.4], considered metal V-belt and V-chain CVTs in which a Coulomb friction model was assumed for the contact with the pulleys. It found the compression V-belt to have the advantage over the other systems considered with a greater power density and quieter running , this last due to the lower contact stress on the pulleys and the negligible polygonal effect with the thin segments used. Its disadvantages were a drastic reduction in power density at small running diameters and difficulties in manufacturing the bands.

This paper also briefly considered values of overall mechanical efficiency. Two graphs from measured results are shown, one of efficiency against speed ratio and the other of efficiency against torque transfer. For most of these two ranges the efficiency is in the mid nineties, the maximum being close to 98%. No details of the test rig are given.

A Department of Energy paper [1.5] dated 1981 reviews the whole field of advanced automotive transmissions and, in particular, examines the operating characteristics of CVTs, describes a number of CVTs under development and gives the development position of each.

The most advanced was the Van Doorne metal V-belt CVT which was expected to be in production in about three years from then. Two traction drives were shown to be fairly advanced in development in spite of the poor showing in Cuypers [1.2], the nutating traction drive by the Vadetec Corporation and the toroidal traction drive of the Perbury type then being developed by British Leyland and now by Torotrak.

The research needs for CVTs were seen to be the development and validation of models with emphasis on the efficiency of the system, identification and reduction of losses, the development of control systems and the optimisation of the complete powertrain.The paper recommends the testing, evaluation and modelling of a CVT as soon as it becomes available.

1.3 The Van Doorne CVTs [1.5]

The first Van Doorne CVT was available in a production car in 1955, the DAF. The variable speed unit, called the Variomatic, was a rubber V-belt running in variable diameter pulleys. The Variomatic was developed over the years and when the DAF company was taken over by Volvo in 1976 was offered in the 1.4 litre Volvo 340. The driveability of the Volvo is good and the overall performance [1.6] is close to that of the Volvo 340 fitted with a manual 5-speed gearbox. The main drawback is the limited life of the twin rubber belts.

In 1966, Van Doorne started work on an improved CVT and by 1969 had conceived the current metal V-belt system. Development work was transferred to an independent company, Van Doorne's Transmissie b.v., in 1972 and the initial production was for industrial drives. From 1976 Ford in collaboration with Van Doorne and Fiat developed the system for automotive use, the design being known as the CTX. In

1980 field trials were run with 1.5 litre Fiat Ritmo taxis but it was not until 1987 that the first production cars appeared, the Fiat Uno and the Ford Fiesta. Since then other vehicle manufacturers, Subaru, Lancia, Rover and Nissan, have offered the transmission in production automobiles. Van Doorne manufactures the belts and, possibly, the pulleys and pumps [1.7] and supplies them to a number of vehicle manufacturers plants for assembly in the transmissions.

It is the only CVT currently offered in production automobiles. Two versions are available, the Ford CTX with two wet, multi plate clutches, one for forward drive and one for reverse, and the Subaru ECVT which uses a magnetic powder clutch.

1.4 The performance of the Van Doorne CVT

The advantages promised for the use of a CVT have apparently not been realised. A magazine article [1.6] entitled 'The Doubtful Future of the CVT' includes an interesting table in which all the cars available at that time offered with the CVT were compared with the corresponding models using a manual 5-speed gearbox. Comparisons were made of top speed, acceleration time and fuel consumptions, both City Cycles and steady speed values. Virtually all the comparisons show the CVT to be inferior to the 5-speed gearbox with the one major exception of the Fiat Panda 1000 with the ECVT which showed a 22% improvement in fuel consumption for the Urban Cycle. This one good figure is open to doubt, though, as the two other automobiles with the ECVT show inferior fuel consumptions and on steady speeds the Panda also shows inferior fuel consumption. However, when compared with equivalent models fitted with conventional automatic transmissions all the CVT vehicles showed better fuel consumptions.

1.5 The necessity for modelling and testing the Van Doorne CVT

When this investigation was commenced at the end of 1988 the Van Doorne CVT was just being offered in production automobiles but was not apparently giving the advantages to be expected from a CVT. A few papers modelling the system had appeared, Gerbert [1.8], Becker [1.9] and Sun[1.10], but only one, Becker's, was backed by any test results. Further, these three papers all diverged in their conclusions. Thus it was considered to be important that a model of the CVT should be developed, that the losses should be investigated and that a control strategy making use of the model and endeavoring to maximise the possibilities of CVT operation should also be developed. It was also important that this theoretical work should be backed by a comprehensive test programme.

1.6 The importance of the overall slip in the investigation

One thing that the three papers mentioned above agreed on was that the shear connection between the belt and the pulleys should be modelled by Coulomb friction as did Cuypers [1.4]. The manufacturers, too, believe this assumption to be correct and include in the design of the belt a surface treatment to aid the exclusion of oil from the contact, Hendriks [1.11].

In view of the amount of oil likely to be present inside the transmission casing when the system is operating, it was considered probable that this shear connection would be viscous in spite of the surface treatment. Results of slip measurements in the paper by Becker [1.9] showed values of up to 3.5% overall slip. As the slip with a Coulomb friction model depends on the stiffness in compression of the belt segments it did not seem likely that slips of this magnitude could be achieved when the segments were

made of steel. Thus arose the emphasis in this work on the importance of measuring the overall slip accurately and on the system model predicting this slip correctly. The starting point of this investigation was the assumption that the model for this shear connection should be viscous. If the assumption of viscous shear should prove to be correct, the amount of slip would obviously depend on the pressure clamping the pulley halves together. This raises the possibility of designing the control system so that the loss due to slip is balanced against the loss from driving the hydraulic pump.

1.7 The objectives of this investigation

This investigation is concerned with:-

(a) the development of a model for the Van Doorne transmission,

(b) the identification and minimisation of the losses in the transmission,

(c) the testing of the transmission in order to validate the model, to determine the performance of the transmission and to measure the magnitude of the losses,

(d) making any proposals that may arise to improve the performance of the transmission.

A parallel project involving a colleague, Markus Guebeli, was concerned with the design of a control strategy for the transmission and with the initial testing of the transmission to be followed later by simulation of, and tests on, the redesigned control system.

CHAPTER 2

Description of the Steel, Compression V-Belt CVT

2.1 Introduction

The transmission tested was a standard Ford CTX unit as fitted in the 1.1 litre Ford Fiesta [2.1]. It has a large ratio range equal to 5.85:1, roughly equivalent to a normal gearbox with six ratios. The lowest overall ratio is 14.08:1 which may be compared with the value of 13.75:1 in the MTX-5, the corresponding 5-ratio manual gearbox alternatively fitted in the Fiesta. The highest overall ratio is 2.41:1 compared with 2.90:1 for the manual.

The transmission is shown diagramatically in figure 2.1. It can be divided into five main parts:

The belt and pulley variable speed unit.

An epicyclic gear system with two, wet multi plate clutches on the transmission input shaft.

A primary reduction gearset plus a final drive reduction gearset, including the differential, between the secondary pulley and the output shafts to the wheels.

A hydraulic gear pump driven off the input shaft.

A hydraulic control unit.

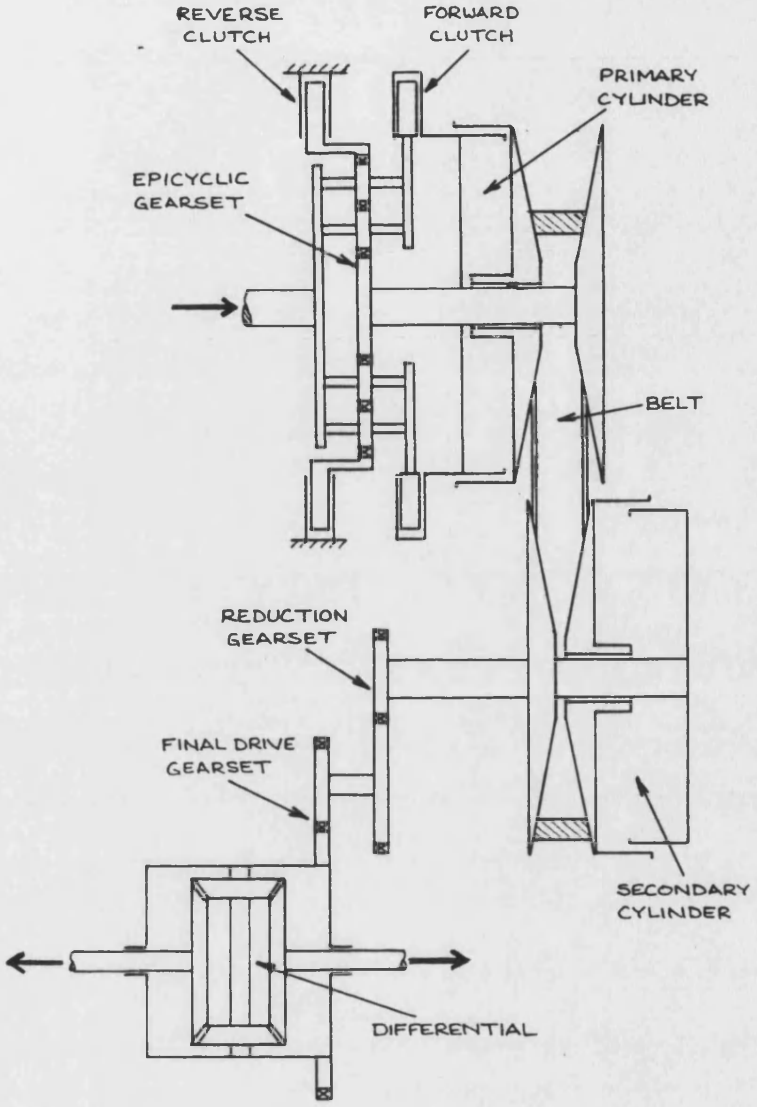

Figure 2.1 A diagram of the Ford CTX transmission

2.2 The belt and pulley system

The heart of the transmission is the belt and pulley system, the essential parts of which are shown in figure 2.2. The two, 22° total angle V-pulleys have conical surfaces and one half of each pulley can move axially under hydraulic control in order to set the transmission ratio. The opposite halves of the pulleys move so that the belt

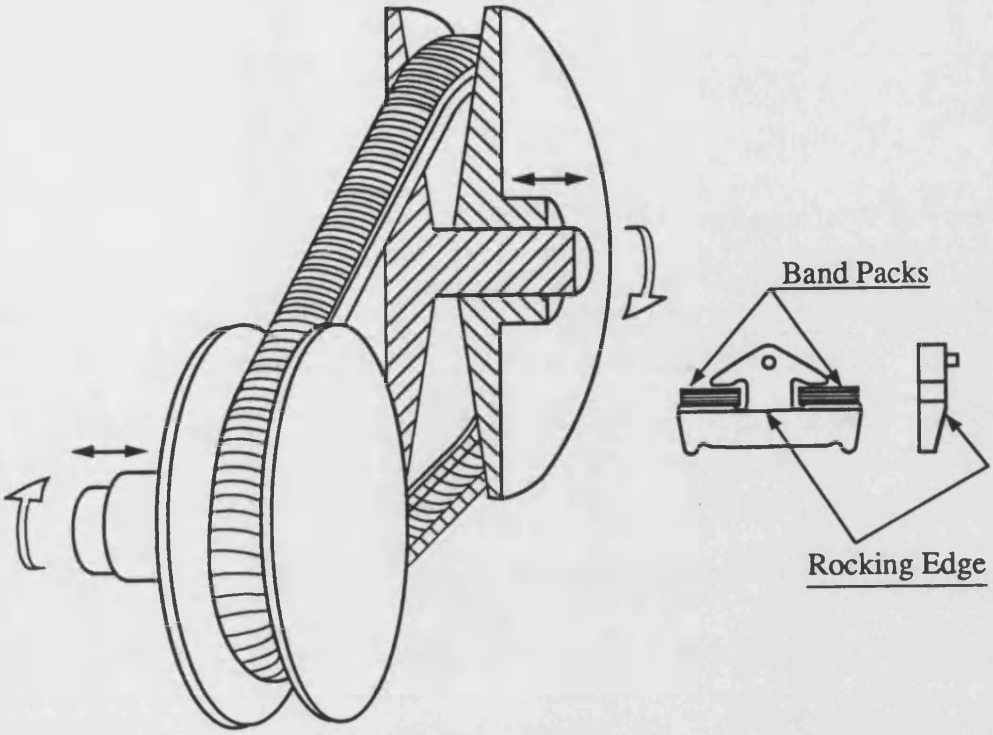

Figure 2.2 The belt and pulley system

runs very nearly, but not completely, in a straight line off one pulley and onto the other.

The belt is made of steel and is very flexible so that it is able to run at a very small radius on a pulley. It consists of a large number of flat segments, shown in figure 2.2, which transfer the torque in compression between the primary and secondary pulleys. Each segment has a peg on its front face which engages with a hole in the rear face of the segment on front. This ensures that the segments run with their planes perpendicular to the direction of motion. The lower half of the front face is cut away to allow the segments to tilt about the 'rocking edge' as they round a pulley.

The segments are held together and constrained to run around the pulleys by two packs of thin, endless steel bands which run in slots in the segments, a pack of thin

bands being used for flexibility. The shoulder on which the bands run is slightly curved in front view so that the band pack runs at the highest point, like a flat belt on a pulley, and does not touch the pulley surface. As will be explained later, the bands move relative to the segments.

The number of segments in the belt and the number of bands in a pack depend on the power rating of the transmission. The transmission tested had 297 segments and 10 bands in each pack.

2.3 The epicyclic gear and clutch system

The wet, multi plate clutches are used to give a smooth take up of the drive, one clutch for forward drive and the other for reverse. The epicyclic gear reverses the direction of the pulleys as required. The clutches are engaged by applying hydraulic pressure to the appropriate cylinder. During normal operation this pressure is sufficient to prevent slip but, when the vehicle is stationary and the engine is idling, this pressure takes up a low value that supplies the same vehicle creep effect as a conventional automatic.

With reference to figure 2.1, the planet gears in the epicyclic are carried on axles which connect the input shaft to the forward clutch disc. When the forward clutch is engaged, the clutch disc is connected to the primary pulley shaft so that the epicyclic is locked and there is direct drive from the input shaft to the pulley. The plates of the reverse clutch then run at the input speed between their stationary pressure plates. When the reverse clutch is engaged, the outer ring of the epicyclic is stationary and the input to the planetary gears causes the primary pulley shaft to rotate in the opposite direction with the forward drive clutch plates rotating freely.

2.4 The primary and final drive reduction gears

These gears transfer the torque from the secondary pulley to the output shafts. The ratio of the primary reduction gear is matched to the particular vehicle application. On the transmission tested this ratio was 1.476:1, slightly different from the usual 1.1 litre Fiesta value of 1.41:1. The final drive has a standard ratio in all cases of 3.842:1.

2.5 The hydraulic pump and control unit

The operation of the control unit is described by Hahne [2.2] who also describes the development of the CTX project.

The hydraulic pump is a normal spur gear pump which is connected directly to the input shaft so that it is always driven whenever the engine is running.

The driver's selector lever has the standard five positions:

P - parking. The secondary pulley is locked

R - reverse drive.

N - neutral.

D - forward drive.

L - low, to provide engine braking on the over-run.

The hydraulic control unit has five input signals:

The driver's selector lever position.

The accelerator pedal position.

The transmission ratio by means of the position of the movable half of the primary pulley.

The engine speed.

The primary pulley speed.

The last two speed inputs are obtained from the pressure generated in a pitot tube immersed in a circular reservoir rotating at the appropriate speed. A diagram of the pulley servo control system is shown in figure 2.3.

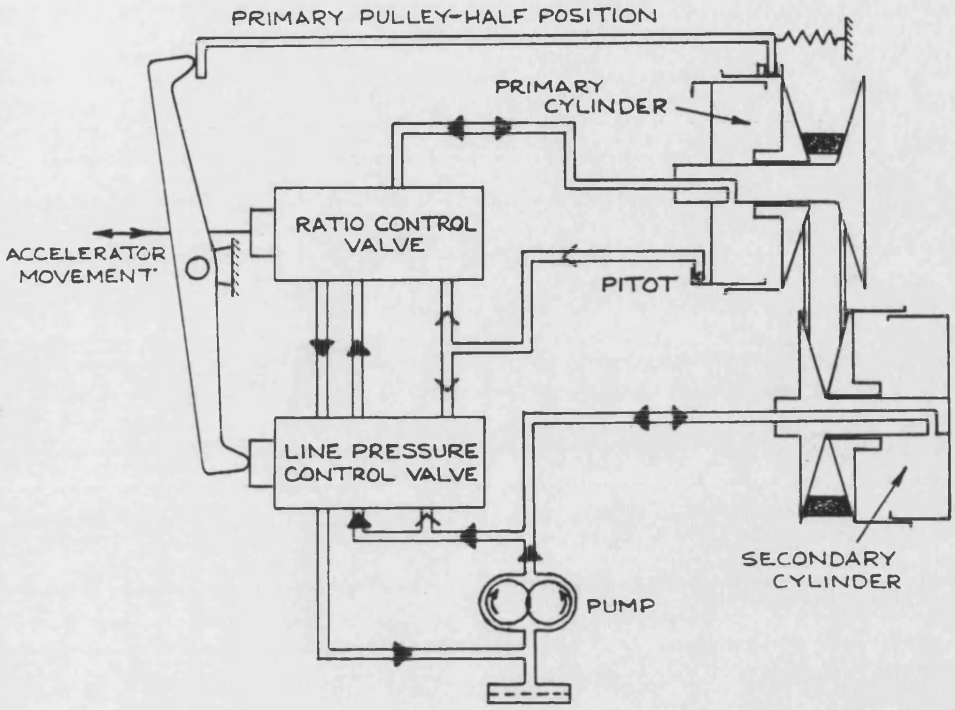

Figure 2.3 The pulley servo control system

The line pressure from the pump passes to the secondary pulley servo cylinder, this serving to tension the belt, and to a line pressure control valve. The control valve modulates the line pressure between approximately 30 bar and 8 bar from inputs of accelerator position, primary pulley speed and transmission ratio. The lowest pressure required to prevent slip is used.

A ratio control valve feeds oil to or from the primary pulley servo cylinder in order to control the transmission ratio. This valve is actuated by inputs of accelerator position and primary pulley speed. The accelerator position programmes a particular

primary pulley speed, which is the engine speed when the clutch is closed, and the valve changes the ratio until the input primary pulley speed is equal to the programmed value.

The clutches are controlled by a further three valves which are also located in the control unit.

Figure 2.4 is a ratio diagram for the CTX, a diagram of vehicle speed plotted against engine speed. On it are shown lines of constant transmission ratio, straight lines radiating from the origin. The low and high ratios for the CTX are shown as well as the five ratios typical of a 5-speed manual gearbox. The point A represents the vehicle

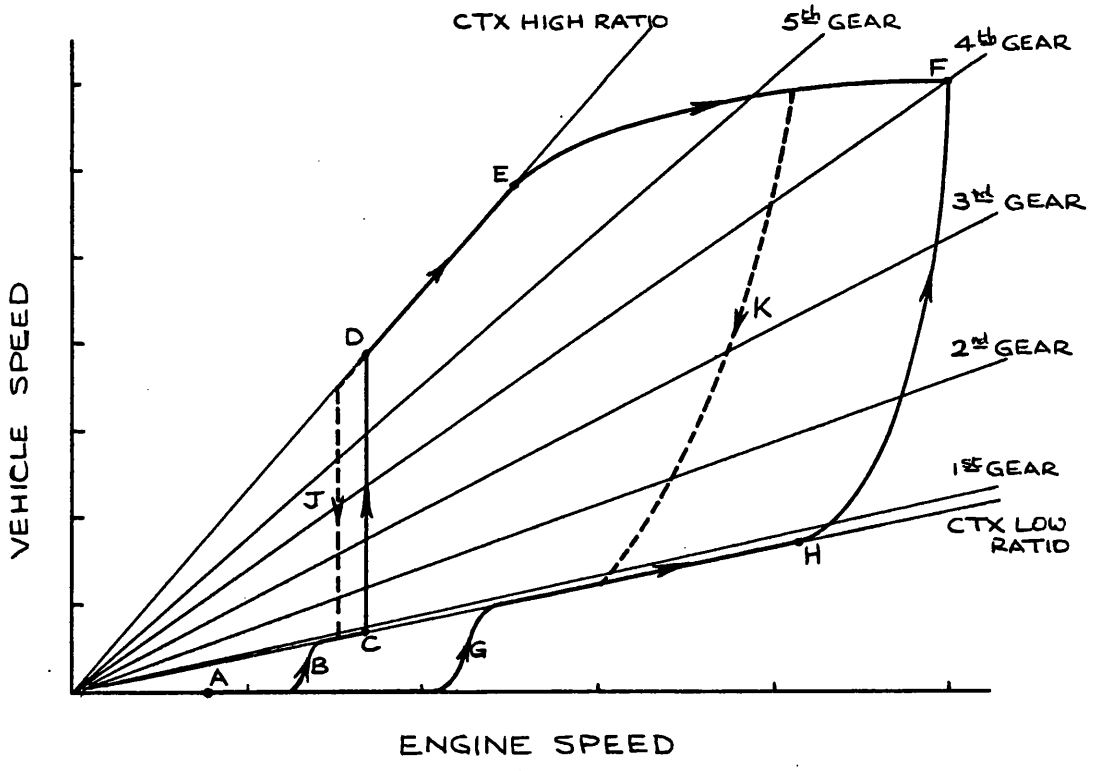

Figure 2.4 The ratio diagram for the CTX control system

at rest with the engine idling.

Once the selector lever is set the vehicle is controlled by the accelerator and brake only. With 'D' selected, if the throttle is slowly opened until it is wide open the minimum acceleration line will be followed. Ideally the clutch will close at B and the transmission will remain in low ratio until the vehicle has accelerated to C. Then the ratio will change at a low, constant engine speed up to the high ratio at D. Thereafter the high ratio line is followed to E where the engine is operating in its most efficient region. To remain in the high efficiency region and then to achieve maximum speed the engine speed must be raised more rapidly by reduction of the ratio up to the maximum speed point F. Any constant speed point will lie on this line.

If a wide open throttle line is followed starting at the point A the clutch now closes at a higher engine speed at G and the transmission stays in low ratio until near the maximum engine speed at H. Then the ratio steadily increases up to the maximum speed point at F. Intermediate accelerations follow a line between these two.

If the throttle is closed at maximum speed the system retraces the first line but passes D still in high ratio and then reduces the ratio to the low value at the lower engine speed shown by the line J. When the low ratio is reached the clutch disengages.

If 'L' has been selected to give engine braking as when decending a steep hill the ratio change towards low comes earlier and the engine speed remains high. The path K is followed.

In reverse, 'R', only the low ratio is available.

These lines are the ideal lines that the designers of the control system endeavour to follow.

2.6 The behaviour of the belt when the transmission is running

Relative motions occur at the contacts between the belt segments and the pulley surfaces, between band number one and the segments and between adjacent bands.

In the forward drive situation the primary pulley transfers a torque to the belt by means of friction at the contact and the pulley surface moves forward relative to the belt. At the secondary pulley the belt transfers the torque to the pulley surface and moves forward relative to the surface.

These transfers result in a compressive force building up in the segments in the primary pulley, remaining in the segments on the straight section between the primary and secondary pulleys and then reducing to zero in the secondary pulley. The presence of a total initial gap between the segments when the belt is assembled means that the segments have no compressive force along the other straight section. Thus the belt segments are pressed tightly together around the pulleys and along the straight from the primary to the secondary pulley. While rounding a pulley the segments contact each other along the line of the rocking edges so that the belt is continuous along this line. The speed of the belt segments along the line of the rocking edges must then be taken as the belt speed.

The bands and the contact between the inner bands and the segment shoulders all lie above the line of the rocking edges. As the belt will tend to act as a solid body when passing round a pulley, the outer bands will tend to be moving faster than the inner bands and all the bands faster than the segments. Hence on the following straight section the bands will move ahead of the segments and the outer bands ahead of the inner.

CHAPTER 3

Consideration of the Coulomb Friction Model

3.1 Introduction

If one considers the contact between the belt segments and the pulleys and the pressure generated by the clamping force on the pulley halves together with the surface treatment of the segment sides by the manufacturers in order to remove the oil film [3.1] and then consults the reference work by Dowson [3.2] one is led to the conclusion that this shear connection lies in the field of Boundary Lubrication. It is then reasonable to make use of a coefficient of friction in the same way as for dry solids but with a reduced value. Authors of papers considering the compression belt transmission have then made the assumption that Coulomb friction applies to this connection and, indeed, to all the other connections in the system.

A Coulomb friction model gives rise to slip between adjacent members whenever a force is being transferred between them. The transfer of the force causes a change in the loading in the member and hence a change in length because of the elasticity of the material. These changes in length result in slip between the two members. Conversely, when there is no slip, there is no change in loading and no force transfer. A well known example of this effect is in the drive between two pulleys with an unlubricated flat belt where Coulomb friction applies. As the belt passes round each

pulley it passes firstly through the 'idle arc', a region of no slip and no torque transfer and secondly through the 'active arc' where there is slip and torque transfer.

It was seen in Chapter 2 that, except for the equal radii case, the bands must slip over the segments when passing round the pulleys. Because of the large pressure between the bands and the segments, the assumption of Coulomb friction would give rise to large tensile force changes in the bands when this slip occurs. The bands would then have a considerable effect on the torque transfer between the pulleys, either assisting or hindering depending on the direction of slip. A Coulomb friction model of the transmission should show this effect.

This chapter reviews the papers on modelling the transmission, considers the overall slip which results from the assumption of Coulomb friction and shows that this slip is very much less than the measured slip.

3.2 Review of papers proposing models of the transmission

The major papers dealing with the transmission are listed in the references [3.3, 3.4, 3.5, 3.6]. All make use of a Coulomb friction model for the shear connections between adjacent, moving members.

G.Gerbert [3.3]

This paper appears to be the first published on the analysis of the steel, pushing V-belt but is of limited use as the author considers only the case of the pulley radii being equal. His work is influenced by his previous work on normal, rubber V-belts [3.7] in that it includes the elastic penetration of the belt in the V groove in the pulleys. This complicates the analysis unnecessarily as the belt and pulleys are very stiff and this penetration is small. Kim and Lee [3.8] considered this aspect of Gerbert's work

and carried out experiments in which they measured the radial displacement of the belt as the belt passed around the pulleys. Their finding was that this displacement is extremely small and difficult to measure.

The paper does include consideration of the effect of the total initial gap between the belt segments on the overall slip, the only one of the papers reviewed here that does so. This work, too, is limited as the author does not address the problem of determining the band speed in relation to the segments, this having an important bearing on the behaviour of the gaps.

H.-J.Becker [3.4]

The analysis in this paper is good and, assuming that the computer processing of the model is correct, gives the definitive result for a Coulomb friction model. The only omission found is that in writing down the equations of motion for a segment the author did not consider the rotation of the segment about an axis parallel to the pulley axis. However, this omission has a relatively small effect on the results.

The measured results presented in the paper include values of overall slip, the only work apart from the present work to do so. Although Becker did not measure the belt operating radii, his deduction of overall slip from his pulley speed results gives values compatible with those obtained in this work.

Becker obtained the value of the belt stiffness in compression required to calculate the overall slips from the slope of one of his overall slip - torque curves. He then used this stiffness to calculate overall slips for comparison with all his measured results, reasonably good agreement being obtained.

However, it is considered that as the overall slip depends on the belt stiffness and as the belt material is steel it is unlikely that the large slips measured could be achieved with a Coulomb friction model. Further, the value of belt stiffness obtained by Becker, $S = 2.29 \times 10^5$ N, did seem small.

It was decided to resolve this issue by determining the slips using a Coulomb friction model together with measured values of stiffness for comparison with the slips in one of the tests carried out by Becker, a full throttle acceleration. Instead of undertaking the lengthy reprocessing of his equations, it was decided to determine the slips as follows:

1. To derive an expression for the slip using a simple model based on Coulomb friction.
2. To measure the belt stiffness in compression.
3. To use the simple expression for slip with Becker's stiffness to confirm that it gives values compatible with his sophisticated model.
4. Then to determine the slips using the simple expression together with the measured stiffness in order to see whether or not it can predict the measured values of slip.

This is carried out in the following sections, 3.3 to 3.5.

D.C.Sun [3.5]

The analysis in this paper does not give one much confidence in the results. The equations of motion for a belt segment include a radial friction force in the idle arc during a ratio change but not in the active arc and moments about an axis parallel to the pulley axis are ignored. In addition there is no attempt to relate the size of the

active arc to the torque being transferred.

T.Fujii, T.Kurokawa and S.Kanehara [3.6]

These two papers do not analyse the belt-pulley system directly but describe measurements of conditions in parts of the system and explain the results. The authors take the paper on rubber V-belts by Gerbert [3.7] as the basis of the explanations in an attempt to relate the well established rubber belt theory to the steel pushing belt. They assume that all shear connections between neighbouring components depend on a Coulomb friction model.

Part 1 deals with the relation between the ratio of the two pulley clamping forces and the transmitted torque and is reasonably close to the results obtained from the model in this present work. It is shown that for the results to be consistent with a Coulomb friction model it is necessary to have different values for the coefficients of friction on the two pulleys. This was also shown in the results of Kim and Lee [3.8]. It is difficult to see why the two coefficients should be different and is a pointer to the Coulomb friction model not being appropriate.

Part 2 however produces results which are at variance with the results from this present work and tending in some respects to support a Coulomb model. The measurements show the segment compression and the band tension during one revolution of the belt for a variety of operating conditions. They were obtained from the use of a telemeter system which included strain gauge transducers, transmitter and batteries mounted on the belt. The compression measurements show the presence of idle and active arcs on the primary pulley which supports a Coulomb model and a more complicated process on the secondary pulley which does not fit either a

Coulomb or a viscous model. The band tension measurements showed considerable changes during one revolution. As the transducers are not able to give measurements of segment compression and of band tension on the straight parts of the belt and the results require some interpretation it may be that another analysis would reveal results more compatible with a viscous model but it is not possible to do this from information given in the paper.

During measurements the conditions in the test rig were very different from those in the real transmission. The input speeds were in the range 150 - 300 rev/min and the belt and pulleys were uncased. It is probable that at these speeds any lubricant film is unable to form and the torques are transferred with metal to metal contact. That the results then tend to support a Coulomb friction model is not very surprising.

3.3 The overall slip with a simple Coulomb friction model

To be acceptable, the model for the shear connection between the belt and the pulleys must produce overall slip values equal to the measured values. In order to test the suitability of the Coulomb friction model, a simple model of the transmission was devised and an expression for the overall slip was obtained as explained below.

The assumptions made to describe the model are:-

1. The belt consists of a large number of flat segments which form the compression part of the belt and which are retained by a band passing round the outside. The band is tensioned by clamping the pulley halves together.
2. The band has no bending stiffness and there is no friction between the band and the segments. The band will then have a uniform tension, T_b.
3. When the compressive load in the segments alters while they are moving round a

pulley the segments must slip relative to the pulley as they change length elastically. When this slip takes place the friction force between segment and pulley will be given by a Coulomb friction model, i.e. μ x normal force.

4. Unless the pulley is operating with the maximum possible torque and gross slip is about to occur, the angle of lap may be divided into two arcs in the same way as the normal tension belt:

   The idle arc at the entrance to the pulley where there is no slip, no friction force and no change in compression in the segments.

   The active arc for the remainder of the angle of lap where there is slip, friction equals μ x normal force and the segment compression alters.

5. The torque is transferred between the pulleys by a compressive force *C* in the segments in one straight section of the belt while the other straight section carries zero load.

6. Gaps between the segments will be ignored.

Figure 3.1 shows a diagram of this model of the belt-pulley system.

F → A → B	The compressive force in the segments is zero. From A to B the belt speed and the speed of the pulley in contact with it are equal.
B → C	The compressive force increases from zero at B to a maximum at C and the belt slips backwards relative to the pulley as its length is compressed.
C → D → E	The compressive force in the segments remains constant and from D to E the belt speed and the speed of the pulley in contact with it are equal.

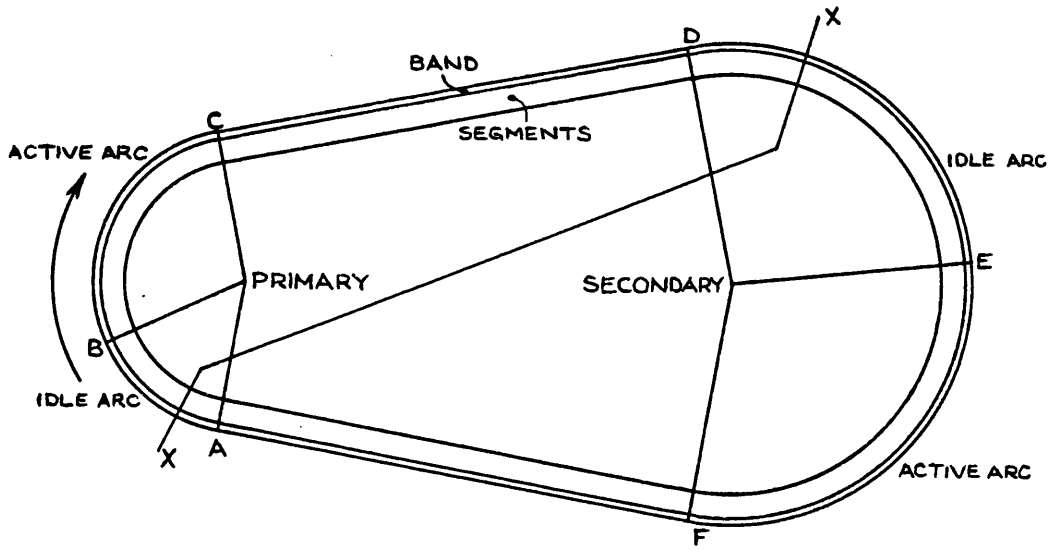

Figure 3.1 The simple model of the belt-pulley system

E → F The compression decreases from a maximum at E to zero at F. The belt lengthens as the load is reduced and slips forward relative to the pulley.

Consider the element shown in the active arc of the primary pulley in figure 3.2. Assume that the line of action of the tangential friction force $2\mu\delta N$ is the same as that of the compressive force in the segments and neglect the mass of the belt.

Radially:

$$-2C.\sin\frac{\delta\alpha}{2} - 2\delta N.\sin\theta + 2T_b.\sin\frac{\delta\alpha}{2} = 0$$

as $\delta\alpha$ is small:

$$-C\delta\alpha + T_b\delta\alpha - 2\delta N.\sin\theta = 0$$

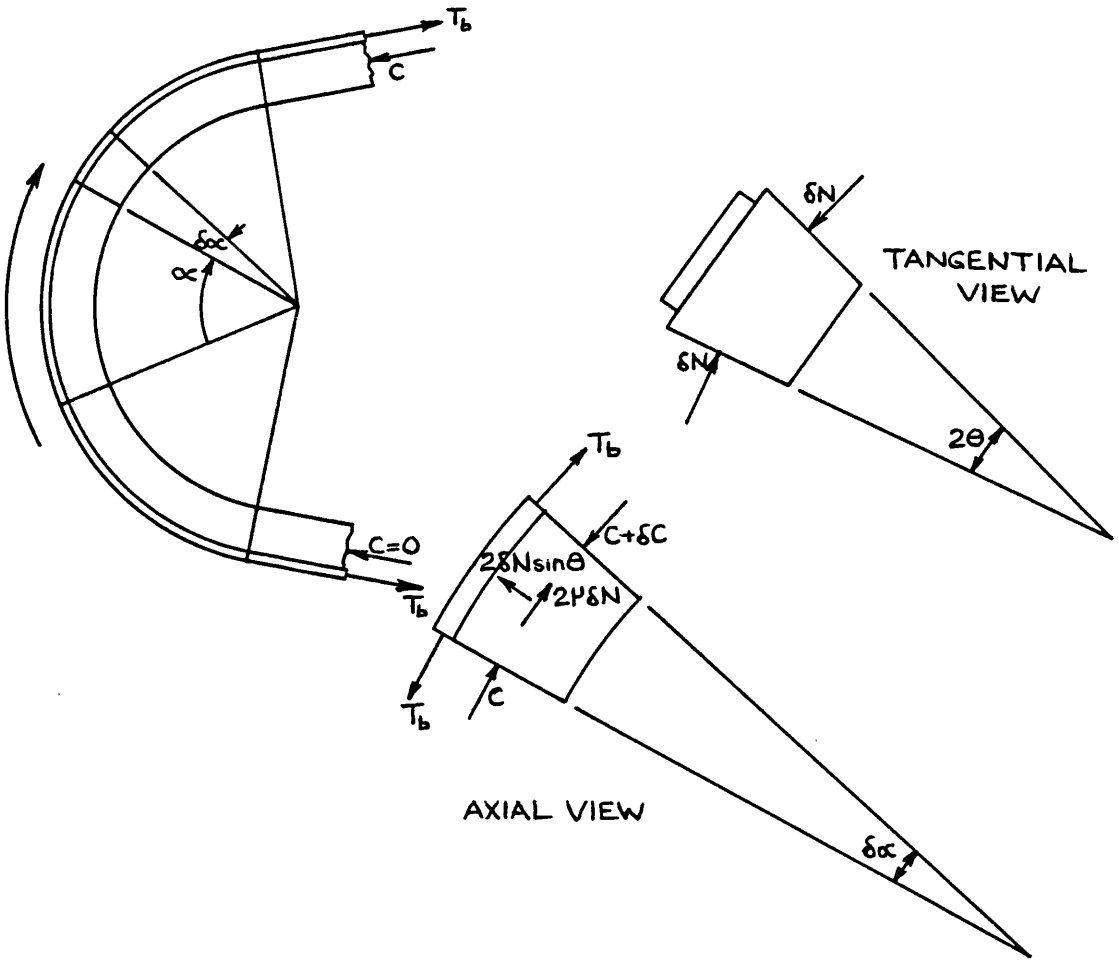

Figure 3.2 Free body diagram for an element in the active arc of the primary pulley

Tangentially:

$$-\delta C + 2\mu\delta N = 0$$

Combine these equations by eliminating δN:

$$\frac{\delta C}{T_b - C} = \frac{\mu}{\sin\theta}\delta\alpha$$

Integrate this equation over the active arc:

$$\frac{T_b}{T_b - C} = e^{\frac{\mu\beta}{\sin\theta}}$$

If R is the effective radius of the segments and T is the moment applied to the pulley:

$$C = \frac{T}{R}$$

As the same values of T_b and C apply to the active arc on both pulleys, the sizes of the two active arcs must be equal.

In order to determine the overall slip consider a boundary XX passing through both idle arcs, see figure 3.1. In steady state the rate of flow of segments across this boundary on the two pulleys must be equal.

If the primary pulley rotates once, a length of segments equal to $2\pi R_p$ will cross XX on the primary pulley.

The same quantity of segments must cross XX on the secondary pulley. Here the segments are carrying a load C and the length of the segments will be $2\pi R_p(1 - \delta_c)$ where δ_c is the strain corresponding to the load C.

The number of turns made by the secondary pulley as this length of segments crosses XX will be:

$$\frac{2\pi R_p(1 - \delta_c)}{2\pi R_s} = \frac{R_p}{R_s}(1 - \delta_c) = \frac{n_s}{n_p}$$

The overall slip is given by:

$$S_1 = 1 - \frac{n_s R_s}{n_p R_p} = \delta_c$$

The slip for the simple model is equal to the strain in the segments corresponding to the compressive load as the segments pass round the idle arc at inlet to the secondary pulley. To use this expression it is necessary to make measurements on the segments in order to produce a load-strain relation or to otherwise deduce the stiffness. It is important that the stiffness is obtained for the segments when they are positioned on a circular path so that the compressive load is conveyed from segment to segment through a line contact at the rocking edge. The stiffness when the segments are in a straight line with their faces in contact is likely to be very different.

Becker [3.4] deduced a value for the segment stiffness from the slope of one of his measured overall slip-torque curves. He determined the stiffness, i.e. the ratio of compressive force/strain, to be:

$$S = 2.29 \times 10^5 \text{ N}$$

As the overall slip from the simple model is to be used to test whether or not the Coulomb friction assumption is appropriate it was decided to make measurements in order to determine the stiffness of the segments.

3.4 Measurement of the stiffness in compression of the belt segments

A support was designed which would hold a number of belt segments in their correct relative positions while on a large radius curve and which would allow a compressive force to be applied to them. As the segment contact is a line contact, the radius of the curve will have no, or little, effect on the stiffness. The support is shown in figure 3.3 set up for testing in a Denison machine. The segment shoulders rest on the curved members of the support which thus take the place of the bands in the normal operation of the belt. The total change in length of the segments under load is equal to the

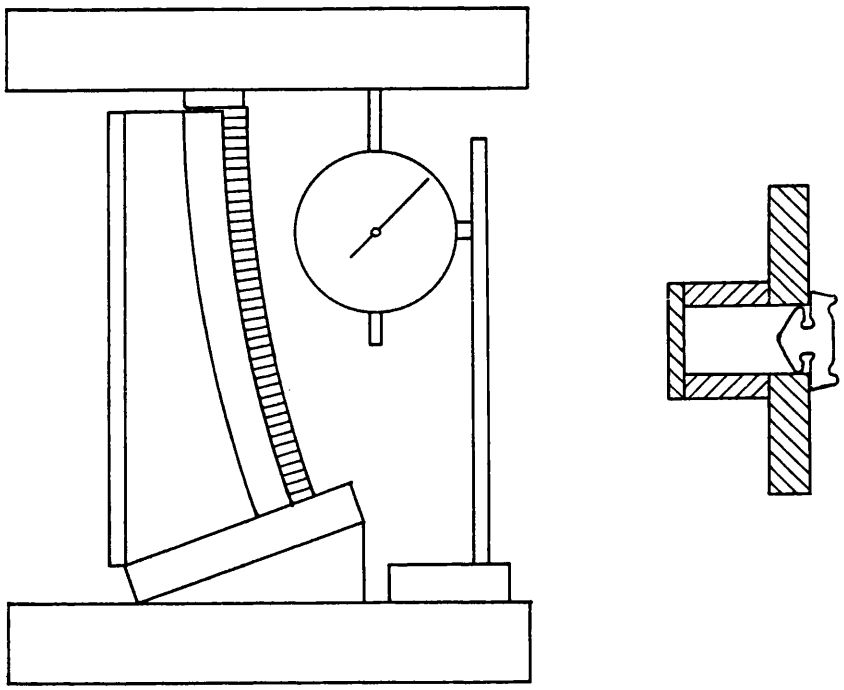

Figure 3.3 The support used for measuring the segment stiffness

vertical movement of the loading block and this was measured with the dial gauge shown. The deformation of the support base is negligible compared with that of the segments as it is relatively massive.

The decrease in length of the segments was measured for a series of compressive loads from zero up to the maximum encountered in operation of the belt system. To ensure that friction between the segments and the support was eliminated, the parts were well oiled and the support was lightly tapped before a measurement was taken. Absence of friction was confirmed by continuing the measurements during unloading, the two load-displacement curves being identical.

The support held 47 segments with a total length of 102.6 mm. Figure 3.4 shows the load-strain curve for the segments resulting from the measurements. Not surprisingly, it shows a stiffness increasing with load due to the flattening of the line contact as the load is increased.

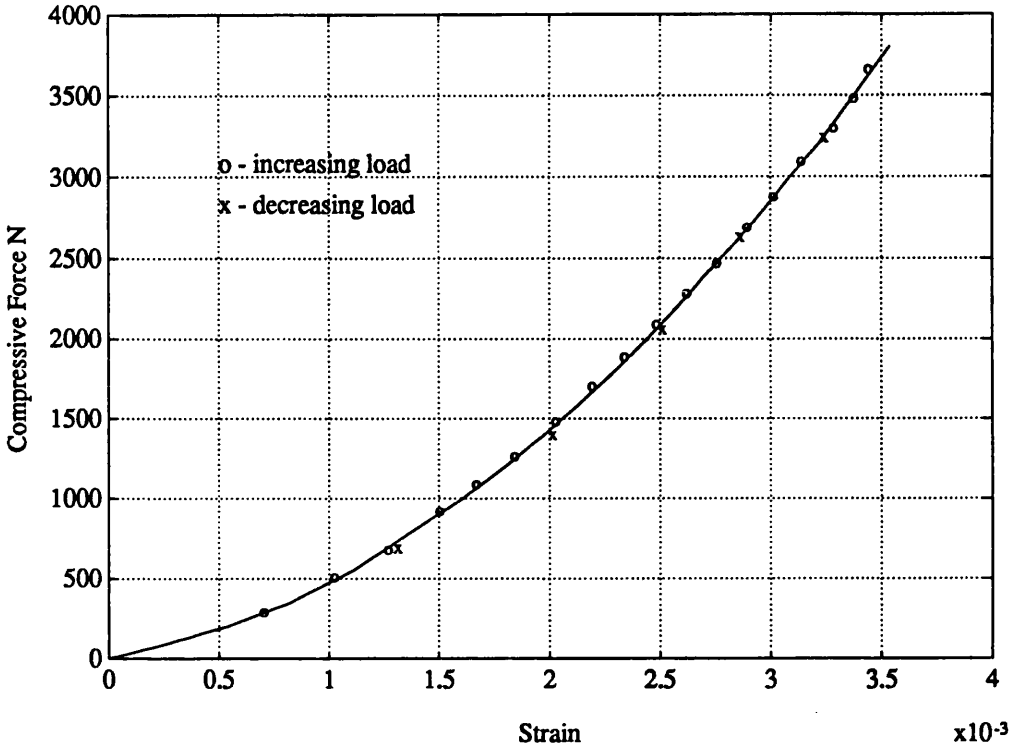

Figure 3.4 Compressive load - strain curve for the belt segments

3.5 Comparison of slip calculated from the simple model with Becker's values

In order to use the simple model together with the measured stiffness to determine whether or not a Coulomb friction model of the shear connection between the segments and the pulleys is able to predict the slips measured during operation of the transmission it is necessary to:

1. show that the slips derived from the simple model using Becker's stiffness are comparable with the slips from his sophisticated model and, if so,
2. to compare the slips calculated from the simple model using the measured stiffness with Becker's measured slips.

Figures 11 and 12 in Becker's paper [3.4] show his measured and calculated values of transmission properties during a full throttle acceleration. Measured and calculated

overall slips are shown together with measured values of transmission ratio and of input torque which can be used to determine the compressive force in the segments entering the secondary pulley. Figure 3.5 shows a copy of Becker's overall slip-time curves. Plotted on it is the overall slip obtained from the simple model using the stiffness determined by Becker, $S = 2.29 \times 10^5$ N. This can be compared with Becker's calculated values and shows that the overall slips determined from the simple model are close to the slips given by his much more complex model.

Having shown that the simple model does predict correct values of slip for a Coulomb friction model it can now be used with the measured values of stiffness for comparison with the measured slips. This second curve is also plotted on figure 3.5. The slips are very much less than the measured slips which shows that a sophisticated Coulomb friction based model like Becker's cannot predict the slips measured during

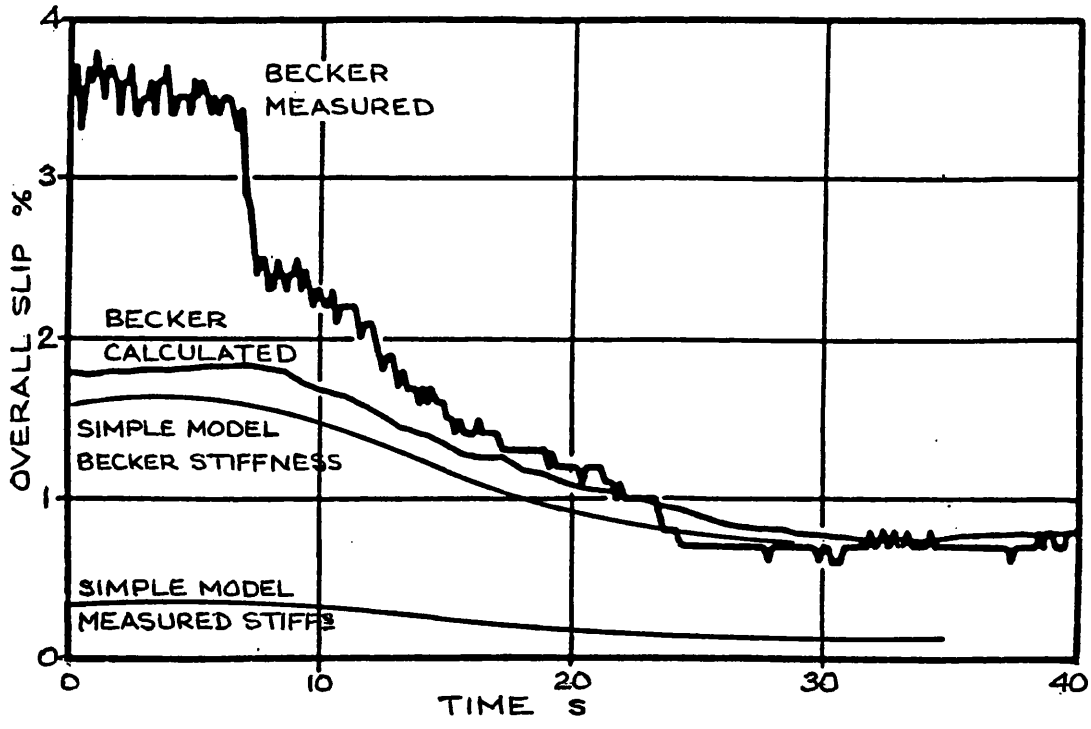

Figure 3.5 Overall slip - time curves from Becker [3.4] with additions

actual operation of the transmission. Some other model for the shear connection is required. A viscous shear model is considered in chapter 4.

3.6 The shear connection between segments and bands

The shoulders on the segments which support the bands are situated a short distance above the line of the rocking edges and consequently the bands normally move relative to the segments, as explained in chapter 2, section 6. This gives rise to a friction force between the two. The authors of the papers considered in this chapter have made the assumption that a Coulomb friction model applies to this connection. The manufacturers of the transmission give details [3.1] of the segments which show that the shoulder carrying the band is curved in side view so that any oil present will be carried into the contact and encounter a wedge shaped passage, see figure 3.6. The underside of the belt is sprayed with oil during operation so that plenty of oil will be available at the contact. Thus a hydrodynamic oil film will be generated and a viscous shear model should be used for this contact.

This connection has an important effect on the overall model. In the introduction to this chapter it was shown that a Coulomb friction model would produce large changes in the tensile force in the bands around the belt. Viscous shear results in only a small force at this contact and the band tension is then close to being uniform.

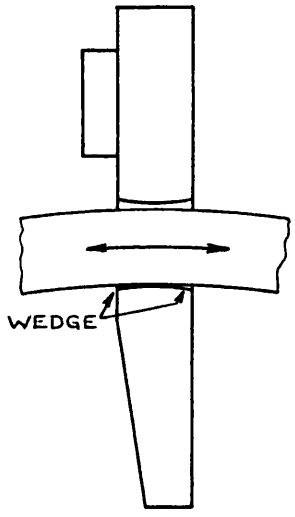

Figure 3.6 Segment - band connection

3.7 Summary of conclusions

1. In section 3.2 previous papers modelling the system were reviewed and the paper by Becker [3.4] was shown to give the definitive model for a Coulomb friction based model.

2. In sections 3.3, 3.4 and 3.5 a simple expression for the overall slip in the transmission which depends on the belt stiffness in compression was developed. It was used to determine slips using the value of stiffness deduced by Becker which were then compared with his calculated slips, good agreement being obtained. An experimental determination of the belt stiffness was described and slips from the simple model using these measured values were compared with the slips measured by Becker. It was shown that a Coulomb friction model for the segment–pulley connection gives overall slip values which are very much less than the slips obtained by measurement and is therefore not appropriate. An alternative viscous model is considered in the next chapter.

3. In section 3.6 the shear connection between the segment shoulder and the moving inner band was considered. It was shown that this, too, should have a viscous model which produces a very different result for the effect on the band tensions. Instead of the large tension changes around the belt which arise from the Coulomb friction model, the band tensions are found to be close to uniform.

CHAPTER 4

Consideration of Viscous Shear Models

4.1 Introduction

In Chapter 3 it was shown that a Coulomb friction model for the shear connection between the belt segments and the pulleys gives very small values for the overall slip compared with the measured values obtained by Becker [4.1] and that a different model is required. In this chapter, a viscous shear model is proposed.

The first model considered was completely empirical, Micklem et al [4.2], and was found to give good agreement with measured slips. Guebeli [4.3] found the model very useful in simulation work to develop a control system for the transmission.

Later an elastohydrodynamic model was used in which established elastohydrodynamic relations determined the oil film thickness and the viscosity was obtained empirically but with reference to published data. An empirical relation for the viscosity was used as data were not available for the oil used and the working temperature was not measured.

Collier and Goldsmith [4.4] carried out a final year project at Bath University to test this model and obtained quite good agreement between their measured results and results from the model.

Viscous shear models are also proposed for the other connections in the system,

between the segment shoulders and the inner band and between the bands.

4.2 Choice of an elastohydrodynamic model

The first viscous model proposed was

shear stress, $\tau = \eta_s . v_{rel} / t_s$

$t_s = k_1 / p_m$

$\eta_s = k_2 + k_3 p_m$

where v_{rel} is the relative speed of one surface to the other, t_s is the oil film thickness and η_s the corresponding viscosity. p_m is the mean pressure in the contact taken as the complete side of the segment. k_1, k_2 and k_3 are empirical constants, k_1 was chosen arbitrarily and k_2 and k_3 were then determined by making calculated and measured results fit [4.2].

Although this model gave useful results it was unsatisfactory as it had no firm basis in lubrication theory. The contact between the flat segment side and the conical pulley surface was taken as the whole area of the segment side whereas it is ideally a line contact in which the pressures would be much higher than the p_m used.

To determine the magnitude of the pressures that are obtained in such a contact, consider the case of the primary pulley working on the minimum radius when the clamping forces on the pulleys are high. Becker [4.1] obtained a measured primary pressure of approximately 13 bar which gives a primary clamping force of 26 kN. On minimum radius the number of segments engaged with the pulley is 34 so that the normal force on the segment side with the 11° wedge half-angle is 26000/34cos11 which equals 779 N. The length of the line contact is 4.6 mm and the width of the Hertzian contact from equation 4.1 is 1.07 mm. The mean pressure in the contact is

then 0.16 GN/m^2. At the other extreme, with low clamping forces and maximum radius, the mean pressure is about 0.04 GN/m^2. These pressures are in the low range of those normally found in elastohydrodynamic lubrication. Thus it was concluded that relations from elastohydrodynamic lubrication should be used when considering this contact.

4.3 The central, Hertzian contact

When the segment is wedged into the pulley, the contact between the flat segment side and the conical pulley surface will be along a line in the radial plane with a non uniform load distribution due to manufacturing discrepancies. Because of the difficulty in dealing with variations in this distribution from segment to segment and pulley to pulley, the load distribution in this analysis is treated as uniform.

The problem of the elastic contact between two non conformable solids was first solved by Hertz, see Johnson [4.5]. For the line contact it can be shown that the pressure distribution in the surface across the contact is close to a semi ellipse. The half width of the contact, a, if the two materials are the same and have a Poisson's ratio equal to 0.3 is given by Cameron [4.6]

$$a = 1.52\left(\frac{W_c R_c}{L_c E}\right)^{1/2} \qquad \textbf{(4.1)}$$

where W_c is the load applied over the contact length L_c and R_c is the reduced radius. As the segment surface is flat, the radius R_c is the radius of the pulley surface at the contact. The end effects are ignored and this width is assumed to apply over the whole length of the contact.

Elastohydrodynamic theory [4.6, 4.7] shows that the presence of the liquid film between the surfaces does not alter the conditions in the surfaces and the pressure in the liquid film is the same semi ellipse with the liquid having a constant thickness h_o apart from a sudden reduction to a minimum thickness h_m near the outlet dictated by conditions of continuity in the flow.

Only the Hertzian contact region needs to be considered when evaluating the shear force. Outside this region the pressures and hence the viscosities are very much smaller and the film thicknesses are greater so that here the contribution to the shear force is negligible when compared with that of the central region.

4.4 The oil film thickness for a line contact

As the segment passes round the pulley, the segment side will be continuously in contact with the pulley surface which will pass over the segment, either forwards or backwards depending on which pulley is being considered. There will be plenty of oil initially present on the pulley surface and on the segment side and this oil will be squeezed as the contact forms. A small amount will pass through the high pressure contact and the remaining oil will build up in front of the contact and act as the oil supply for the continuing contact. Some of this oil will be lost around the ends of the contact but the remainder will be replenished by the small amount of oil coming through the contact ahead and also from the outward flow of oil between the front and rear faces of adjacent segments induced by centrifugal action. This radial flow will be obstructed by the contact of the segments along the rocking edge and diverted sideways into the contact regions. It is considered likely that the centrifugal action will maintain the oil reservoir for the whole of the segment contact with the pulley as there

is an oil spray in the transmission directed at the underside of the belt.

The contacting surfaces, then, can be considered as a stationary surface, the segment side, with a curved continuous surface, the pulley surface, passing over it. The oil film separating them is continuously being formed from the entrainment of oil in the reservoir built up in front of the contact. This contact is similar to that between the loaded discs in a disc machine in the limiting condition when one disc is stationary and the other is turning slowly so that its surface slips over that of the stationary disc. Thus the film thickness in the transmission should be given by the same expression as that between the loaded discs. The film thickness, h_o, on the centre line of the contact between the discs is given by Gohar [4.7]:-

$$\frac{h_o}{R_c} = 1.90\left(\frac{\eta_o U}{ER_c}\right)^{0.69}(E\alpha)^{0.56}\left(\frac{ER_cL_c}{W_c}\right)^{0.10} \qquad (4.2)$$

where U is the rolling speed, the sum of the two surface speeds,

R_c is the reduced radius of curvature of the surfaces,

W_c is the normal load carried by the line contact, length L_c.

Relative to the contact, the surface speed of the stationary disc, or segment side, is zero while the moving disc, or pulley surface, will be moving with the slip speed v_{sl}. Thus $U = v_{sl}$.

At the entrance to a pulley the oil film thickness is likely to be large as:-

(a) the segment and pulley surface are both coming together at their actual running speeds so that here the value of U is large, and

(b) the load on the segment side is reduced because of the delay in wedging the segment into the pulley caused by the time required for the

process (see chapter 7).

It is assumed that this thick film will be rapidly removed by the oil flow through the contact area and the thinner film predicted by the shear model quickly established. The relation, equation 4.2, was used to estimate the oil film thickness, t_s, with the rolling speed U replaced by the slip speed, v_{sl}.

$$\frac{t_s}{R_c} = 1.90\left(\frac{\eta_o v_{sl}}{ER_c}\right)^{0.69}(E\alpha)^{0.56}\left(\frac{ER_cL_c}{W_c}\right)^{0.10} \qquad (4.3)$$

It will be assumed that the thickness, t_s, applies uniformly over the whole Hertzian contact area.

4.5 Radius of curvature of the pulley surface at radius *R*

Figure 4.1 shows the pulley half when the pulley has a wedge angle 2θ. The radius of curvature is required at the contact point A where the belt radius is R.

The equation to the curve produced by the plane AB, perpendicular to a radial line in the pulley surface, cutting the conical surface of the pulley is:-

$$y^2 = \frac{R^2}{\sin^4\theta} - x.\frac{2R\cos^2\theta}{\sin^3\theta} + x^2(\cot^2\theta - 1) \qquad (4.4)$$

where x is measured from the point B and y is the half width of the curve at point C. The curvature at a point on the curve is equal to $-d^2x/dy^2$ at that point and the radius of curvature is 1/curvature.

Differentiating this equation twice and putting $x = R/\sin\theta$ and $y = 0$ gives the radius

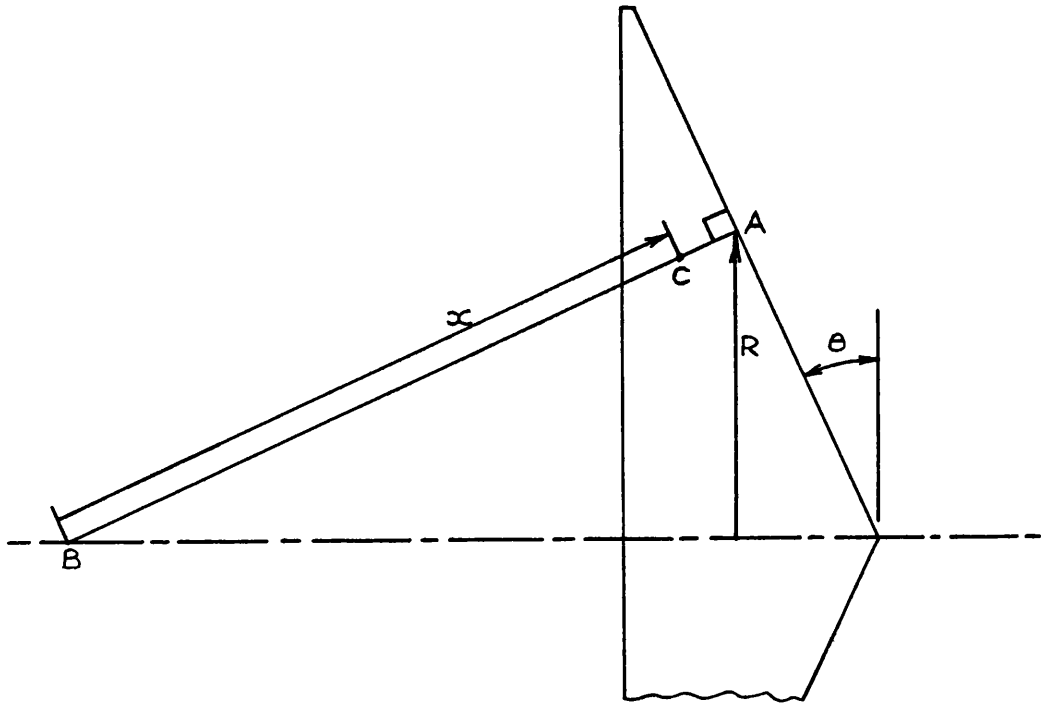

Figure 4.1 Contact point A, radius *R*, on the surface of a pulley half

of curvature at A as:-

$$R_c = \frac{R}{\sin\theta} \qquad (4.5)$$

4.6 Viscosity values for the central contact region

The viscosity values used were determined empirically but with reference to the work of Evans and Johnson [4.8]. In that work a disc machine was used to measure the rheological properties of three lubricants at elastohydrodynamic pressures. A number of constant temperature curves of log(mean viscosity) against mean pressure in the contact are plotted for each lubricant. These curves show that, at the relatively low pressures encountered in the contact in the transmission and provided that the operating temperatures are assumed to be constant, a linear relation between $\log\eta$ and

p_m is a reasonable representation. This relation may be written in the same form as the Barus Law:-

$$\eta_s = \eta_{os} e^{\alpha_s p_m} \qquad (4.6)$$

where η_{os} and α_s are particular constants for a small range only.

As data for the oil used were not available and as the operating temperature inside the transmission was not measured it was not possible to evaluate these constants except in an empirical manner by making the calculations fit the measured results at two operating points. The values obtained were consistent with the results of Evans and Johnson [4.8].

4.7 Asperity contact

The film thicknesses predicted by equation 4.3 are such that for some conditions of operation of the transmission there is probably considerable asperity contact. In spite of this the viscous model usually gives overall slip results which agree well with the measured values. Johnson, Greenwood and Poon [4.9] have shown that, with light asperity contact, the actual mean separation is very nearly equal to the film thickness between smooth surfaces. As the viscous model still gives reasonable results it may be that the majority of the asperities approach each other in such a way as to produce micro ehd films with a relatively low friction force [4.7] rather than giving direct contact with a much greater friction result. There is some support for this in a review paper by Kaneta [4.10]. The asperities in the contact region on the pulley surface are longitudinal, the machining marks on the pulleys being circumferential, while the segment sides tend to be worn smooth. Kaneta shows interferograms of a contact with

longitudinal bumps, each bump with an ehd film, which verifies numerical results obtained by Karami et al [4.11] using longitudinal model asperities.

However, there are some cases where the predicted film thickness is very small and the calculated overall slip is then much less than the measured slip. These would appear to correspond to the cases where the surfaces reach their minimum separation due to asperity contact and were dealt with by specifying a minimum thickness for the film, t_{smin}. This device enabled the viscous friction model to give good results over the whole operating range of the transmission. The minimum thickness was taken to be the calculated film thickness when this effect first appears.

4.8 The viscous model for the segment-pulley contact

The shear force between the segment side and the pulley is determined from the shear stress given by:-

$$\tau_s = \eta_s \frac{v_{sl}}{t_s} \qquad (4.7)$$

applied uniformly over the area of the Hertzian contact, $2aL_c$.

The width of the contact, $2a$, is determined from equation 4.1, the film thickness, t_s, from equation 4.3, subject to a minimum value of t_{smin}, and the viscosity, η_s, from equation 4.6. The radius of curvature, R_c, of the pulley surface is obtained by using equation 4.5. The mean pressure, p_m, = $W_s/2aL_c$

4.9 Comparison of values from the viscous model with measured results

Two students, Collier and Goldsmith [4.4], carried out a final year research project to

test this viscous model. They supported a single, stationary segment in a slowly rotating pulley and measured the capacitance between the segment and the pulley. From this a value was obtained which, for a uniform film over a constant area, would be proportional to the oil film thickness. They also measured the drag force on the segment. This was done for a series of radial loads on the segment, a series of pulley speeds and a series of radii covering the whole operating range of the transmission. Their apparent film thickness measurements showed that, for a given slip speed, the relative film thickness decreased as the load on the segment increased and normally dropped to a small residual value at the higher loads. The higher slip speeds showed bigger initial thickness. A typical result from their report is shown in figure 4.2, the apparent relative film thicknesses for a radius of 75 mm.

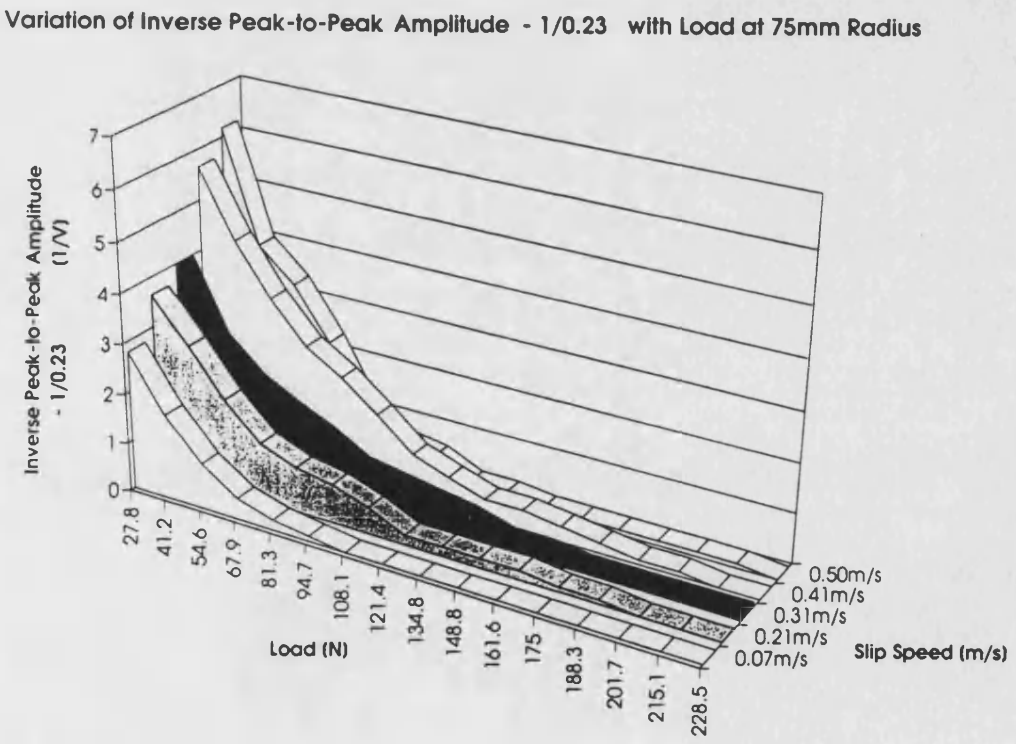

Figure 4.2 Variation of relative film thickness between segment and pulley surface with load and slip speed. From Collier and Goldsmith [4.4]

The small residual value appears to correspond to the minimum thickness, t_{smin}, used in the model. The measured thicknesses are all relative and were compared with the corresponding calculated results by scaling the values. The same factor was used for all the results and was determined by making the measured and calculated values agree at one point. The minimum film thickness was chosen to give the best fit between the shapes of the measured and calculated curves, the value determined being $t_{smin} = 118 \times 10^{-9}$ m. The results are shown in figures 4.3, 4.4, 4.5 and 4.6 for radii of 39.3, 50.0, 60.0 and 71.3 mm respectively. In many cases the measured and calculated curves have the same form which supports the use of the viscous model.

The measured drag forces together with the corresponding calculated values are shown similarly in figures 4.7, 4.8, 4.9 and 4.10. By comparing the film thickness and the drag force curves for the same radius, e.g. figures 4.5 and 4.9 for a radius of 60.0 mm, it can be seen that where the calculated film thickness is greater than the minimum, t_{smin}, there is excellent agreement between the measured and calculated drag force curves. Use of the value of t_{smin} given, usually at the lower slip speeds, results in the calculated shear force being much less than the measured force. Reducing the value of t_{smin} gives better agreement on the drag force results but worse on the shape of the film thickness curves. The value of t_{smin} used is small when compared with the likely RMS value for the surface roughness but may be appropriate when the asperities are compressed in the contact.

4.10 Consideration of an extension to the model to allow for asperity contact

A more complicated model can be devised to allow for the effect of the asperity contact in the cases where the calculated value of the film thickness is less than the

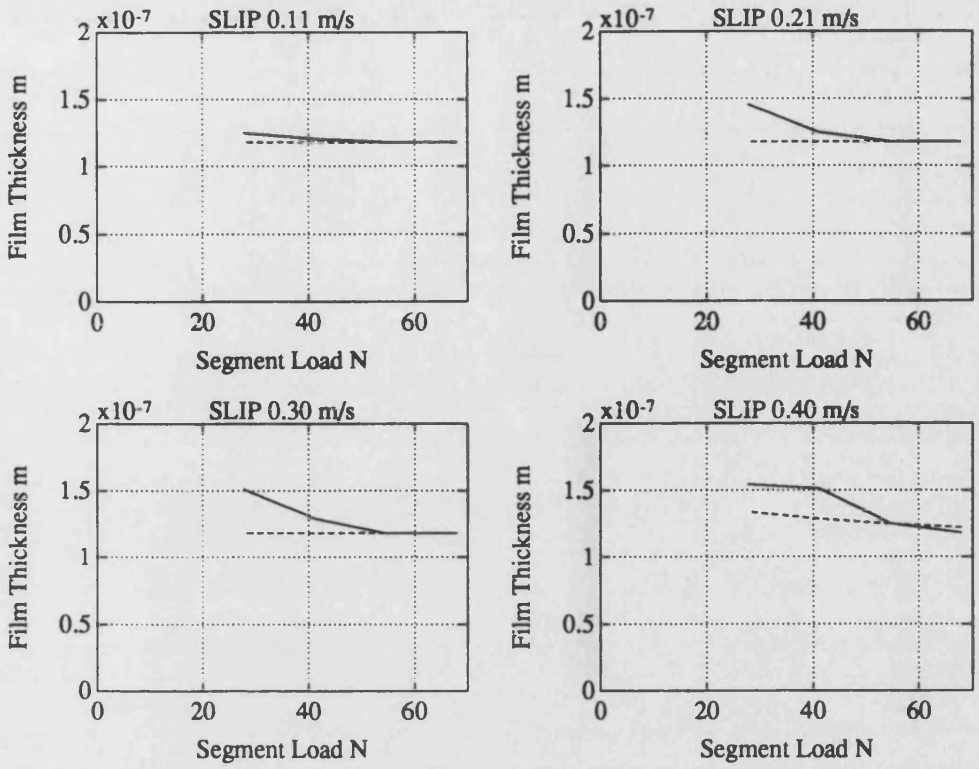

Figure 4.3 Measured (—) and calculated (---) film thickness - 39.3 mm radius

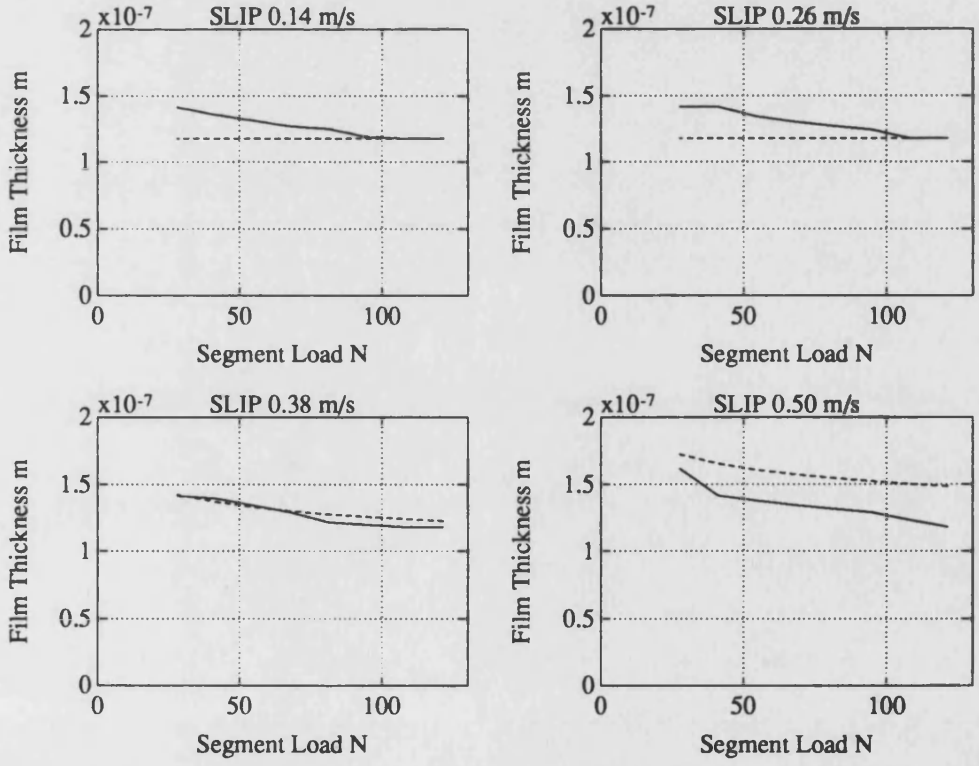

Figure 4.4 Measured (—) and calculated (---) film thickness - 50.0 mm radius

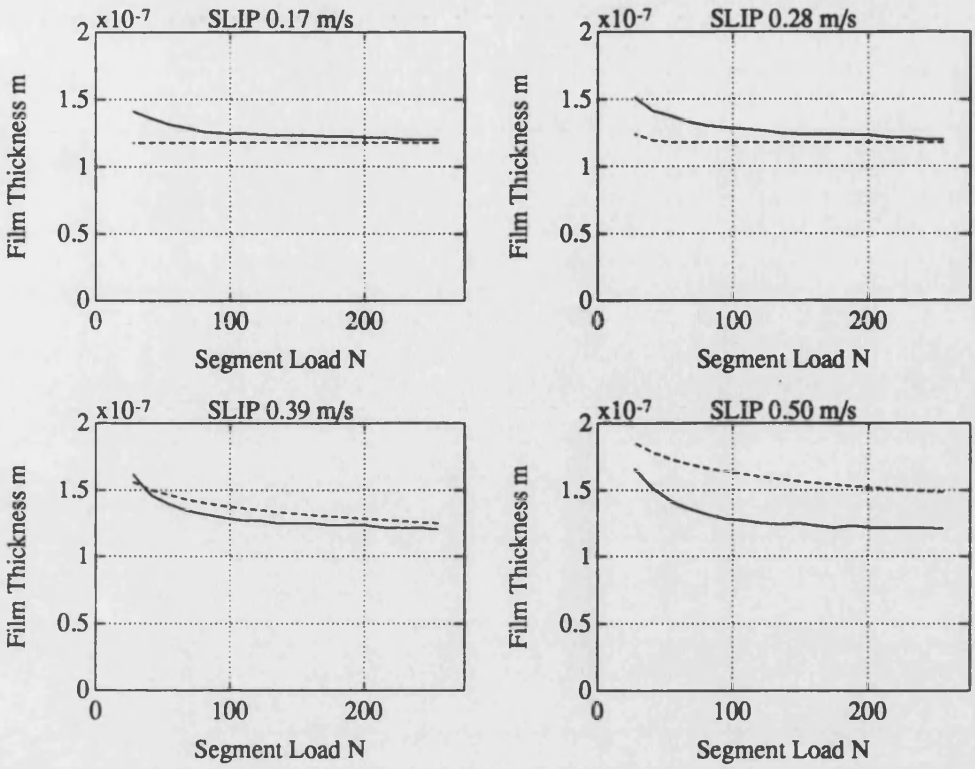

Figure 4.5 Measured (—) and calculated (---) film thickness - 60.0 mm radius

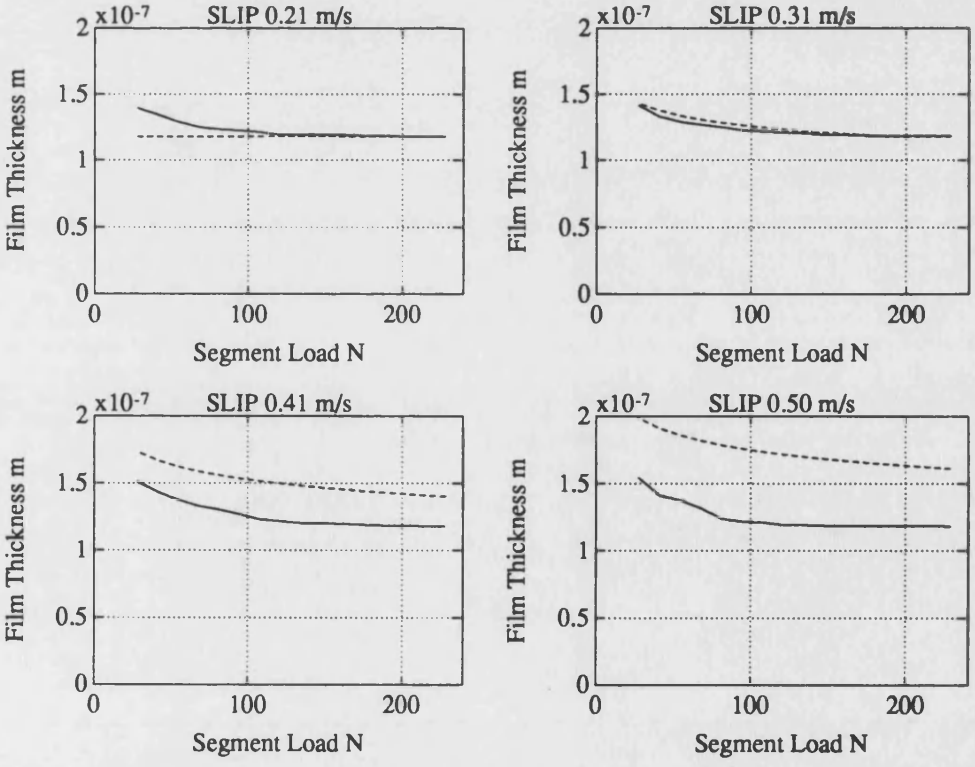

Figure 4.6 Measured (—) and calculated (---) film thickness - 71.3 mm radius

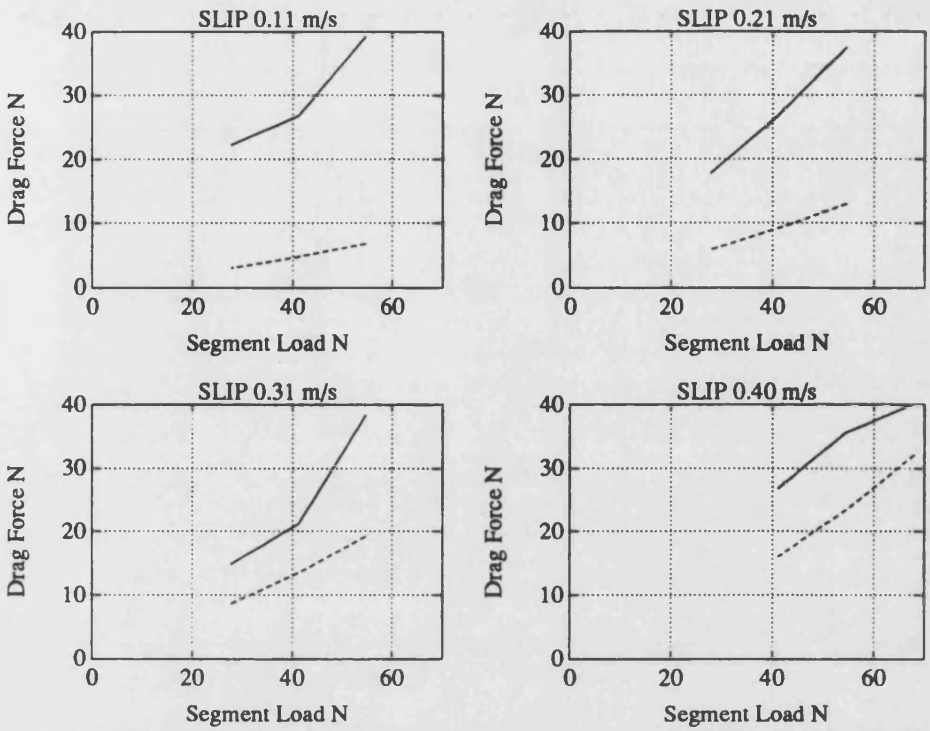

Figure 4.7 Measured (—) and calculated (---) drag force on segment - 39.3 mm radius

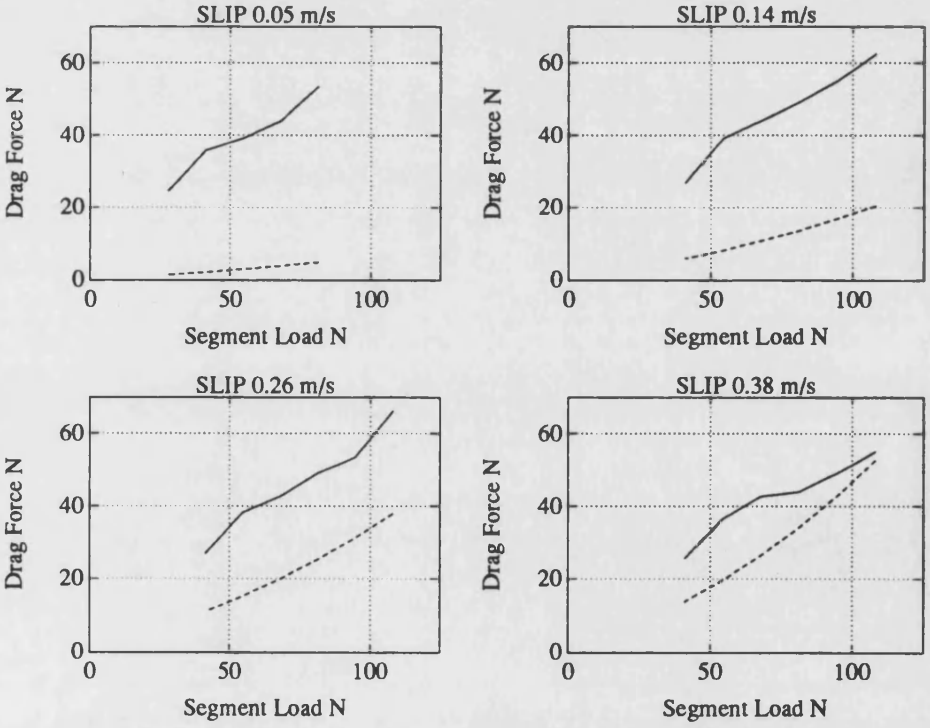

Figure 4.8 Measured (—) and calculated (---) drag force on segment - 50.0 mm radius

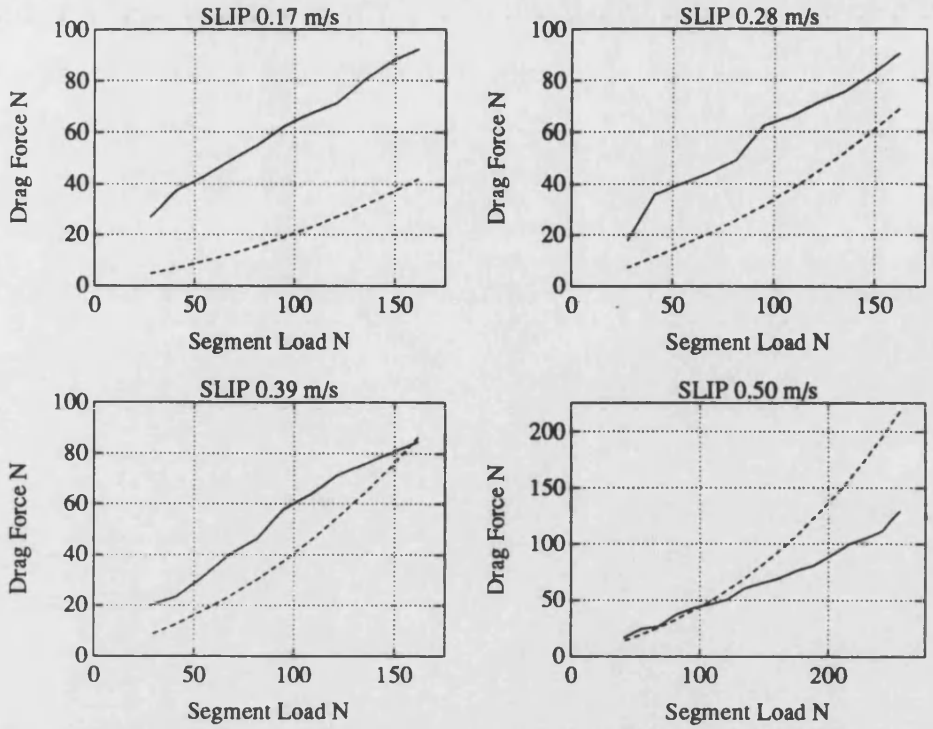

Figure 4.9 Measured (—) and calculated (---) drag force on segment - 60.0 mm radius

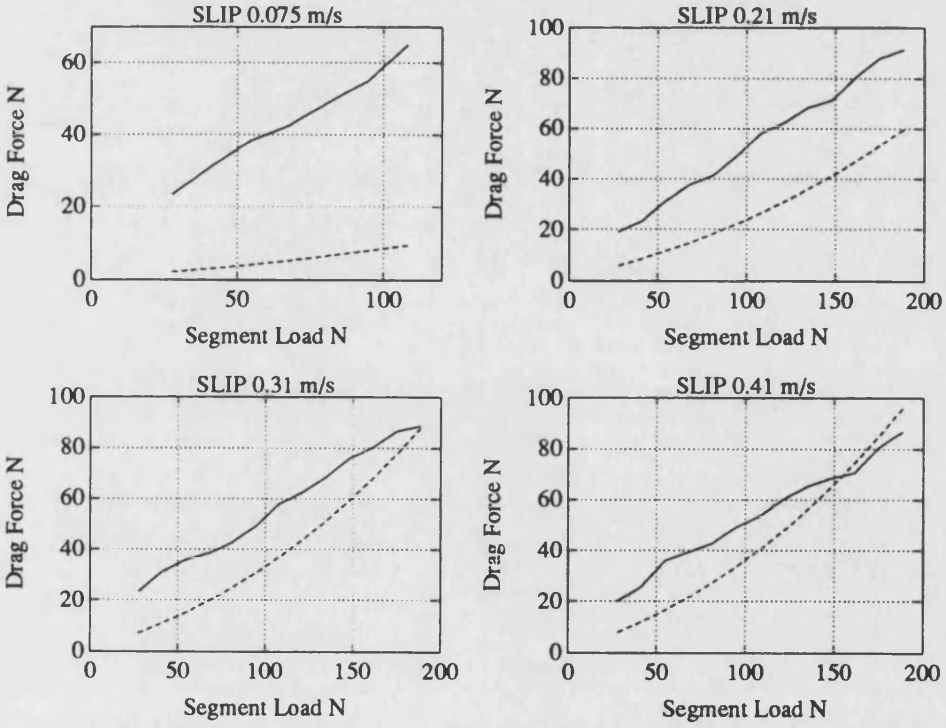

Figure 4.10 Measured (—) and calculated (---) drag force on segment - 71.3 mm radius

minimum value, t_{smin}.

In these cases assume that the normal load between the segment side and the pulley surface is carried partly by the pressure in the oil film and the remainder by the direct contact of the asperities. Only the mean pressure in the Hertzian contact will be used in determining the loads, the pressures in the oil film outside this region being relatively very small.

The load carried by the oil pressure in the film can be determined from the film thickness expression, equation 4.3, by putting t_s equal to t_{smin}. Then the shear force due to viscous shear can be determined from the simple viscous model using this load. The remainder of the total load is carried by the asperities and the shear force arising from this direct contact is assumed to be given by the simple friction expression, μ x asperity load. Note that this does not imply a reversion to a Coulomb friction model. The expression is an approximation to enable the shear force arising from asperity contact when there is a slip speed to be determined. This shear force may be due to direct metal to metal contact of the asperities or to the formation of micro ehd films on the asperities. The amount of slip will be controlled by the viscous part of the connection.

This model was tested by applying it to the drag results for 50.0 mm radius. It can be seen in figure 4.4 that the film thickness with the lower slip speeds is equal to t_{smin} while the higher speeds generate thicker films. This is reflected in the drag force results shown in figure 4.8 where there is considerable discrepancy between measured and calculated values at the lower slip speeds. The revised drag values are shown in figure 4.11 where it can be seen that this more complicated model does give much better results. The coefficient of friction, μ, used was 0.13, a value that is very

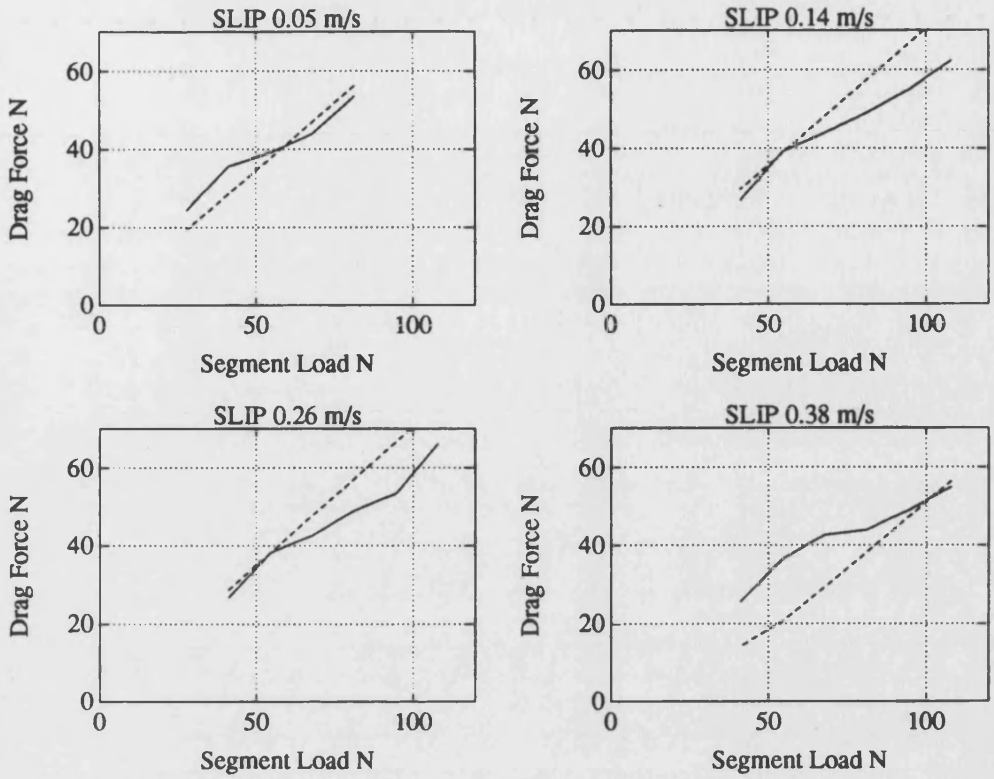

Figure 4.11 Measured (—) and calculated (---) drag force on segment using the model that includes the effect of asperity contact - 50.0 mm radius

reasonable.

However, the simple model does give good results for the complete transmission, as will be shown later, and it is not considered that use of the more complicated model would be an advantage. Why the simple model should give good results is not immediately apparent if graphs such as those in figure 4.10 are considered where considerable discrepancy is shown between values calculated from the model and the measured values. The reason is that both the measured and the calculated slip speeds in the transmission are usually greater than 0.25 m/s and often considerably greater so that the transmission operates under conditions where the discrepancy is normally small. It is only with the very small torque transfers that the discrepancies appear.

4.11 The shear connections between the segment shoulders and the inner band and between neighbouring bands

1. Between the segments and the inner band

As explained in section 3.6, a viscous shear relation is appropriate for this connection as a hydrodynamic oil film will be generated by the relative motion of the band over the segment shoulders.

The pressure in this oil film is small. The maximum value of the total band tension is approximately 4000 N and, when the belt is passing round a pulley at the minimum radius, this tension produces a mean pressure in the film of about 10 MN/m^2. Hence the basic viscosity, η_o, can be used to determine any shear stress.

As this shear force is small, a uniform film thickness, t_{f1}, is assumed in order to evaluate the force. A more elaborate calculation would complicate the transmission model unnecessarily.

2. Between neighbouring bands

The surface of the bands has a 'herring bone' pattern etched in the surface which will maintain an oil film between the bands because of their relative motion. Once again the pressures are low and a uniform film thickness, t_f, is assumed, the same value applying to all the bands.

4.12 Summary of the viscous shear models at the contacts

Figure 4.12 is a side view of a segment with the pack of ten bands in place. The locations are shown of the three contacts where there is relative motion between adjacent parts. The viscous models assumed for the contacts are summarised.

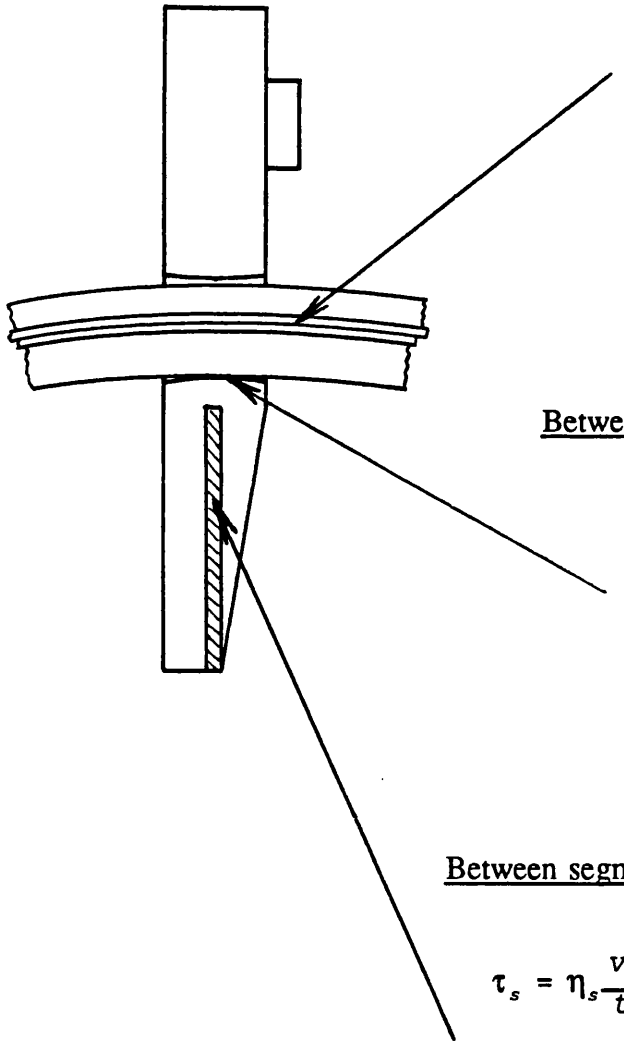

Between adjacent bands

$$\tau = \eta_o \frac{v_{surf.n} - v_{surf.n-1}}{t_f}$$

where t_f is uniform

and $v_{surf.}$ is the speed of the surface at the contact

Between inner band and segment shoulder

$$\tau = \eta_o \frac{v_{surf.1} - v_{surf.s}}{t_{f1}}$$

where t_{fl} is uniform

Between segment side and pulley surface

$$\tau_s = \eta_s \frac{v_{s1}}{t_s}$$

Determined as detailed in section 4.8

Figure 4.12 Summary of the viscous shear models

CHAPTER 5

The System Model

5.1 Introduction

In this chapter the transmission is analysed and a system model presented. The viscous shear relations developed in chapter 4 are used in the analysis.

The inherent losses in the system are identified and it is shown how these can be minimised in order to obtain the most efficient operation of the system.

5.2 Assumptions made in the analysis of the transmission

1. The segments move in a circular path when engaged with a pulley as the radial stiffness is large.

   The radial positions of the segments around the pulleys were measured by Kim and Lee [5.1] and their results justify this assumption.

2. All inertia forces are negligible except for those dealing with the centripetal acceleration of the belt components when rounding a pulley.

   The angular accelerations of the pulleys and the linear acceleration of the belt are all limited by the large inertia of the vehicle.

3. Whenever there is relative motion between neighbouring components a viscous

shear stress exists in the oil film at the interface given by:

$$\tau = \eta \frac{v_{rel}}{t_c}$$

The viscosity and film thickness for the contact between the segment sides and the pulley surfaces will be obtained as described in chapter 4, section 8. The values for the contacts between adjacent bands and between the inner band and the segments are described in chapter 4, section 11.

4. Cases involving a ratio change are dealt with by superimposing a radial velocity on the belt as it rounds a pulley.
5. Changes in relative speed between components due to increasing or decreasing deformations as the segments round the pulleys and the compressive load is altered will be neglected. The effect is small.
6. When the band packs are assembled the ten bands fit closely together without any initial tensions or compressions.

5.3 Division of the belt into regions

It is convenient to divide the belt into four different regions, the section on the primary pulley, the two straight sections and the section on the secondary pulley. Figure 5.1 shows the belt divided into these four regions by the four stations shown.

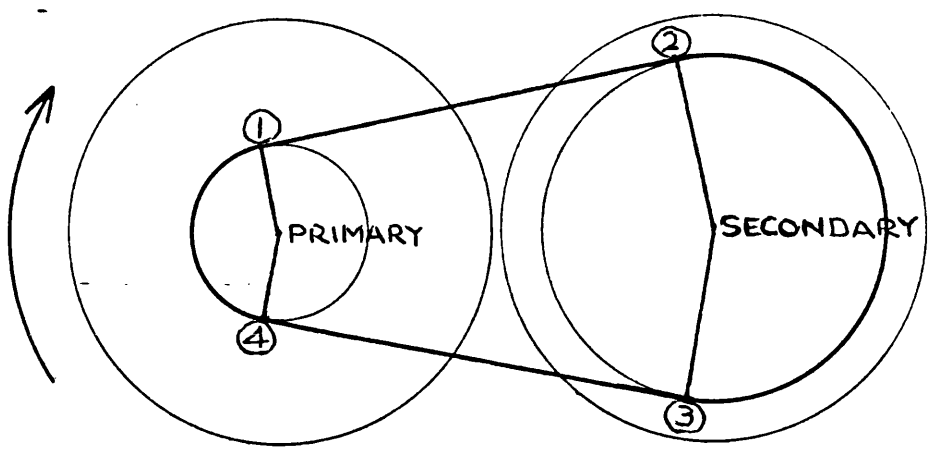

Figure 5.1 The four stations on the belt

5.4 The belt geometry

The effective line of action of the belt is through the rocking edges (see figure 5.5) on the segments. The operating part of the belt is continuous along this line and this gives meaning to a belt speed. There is a small total gap between the segments after assembly of the belt as the segments are not tightly pressed together. As is explained in chapter 8, during normal running this total gap is distributed between segments moving from the secondary pulley between stations 3 and 4. This gap and the additional effect of the lengthening of the bands under tension are neglected in the belt geometry as they are small.

The diagram, figure 5.2, shows the belt as a line along the rocking edges passing around the two pulleys. The belt length can be expressed in terms of the quantities shown and equated to the actual length to give an equation relating the two radii.

The equation assumes that, as the segments are thin, the line joining the rocking edges around a pulley approximates to the arc of a circle.

$$L = R_p\beta_p + R_s\beta_s + 2\sqrt{X^2 - (R_s - R_p)^2} \tag{5.1}$$

where

$$\beta_p = \pi - 2\alpha \qquad \beta_s = \pi + 2\alpha \tag{5.2}$$

and

$$\sin\alpha = \frac{R_s - R_p}{X} \tag{5.3}$$

The radial velocity of a segment on a pulley, $v_R = dR/dt$

The relationship between the two radial velocities can be determined by differentiating the above relations with respect to time. After manipulation,

$$v_{Rs} = -v_{Rp}\frac{\beta_p}{\beta_s} \tag{5.4}$$

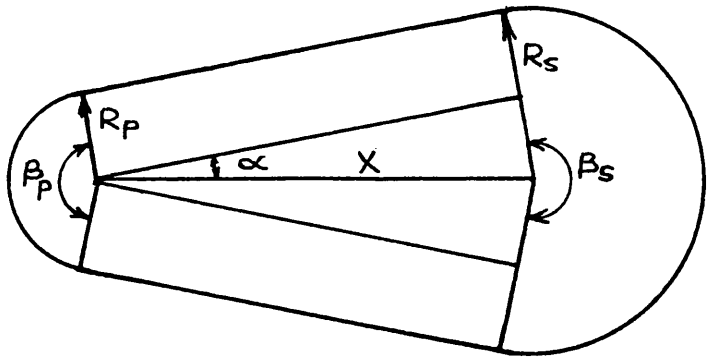

Figure 5.2 The belt geometry

5.5. Speeds of the bands relative to the speed of the segments

From assumption 2, any acceleration of a band in a direction along its length is negligible so that the resultant force on the band in this direction must be zero. This resultant force is made up from the shear stresses arising from the shearing of the oil films separating the bands. Figure 5.3 shows the shear stresses applied to band 10, the outer band.

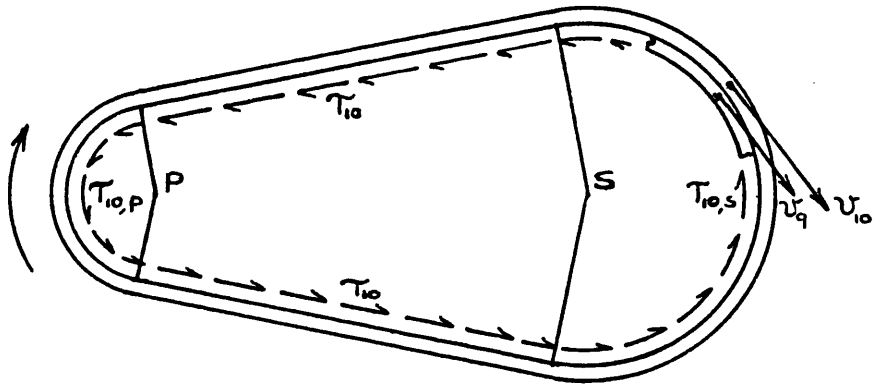

Figure 5.3 The shear stresses acting on band 10

It shows a general case that assumes band 10 is moving ahead of band 9 everywhere. Writing down the equation stating that the resultant shear force is zero produces an expression that gives the ratio v_{10}/v_9.

The remaining bands have shear stresses applied to both surfaces. However, for band 9 the force on the outer surface has already been shown to be zero when considering band 10 so that only the shear force on the inner surface needs to be equated to zero and so on for all the other bands down to band 2.

The following relation giving the ratio of speeds v_n/v_{n-1}, where n has values from 2 to 10, can be derived noting the following points:

1. The shear force on a region of the band is equal to

$$\eta_o \frac{v_{rel}}{t_f}.area$$

2. From assumption 3, t_f is uniform for a band.

3. Around a pulley, v_{rel} = speed of inner surface of band n

- speed of outer surface of band $(n - 1)$.

Hence $$v_{rel} = v_n \frac{R + x + (n - 1)t_b}{R + x + (n - 0.5)t_b} - v_{n-1} \frac{R + x + (n - 1)t_b}{R + x + (n - 1.5)t_b}$$

and the surface area involved is $(R + x + (n - 1)t_b)\beta w$

4. On the straight parts of the belt, $v_{rel} = v_n - v_{n-1}$

and the area = $(L - R_p\beta_p - R_s\beta_s)w/2$

$$\frac{v_n}{v_{n-1}} = \frac{\frac{(R_p+x+(n-1)t_b)^2\beta_p}{R_p+x+(n-1.5)t_b}+(L-R_p\beta_p-R_s\beta_s)+\frac{R_s+x+(n-1)t_b)^2\beta_s}{R_s+x+(n-1.5)t_b}}{\frac{R_p+x+(n-1)t_b)^2\beta_p}{R_p+x+(n-0.5)t_b}+(L-R_p\beta_p-R_s\beta_s)+\frac{(R_s+x+(n-1)t_b)^2\beta_s}{R_s+x+(n-0.5)t_b}} \qquad (5.5)$$

The speed of band 1 relative to that of the segments is found similarly except that, when rounding a pulley, the surface area between band 1 and the segments is affected by the opening up of the segments and equals $R\beta w$.

$$\frac{v_1}{v_s} = \frac{L+2\pi x}{\frac{R_p\beta_p(R_p+x)}{R_p+x+0.5t_b}+(L-R_p\beta_p-R_s\beta_s)+\frac{R_s\beta_s(R_s+x)}{R_s+x+0.5t_b}} \qquad (5.6)$$

5.6 The forces on a segment engaged with a pulley

A Free Body Diagram for a segment engaged with the primary pulley under driving conditions is shown in figure 5.4. Because of the viscous shear in the oil film between the belt and the pulley surface, there is a slip speed in the direction of rotation with the segment trailing behind the pulley surface together with a velocity radially outwards due to a ratio change. A similar diagram will apply to the secondary pulley but with W in the opposite direction as the segment is now sliding forward over the pulley surface.

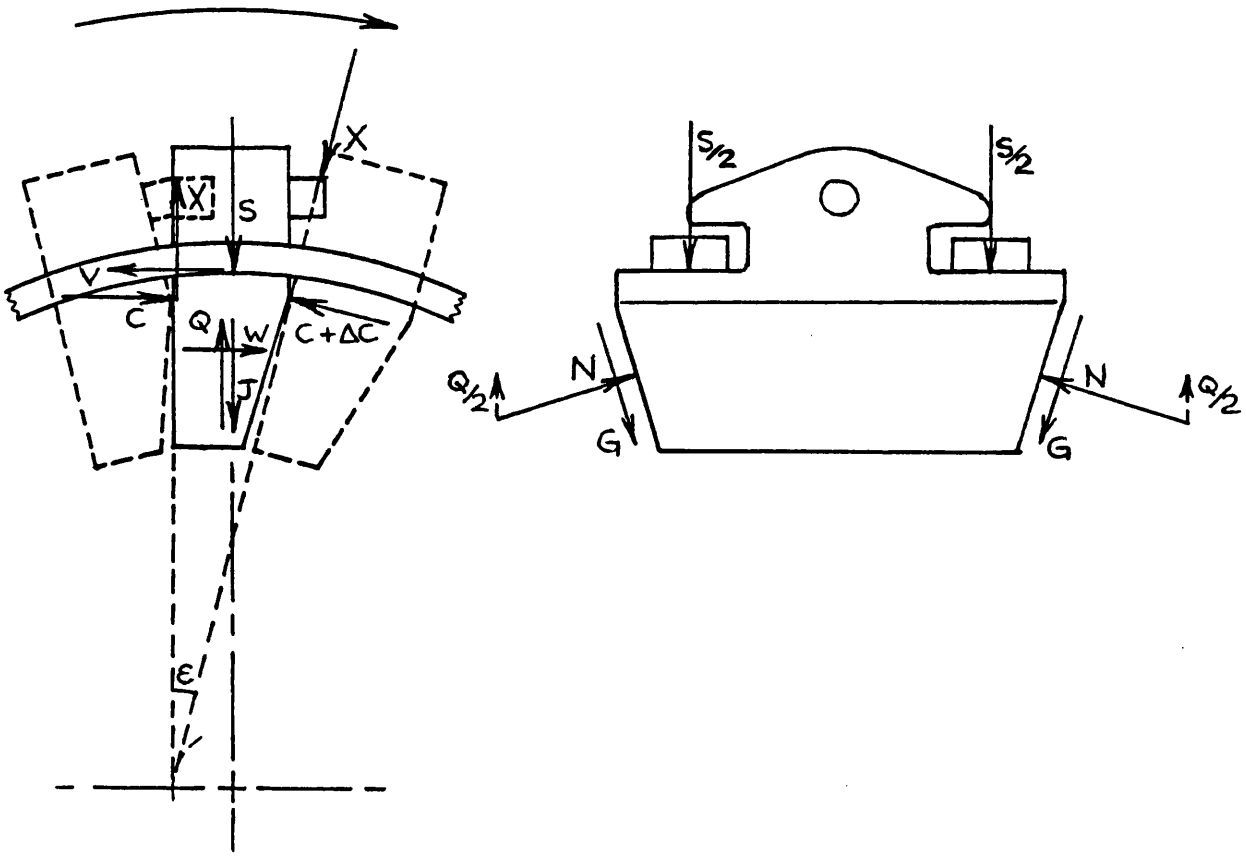

Figure 5.4 Free body diagram for a segment engaged with the primary pulley

The forces shown are:-

$-N$	The normal force between pulley and segment
Q	the radial component of the two forces N.
W	the tangential component of the shear force produced by the relative motion of the segment over the pulley surfaces, $W/2$ each side.
C	the compressive force between segments.
V	the tangential force between the inner band and the segment due to their relative motion
S	the force applied by the bands to the segment due to the band tension.
G	the component in the radial plane and parallel to the pulley surface of the shear force produced by the relative motion of the segment over the the pulley
J	the radial component of the two forces G.
X	the forces in the 'peg and hole' connections between the segments required to balance the moments on the segment.

As the acceleration in the tangential direction is negligible, assumption 2, the resultant force in that direction is zero:

$$W + C - (C + \Delta C)\cos\varepsilon - V - X\sin\varepsilon = 0$$

Take moments about an axis parallel to the pulley axis and passing through a point on the centre line of the segment and level with the rocking edge. It may reasonably be assumed that the lines of action of the forces Q, S, J and the inertia force from the mass of the segment rounding the curve lie close enough to this point for the moments

to be neglected. The line of action of W is $\bar{y}$ below this point.

$$W\bar{y} + Vx + (C + \Delta C)\sin\varepsilon\frac{s}{2} - X\frac{s}{2} - X\cos\varepsilon\frac{s}{2} = 0$$

ε is small and equals s/R

Combining these three equations gives:

$$\Delta C = W(1 - \frac{\bar{y}}{R}) - V(1 + \frac{x}{R}) \qquad (5.7)$$

The surface of the segment in contact with the pulley is assumed to be a Hertzian line contact, as explained in chapter 4. This is a rectangle, width $2a$, which starts at the level of the rocking edge and lies in the radial direction as shown in figure 5.5.

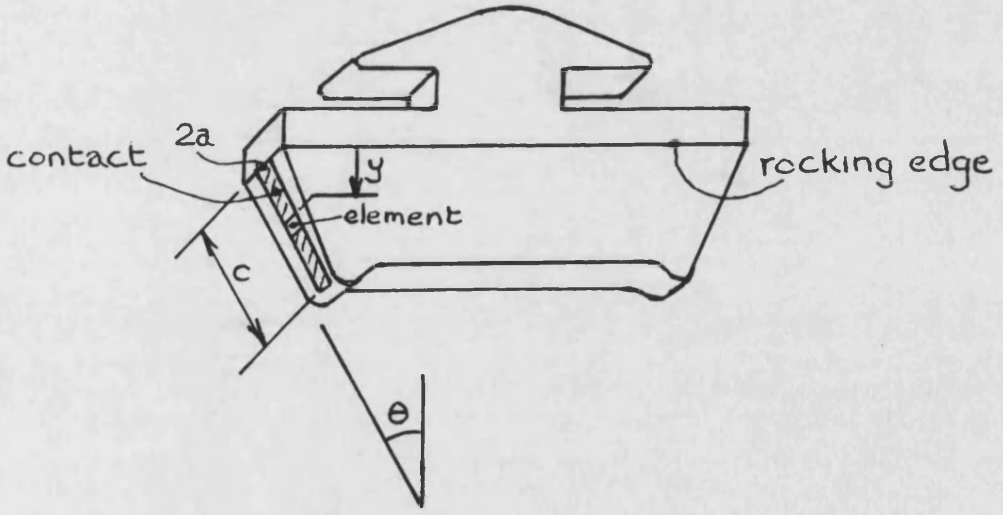

Figure 5.5 The contact between segment and pulley

At the element shown:

- the speed of the segment = $v_s(R - y)/R$

  the speed of the pulley surface = $n(R - y)$

  the shear stress in the oil film

$$= \frac{\eta_s}{t_s}\left(n(R - y) - \frac{v_s(R - y)}{R}\right)$$

acting over the area $2a.dy/\cos\theta$

Writing down the resulting force and integrating over both edges of the segment gives:

$$W = 2\frac{\eta_s}{t_s}(n - \frac{v_s}{R})(2Rc - c^2\cos\theta)a \qquad \textbf{(5.8)}$$

Multiplying the force on the element by the operating radius $(R - y)$ and integrating gives the pulley torque contributed by the segment.

$$T_{seg} = 4\frac{\eta_s}{t_s}(n - \frac{v_s}{R})(R^2c - Rc^2\cos\theta + \frac{c^3\cos^2\theta}{3})a$$

The distance of the line of action of W below the rocking edge, $\bar{y}$, as

$T_{seg} = W(R - \bar{y})$ is given by:-

$$\bar{y} = R - \frac{2(R^2c - Rc^2\cos\theta + \frac{c^3\cos^2\theta}{3})}{2Rc - c^2\cos\theta} \qquad \textbf{(5.9)}$$

The mean slip speed between the segments and the pulley at the radius of the line of action of W, v_{sl}, is given by

$$v_{sl} = (n - \frac{v_s}{R})(R - \bar{y}) \qquad (5.10)$$

To evaluate the force V:

the speed of the segment at the shoulder = $v_s(R + x)/R$

the speed of the inner surface of band 1

$$= v_1 \frac{R + x}{R + x + 0.5t_b}$$

and the stress is applied over an area equal to ws

Hence

$$V = \frac{\eta_o ws}{t_{fl}} \left(\frac{v_s}{R} - \frac{v_1}{R + x + 0.5t_b} \right) (R + x) \qquad (5.11)$$

The force G arises from the radial velocity of the segment over the pulley surface. The segments and the pulley surface are separated by an oil film generated by the tangential slip speed and the addition of v_R will have little effect on the film thickness. The values of viscosity and film thickness used to determine G will be the same as the values determined for the tangential motion.

The radial component of the shear stress in the plane of the segment side

$$= \eta_s \frac{v_R/\cos\theta}{t_s}$$

which acts on an area $2ac$.

Therefore:

$$G = \frac{\eta_s v_R 2ac}{t_s \cos\theta} \qquad (5.12)$$

5.7. Overall relationships for a pulley and a section of belt engaged with it

Figure 5.6 shows Free body diagrams for an element of the belt engaged with a pulley and for the pulley halves. The segments are treated as continuous with the two bandpacks combined into one for simplicity. The force in the n^{th} band is shown, the others are similar. The number of segments in the element is $R.\delta\gamma/s$.

The radial equation of motion for the belt element is:

$$\sum_{n=1}^{n=10} T_n \delta\gamma - C\delta\gamma - 2\delta N\sin\theta + 2\delta G\cos\theta = \frac{m_s v_s^2}{s}\delta\gamma + \sum_{n=1}^{n=10} m v_n^2 \delta\gamma$$

The axial equation for a pulley half is:

$$\delta F - \delta N\cos\theta - \delta G\sin\theta = 0$$

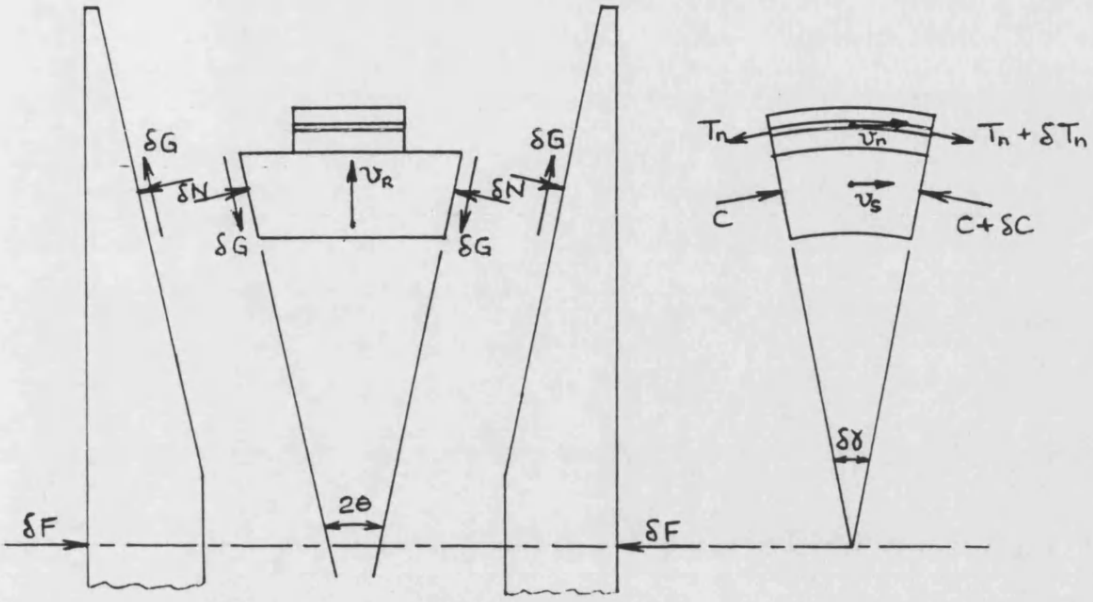

Figure 5.6 An element of belt engaged with a pulley

δG = G x the number of segments in the element,

where G can be obtained from equation 5.12. Then:

$$\delta G = \frac{\eta_s v_R 2ac}{T_s \cos\theta} \cdot \frac{R\delta\gamma}{s}$$

The angle subtended at the axis by a segment is small so that these equations can be applied to a segment.

Then $\delta\gamma = s/R$

Combining these equations and eliminating N and G results in:

$$\Delta F_{seg} = \frac{s}{2R\tan\theta}\left(\sum_{n=1}^{n=10} T_n - C + \frac{\eta_s v_R 4acR}{st_s\cos^2\theta} - \frac{m_s v_s^2}{s} - \sum_{n=1}^{n=10} mv_n^2\right) \qquad (5.13)$$

In determining the conditions in the oil film between the segment side and the pulley surface it is necessary to know the value of the normal load/segment side, W_c.

$$W_c = \frac{\delta N}{\frac{R\delta\gamma}{s}} = \frac{s}{R}\frac{\delta N}{\delta\gamma}$$

Using the equations above results in:

$$W_c = \frac{s}{2R\sin\theta}\left(\sum_{n=1}^{n=10} T_n - C - \frac{m_s v_s^2}{s} - \sum_{n=1}^{n=10} mv_n^2\right) + \frac{2a\eta_s v_R}{t_s\sin\theta} \qquad (5.14)$$

and the mean pressure in the Hertzian contact area is:

$$p_m = \frac{W_c}{2ac} \qquad (5.15)$$

5.8 Relationships between the band tensions

Figure 5.7 shows the centre lines of bands n and (n-1).

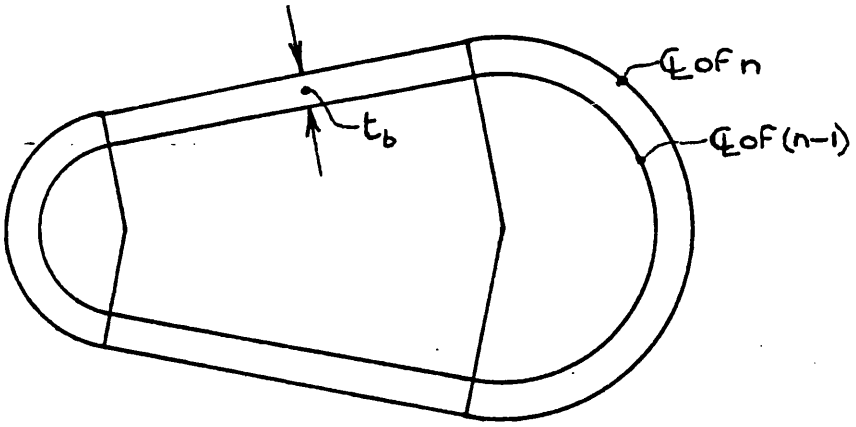

Figure 5.7 The centre lines of bands n and (n - 1)

As the bands must fit closely together at all times, band n must always be $2\pi t_b$ longer than (n-1) and, when loaded, the extensions of the two must be equal. As the extensions of all bands under load must then be equal, by equating the extension of band n to the extension of band 1 the tension in band n can be put in terms of the tension in band 1.

Each of bands 2 to 9 has a pair of adjacent bands moving with virtually equal and opposite relative speeds. From assumption 2, the shear stresses on each side of these bands will then be equal and opposite and the band tension will be uniform. Only bands 1 and 10 experience any changes in tension.

The changes in tension between stations for band 10

The shear stresses acting on band 10 are shown in figure 5.3. The change in band

tension between two adjacent stations is equal to the shear force arising from these shear stresses, the force being determined as explained in section 5.5.

$$\Delta T_{10,1-2} = \Delta T_{10,3-4} = \eta_o \cdot \frac{v_{10}-v_9}{t_f} \cdot \frac{w(L-R_s\beta_s-R_p\beta_p)}{2} \qquad (5.16)$$

$$\Delta T_{10,2-3} = -\frac{\eta_o}{t_f}\left(v_9\frac{R_s+x+9t_b}{R_s+x+8.5t_b} - v_{10}\cdot\frac{R_s+x+9t_b}{R_s+x+9.5t_b}\right)w(R_s+x+9t_b)\beta_s \qquad (5.17)$$

$$\Delta T_{10,4-1} = -2\Delta T_{10,1-2} - \Delta T_{10,2-3} \qquad (5.18)$$

The changes in tension between stations for band 1

Figure 5.8 shows the shear stresses acting on band 1. The changes in tension may be determined in the same way as for band 10:

$$\Delta T_{1,1-2} = \Delta T_{1,3-4} = \eta_o\left(\frac{v_1-v_s}{t_{fl}} - \frac{v_2-v_1}{t_f}\right)\frac{w(L-R_s\beta_s-R_p\beta_p)}{2} \qquad (5.19)$$

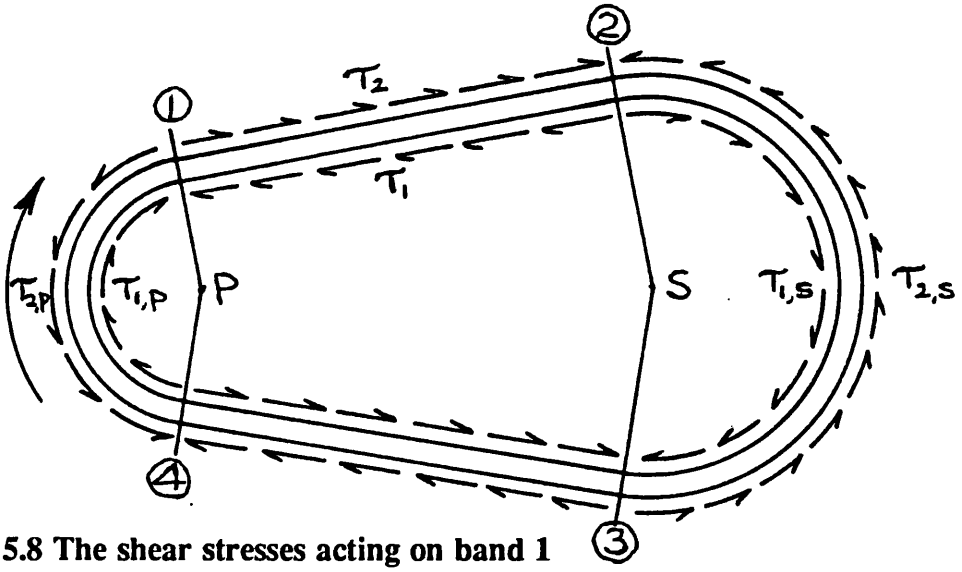

Figure 5.8 The shear stresses acting on band 1

$$\Delta T_{1,2\text{-}3}=\frac{\eta_o}{t_f}\left(v_1\cdot\frac{R_s+x+t_b}{R_s+x+0.5t_b}-v_2\cdot\frac{R_s+x+t_b}{R_s+x+1.5t_b}\right)w(R_s+x+t_b)\beta_s$$

$$-\frac{\eta_o}{t_{fl}}\left(v_s\cdot\frac{R_s+x}{R_s}-v_1\cdot\frac{R_s+x}{R_s+x+0.5t_b}\right)wR_s\beta_s \qquad \textbf{(5.20)}$$

$$\Delta T_{1,4\text{-}1}=-2\Delta T_{1,1\text{-}2}-\Delta T_{1,2\text{-}3} \qquad \textbf{(5.21)}$$

The tension in band *n*, where *n*=2 to 9, in terms of $T_{1,1}$

Writing down the equation: extension$_n$ = extension$_1$ gives:-

$$T_{n,1} = \frac{Y_1}{Y_n}\left(T_{1,1}+\Delta T_{1,1\text{-}2}+\frac{\Delta T_{1,2\text{-}3}}{2}\right) \qquad \textbf{(5.22)}$$

where $$Y_n = L + 2\pi(x + (n-0.5)t_b) \qquad \textbf{(5.23)}$$

The tension in band 10 in terms of $T_{1,1}$

Similarly, the equation extension$_{10}$ = extension$_1$ gives:

$$T_{10,1} = \frac{Y_1}{Y_{10}}\left(T_{1,1}+\Delta T_{1,1\text{-}2}+\frac{\Delta T_{1,2\text{-}3}}{2}\right)-\Delta T_{10,1\text{-}2}-\frac{\Delta T_{10,2\text{-}3}}{2} \qquad \textbf{(5.24)}$$

5.9. The change in segment compression along the straight parts of the belt

The segment compression is altered by the shear stress between the inner bands and the segments caused by the band moving faster then the segments. Neglecting any gaps that might appear between the segments over a part of this length,

$$\Delta C_{1\text{-}2} = \Delta C_{3\text{-}4} = \frac{\eta(v_1 - v_s)}{t_{fl}} \, w \, \frac{(L - R_s\beta_s - R_p\beta_p)}{2} \qquad (5.25)$$

5.10 The torque required to drive the oil pump, T_s

The oil supply required to operate the transmission control system is delivered by a gear pump driven directly from the input shaft. As described in chapter 2, the control system modulates the oil pressure and delivers it directly to the secondary pulley cylinder. Hence the torque required to drive the pump can be related to the secondary pulley clamping force.

The secondary pulley cylinder incorporates a spring to assist return of the transmission to the starting position when it is shut down. As the axial movement of the pulley halves is small in relation to the compression of the spring, the force exerted by this spring is treated as a constant, F_{sp}.

If the volumetric flow through the pump is V_p and the mechanical efficiency is η_{mp},

$$T_g = \frac{2V_p(F_s - F_{sp})}{\eta_{mp}\pi^2(D_{s1}^2 - D_{s2}^2)} \qquad (5.26)$$

where F_s is the clamping force on the secondary pulley and D_{s1} and D_{s2} are the outer and inner diameters of the pulley cylinder.

5.11 Inherent losses in the transmission system

There are three significant losses inherent in the pushing belt transmission.

One is the loss caused by belt slip at the pulleys and by slip between the bands which has already been included in the model by the viscous treatment of these slips.

The second is the belt torque loss caused by the resistance to the radial sliding as the belt segments are continuously wedged into and out of the pulleys. This loss is considered separately in chapter 7.

The third is the energy lost in driving the hydraulic pump required to provide the clamping force on the pulleys, The expression for the torque required is shown in section 5.10.

As these three inherent losses are related there is the possibility of programming the control system for the transmission in order to minimise the sum of the losses. This was considered by Guebeli and presented in a conference paper [5.2].

Other losses in the transmission such as losses in gears and bearings are common to all types of transmission and can be treated conventionally.

The magnitudes of the losses in the transmission are considered in chapter 10, section 8.

CHAPTER 6

The Test Rig and the Instrumentation

6.1 The Design Philosophy

This project on the Van Doorne continuously variable transmission system followed on from a long series of vehicle transmission projects in the School of Mechanical Engineering with the expectation that it, in turn, would be followed by other projects. As these future projects would probably be concerned with the combined control of the transmission and engine in the operation of a complete vehicle, it was decided that the test rig should simulate such a vehicle.

An important requirement of the project is that any modifications to the transmission required to incorporate it in the test rig should be such that the normal operation is not disturbed. Any results would then be representative of conditions in the vehicle.

As the transmission tested has been commercially available in the Ford Fiesta, a representative small car, this vehicle was chosen as the one to be simulated. The test rig would then be suitable for the simulation of any small road vehicle.

In order to facilitate changes in engine and/or type of transmission the inclusion of a flat surface at the front end of the test bed was considered to be desirable. These components could then be easily bolted down at any convenient point. Torque meters mounted in cradles could also be bolted down on the surface and included in the drive

shafts.

The inclusion of a flywheel mounted towards the rear of the test bed simulated the total vehicle inertia. As it is normal for small road vehicles to have a transversely mounted engine with the output shafts from the transmission running at the vehicle wheel speed it was decided that the flywheel should be directly coupled to the output shaft and run at the same speed as the wheels.It was thought desirable to include a facility for changing the inertia of the flywheel so that various vehicle loads could be simulated.

The dynamometer was chosen to be of the hydrostatic type and was mounted at the rear of the test bed. An earlier research project in the Department had considered the use of a hydraulic pump as a dynamometer and had found it to be satisfactory. A colleague, Markus Guebeli, undertook the design of the dynamometer and the programming of the control system.

A schematic diagram of the test rig is shown in figure 6.1 and a photograph is shown in figure 6.2.

6.2 The major components of the test rig

1. The test bed

The bed was constructed from channel section steel members, two longitudinal ones which were connected by shorter lengths of the same section placed on top and welded to them.

The overall length was dictated by the sum of the lengths of the components plus suitable lengths for the connecting shafts. The longest shaft was that between the

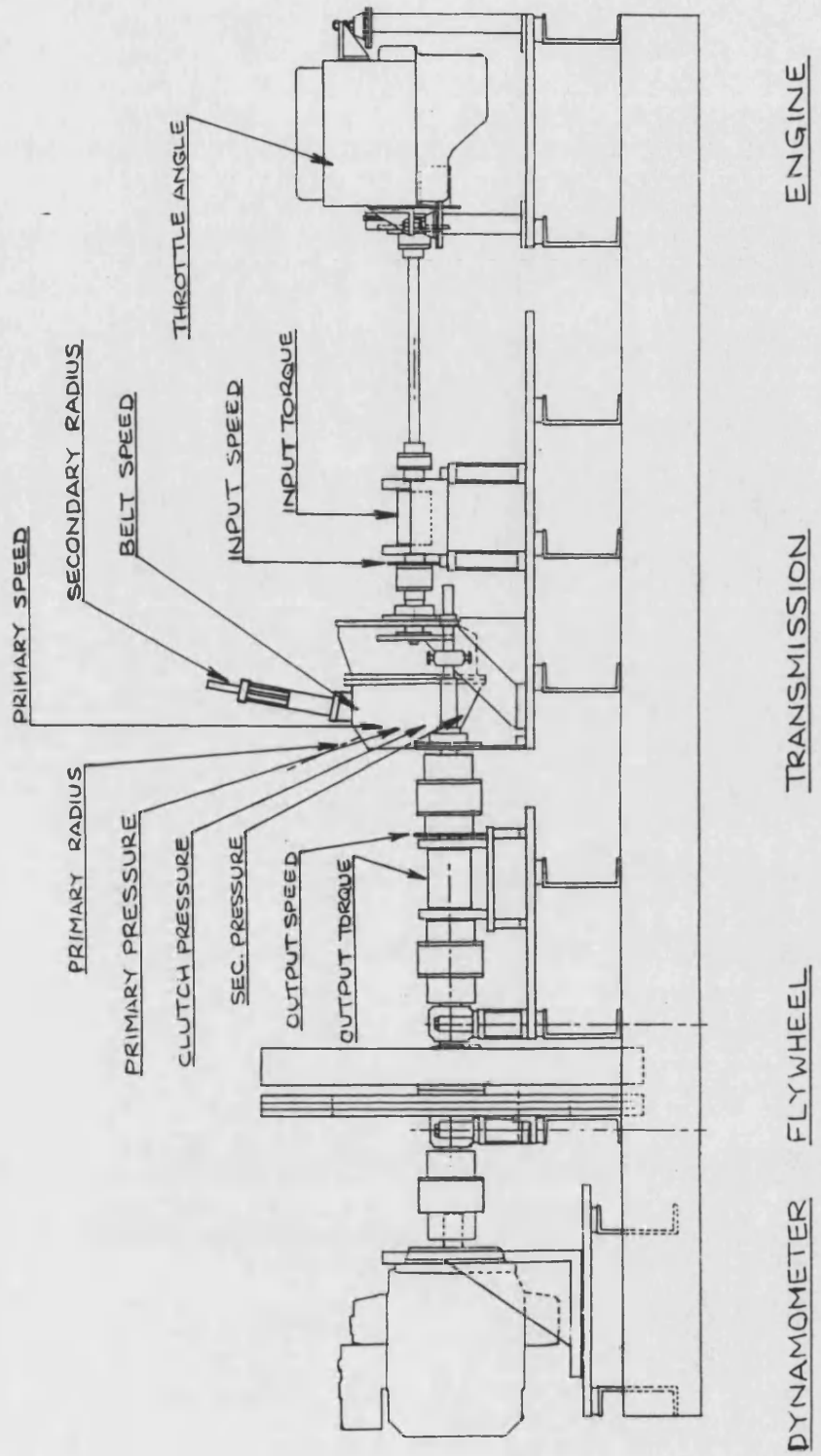

Figure 6.1 Schematic diagram of the test rig

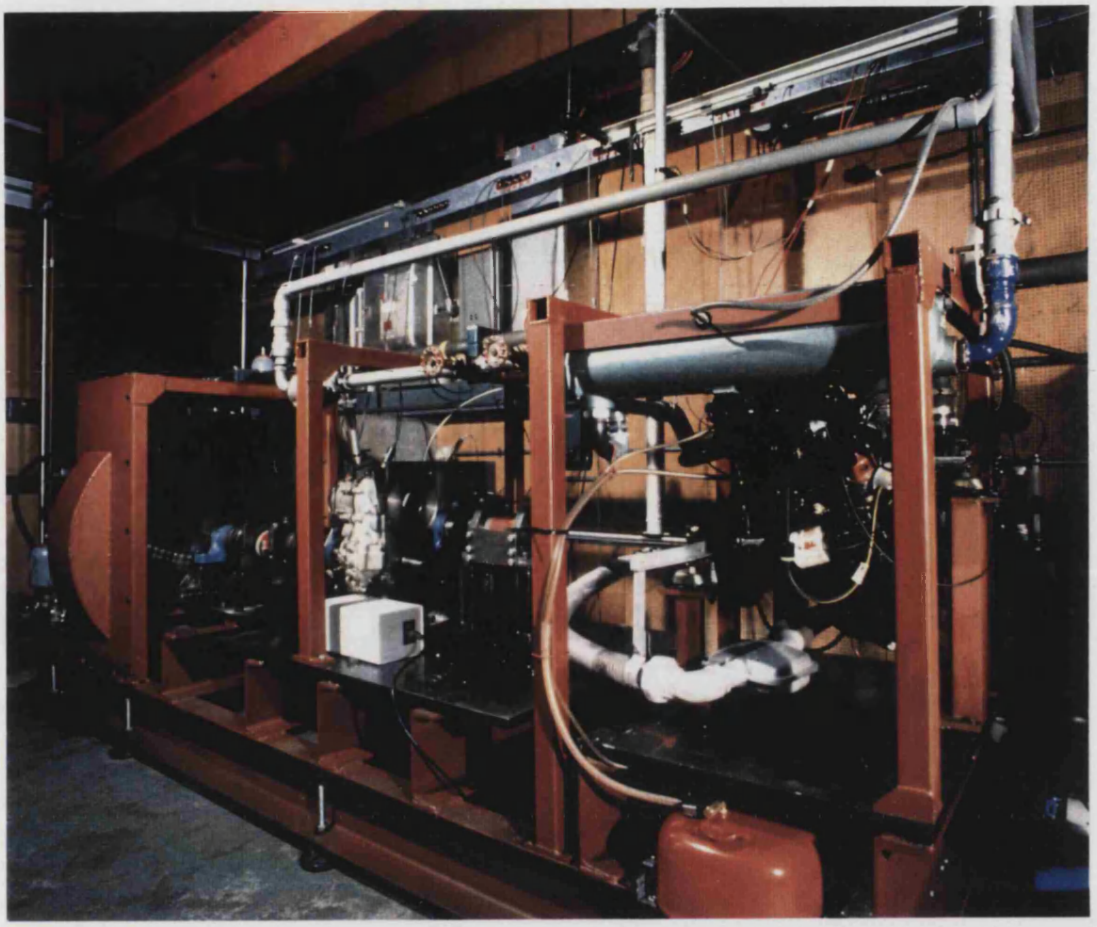

Figure 6.2 A photograph showing the test rig

engine and the first torque transducer. Its length was determined from the allowable angular displacement of the flexible couplings and the likely movement of the engine on its flexible mountings.

The height of the channel sections was determined from the clearance between the flywheel, diameter 1 m, and the longitudinal members, which fixed the height of the output shaft from the transmission, and the desirability of keeping the engine and transmission supports to a reasonable length.

The flat plates for mounting the components were made from steel plate ground flat on both sides to give a final thickness of 20 mm. The plates were mounted on small

packing blocks welded to the cross channels which were carefully ground, with the aid of a long straight edge, to ensure that their top surfaces were all in one plane. The steel plates were bolted down onto these blocks. Because of the size of the hydraulic pump to be used for the dynamometer, its mounting plate and the two cross members supporting it were positioned lower down than the others.

2. The dynamometer

The load for the engine and transmission on the test bed to work against was provided by a large hydraulic pump, the torque required to drive the pump depending on the oil flow rate, controlled by the pump swivel angle, and the pump delivery pressure, controlled by means of a poppet valve in the delivery line. The pump could also be operated as a motor to drive the transmission from the output side when required as, for example, when simulating the car descending a hill. The dynamometer hydraulic system is shown in figure 6.3.

The control system for the dynamometer provided two separate facilities. One maintained the pump speed and hence the transmission output speed at a constant, selectable value. The alternative provided a resisting torque at the pump equal to the road load experienced by the car at the speed concerned, including the effect of a selectable gradient, so that the car operation could be simulated [6.1].

The dynamometer can be seen in the photograph shown in figure 6.4.

3. The flywheel

The flywheel was designed to represent the inertia of the Ford Fiesta car. The basic flywheel was chosen to be a circular steel disc of uniform thickness and the largest

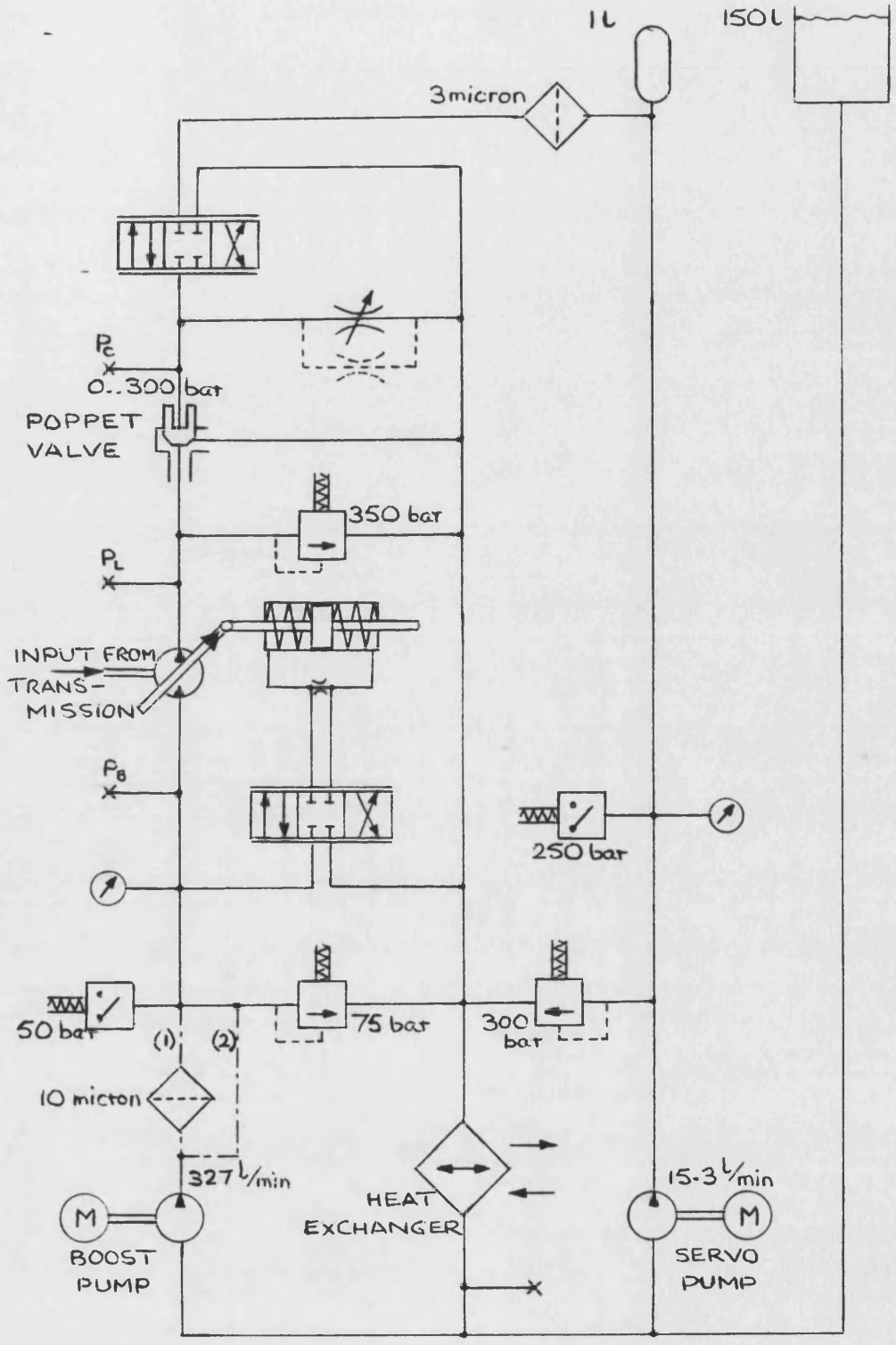

Figure 6.3 Schematic diagram of the dynamometer hydraulic system

practical diameter was taken to be 1 m. This was to represent the inertia of a lightly loaded car, the basic car plus a small amount of fuel and a driver. One, two or three equal steel rings with the same outside diameter as the flywheel and with a thickness of 15 mm can be bolted to the flywheel to give three extra increments of inertia up to that of a fully loaded car.

In determining the dimensions of the flywheel, the inertia of the car mass and the combined moment of inertia of the four wheels only need to be considered. The rotational inertia of the engine and transmission are already included in the test rig.

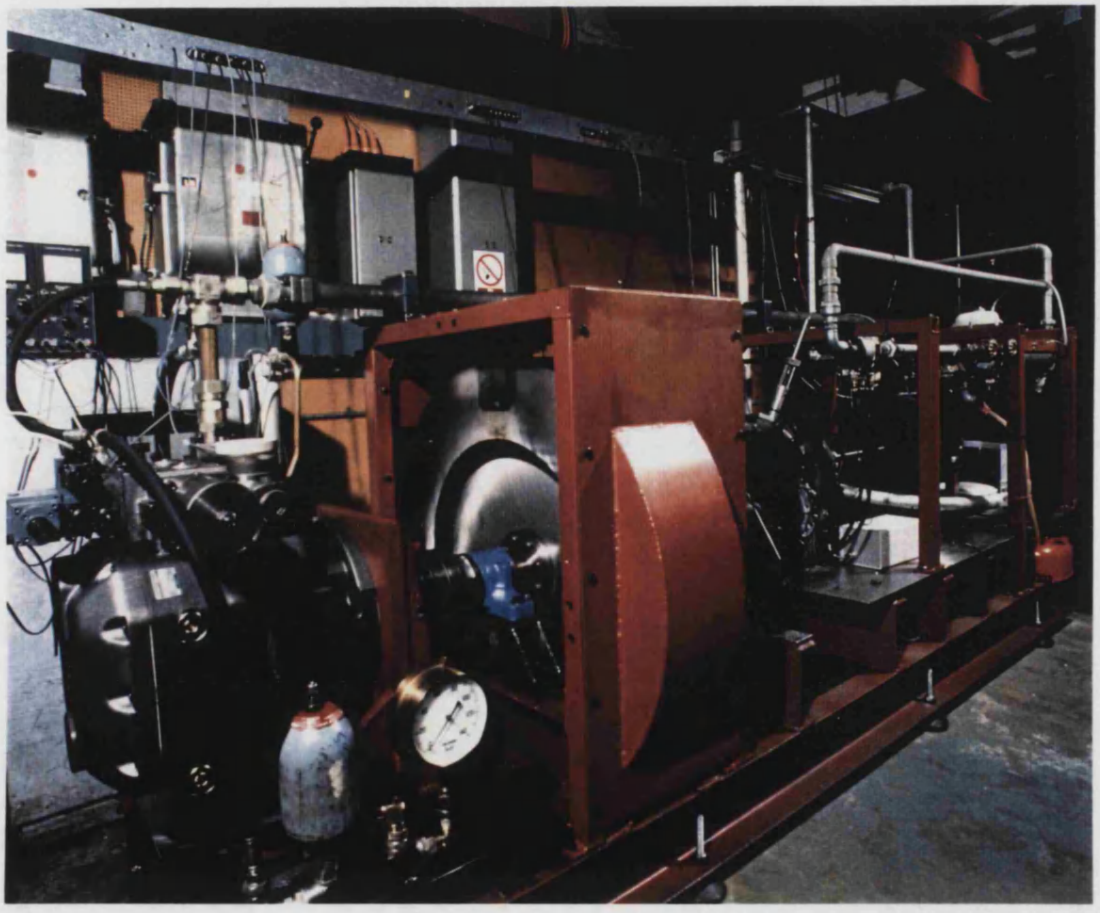

Figure 6.4 The dynamometer and flywheel on the rear of the test rig

If ω = wheel angular speed = flywheel speed

r = road wheel radius

then ωr = the vehicle speed

Equating the kinetic energy of the car to that of the flywheel:

$$\frac{1}{2}m(\omega r)^2 + \frac{1}{2}I_w\omega^2 = \frac{1}{2}I\omega^2$$

where m is the mass of the car

I_w is the combined moment of inertia of the car wheels

I is the moment of inertia of the flywheel.

Hence $I = mr^2 + I_w$

For the Ford Fiesta:-

mass of the lightly loaded car = 825 kg

mass of the fully loaded car = 1200 kg

road wheel radius = 0.28 m

combined moment of inertia of the wheels, I_w, = 1.23 kg m^2

Thus the moment of inertia of the basic flywheel to represent the lightly loaded car is equal to 65.91 kg m^2.

The square of the radius of gyration of a solid disc = radius^2/2,

and the density of steel = 7820 kg/m^3.

As the basic flywheel is a solid disc with an outside diameter of 1 m, the required thickness of the disc is 86 mm.

Each of the three additional rings represents 1/3 of the increase in vehicle inertia from light to full load. Then the moment of inertia of each ring = 125 x 0.28^2 = 9.80 kg m^2.

As each ring has an outside diameter of 1 m and a thickness of 15 mm, the inner diameter to give the required inertia is 0.622 m.

The disc and the rings were each flame cut from mild steel plate, slightly oversize, the disc having a central hole for a hub. They were then stress relieved, ground on both faces to the final thickness and finally machined on the inner and outer diameters to the required size.

To ensure that the rings were correctly located they were bolted to the main disc by eight shoulder bolts in reamed holes. The circumferences of the disc and rings were all marked to ensure correct angular positioning. The disc and rings were all dynamically balanced by drilling appropriate holes in the circumferences.

The hub is a pressed fit in the main disc and the two are bolted together by eight shoulder bolts in reamed holes passing through a flange in the hub. The hub is keyed to the shaft. The integrity of the flywheel shaft was considered in the event of a siezure of a major component in the test rig. Only the sudden stoppage of the dynamometer presented any problem. To ensure that the shaft would fail outside the flywheel bearings, a groove was cut around the shaft between the dynamometer and the adjacent bearing in order to provide a stress raiser.

A section of the flywheel is shown in figure 6.5. The flywheel and the three additional

rings, in this case not in use and bolted to brackets attached to a frame on the test bed, can be seen in the photograph shown in figure 6.4.

The maximum speed of the car is about 95 mile/h which gives a maximum speed for the flywheel of 1450 rev/min. A rough idea of the stresses involved in the flywheel at this speed was obtained by use of the stress relations for a rotating cylinder. At the central plane of a hollow rotating cylinder, the tangential, radial and longitudinal stresses, σ_θ, σ_r and σ_z respectively, are given by:

$$\sigma_\theta = \frac{\rho\omega^2}{8}\left[\left(\frac{3-2\nu}{1-\nu}\right)\left(a^2+b^2+\frac{a^2b^2}{r^2}\right)-\left(\frac{1+2\nu}{1-\nu}\right)r^2\right]$$

$$\sigma_r = \frac{\rho\omega^2}{8}\left(\frac{3-2\nu}{1-\nu}\right)\left(a^2+b^2-\frac{a^2b^2}{r^2}-r^2\right)$$

$$\sigma_z = \frac{\rho\omega^2}{4}\left(\frac{\nu}{1-\nu}\right)\left(a^2+b^2-2r^2\right)$$

where a and b are the inner and outer radii respectively;

ν is Poisson's ratio for the material which = 0.3;

ρ is the material density which = 7820 kg/m^3 for steel;

ω is the angular velocity of the cylinder.

For the main disc, a = .050 m and b = 0.500 m. Then at a speed of 1450 rev/min:

σ_θ has a maximum value at the minimum radius equal to 38.70 MN/m^2,

σ_r has a maximum value when $r^2 = ab$ equal to 15.65 MN/m^2,

σ_z has a maximum value at the minimum radius equal to 4.78 MN/m^2.

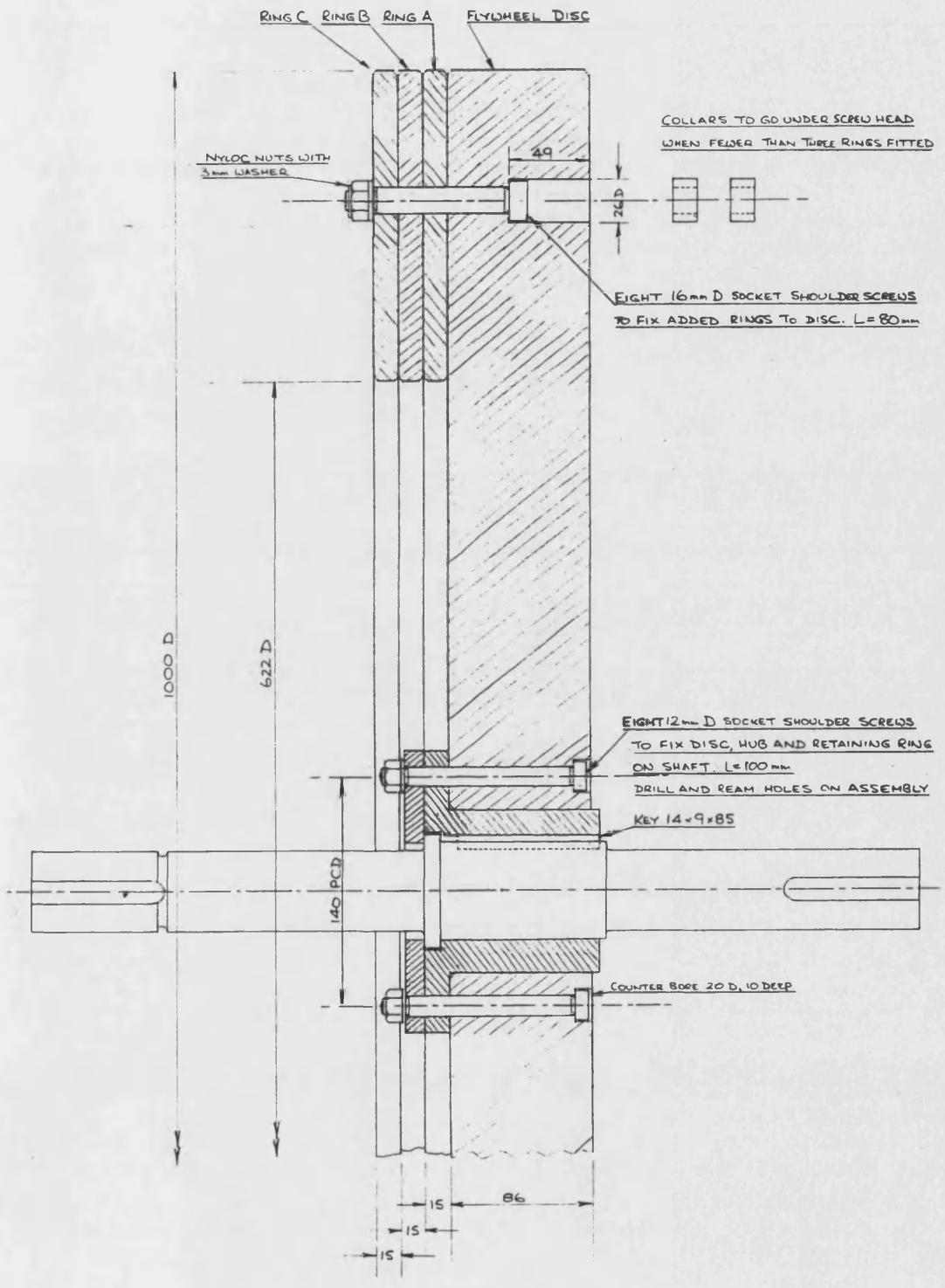

Figure 6.5 Sectional drawing of the flywheel and additional rings

All these stresses are well below the yield stress for the material which is 200 MN/m^2.

For the additional rings, a = 0.311 m and b = 0.500 m.

The maximum value of the tangential stress, once again at the minimum radius, is equal to 41.11 MN/m^2 which is also well below the yield stress.

When the flywheel was installed on the test bed it was run up to 1800 rev/min without and with the extra rings by using the dynamometer as a motor. The running was very smooth showing that no undue distortion occurs at this speed and large stresses are then not likely to be present. As the stresses depend on the square of the speed, this speed would give stresses about 1.5 times the stresses at the normal maximum of 1450 rev/min.

The bending stresses in the 50 mm diameter flywheel shaft under the weight of the flywheel were determined in order to check that they are not likely to lead to a fatigue failure.

The centre lines of the bearings are 276 mm apart and the flywheel is 120 mm from one bearing. As the mass of the complete flywheel is 720 kg, the maximum bending moment in the shaft is approximately 480 N m.

The second moment of area for the circular section is $\pi d^4/64$.

Hence the maximum stress in the shaft is 39.1 MN/m^2. This is a very modest stress which is not likely to lead to fatigue problems.

4. The transmission

The Ford CTX transmission was mounted on a vertical plate fixed to the test bed. A photograph of the transmission mounted on the test rig is shown in figure 6.6. The input shaft is on the right and the output on the left.

When the transmission is bolted to the rear of the engine as in normal operation in a car, the drive from the engine enters the transmission through a torsion damper bolted to the engine flywheel. On the test rig, the same torsion damper is used but bolted to a flange on the end of the drive shaft from the engine.

The output from the transmission comes through a casting, carried on the final drive

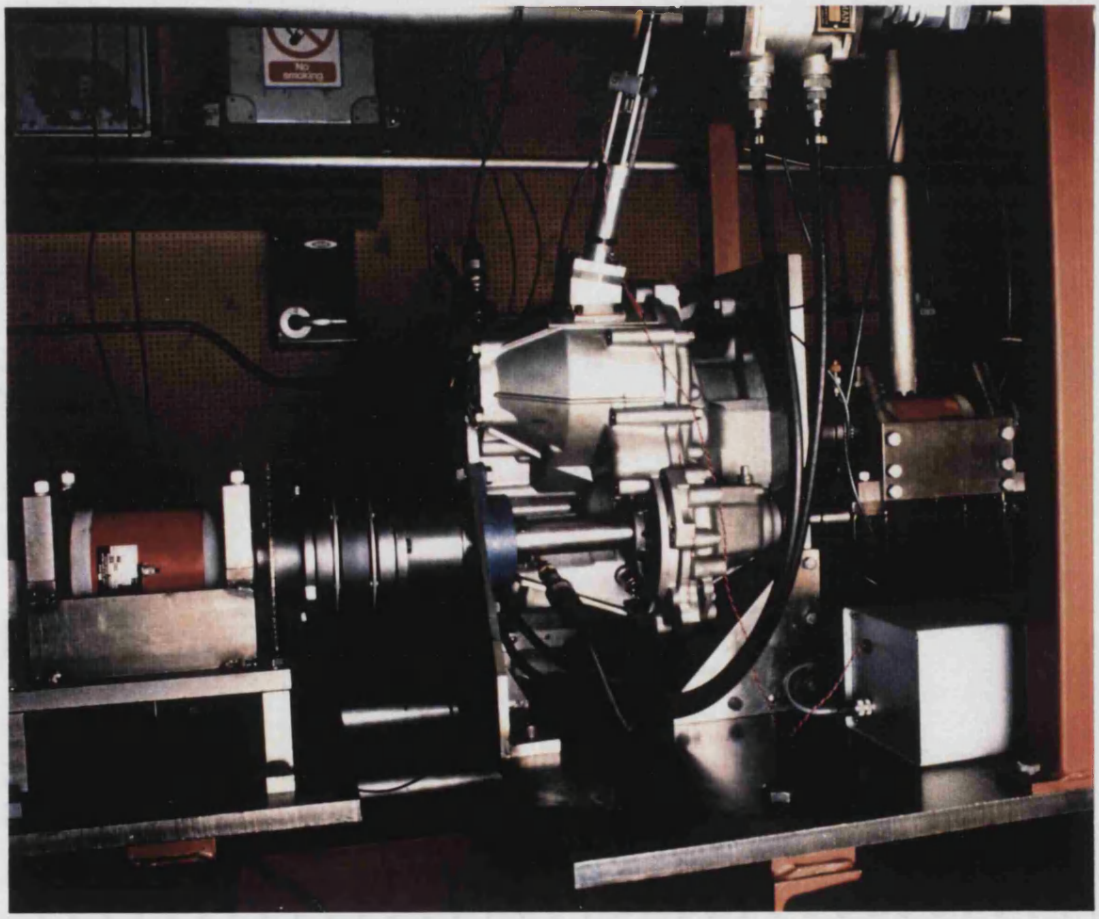

Figure 6.6 The transmission mounted on the test rig

gear, which contains the differential and supports fittings for the two final drive shafts, one to each of the front wheels of the car. This had to be modified so that the output was through a single shaft. The two fittings for the ends of the drive shafts were removed and the differential was removed and replaced by a special connecting block. The normal differential assembly and the special block that replaced it are shown in figure 6.7. This block was attached to the casting by the two bolts shown which replaced the pin through the differential. Thus the normal operation of the transmission was not disturbed.

The single output shaft from the transmission to the flywheel and dynamometer was keyed to this special block. The maximum diameter available for this output shaft without disturbance to the transmission was 28 mm and this restriction gave rise to the most highly stressed component on the test rig. It was determined that the maximum torque to be transferred from the block to the shaft was 1170 N m when the transmission was accelerating in low ratio with a wide open engine throttle. This gave a maximum shear stress in the shaft, including a stress raising factor for a step in the shaft, equal to 434 MN/m^2. A high grade steel, En 16T, was specified for the shaft with a yield stress of 680 MN/m^2 giving a safety factor of about 1.5 before permanent deformation.

By means of these modifications the transmission was operated on the test rig as if it were in a vehicle. It was firmly mounted and the input and the output torques entered and left the transmission in the same way as normal.

When installed in a car, the transmission has a heat exchanger mounted in the engine radiator water in order to cool the circulating oil. The test rig had a small heat

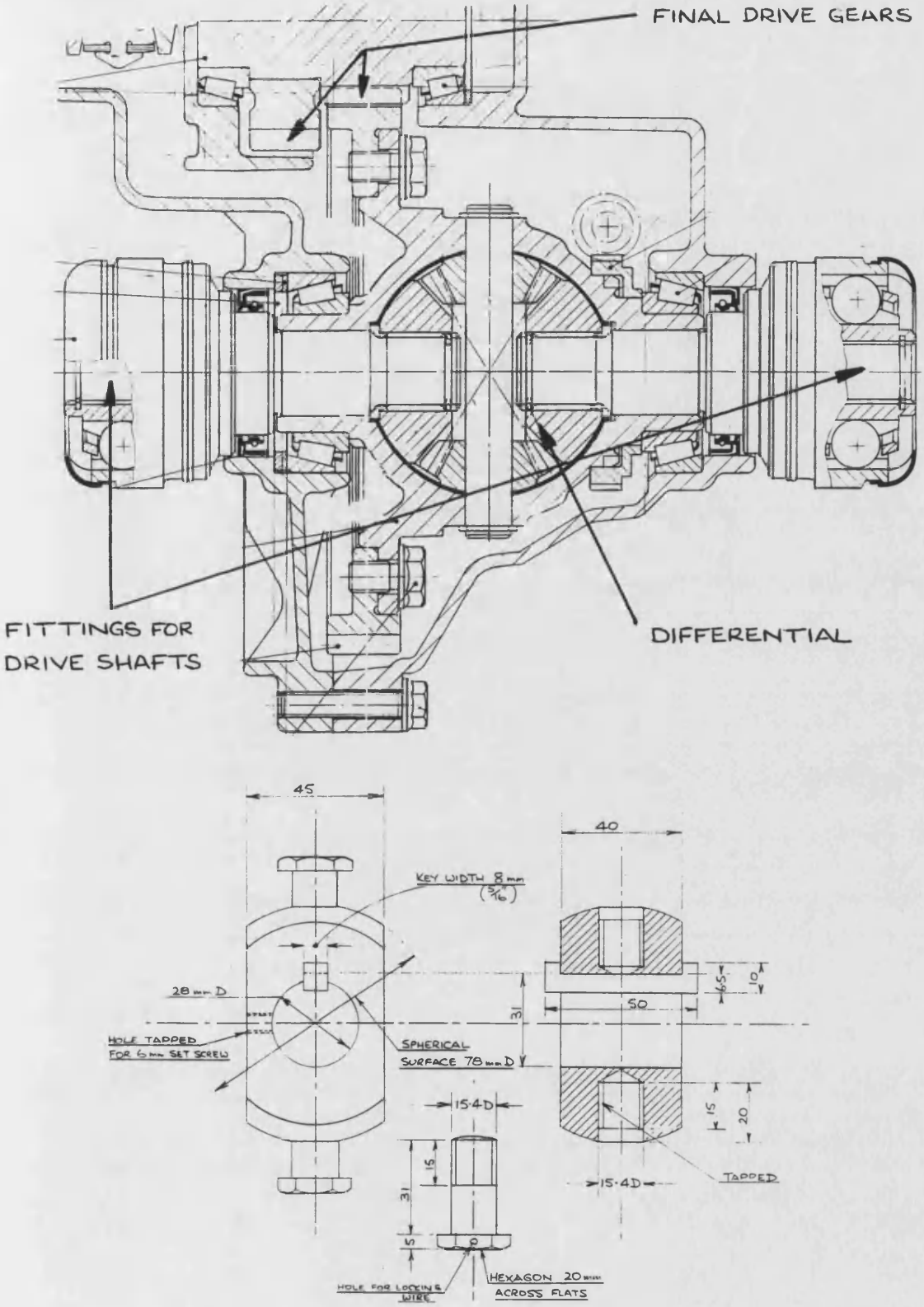

Figure 6.7 The differential assembly and the replacement block

exchanger for this purpose, the coolant being water from the laboratory cooling circuit.

The control system for the transmission used in the first series of tests was the standard hydro-mechanical system situated under the transmission. This supplies oil at the appropriate pressures to the clutch operating cylinder, the secondary pulley cylinder and the primary pulley cylinder in response to inputs of engine throttle opening (accelerator position), opening of the primary pulley halves and hydraulic signals of engine speed and primary pulley speed.

For later tests the normal control system and the hydraulic pump were removed and the transmission was operated by a separate hydraulic system controlled by computer. This separate system was designed by Guebeli for his study on frequency control. It enabled any values of clutch, secondary pulley and primary pulley pressures to be fed into the transmission. All the remaining tests for this project were carried out with fixed pulley radii. When the normal transmission is in low ratio with the primary pulley at its smallest radius, the moveable primary pulley half rests on a shoulder on its shaft and no primary pressure is required, the belt being tensioned by the secondary pressure. By inserting rings of various thicknesses against this shoulder the position of the pulley half can be adjusted and any operating radius obtained, still with no primary pressure being required. This does not in any way alter the normal operation of the belt system. A series of five sets of radii covering the whole range were used by employing either the basic shoulder or one of four additional rings. The clutch pressure was maintained at a value that prevented clutch slip. The secondary pressure was set to any desired value.

5. The engine

One of the engines used in the Ford Fiesta series of cars, a 1.1 litre petrol engine, was used in the test rig. It can be seen in the front of the photograph in figure 6.2.

The engine was mounted on three pillars attached to the base plate, each pillar having a Cushyfloat mounting at the top. Two arms bolted to the flange at the rear of the crankcase went respectively to two of the pillars while a bracket bolted to the front mounting point went to the third.

The normal engine cooling system was utilised with the hot water from the engine passing through a heat exchanger mounted on the test rig and then back to the engine. The heat exchanger coolant was water from the laboratory cooling circuit.

Petrol was supplied to the engine from a small tank, as used in small boats, positioned under the test rig. For filling, the tank could be easily removed and the fuel line disconnected without spillage at a quick release connector.

The engine throttle was operated by means of a small hydraulic piston and cylinder which gave either remote manual control or control through a computer as required. For the first series of tests the normal linkage between the engine throttle and the transmission was utilised.

6.3 The Instrumentation

1. The quantities to be measured

For any transmission test it is necessary to measure the shaft torque and speed at input to and at output from the transmission.

For this project it was extremely important to determine the slip accurately and this can only be done if the belt radius on the two pulleys is known. Thus the primary radius and the secondary radius are to be measured. As the drive from the input shaft to the primary pulley passes through the clutch it is also necessary to ensure that slip is not occurring in the clutch. This was done by measuring the primary pulley speed in addition to the input shaft speed. In order to separate the slips on the two pulleys it is desirable to measure the belt speed.

The hydraulic pressures supplied by the control system to the operating cylinders on the secondary pulley, the primary pulley and the clutch are important and are to be measured.

It is also desirable to measure the engine throttle angle so that there is an indication of the engine operating point during a test.

Hence the following twelve quantities are to be measured:-

1. shaft torque at input to the transmission
2. speed of input shaft
3. speed of the primary pulley
4. shaft torque at output from the transmission
5. speed of output shaft
6. belt radius on primary pulley

7. belt radius on secondary pulley

8. speed of the belt

9. pressure in the primary pulley cylinder

10. pressure in the secondary pulley cylinder

11. pressure in the clutch operating cylinder

12. engine throttle angle.

The locations of these measurements on the test rig are shown in figure 6.1.

2. Torque measurement

Strain gauge type torque transducers were used in the input and the output shafts.

The maximum torque that can be delivered by the engine is 83 N m and the transducer in the input shaft to the transmission was an EEL size CA with a normal torque range of 0 - 135 N m.

The maximum torque in the output shaft from the transmission was determined to be about 1170 N m and here an EEL size DC transducer with a range of 0 - 1350 N m was used.

The two torque transducers, mounted in their cradles, can be seen to right and left in the photograph of the transmission in figure 6.6.

Both transducers were calibrated by removing the couplings on each side, bolting a locking arm to one flange and a horizontal loading arm to the other. A series of weights was hung on the end of the loading arm to cover the full range required and the factors for converting the signals to torques determined.

3. Speed measurements

The four speed measurements were made using electro-magnetic pickups to generate pulses which were processed in a Frequency to Voltage circuit developed in the School [6.2]. The accuracy is within 0.1% of the maximum value.

For the input and the output shafts, toothed wheels were used to generate the pulses. These were mounted on the torque transducer coupling flanges, on the transmission side in both cases, and can be seen in the photograph in figure 6.6.

For the primary pulley advantage was taken of a pressed steel plate with evenly spaced indentations for stiffening purposes attached to the pulley. Mounting a pickup close to the circumference produced suitable pulses.

For the belt speed, the belt segments moving round a pulley were used. When rounding a pulley the segments contact each other at the level of the rocking edges and open up at the outer radius. The pickup was mounted close to the segments on the end of the probe measuring belt radius on the secondary pulley.

4. Belt radius measurement

Two probes were used to measure the belt radii on the pulleys, one mounted over the primary pulley and the other over the secondary. A diagram of a probe is shown in figure 6.8 and the probe for the secondary pulley can be seen on top of the transmission in the photograph in figure 6.6.

A linearly guided, spring loaded rod holds a wheeled assembly onto the top of the belt, the wheels running on the two band packs. The rod moves in a radial plane from the pulley axis in a direction parallel to the surface of the fixed pulley half. The position of the probe is measured with a linear variable displacement transducer

(LVDT) supported on top of the probe assembly. Two holes were cut in the casing to gain access to the pulleys. The light touch of the wheels on the belt will not affect the normal running of the transmission.

To calibrate the probes, the outputs from the LVDTs were measured with the belt in a known position. Then, knowing the calibration of the LVDT, any output can be readily turned into a radius. To put the belt in the known position, the transmission was set in the 'Drive' position with the engine idling and the output shaft stationary. This pressurises the secondary pulley cylinder and tensions the belt with the primary pulley halves at their maximum opening and hence with the belt at its minimum radius. With the probes removed and with the aid of a depth gauge, the depths of the belt below the outer circumferences of the pulleys was measured and the two pulley radii determined. The probes were then replaced and the LVDT outputs measured. As a precaution, when radius measurements were first

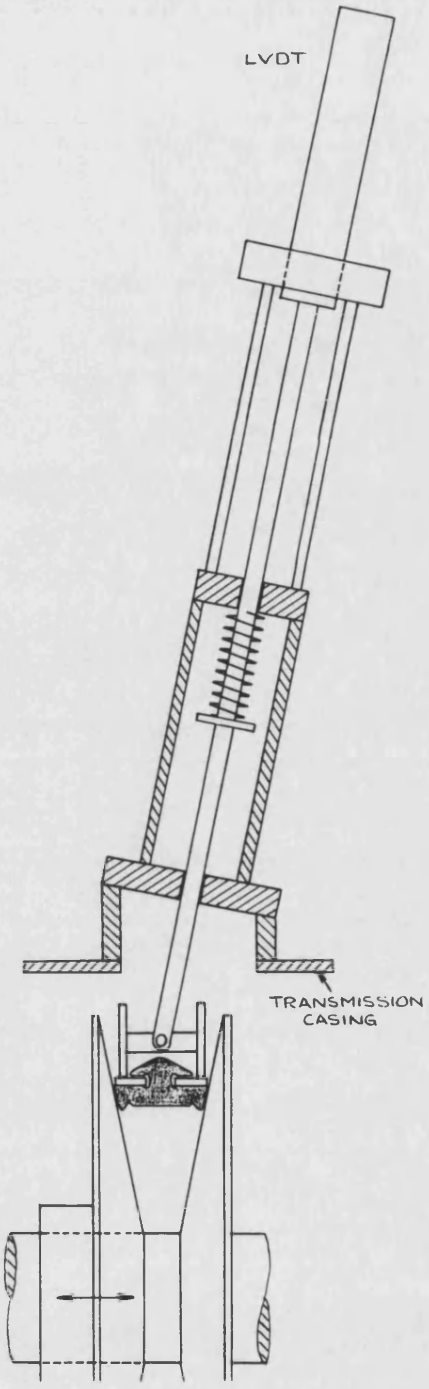

Figure 6.8 Belt radius probe

obtained with the transmission running, the values obtained were checked for compatibility using the geometric relations developed in chapter 5. At all times when the transmission was running the probes were very steady giving confidence in the measuring system.

5. Pressure measurements

The pressures in the primary and the secondary pulley cylinders and in the clutch operating cylinder were measured using strain gauge pressure transducers. These were inserted into the oil lines supplying the cylinders at points as close as possible to the cylinders in order to minimise pressure loss errors when changes were occurring.

6. Engine throttle angle

This angle was measured by means of a rotary potentiometer attached to the throttle spindle.

7. Data collection

The signals from the transducers were conditioned as required to produce analogue signals of the quantities measured. A computer system was used to convert these analogue signals into digital form before collection in the computer.

Chapter 7

Belt Related Torque Loss

7.1 Introduction

The losses in rubber V-belts have been extensively analysed, for example: Childs and Cowburn [7.1], showing that there is an important belt related torque loss mainly due to:

1. sliding losses as the belt is wedged into and pulled out of the pulley groove at inlet to and at outlet from a pulley;

2. hysteresis loss as the belt is bent on and off a pulley.

Little has been published on a similar loss in the steel, pushing V-belt transmission. Roovers [7.2] shows that there is a significant loss dependent on the clamping force on the secondary pulley. Unfortunately his paper gives no information on how the data was obtained. None of the papers on modelling the system which were considered in chapter 3 includes this loss.

The results of measurements are presented in this chapter which show that the belt related torque loss is important and dependent on the belt configuration as well as on the pulley clamping force. Only the sliding loss as in 1. above is considered to be

important as the steel belt has little bending stiffness.

A semi-empirical model is proposed to explain the loss and calculations from this model are compared with the measured results. The agreement between measured and calculated values is good.

7.2 Belt torque loss

This loss is caused by the radial sliding losses as the belt is continuously wedged into and out of the pulleys. As the segment enters a pulley, the pulley halves will distort as they are locally pushed apart and the segment will be laterally compressed. As these small deformations take place the segment will move a small distance radially inwards against friction forces between the segment sides and the pulley surfaces. The torque loss supplies the energy that must be used to overcome these friction forces both on entry and, similarly, on exit. To insert the segments into the pulley wedge angle at inlet to the pulley and to withdraw the segments at outlet in the very short time available requires quite large radial forces.

At the entrance to a pulley this radial force arises from the normal curvature of the bands giving an inward component to the tensions in the bands. As the insertion of the segment will take a finite time, the pulley will turn through a small angle while the process occurs and the belt will enter the pulley at a radius greater than the equilibrium radius. This equilibrium radius will be achieved after a small angular movement of the pulley and it will be assumed that the segment moves round the remainder of the pulley at this, uniform, radius. Justification of this assumption can be found in the measurements of the belt radius around a pulley made by Kim and

Lee [7.3].

At the exit from a pulley the segment will tend to stay wedged in the pulley until the reverse angle in the belt provides a sufficient outward component from the tensions in the bands to withdraw the segment. Thus the belt will tend to leave a pulley at a radius less than the equilibrium radius.

These variations in the actual belt radii from the ideal, equilibrium radii give rise to an increase in the input torque required, the extra torque providing the energy which is dissipated in the sliding losses.

7.3. Torque loss on no-load

Based upon the above argument, the line of the belt is shown in figure 7.1 with a reduced radius at exit from a pulley and an increased radius at entrance to a pulley.

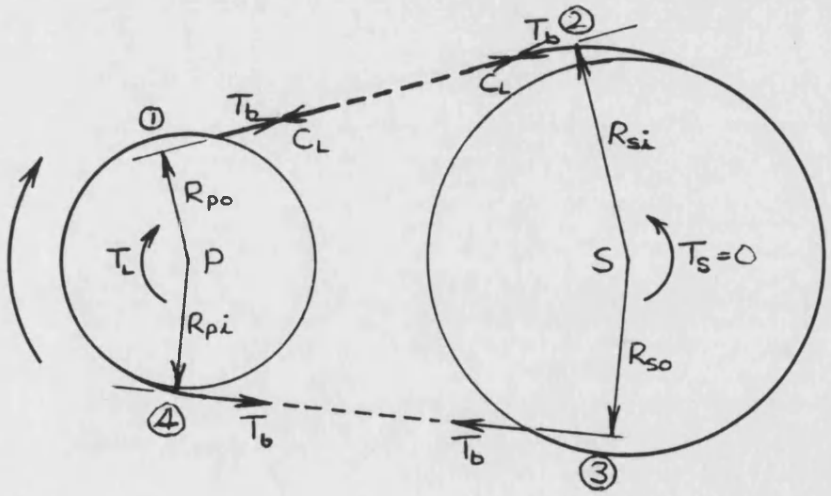

Figure 7.1 The line of the belt on no-load

Neglecting any viscous shear connection between the bands and the belt segments, the total band tension, T_b, will be uniform. As this is a no load case, the secondary pulley torque, T_s, equals zero and to achieve this it is necessary to have a small compressive load, C_L, in the segments between stations 1 and 2. Neglecting the small difference in the lines of action of the tensions and compressions in the belt:

$$C_L = T_b\left(1 - \frac{R_{so}}{R_{si}}\right) \qquad (7.1)$$

$$\text{and} \quad T_L = T_b R_{po}\left(\frac{R_{pi}}{R_{po}} - \frac{R_{so}}{R_{si}}\right) \qquad (7.2)$$

This is the Belt Torque Loss, the torque required to insert the segments into the pulleys and then to remove them.

As the loss mechanism is fundamentally of the same form at entry and exit and as R_i and R_o are only slightly different from the equilibrium radius, it is assumed that the entry and exit radii are related to the equilibrium radius by the same factor, k_p for the primary pulley and k_s for the secondary.

$$R_{po} = k_p R_p \qquad \text{and} \qquad R_{pi} = R_p/k_p$$

$$R_{so} = k_s R_s \qquad \text{and} \qquad R_{si} = R_s/k_s$$

k_p and k_s will have different values as the radial stiffness of the belt in the pulleys will depend on the radius. Substituting these values in equation (7.2) gives:

$$T_L = T_b R_p k_p \left(\frac{1}{k_p^2} - k_s^2 \right) \qquad (7.3)$$

In order to determine the values of k_p and k_s, consider the belt at outlet from the primary pulley i.e. at station 1 in figure 7.1. The force C_L is small and may be neglected. The detail is shown in figure 7.2.

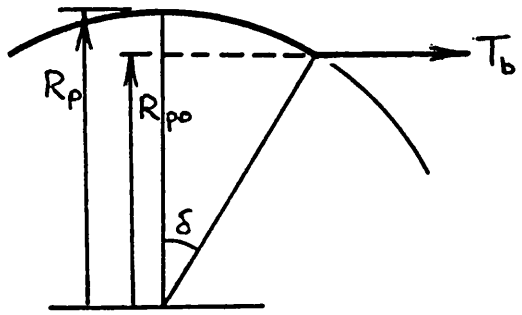

Figure 7.2 The belt at outlet from the primary pulley

The belt shape as the segments leave the pulley is likely to be a more gradual curve than the abrupt angle shown. However, in the absence of a full investigation of the mechanism, this simple approximation may be used with the assumption that the force required to withdraw a segment is proportional to the clamping force carried by the segment, that is

$$T_b \sin\delta \quad \propto \quad \frac{F_p}{\frac{R_p \beta_p}{s}}$$

From equation 5.13 it can be shown that, approximately,

$$T_b = \frac{2F\tan\theta}{\beta} + \frac{C}{2} + m_b v_s^2$$

so that at low speed and with no load

$$T_b = \frac{2F_p\tan\theta}{\beta_p} \quad \text{also} \quad k_p = \cos\delta$$

From which

$$R_p\sqrt{1 - k_p^2} = \text{constant}_1$$

$$R_s\sqrt{1 - k_s^2} = \text{constant}_2$$

Assuming the two pulleys are similar, these two constants will be equal and

$$R\sqrt{1 - k^2} = \text{constant} = K \qquad (7.4)$$

The constant, K, can be determined from measurements of the torque loss and of the corresponding pulley radii in a single no-load case.

7.4. Measurement of the torque loss on no-load

The rig described in chapter 6 was used to measure the torque loss on no-load. During the tests the secondary pulley cylinder was supplied with oil from a separate, external system giving control over the clamping pressure while the primary cylinder was

unpressurised with the moveable pulley-half resting on one of a series of stops giving a variety of fixed, operating radii. No load conditions were obtained by disconnecting the output shaft and various input speeds were obtained by setting the engine throttle. The losses along the input shaft, including drag in the reverse clutch, were obtained first by running the transmission with the belt removed and measuring the torque inputs for a series of input speeds. The belt was replaced and torque inputs were again measured for a series of input speeds, secondary pressures and operating radii. The torque loss was obtained by subtracting from each of these last values the input shaft loss corresponding to the particular input speed. The results are shown in figure 7.3. Speed has little effect on the torque loss with the smaller values of primary radius and

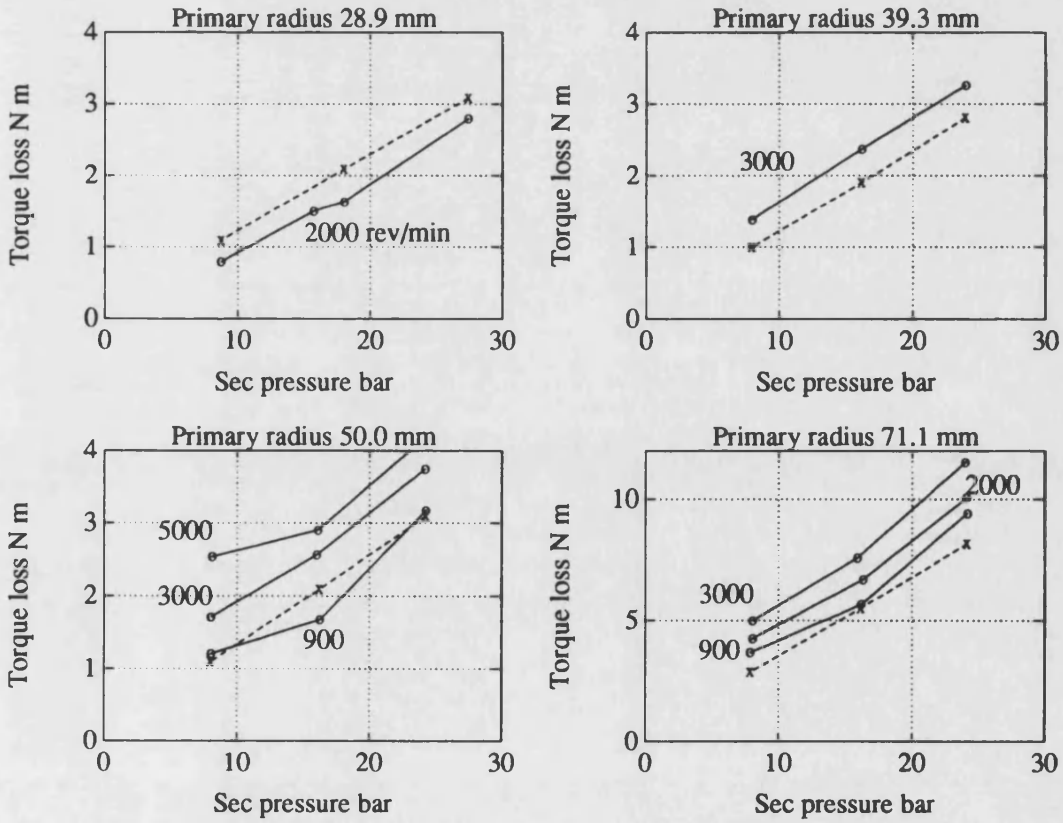

Figure 7.3 Measured (—) and calculated (---) belt torque loss on no-load

a relatively small effect only at the higher values.

The constant in equation 7.4 was determined from a measurement of the torque loss when R_p was equal to 0.050 m and R_s was 0.0579 m. The point chosen was at the fairly low speed of 900 rev/min and a secondary pressure of 8 bar. The value obtained for the constant was 0.0055 m. The variation in the effective belt radius from the nominal radius is then about 0.25 mm at the maximum radius, 0.35 mm at mid radius and 0.6 mm at the minimum radius. Calculated values for the torque loss at low speeds are also shown with the measured results in figure 7.3. The calculated torque loss at higher speeds will be greater than the low speed value as the band tension increases with speed.

The measured and calculated torque losses at low speed show very good agreement which justifies the use of the semi-empirical model. It is very encouraging that, although the constant in equation 7.4 was determined from a single no-load test, the slopes of the calculated curves in figure 7.3 are very close to the slopes of the measured curves.

7.5. Torque loss when the transmission is delivering a torque

Assuming that the same mechanism applies when the system is transferring a torque, it can be seen that conditions will be altered in the section between stations 1 and 2 where the segments are carrying a compressive force and not at all between stations 3 and 4 where the segments are slack. Considering the belt at station 1, the effect of the compressive force is to make the segment less tightly wedged into the pulley than in the no load case and to reduce the withdrawing force from $T_b \sin\delta$ to $(T_b - C)\sin\delta$.

Assuming, further, that these two effects are in proportion, it seems reasonable to use the same values for k_p and k_s at stations 1 and 2 respectively as in the no load case.

Consider the system when the secondary pulley is delivering a torque T_s. Figure 7.4 shows an ideal system with no torque loss and, hence, with the belt entering and leaving the pulleys tangentially.

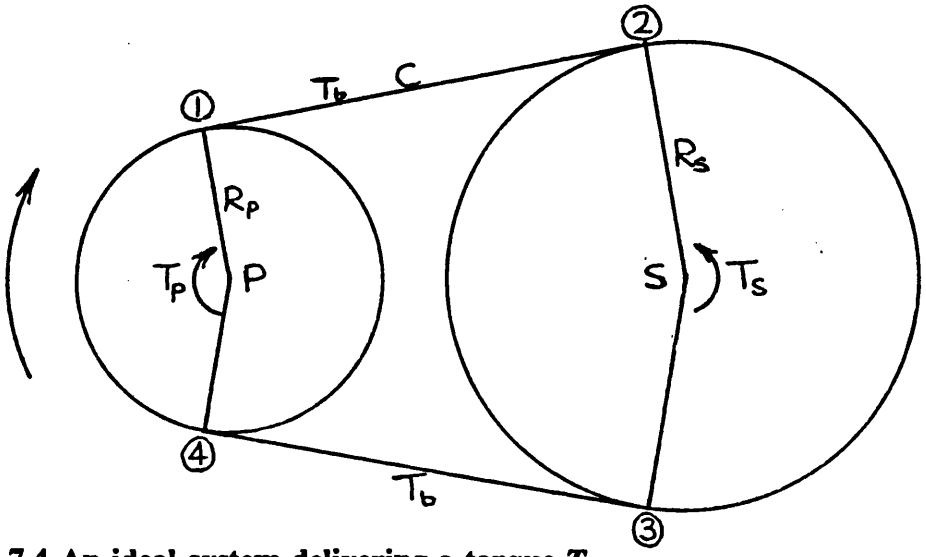

Figure 7.4 An ideal system delivering a torque T_s

$$C = \frac{T_s}{R_s} \quad \text{and} \quad T_p = T_s \times \frac{R_p}{R_s}$$

Figure 7.5 shows a system with torque loss occurring but still delivering a torque T_s. The compression in the segments between stations 1 and 2, C_x, must now be greater than C in the ideal case to overcome the adverse torque from the band tension.

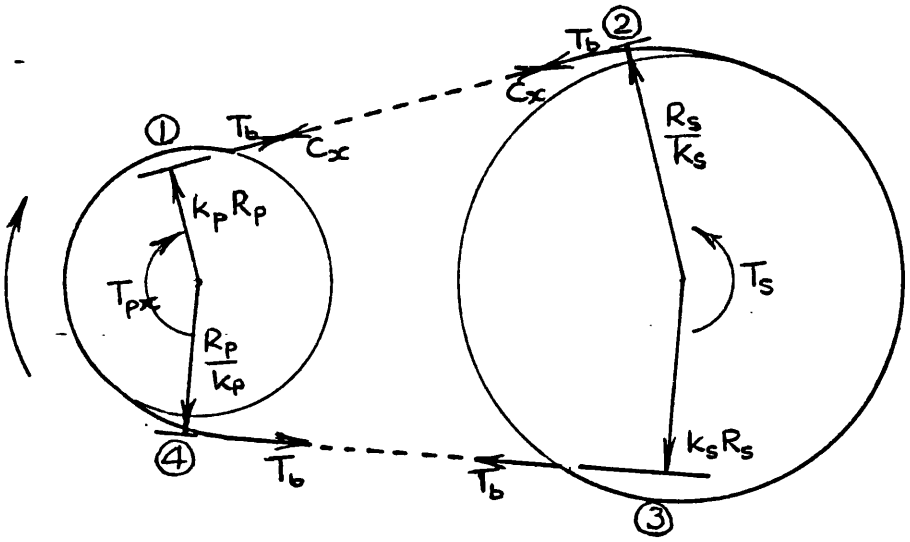

Figure 7.5 System with torque loss

From moments applied to the secondary pulley:-

$$C_x = \frac{k_s T_s}{R_s} + T_b(1 - k_s^2)$$

From moments applied to the primary pulley:-

$$T_{px} = \frac{k_p k_s T_s R_p}{R_s} + T_b R_p k_p \left(\frac{1}{k_p^2} - k_s^2\right)$$

The belt torque loss, T_{Lx}, is the amount by which T_{px} exceeds the ideal T_p.

$$T_{Lx} = T_b R_p k_p \left(\frac{1}{k_p^2} - k_s^2\right) - \frac{T_s R_p}{R_s}(1 - k_p k_s) \qquad \textbf{(7.5)}$$

The first term is equal to the no load torque loss, equation (7.3).

The expression for the loss when the transmission is transferring a torque was determined with the assumption of a reverse bend in the belt at station 1. This is not likely to occur when the segments are loaded in compression as the belt then has a very high bending stiffness in the reverse direction. Probably what happens is that the belt leaves the pulley tangentially and the belt between stations 1 and 2 acts as a lever withdrawing the segments and applying a small, local moment to the primary pulley as it does so. Attempts to model this proved abortive but as the energy involved in the withdrawal process will be the same whichever model applies it is permissible to use the derived expression to evaluate the torque loss.

The behaviour of the belt at the other three stations will not be altered by the addition of a load.

7.6. Comparison of calculated and measured torque losses on load

A series of steady state tests was run using a variety of primary pulley stops to give a range of belt configurations. For each set the primary radius, the output speed and the secondary cylinder pressure were fixed and the conditions were measured for a series of input torques set by adjustment of the engine throttle.

The belt torque loss was deduced from the measurements by subtracting the ideal torque input, $T_s.R_p/R_s$, from the measured torque input less the loss along the input shaft.

The torque loss was calculated from equation (7.5), the band tension, T_b, being calculated from the system model described in chapter 5.

The calculated and measured torque losses are shown in figures 7.6 and 7.7 for input torques of 32 and 64 N m respectively. Each figure shows the losses plotted against the secondary pressure for four values of primary radius.

Although the values of torque loss deduced from measurements when the transmission is on load are open to some inaccuracy as they are the small difference between two large values, there is good agreement between them and the calculated values and they are compatible with the no-load values which were directly measured.

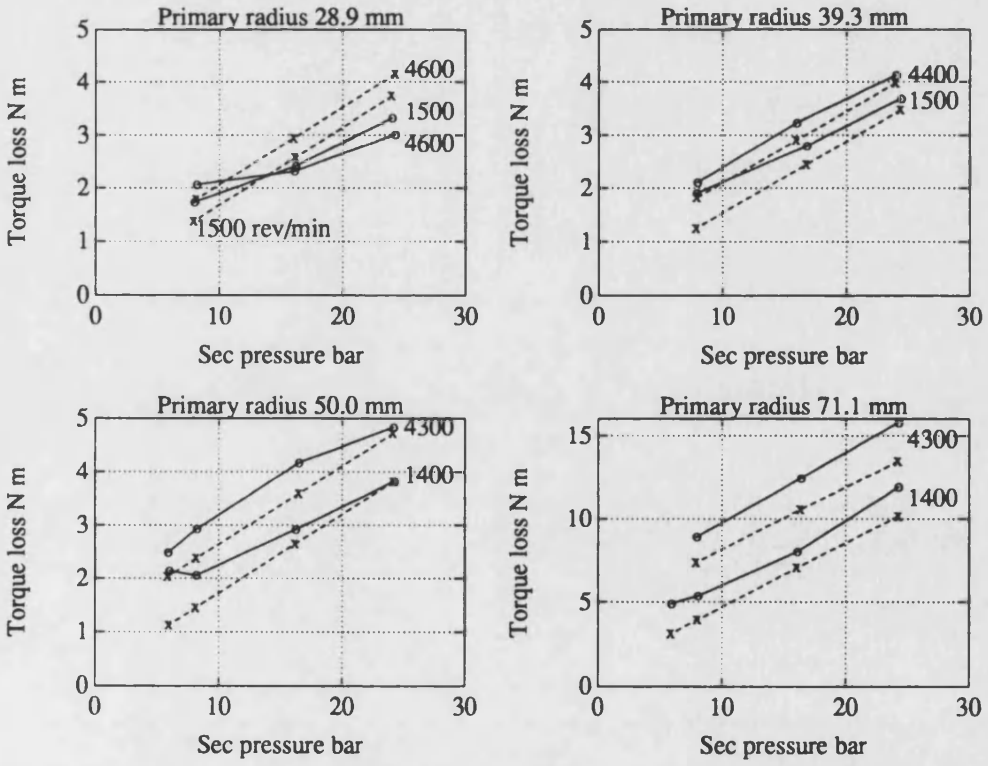

Figure 7.6 Measured (—) and calculated (---) torque losses - 32 N m input

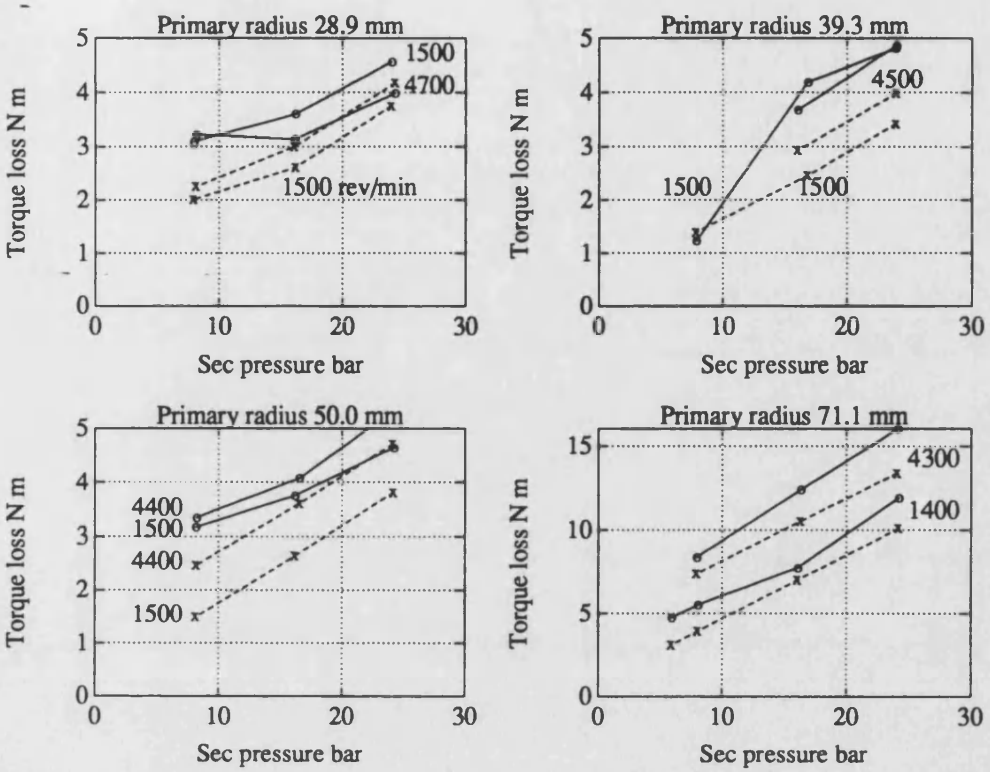

Figure 7.7 Measured (—) and calculated (---) torque losses - 64 N m input

7.7. Inclusion of the torque loss in calculations on the transmission

To include the torque loss in calculations using the overall transmission model it must be dealt with in two parts:

First, to provide for the effect on the secondary pulley, the torque transfer between the segments and the pulley which is ideally the torque delivered, T_s, must be increased by:

$$T_{Ls} = \frac{C_x R_s}{k_s} - CR_s = \frac{T_b R_s}{k_s}(1 - k_s^2) \qquad (7.6)$$

This effect at the secondary pulley will result in extra slip at the secondary pulley, a greater torque transfer at the primary pulley and a correspondingly greater slip at the primary pulley.

Second the torque transfer along the input shaft to the primary pulley must be further increased to provide for the effect on the primary pulley by an amount:

$$T_{Lp} = T_{Lx} - (C_x k_p R_p - C R_p) = \frac{T_b R_p}{k_p}(1 - k_p^2) \qquad (7.7)$$

This will result in an additional extra slip on the primary pulley.

This mechanism of loss not only results in a loss in torque but also in a further small loss due to extra slip.

7.8 The torque loss when the transmission is in an overdrive ratio

Figures 7.3, 7.6 and 7.7 show that the torque loss becomes large when the transmission is in an overdrive ratio and the secondary pulley is operating at the minimum radius. The reason for this is evident if the low speed, no load case is considered.

Introducing the factor k_s into equation 7.1 and then using equation 7.4 gives:-

$$C_L = T_b(1 - k_s^2) = T_b \frac{K^2}{R_s^2}$$

From equation 5.13 it can be shown that at low speed and on no load:

$$T_b = \frac{2F_s \tan\theta}{\beta_s} \qquad \text{so that} \qquad C_L = \frac{2F_s \tan\theta}{\beta_s} \cdot \frac{K^2}{R_s^2}$$

In overdrive, both R_s and β_s are small so that for a given clamping force, F_s, C_L has its largest value. Further, this high value of C_L is then applied to the primary pulley at its largest radius so that the extra torque required is very large when compared with the extra torque at other radii. This effect is ameliorated somewhat as a reduced secondary clamping force can be used when the secondary radius is small without the overall slip becoming excessive. However, this large torque loss in the overdrive ratio is an important feature of the transmission and is commented on further in the discussion of results in chapter 11.

CHAPTER 8

The Effect of Gaps Between the Segments

8.1 Introduction

If two adjacent segments in the belt are pushed apart it will be found that there is an initial total gap, Δ, present. When the belt is operating the lengthening of the bands under tension and the shortening of the segments under compression will both increase this total gap. When the belt is running this gap will be spread out over a length of the belt so that a number of segments will be separated by small gaps. The position of this length is important as if it enters the primary pulley it will cause additional slip in the transmission. This effect was considered by Gerbert [8.1] in 1984 but has not been commented on by other authors since then. His analysis is rather limited as he considers only the case of the pulley radii being equal and does not really address the problem of determining the band speed which has a large influence on the position of the gaps.

8.2 Extra overall slip caused by gaps between segments in the primary pulley

As the belt passes round the primary pulley a compressive force will be built up in the segments because of the torque transfer between the pulley and the segments. During this process the pulley surface will slip forward relative to the segments. If

segments enter the pulley separated by gaps they will be carried round by the pulley with no slip until they meet the slower moving line of closed up segments ahead. This will have the effect of reducing the length of the part of the belt over which the torque is being transferred, the active arc, and will require an increased slip to produce the increase needed in the shear stress. The secondary pulley is unaffected by the presence of gaps.

Gaps in the primary pulley result in extra slip even at zero load. In steady state, continuity requires that the rate of flow of segments across any section perpendicular to the length of the belt is uniform. The closed up line of segments has a speed v_s. If the thickness of a segment is s and h is the gap between segments at a section of the belt where the speed is v, the rates of flow of segments at this section and at a section across the closed up line must be equal and

$$\frac{v_s}{s} = \frac{v}{s+h} \qquad \text{so that} \qquad v = \frac{s+h}{s} v_s \qquad (8.1)$$

Consider the transmission with belt radii R_p and R_s delivering a very small torque so that the active arc on the primary pulley is very small. The segments on the primary pulley where the gaps are equal to h and the speed equal to v will be carried round with zero slip and the pulley speed, n_p, will be v/R_p.

$$n_p = \frac{s+h}{s} \cdot \frac{v_s}{R_p}$$

The segments will pass round the secondary pulley with effectively zero slip as the torque is very small and the pulley speed, n_s, will be given by

$$n_s = \frac{v_s}{R_s}$$

The overall slip, S_l, is given by

$$S_l = 1 - \frac{n_s R_s}{n_p R_p}$$

and, in this case on effectively zero load,

$$S_{lo} = \frac{h}{s + h} \qquad (8.2)$$

Because of this effect of the gaps possibly causing extra slip it is important to determine where on the belt the gaps occur and, in particular, whether or not they occur in the primary pulley.

8.3 The possible positions of the gaps

From the start of the active sector on the primary pulley right round to the outlet from the secondary pulley the belt segments are carrying a compressive load and are tightly pressed together. Thus the gaps can only occur in the remainder of the belt i.e in the straight section as the belt returns from the secondary to the primary pulley and in the inlet sector on the primary pulley.

There are two possible mechanisms for separating the segments:

1. At outlet from the secondary pulley the bands are moving faster than the segments and, because of the shear connection between the two, the bands may carry the segments along the following straight section at a speed greater than v_s and, consequently, with gaps.

2. At inlet to the primary pulley the pulley surface is moving faster than v_s because of slip and may take in segments and carry them round with zero slip, once again at a speed greater than v_s and with gaps, until they meet the slower moving line of closed up segments ahead at the start of the active sector.

There are three likely possibilities for the position of the gaps which are depicted in Figure 8.1.

(a) The segments are separated by the first mechanism at the outlet from the secondary pulley and the total gap available is such that the length of the section with gaps does not extend to the primary pulley and the segments reach the primary pulley as a closed up line moving at v_s.

(b) The segments are separated as in (a) and the section with gaps does extend to the primary pulley. The segments then enter the pulley with gaps, altered by the second mechanism at the entrance, until they meet the closed up line part of the way round the pulley.

(c) The shear force between the bands and the segments at outlet from the secondary pulley is not sufficiently great to separate the segments which will tend to stick together because of the oil film between them. Then the segments will move as a closed up line to the primary pulley with a speed v_s where they will be separated by the second mechanism and enter the pulley with gaps.

There are other possibilities, for example, the shear force between the bands and the segments may not be great enough to separate each segment as it emerges from the secondary pulley but may be so after a number of segments have extended along the straight. Then the segments will continue along the straight as a series of blocks containing equal or differing numbers of segments until they meet the closed up line

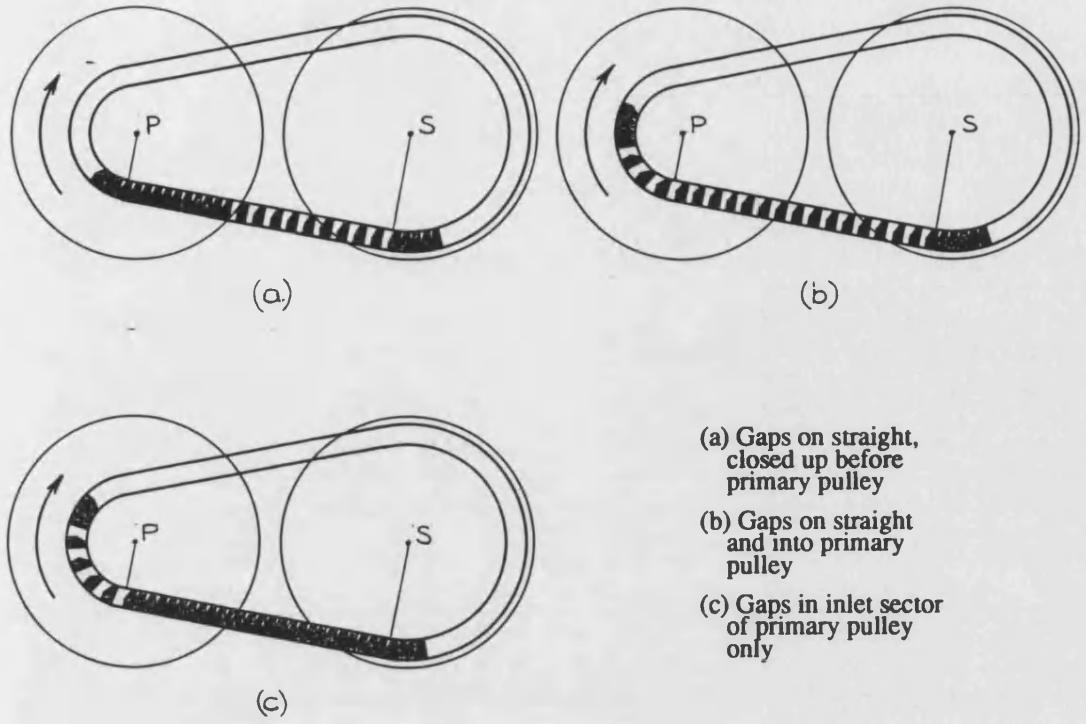

Figure 8.1 The possible positions of the gaps between the segments

ahead as in (a) or (b).

It was shown in chapter 7 that there is likely to be a reverse bend in the belt at outlet from the secondary pulley in order to produce the outward force required to withdraw the segment from the pulley. At the reverse bend the segments must pivot about the outer edge of the segment behind, see figure 8.2, which will ensure that they will all be separated. Thereafter possibility (a) or (b) will occur.

8.4 Experimental determination of the position of the gaps

The position occupied by the gaps between the segments was deduced from measurements of the overall slip for a full range of input torques using belts with three different values of initial total gap, Δ. The standard belt was found to have a total gap equal to 0.80 mm. After testing this was increased to 1.20 mm by grinding

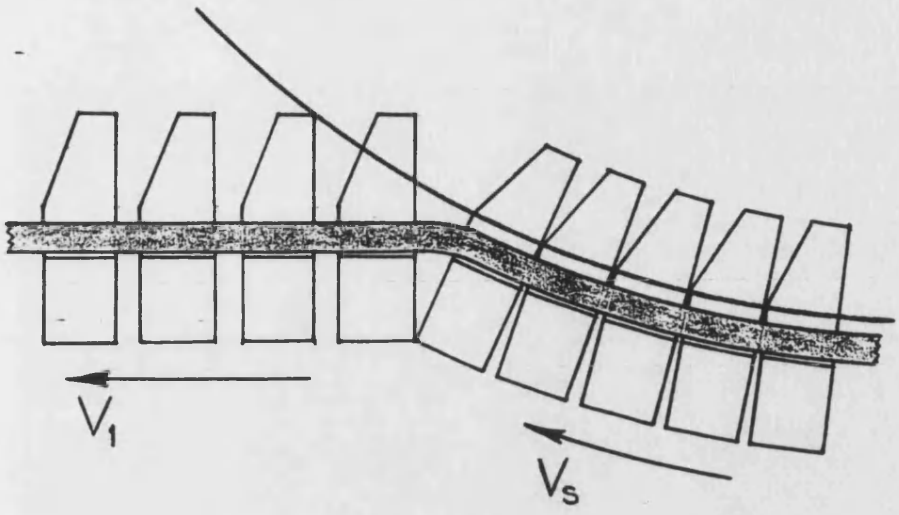

Figure 8.2 Separation of segments by reverse bend in belt at outlet from secondary pulley

0.40 mm off the rear face of one segment and off the locating peg on the segment behind. A final test was carried out with the large gap of 2.984 mm obtained by removing one segment from the belt.

For each set of tests the secondary pulley cylinder was supplied with oil from the separate, external system so that the secondary clamping pressure could be adjusted. The primary cylinder was unpressurised with the moveable pulley half resting on a stop so that the operating radii were fixed. The overall slips in the transmission were measured for a series of constant secondary pressures and input speeds over a full range of input torques.

Figures 8.3 and 8.4 show a comparison of the slips for the standard belt and the belt with the shaved segment with a low and a high input speed respectively. The results show no change in the slip as the initial gap is altered so that the gaps in the belt cannot be entering the primary pulley. The belt must behave as in figure 8.1(a). If behaviour as in (b) or (c) occurred the extra initial gap would increase the length of

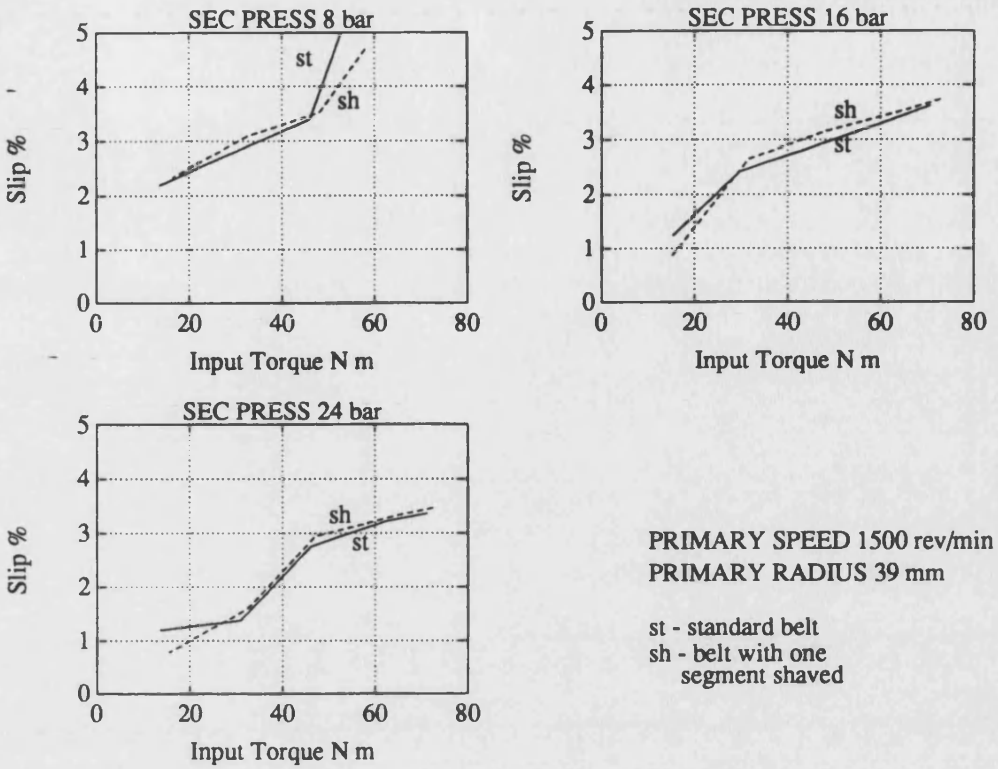

Figure 8.3 Slip measurements with two values of belt total gap

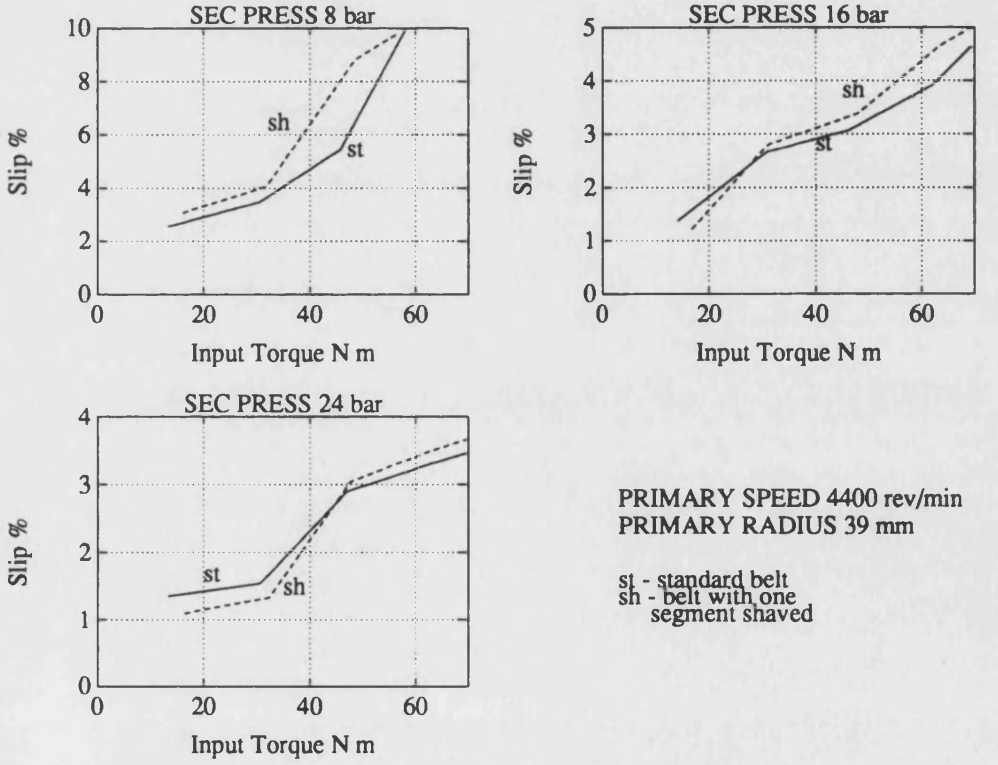

Figure 8.4 Slip measurements with two values of belt total gap

the inlet sector on the primary pulley and give rise to an increased slip.

To ensure that a large gap does give an increased slip the tests were repeated with a segment removed from the belt. The results are shown in figure 8.5 and it can be seen that the extra gap does give the expected increase in slip. Here the belt must be behaving as in figure 8.1(b).

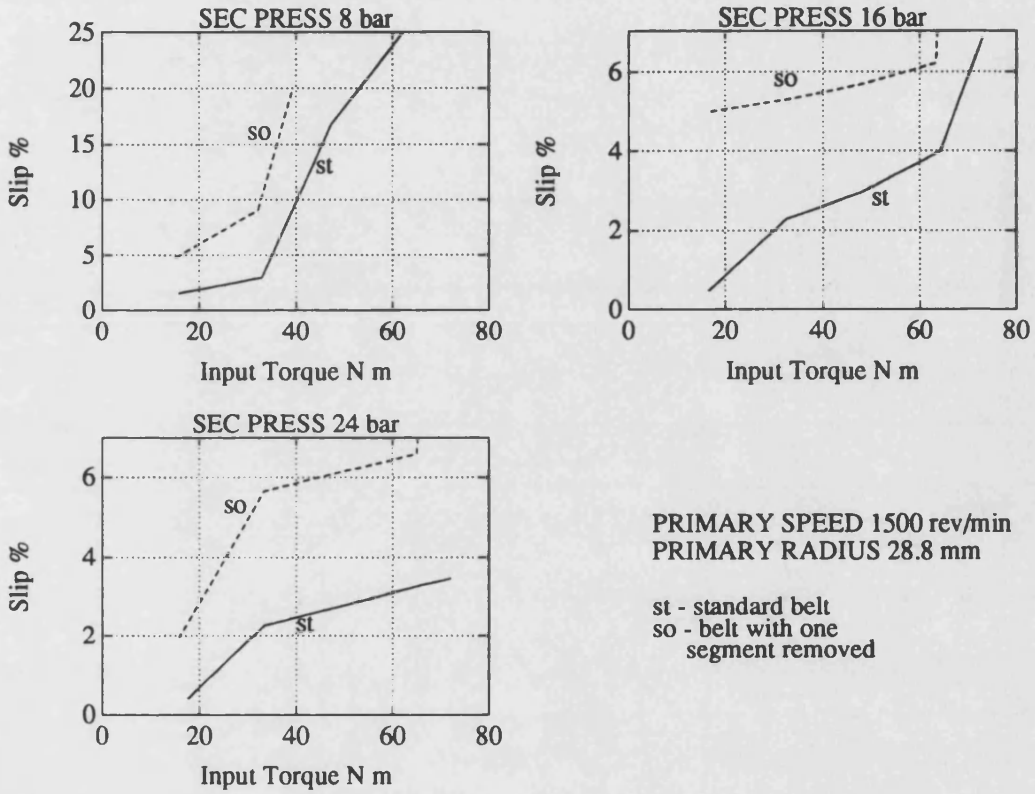

Figure 8.5 Slip measurements with large gap compared with standard

8.5 Theoretical verification of the effect of gaps on slip

The equations governing the effect of the gaps are as follows.

Assume that the separated segments leaving the secondary pulley are carried along with the speed of the inner band, v_1.

Then from equation 8.1 the magnitude of the gaps between the segments on the

straight section is given by

$$h_{st} = s\left(\frac{v_1}{v_s} - 1\right) \qquad (8.3)$$

The total gap, g_t, allowing for the extension of the bands but neglecting the compression of the segments which is small is given by

$$g_t = \Delta + \frac{T_1 L}{w t_b E} \qquad (8.4)$$

If g_t is sufficiently small for the extent of the section with gaps, L_g, to be less than the length of the straight section

$$L_g = \frac{g_t}{h_{st}}(s + h_{st}) = g_t \frac{v_1}{v_1 - v_s} \qquad (8.5)$$

The ratio v_1/v_s is given by equation 5.6. Substituting this expression in equation 8.5 results in

$$L_g = g_t \frac{L + 2\pi x}{L + 2\pi x - Z} \qquad (8.6)$$

where $$Z = \frac{R_p\beta_p(R_p + x)}{R_p + x + 0.5t_b} + (L - R_p\beta_p - R_s\beta_s) + \frac{R_s\beta_s(R_s + x)}{R_s + x + 0.5t_b}$$

The coefficient of g_t in equation 8.6 alters very little with radius and has a value of 80.775 when either radius is a minimum and 80.748 when the radii are equal. The model described in chapter 5 was used to determine the greatest value of the band tension T_1. This was found to be about 800 N when the input torque and speed were as large as possible, the secondary radius was a minimum and the secondary pressure had the very high value of 30 bar. The maximum value of g_t, from equation 8.4, is thus 1.56 mm and the greatest possible value of L_g from equation 8.6 is 126 mm.

The length of the straight section, L_{st}, is

$$L_{st} = \frac{L - R_p\beta_p - R_s\beta_s}{2} \qquad (8.7)$$

It can be shown that the magnitude of L_{st} does not alter much as the belt geometry is altered and is always about 150 mm. The value of the length of the belt with gaps, L_g, is much less than this showing that with the standard belt it is impossible for gaps to enter the primary pulley and cause extra slip.

If, however, the initial gap Δ is sufficiently large for the gaps to enter the primary pulley the equations required are as follows.

The total gap utilised along the straight section, g_{st}, is the number of segments along the straight multiplied by h_{st}.

$$g_{st} = \frac{L_{st}}{s + h_{st}} h_{st} \qquad (8.8)$$

The remaining gap available for the inlet sector of the primary pulley, g_p, is given by

$$g_p = g_t - g_{st} \qquad (8.9)$$

The segments in the inlet sector are carried round by the pulley without slip so that their speed is n_pR_p.

The magnitude of the gap between the segments, from equation 8.1, is then

$$h_p = s\left(\frac{n_pR_p}{v_s} - 1\right) \qquad (8.10)$$

The number of segments in the inlet sector is g_p/h_p and the magnitude of the inlet sector, β_{pi}, is given by

$$\beta_{pi} = \frac{g_p}{h_p} \frac{(s + h_p)}{R_p} \qquad (8.11)$$

The active sector in the inlet pulley, β_{pa}, available for transferring torque is then

$$\beta_{pa} = \beta_p - \beta_{pi} \qquad (8.12)$$

Figure 8.6 shows measured and calculated overall slips plotted against input torque for the standard belt and for the belt with one segment removed. The value of the initial gap, Δ, with one segment removed is sufficiently large for gaps to enter the primary pulley as is shown by the increased slips. The calculated values for this belt were obtained from a computer programme using the system model developed in chap. 5

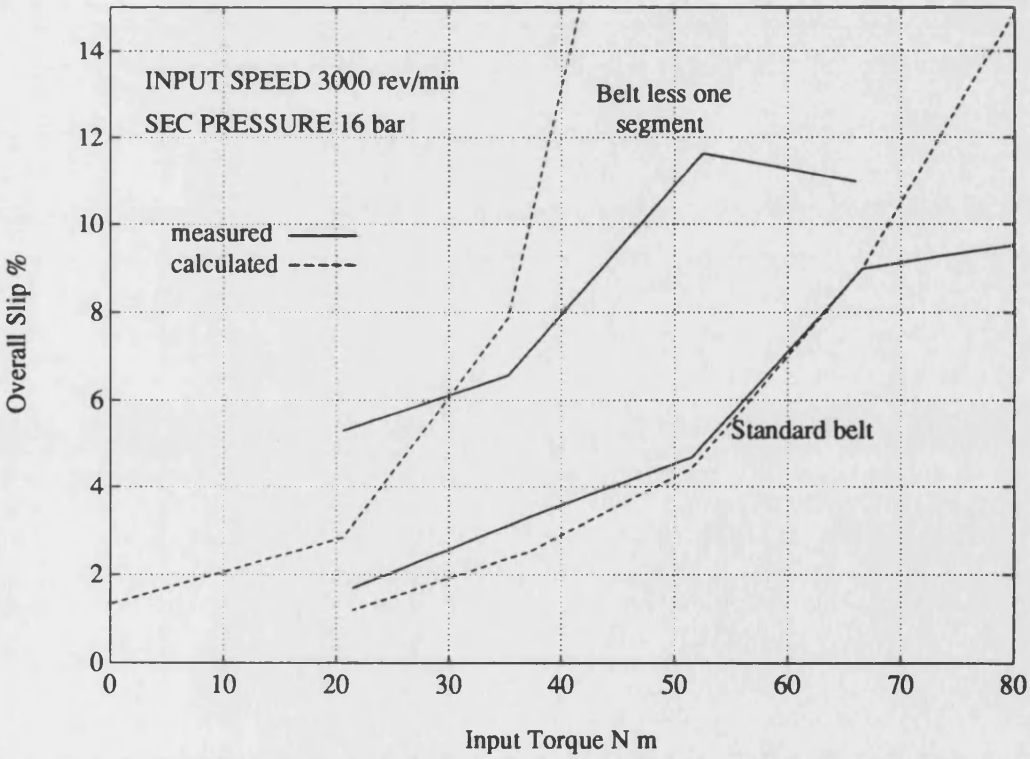

Figure 8.6 Measured and calculated slips for standard belt and belt less one segment - primary radius 29 mm

with the addition of the equations from this chapter. The slip on no-load was obtained by use of equation 8.2.

There is reasonable agreement between the measured and calculated values and the measured curve for the standard belt shows a tendency to pass through the origin as it ought. It is clear that gaps can only affect the overall slip when the initial total gap in the belt is very large. Normal belts have relatively small gaps.

CHAPTER 9

Use of the Model to Determine the Conditions in the Transmission

9.1 Introduction

In this chapter it is shown how the equations developed earlier can be used in order to determine the conditions in the transmission. The procedure proposed was used in the preparation of the computer programmes used to obtain the calculated values of properties for comparison with the values obtained by experiment.

A number of similar computer programmes, all written in Basic, were used, the variations being dictated by such factors as the development of the viscous shear model, alterations in the necessary input parameters and the investigation of the effect of factors like the location of the gaps between the segments. The final programme which embodies all the effects determined in the course of the research is listed in Appendix 3.

The complete programme deals with the conditions on each segment, one by one around a pulley. An alternative procedure is proposed which uses an average condition applied to all the segments on a pulley at once. This gives a very much shorter computation time and the results are still very close to the measured values.

9.2 Choice of the input parameters

The operation of the transmission is fixed by assigning values to five independent parameters. Suitable ones can be chosen by consideration of the standard control system. This controls the operation by means of the two pulley cylinder pressures. The secondary pulley pressure determines the band tension while the primary pressure is used to adjust the belt radii, these quantities being related at an instant by the geometry. As it is easier to determine the primary pressure from the radial velocity of the belt on the pulley rather than the reverse, three of the parameters can usefully be:

the secondary pulley cylinder pressure,

the belt radius on the primary pulley,

the radial velocity of the belt on the primary pulley.

If the calculation was part of a simulation of the vehicle operation, the last two quantities would be known from the previous history. If the secondary pulley pressure is known, it is convenient to start the calculation at this pulley. In order to reduce the amount of iteration in the programme, two further parameters at or near this pulley can be specified, e.g.:

the torque on the output shaft,

the speed of the output shaft.

These five quantities were chosen to be the inputs to the sequence of calculations given below.

9.3 A possible sequence of calculations

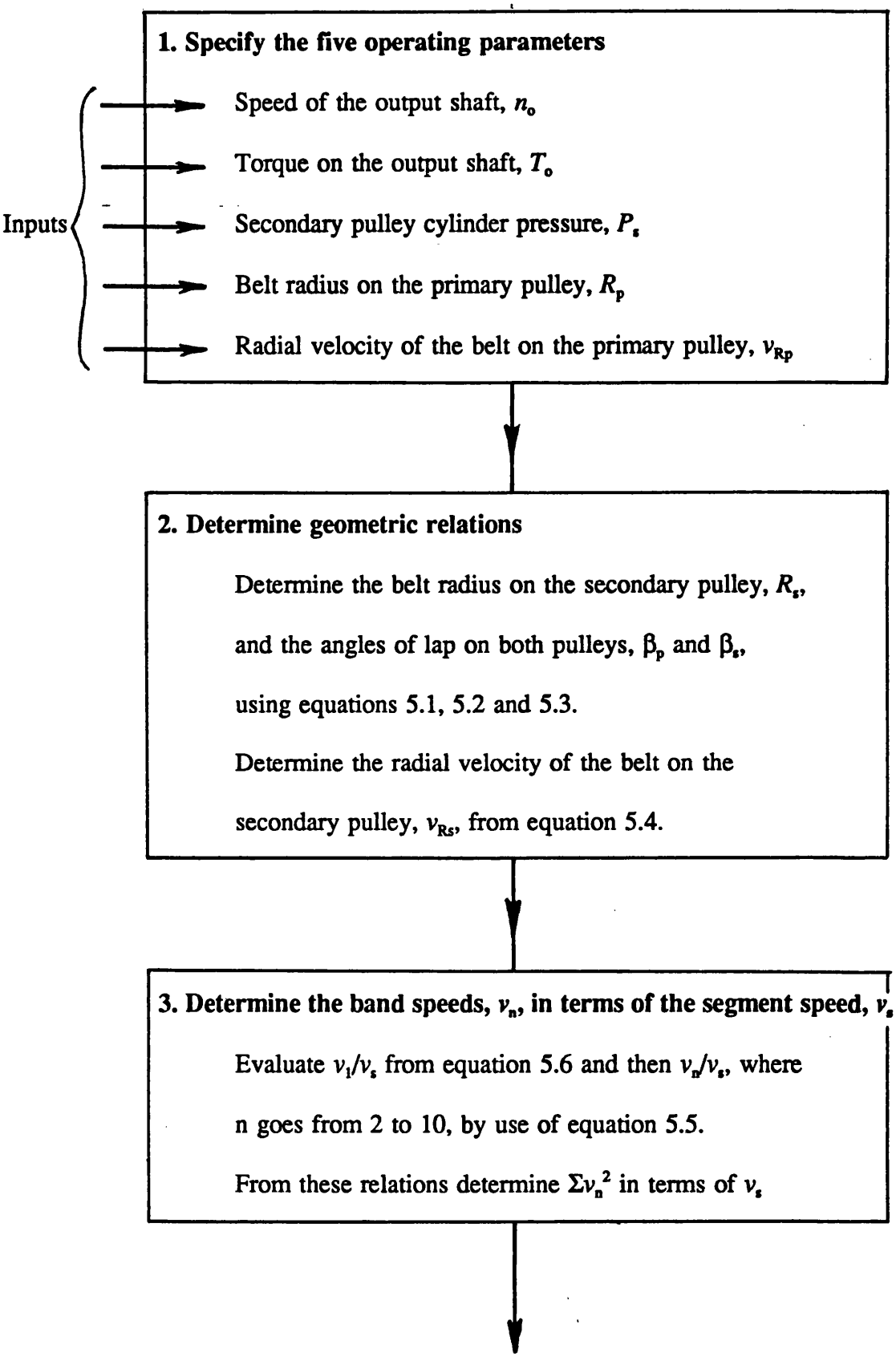

4. Determine the conditions at the secondary pulley

Secondary pulley speed, $n_s = n_o \times R_d$

where R_d is the final drive speed ratio

Secondary pulley torque, $T_s = T_o / R_d \eta_{md}$

where η_{md} is the mechanical efficiency of the final drive

The pulley clamping force, F_s (see section 5.10):

$$F_s = P_s \frac{\pi}{4} (D_{s1}^2 - D_{s2}^2) + F_{sp}$$

5. Evaluate the extra torques, T_{Ls} and T_{Lp}, that must be transferred at the pulleys due to Belt Torque Loss

Evaluate k_p and k_s from equation 7.4

Estimate the total band tension, T_b, from equation 5.13:

multiply the equation by the number of segments on the pulley $R_s\beta_s/s$; assume that the segment compression, C, increases linearly from inlet to outlet; neglect the third term in the brackets; put $v_s = v_n = n_s R_s$ and $C_2 = T_s/R_s$ and note that $C_3 = 0$. Then:

$$\Sigma T_n = T_b = \frac{2F_s \tan\theta}{\beta_s} + \frac{C_2}{2} + v_s^2 \left(\frac{m_s}{s} + \Sigma m\right)$$

Determine T_{Ls} from equation 7.6 and T_{Lp} from 7.7

New ΣT_n

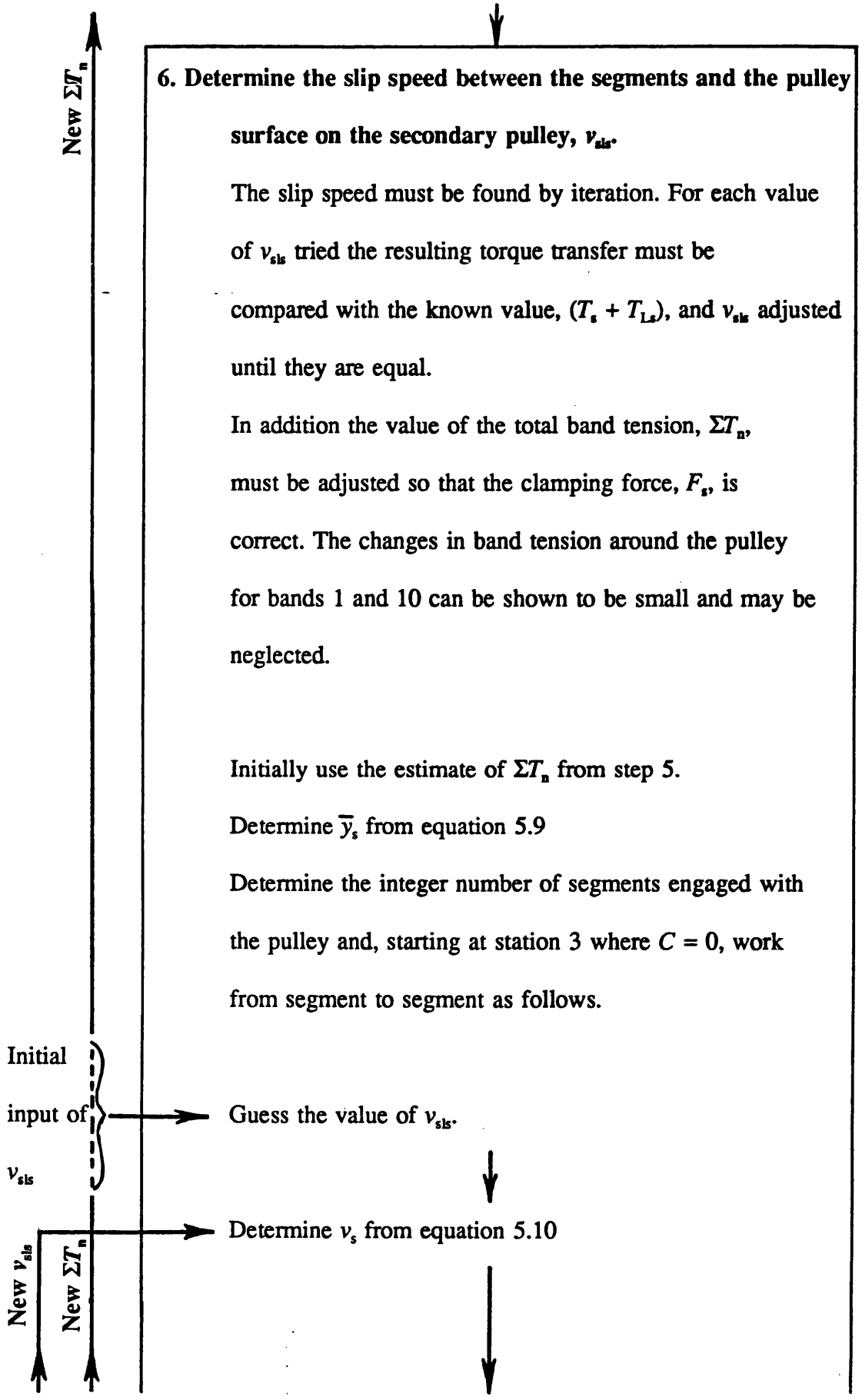
New ΣT_n
6. Determine the slip speed between the segments and the pulley surface on the secondary pulley, v_{sls}.
The slip speed must be found by iteration. For each value of v_{sls} tried the resulting torque transfer must be compared with the known value, $(T_s + T_{Ls})$, and v_{sls} adjusted until they are equal.
In addition the value of the total band tension, ΣT_n, must be adjusted so that the clamping force, F_s, is correct. The changes in band tension around the pulley for bands 1 and 10 can be shown to be small and may be neglected.
Initially use the estimate of ΣT_n from step 5.
Determine $\bar{y}_s$ from equation 5.9
Determine the integer number of segments engaged with the pulley and, starting at station 3 where $C = 0$, work from segment to segment as follows.
Initial input of v_{sls}
Guess the value of v_{sls}.
Determine v_s from equation 5.10
New v_{sls}
New ΣT_n

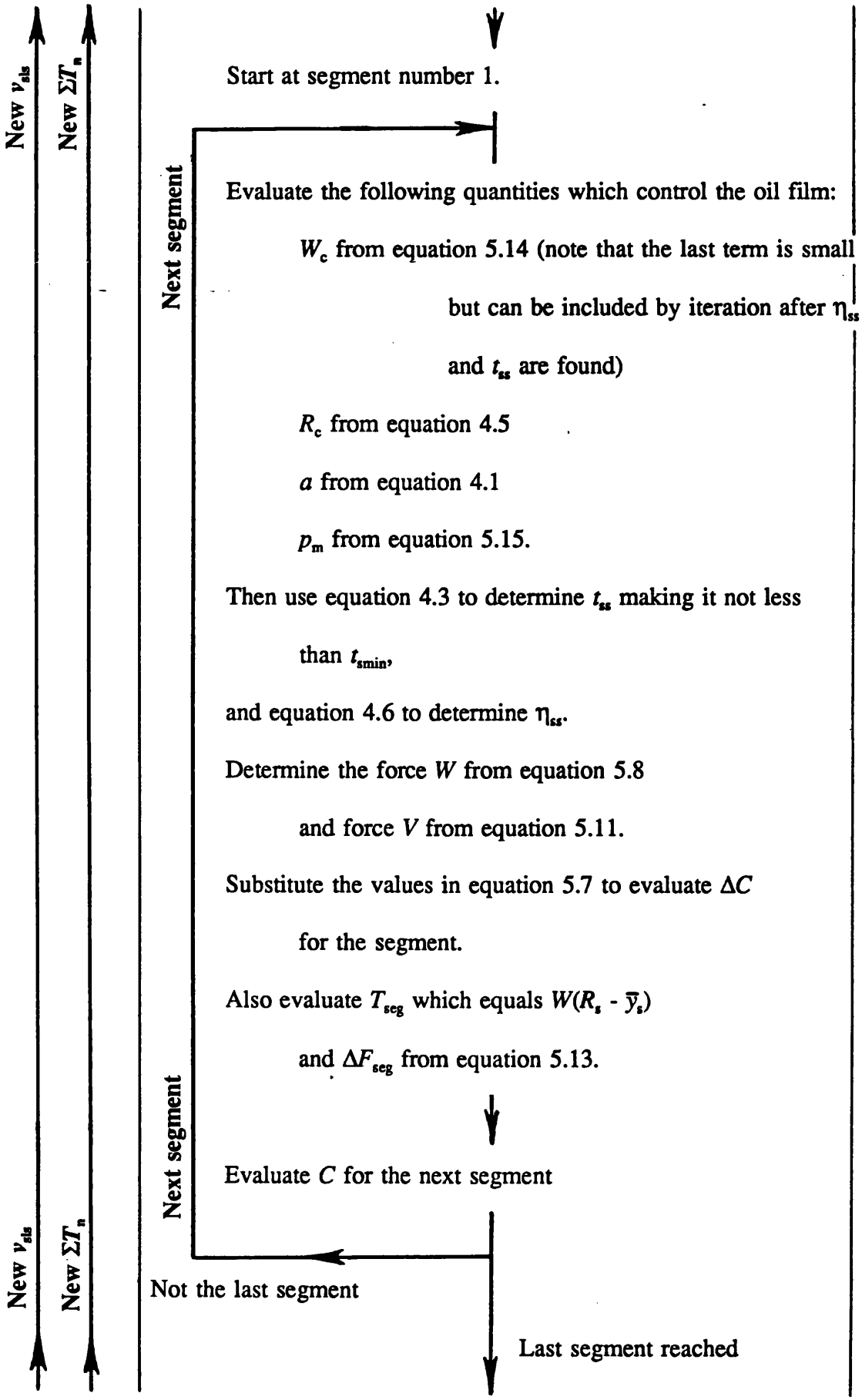
New v_{sls}
New ΣT_n
Start at segment number 1.
Next segment
Evaluate the following quantities which control the oil film:
W_c from equation 5.14 (note that the last term is small but can be included by iteration after η_{ss} and t_{ss} are found)
R_c from equation 4.5
a from equation 4.1
p_m from equation 5.15.
Then use equation 4.3 to determine t_{ss} making it not less than t_{smin},
and equation 4.6 to determine η_{ss}.
Determine the force W from equation 5.8
and force V from equation 5.11.
Substitute the values in equation 5.7 to evaluate ΔC for the segment.
Also evaluate T_{seg} which equals $W(R_s - \bar{y}_s)$
and ΔF_{seg} from equation 5.13.
Next segment
Evaluate C for the next segment
Not the last segment
Last segment reached
New v_{sls}
New ΣT_n

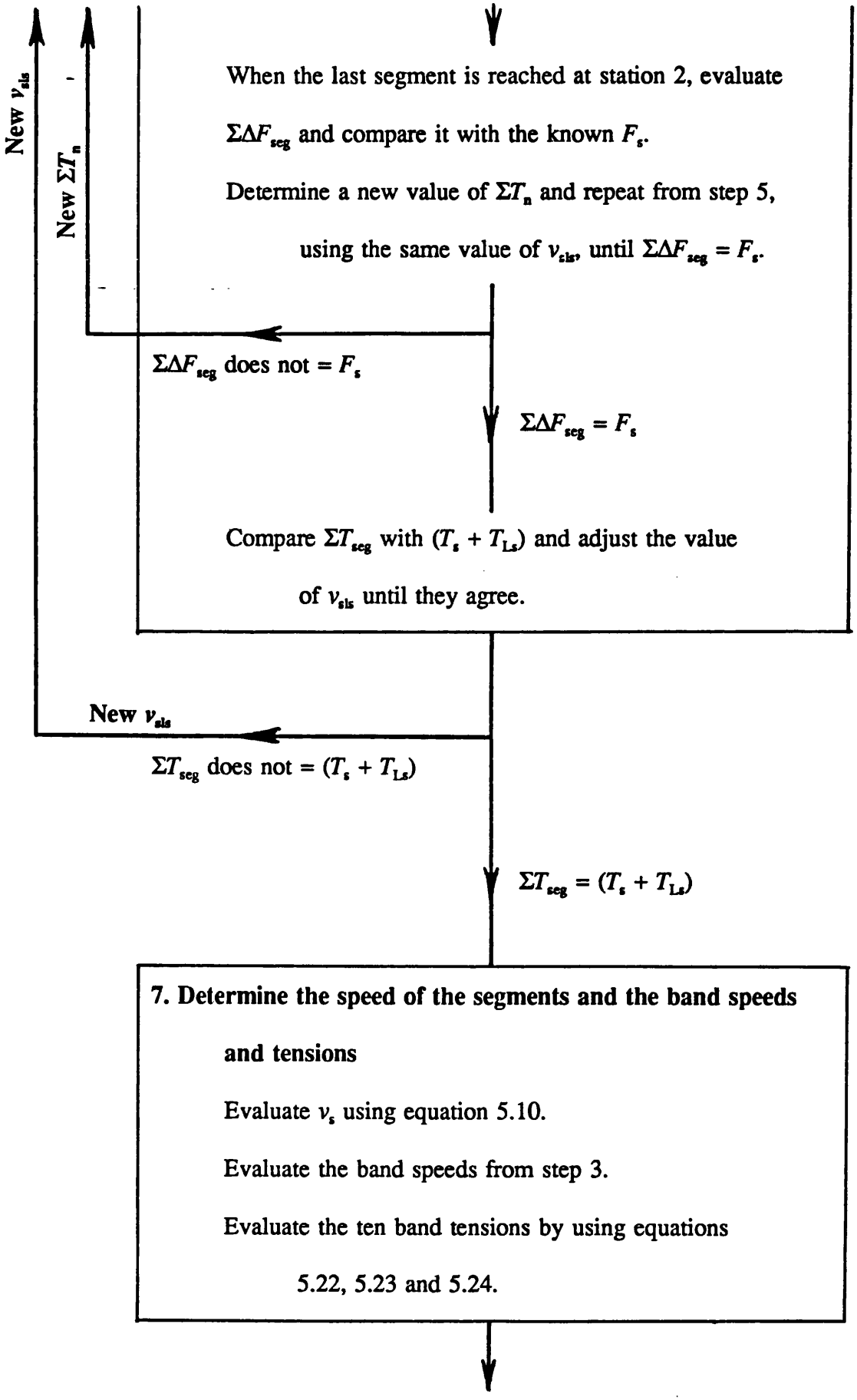
When the last segment is reached at station 2, evaluate
$\Sigma\Delta F_{seg}$ and compare it with the known F_s.
Determine a new value of ΣT_n and repeat from step 5,
using the same value of v_{sls}, until $\Sigma\Delta F_{seg} = F_s$.
New ΣT_n
New v_{sls}
$\Sigma\Delta F_{seg}$ does not = F_s
$\Sigma\Delta F_{seg} = F_s$
Compare ΣT_{seg} with $(T_s + T_{Ls})$ and adjust the value
of v_{sls} until they agree.
New v_{sls}
ΣT_{seg} does not = $(T_s + T_{Ls})$
$\Sigma T_{seg} = (T_s + T_{Ls})$
7. Determine the speed of the segments and the band speeds
and tensions
Evaluate v_s using equation 5.10.
Evaluate the band speeds from step 3.
Evaluate the ten band tensions by using equations
5.22, 5.23 and 5.24.

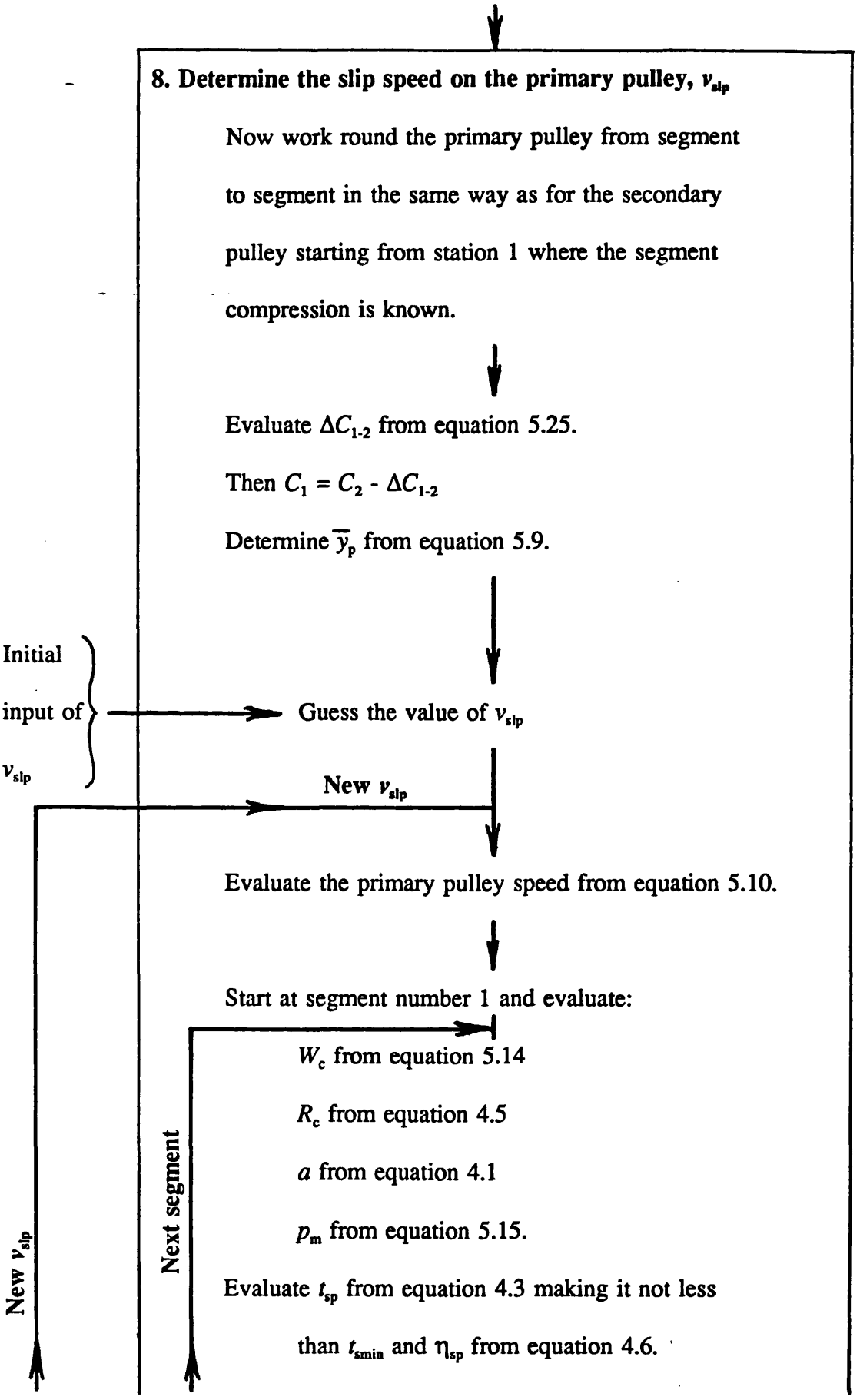
8. Determine the slip speed on the primary pulley, v_{slp}
Now work round the primary pulley from segment to segment in the same way as for the secondary pulley starting from station 1 where the segment compression is known.
Evaluate $\Delta C_{1\text{-}2}$ from equation 5.25.
Then $C_1 = C_2 - \Delta C_{1\text{-}2}$
Determine $\bar{y}_p$ from equation 5.9.
Initial input of v_{slp}
Guess the value of v_{slp}
New v_{slp}
Evaluate the primary pulley speed from equation 5.10.
Start at segment number 1 and evaluate:
W_c from equation 5.14
R_c from equation 4.5
a from equation 4.1
p_m from equation 5.15.
Evaluate t_{sp} from equation 4.3 making it not less than t_{smin} and η_{sp} from equation 4.6.
Next segment
New v_{slp}

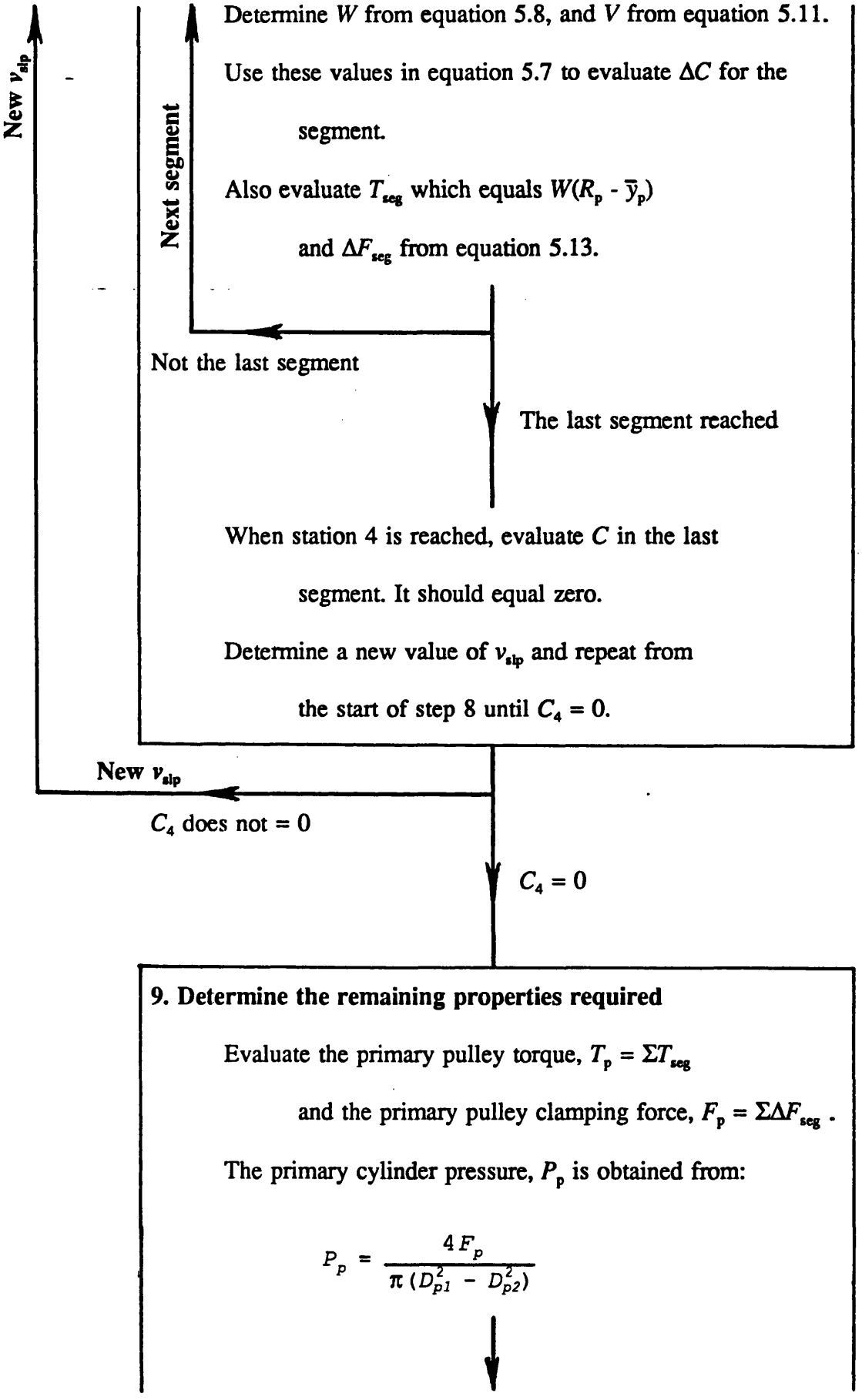
New v_{slip}
Next segment
Determine W from equation 5.8, and V from equation 5.11.
Use these values in equation 5.7 to evaluate ΔC for the segment.
Also evaluate T_{seg} which equals $W(R_p - \bar{y}_p)$
and ΔF_{seg} from equation 5.13.
Not the last segment
The last segment reached
When station 4 is reached, evaluate C in the last segment. It should equal zero.
Determine a new value of v_{slip} and repeat from the start of step 8 until $C_4 = 0$.
New v_{slip}
C_4 does not = 0
$C_4 = 0$
9. Determine the remaining properties required
Evaluate the primary pulley torque, $T_p = \Sigma T_{seg}$
and the primary pulley clamping force, $F_p = \Sigma \Delta F_{seg}$.
The primary cylinder pressure, P_p is obtained from:
$$P_p = \frac{4F_p}{\pi (D_{p1}^2 - D_{p2}^2)}$$

Evaluate the torque required to drive the oil pump, T_g from equation 5.26.

The torque input to the transmission, T_i, is:

$$T_i = T_p + T_{Lp} + T_g$$

Determine the overall slip from:

$$S_l = 1 - \frac{n_s R_s}{n_p R_p}$$

and the overall efficiency from $\eta_{mo} = T_o n_o / T_i n_p$

10. Output of the properties determined

The following properties, determined during the calculations, can be printed out:

Pulley radii, R_p and R_s

Pulley angles of lap, β_p and β_s

Radial velocity of belt on pulleys, v_{Rp} and v_{Rs}

Belt speed, v_s

Band speeds, v_1 to v_{10}

Compression in segments at station 2, C_2

Band tensions at station 1, $T_{1,1}$ to $T_{10,1}$

Pulley clamping forces, F_s and F_p

Pulley cylinder pressures, P_s and P_p

Input and output speeds, n_i and n_o

Input and output torques, T_i and T_o

Torque to drive the oil pump, T_g

Extra torques on pulleys from torque loss, T_{Ls} and T_{Lp}

Overall slip, S_i

Overall mechanical efficiency, η_{mo}

9.4 A simplified sequence of calculations

The computation time can be considerably reduced if the segment by segment treatment of the belt around the pulleys is replaced by an average treatment of the segments.

In step 6 for the secondary pulley, when the quantities which control the oil film are evaluated, the average value of W_c can be found as follows.

If equation 5.13 is applied to the average segment and then multiplied by the number of segments engaged with the pulley, $R_s\beta_s/s$, the left hand side of the equation becomes F_s:

$$F_s = \frac{\beta_s}{2\tan\theta}\left[\Sigma T_n - C - \frac{m_s v_s^2}{s} - \Sigma m v_n^2\right] + \frac{2acR_s\beta_s}{s\sin\theta\cos\theta}\cdot\frac{v_{Rs}\eta_{ss}}{t_{ss}}$$

The part in the square brackets is the average value for the segments and can be substituted directly into equation 5.14 to give the average value of W_c.

$$W_c = \frac{sF_s}{R_s\beta_s\cos\theta} - \frac{2av_{Rs}\eta_{ss}}{t_{ss}\sin\theta}\left(\frac{cs}{\cos^2\theta} - 1\right)$$

Proceed with the calculation to determine the average value of the force W and determine the torque on the pulley:

$$T = W(R_s - \bar{y}_s) \text{ x number of segments}$$

Then adjust the value of the slip speed, v_{sk}, until this torque is equal to the known torque ($T_s + T_{Ls}$).

The primary pulley is treated similarly.

This average treatment of the segments reduces the computation time considerably and gives results very close to those from the segment by segment treatment as will be shown in Appendix 2.

CHAPTER 10

Description of Tests Carried Out and Evaluation of Results

10.1 Introduction

The tests carried out on the transmission can be divided into three sets.

The First set involved accelerations at full throttle from rest and decelerations from high speed with closed throttle both on a simulated level road and up a 10% gradient, the standard control system incorporated in the transmission being used. These tests were done to investigate the characteristics of the control system and to check the instrumentation. Test 2, acceleration on a level road, resulted in the belt radii moving over most of the range with large changes in the pulley cylinder pressures and was used to evaluate the two empirical viscous constants, η_{oil} and α_{η}. A similar test was used by Becker [10.1] to validate his model and a comparison of the two results is of interest.

The Second set was a series of steady state tests, still with the standard control system, in each of which the output shaft from the transmission was constrained by the dynamometer to run at a constant speed. It provided interim data for the development of the transmission model but was later superseded by the third set of tests which were able to cover the whole operating envelope of the transmission by using a separate control system. A few tests in the second set, with high input torques

and the primary radius a minimum, revealed very large overall slip values. In order to determine whether the large slip was occurring between the belt and the pulleys or in the clutch, a further speed transducer was fitted to measure the primary pulley speed. This revealed that the clutch was slipping in these cases. A further test showed that the reverse clutch could be made to slip with quite modest input torques.

In an attempt to resolve a controversy which had arisen over whether or not the magnitude of the initial gap between the segments affected the overall slip, the whole set of tests was repeated with a larger initial gap obtained by the removal of a segment from the belt. This did show increased slips which misled the development of the transmission model until the issue was eventually resolved as explained in Chapter 8.

The Third and final set was also a series of steady state tests but with the transmission under external pressure control and with the belt radii fixed so that the whole operating envelope was covered. The pressurising oil pump was not needed in these tests and was removed. The results showed that under light load conditions the viscous shear model could be improved by the addition of an empirical minimum film thickness, t_{smin}. Further tests were carried out in this set in order to resolve particular problems. In one series, the transmission was run without a belt to measure the losses in the input line over a range of speeds. In another, the transmission was run with a coupling in the output shaft removed so that the no-load torque loss could be measured. Finally the effect of the initial gap in the belt on the overall slip was resolved by running a series of tests at a particular pair of radii first with one segment removed from the belt and then with the segment replaced but reduced in thickness by 0.4 mm to give a small increase in the total gap. This last was the final test as the

belt was now in a non standard condition.

Tables of measured values are shown in Appendix 4.

10.2 Checks on the instrumentation

When the first measurements were obtained they were assessed to ensure that they were reliable. The following comments may be made about some of them:

1. Belt radius measurements

The running of the probe wheels on the belt, figure 6.8, was found to be very satisfactory. The visible parts of the probe spindle were seen to be very steady during running and whenever the transmission was returned to the low ratio position the measured values, too, returned to the calibrated values. The geometrical equations in chapter 5, equations 5.1, 5.2 and 5.3, can be used to check the compatibility of the measured values away from the calibration points.

For example, from the steady state results line B1, Appendix 4, Table 1:

R_p = 28.80 mm $\quad$ R_s = 74.54 mm $\quad$ C = 889 N

P_s = 22.69 bar $\quad$ v_s = 4.62 m/s

These radii are in the calibration position and may be assumed to be correct.

Using the equations with X = 155 mm, the belt length, L = 648.25 mm.

The approximate equation for the band tension, from equation 5.13:

$$T_b = \frac{2F_s \tan\theta}{\beta_s} + \frac{C}{2} + m_b v_s^2 \qquad (10.1)$$

can be used to show that the total band tension is 2866 N.

This tension gives an increase in the length of the bands equal to 0.27 mm so that the unloaded length of the belt is 647.98 mm.

At the other extreme in high ratio, e.g. line B14

R_p = 72.75 mm R_s = 32.00 mm C = 290 N

P_s = 7.48 bar v_s = 27.15 m/s

Here the tension is 2361 N giving an increase in the length of the bands of 0.22 mm Hence the band length in this case is 648.20 mm.

If the measured value of R_p is correct, R_s ought to be 31.36 mm and the error in measuring R_s is +0.64 mm.

But if the measured R_s is correct, R_p ought to be 72.30 mm and the error in measuring R_p is + 0.45 mm.

As both probes are identical it is considered likely that both will be equally in error in high ratio when both are furthest from the calibration position. Halving both errors gives results compatible with the belt length so that both radii are probably in error by about +0.30 mm, an acceptable amount.

As a check that intermediate values are equally in agreement, consider a case where the two radii are approximately equal, e.g. line B3. A similar process dividing the error equally between the two measurements shows the error to be about +0.04 mm, a negligible amount.

It appears that, away from the calibration position in low ratio, both probes give measurements which are slightly too big but are not appreciably in error until close to the high ratio position. The maximum error is in the region of 0.30 mm, about 0.7% of the radii range, an acceptable result.

2. Speed measurement

When the rig was first run, the measured speeds of the input and output shafts were checked against a hand held tachometer which counted the revolutions of the shaft couplings. The results agreed within a few revolutions per minute.

When the primary pulley speed was introduced the measurements of the input shaft speed and the primary pulley speed which must be equal were very close. The pulley speed was usually greater than that of the input shaft but the two were mostly within 6 rev/min of each other. The biggest difference, recorded on one occasion only, was 13 rev/min. At all other times the values were within 10 rev/min. The claimed accuracy of the counting circuit was that a measurement would be within 0.1% of the maximum. With a maximum speed of 5000 rev/min, the maximum error would then be 5 rev/min which is compatible with virtually all of the measurements.

The belt speed was found to be compatible with the pulley speeds, being between the two pulley surface speeds in a convincing way. The surface speed of a pulley was determined at the radius of the rocking edge on the segments, the effective belt radius. The following table shows the pulley surface speeds and the belt speed, all in m/s, for three sets of results from the first steady state tests, B1, B3 and B14. The primary radius for the three is, respectively, minimum, mid and maximum.

	Primary	Belt	Secondary
B1	4.78	4.62	4.44
B3	10.31	10.22	10.04
B14	27.53	27.15	26.86

It appears likely that the claimed accuracy for the speed measurements, 0.1% of the maximum value, was achieved.

3. The overall slip

The overall slip, S_1, for the transmission is an important quantity in this work and very dependent on the accuracy of the measurements. It is given by:

$$S_1 = 1 - \frac{n_s R_s}{n_p R_p} \qquad (10.2)$$

The slips used in the analysis in this work were calculated from the recorded values. The range of error is shown in the following table which takes as an example the same three steady state tests as before, B1, B3 and B14. It assumes that the speeds have errors of ±0.1% of the maximum. Overall slips %:

	Recorded values	Max value	Min value	Range%
B1	7.10	8.70	5.50	±23
B3	2.66	3.37	1.95	±27
B14	2.45	2.68	2.21	±10

If the measured radii are corrected as deduced in section 1 above, the slip for B14 is 3.09%, an error of +26% on the slip used.

It would appear that the calculated slips have a range of error approaching ±30%. This is perhaps shown by the scatter on the slip values for Test 2, Figure 10.2(a). This graph shows a succession of about 420 slips calculated from a series of measurements.

10.3 The first set of tests

These tests were carried out with the transmission controlled by the standard control system and with the dynamometer providing a resisting torque simulating the road load for the vehicle.

For the acceleration tests the simulated vehicle started from rest, i.e. with the flywheel stationary and the engine idling. The data collection system was set to record measurements at small intervals and the engine throttle was opened fully. The deceleration tests were run similarly but starting with the rig running at near maximum speed with the throttle wide open. Immediately after the data collection was started the throttle was fully closed.

Test 1 was used to investigate the starting sequence for the control system and the recording interval was 10 ms, the test lasting only 7 seconds. The results of this test are shown in figure 10.1(a) and (b), all the measured quantities being plotted against time. The graph for the throttle angle is marked with the control operations that can be deduced from the test results.

Test 2 was a full throttle acceleration test to near maximum speed with 50 ms recording intervals and lasting 26 seconds. The measured results plotted against time are shown in figure 10.2(a) and (b). It can be seen that the control system allows the engine speed to rise steadily from 4000 to 4700 rev/min during the run giving quite a good acceleration but not the maximum possible which would be obtained with the engine at 5000 rev/min. A car speed of 100 kilometers per hour occurs at a transmission output speed of 945 rev/min so that the 0 - 100 km/h acceleration time

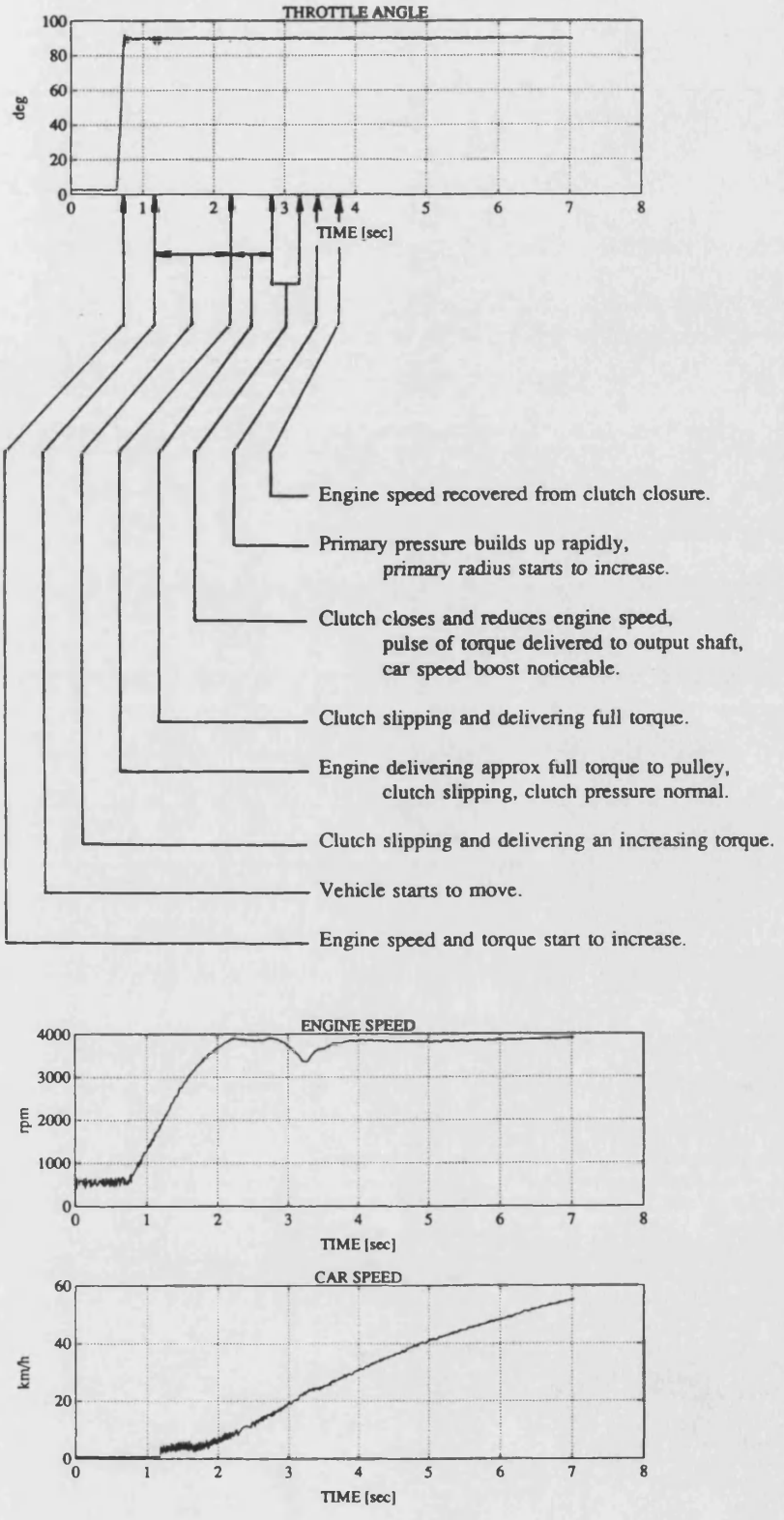

Figure 10.1(a) Test 1. Results for a full throttle acceleration showing the starting sequence for the standard control system

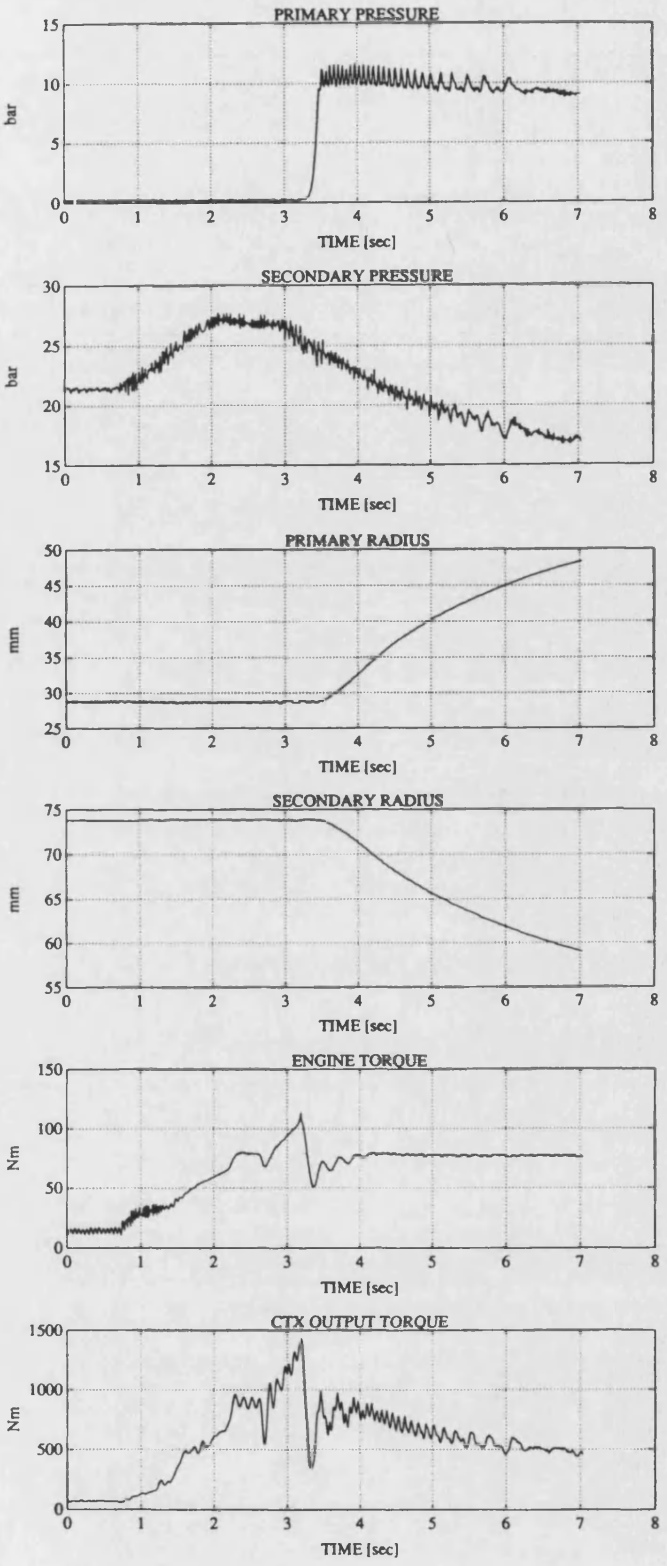

Figure 10.1(b) Test 1. Results for a full throttle acceleration (continued)

is about 17 seconds, a modest value.

It can be seen that the secondary pressure is high at the start of the acceleration to avoid excessive slip on the primary pulley where the engine torque is being fed into the belt at a small radius. It steadily reduces as the primary radius increases so that when this radius is large both the pump loss and the belt torque loss will be limited. The overall slip curve starts at the time of 5 seconds, after the clutch has closed, to avoid the curve starting at 100% slip and then suppressing the detail over the majority of the time when the slips are small.

In his paper, Becker [10.1] showed results from a full throttle acceleration test. One of his graphs showed Overall Slip plotted against Time and may be directly compared with the slip graph in figure 10.2(a). His graph is reproduced in figure 3.5. The slips agree at about 5 seconds but at 25 seconds his slip is only about one third of the value obtained here. The slips determined here are considered to be the more accurate as they are based on radius measurement while his were not.

Test 3 was a deceleration from maximum speed shown in figure 10.3. The output speed at the start of the test corresponds to a vehicle speed of approximately 92 miles per hour. As this is close to the normal maximum speed of the vehicle simulated it can be seen that the road load relation used in the programme for the dynamometer is accurate. The immediate reaction of the control system to the throttle closure is to reduce both pulley pressures and then to rapidly raise the primary pressure so that the belt moves to a maximum radius position on the primary pulley, causing the engine speed to reduce. Thereafter the braking effect on the vehicle is small so that the speeds slowly reduce with other conditions in the system remaining constant. The time

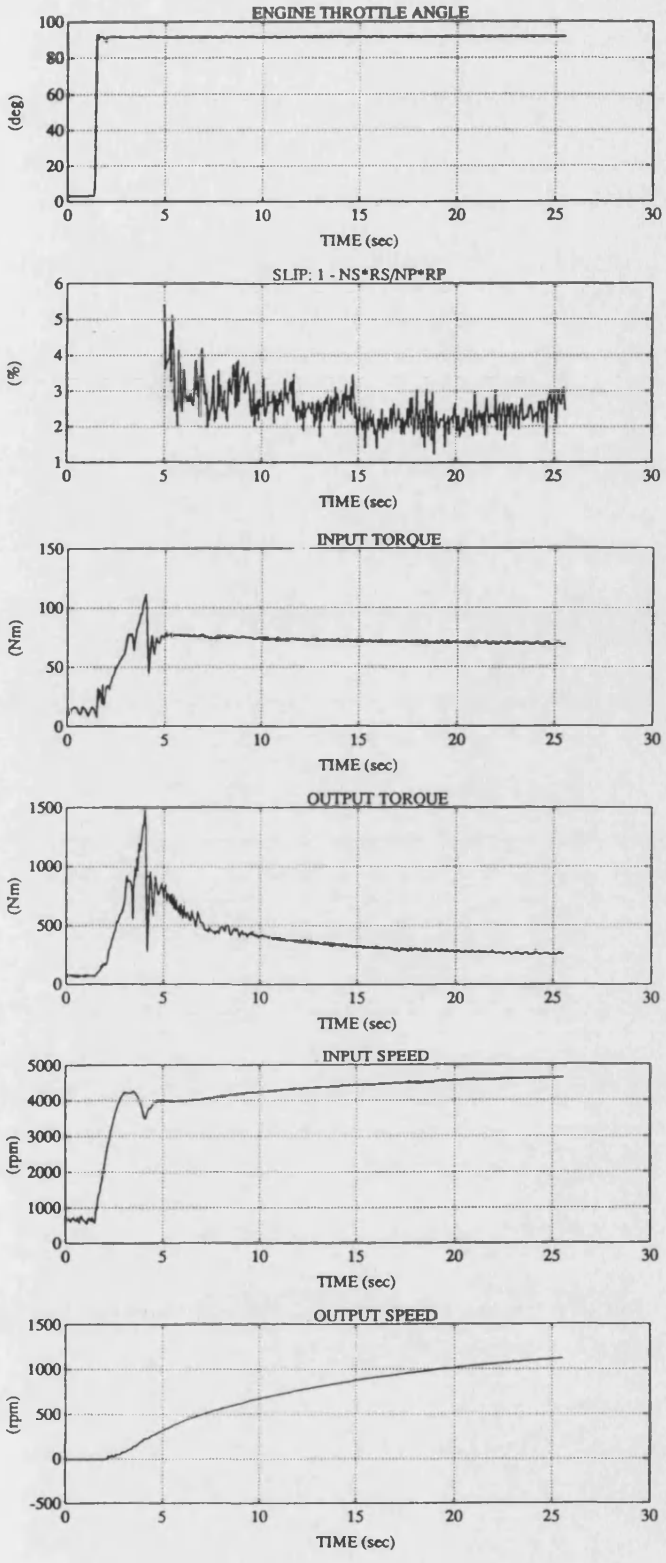

Figure 10.2(a) Test 2. Results for a full throttle acceleration on a level road to near maximum speed

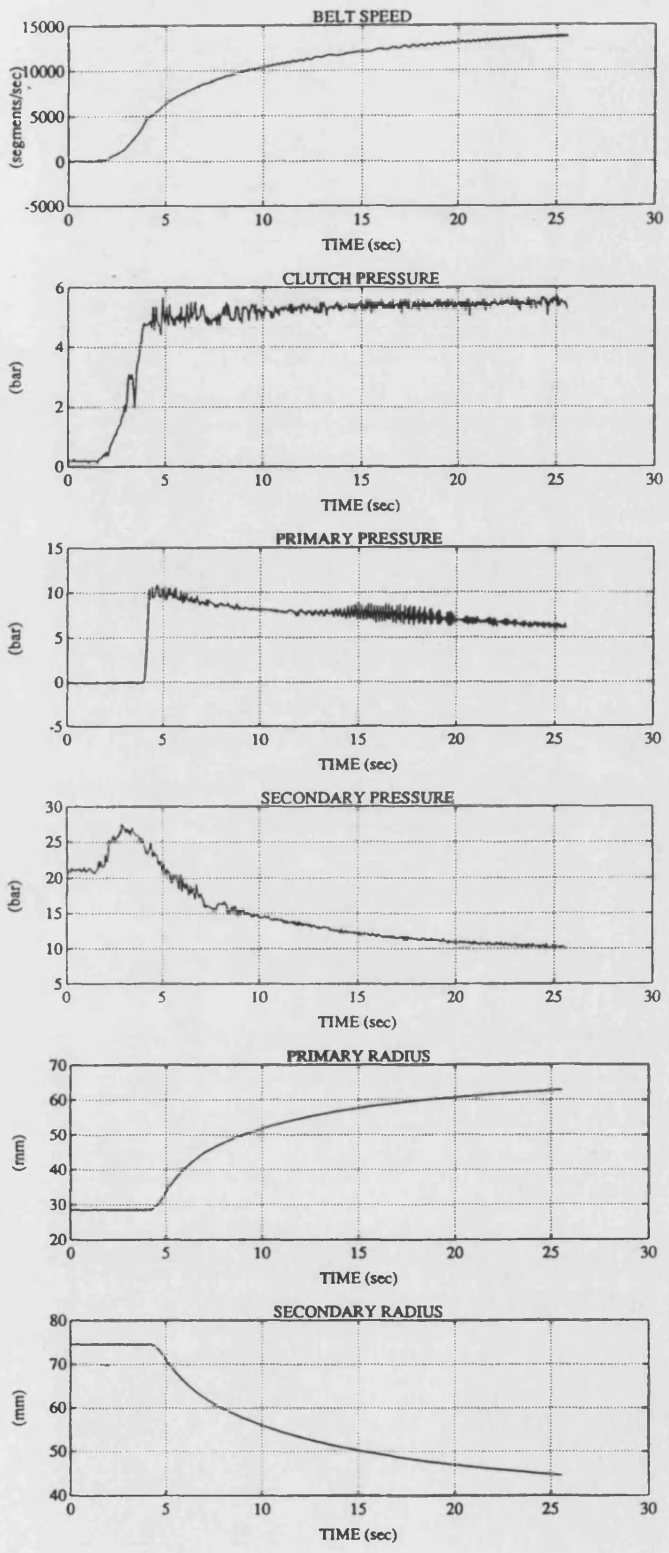

Figure 10.2(b) Test 2. Results for a full throttle acceleration (continued)

available for the test was not long enough for the vehicle to come to rest and the control sequence for stopping is not shown.

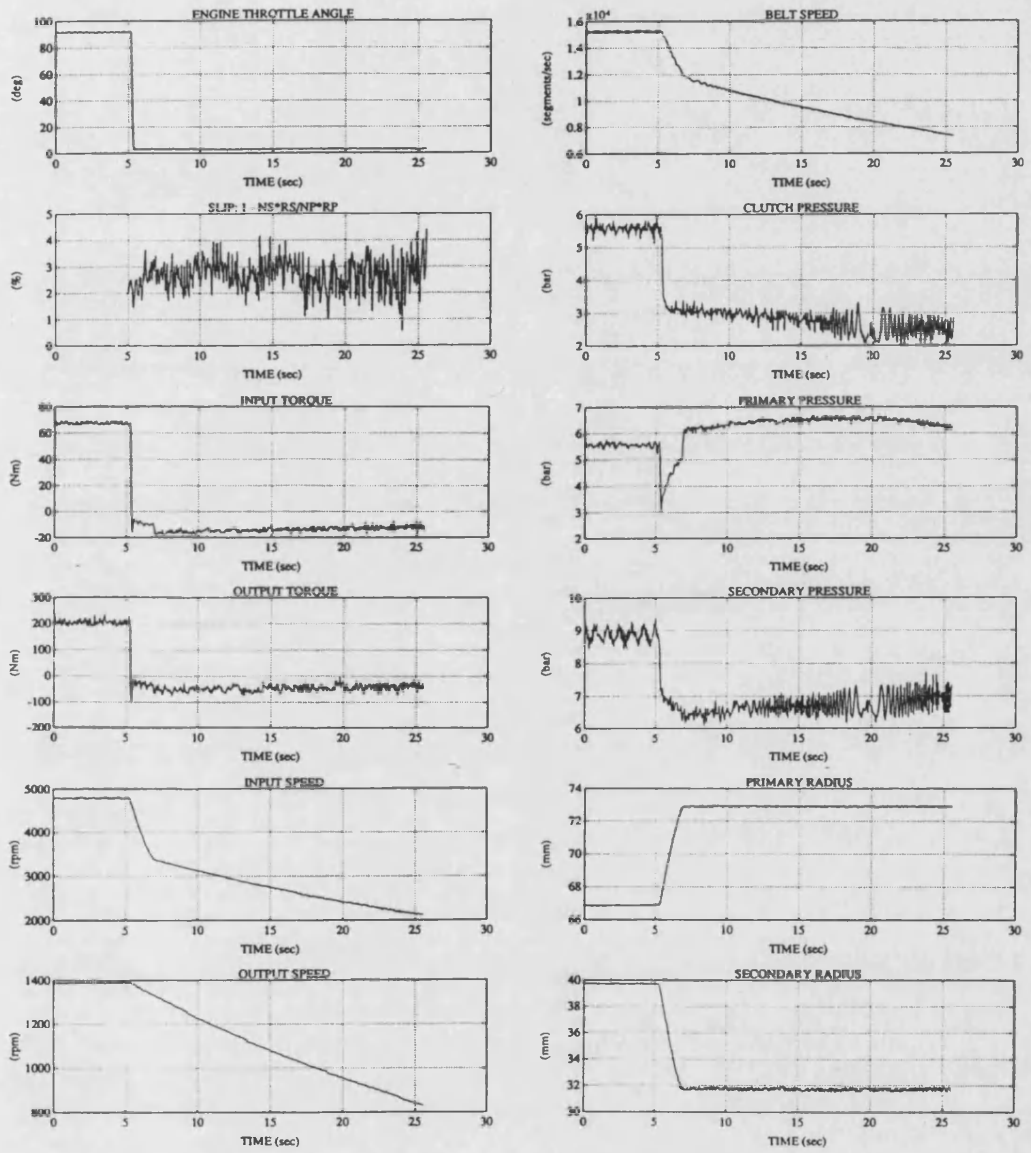

Figure 10.3 Test 3. Results for a closed throttle deceleration on a level road from maximum speed

Test 4, an acceleration up a 10% incline, is shown in figure 10.4. It shows that there are no particular control changes to deal with the extra load, the normal changes are just delayed. The results are virtually the first 13 seconds of Test 2 expanded to fill the 26 seconds.

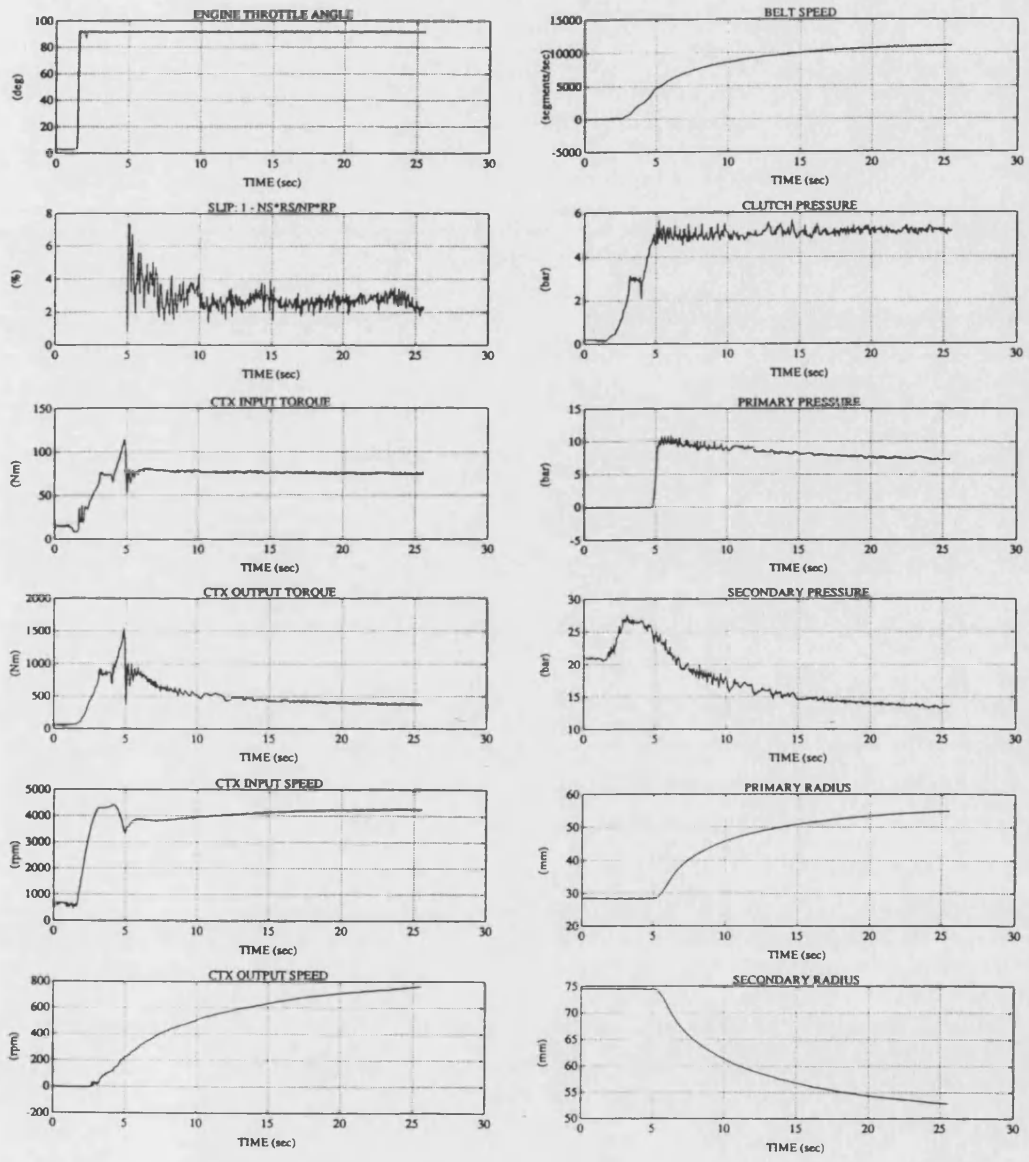

Figure 10.4 Test 4. Results for a full throttle acceleration from rest up a 10% incline

Test 5, a deceleration from maximum speed with closed throttle up a 10% incline, is shown in figure 10.5. Towards the end of the test the rig comes to rest so that the control sequence during stopping is shown. The initial, maximum speed up the incline is only 55 miles per hour. The control system could improve on this by means of a

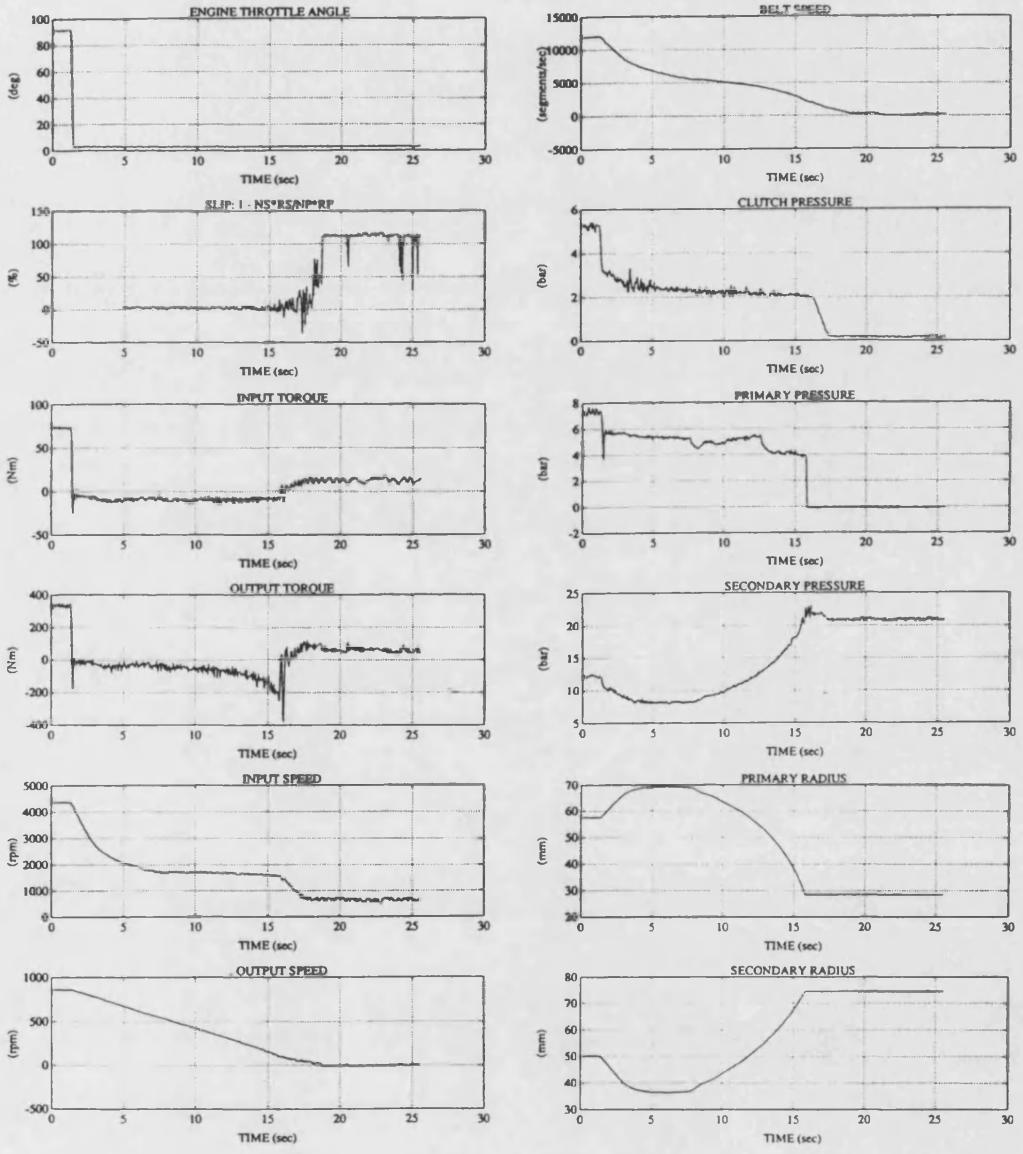

Figure 10.5 Test 5. Results for a closed throttle deceleration from maximum speed up a 10% incline

small change in the pulley radii to raise the engine speed to 5000 rev/min. For the stopping sequence, when the input speed, i.e. the primary pulley speed, has fallen to approximately 1700 rev/min the secondary pressure starts to build up while the primary pressure stays constant. This causes the primary radius to reduce keeping the input speed steady. When the minimum radius is reached, the primary pressure drops to zero as the moveable pulley half comes against the shoulder on the shaft. The input speed then steadily decreases together with the output speed and as the vehicle speed approaches zero the clutch pressure decreases to close to zero. Just enough clutch pressure is present to give vehicle creep on the level. The pulley radii are now in their low ratio, start positions and the secondary pressure is high ready to cope with any acceleration demanded.

10.4 Validation of the viscous shear model using Test 2

As the results from Test 2 covered large ranges in pulley radii and in pulley cylinder pressures, the opportunity was taken to use them in order to determine the empirical constants in the viscous shear model, η_{os} and α_s. These constants were then used with the system model developed in chapter 5 to compare calculated results with measured values.

The slip on the primary pulley can be determined from the measured values of primary pulley speed and radius and the speed of the belt, the equation relating these quantities being 5.10. The slips on the primary pulley during Test 2, determined from measured results, are shown in figure 10.6. Not surprisingly, there is considerable fluctuation in the values but a reasonable mean line can be drawn. The mean values at 5 and 25 seconds respectively can be used to evaluate the two unknown constants.

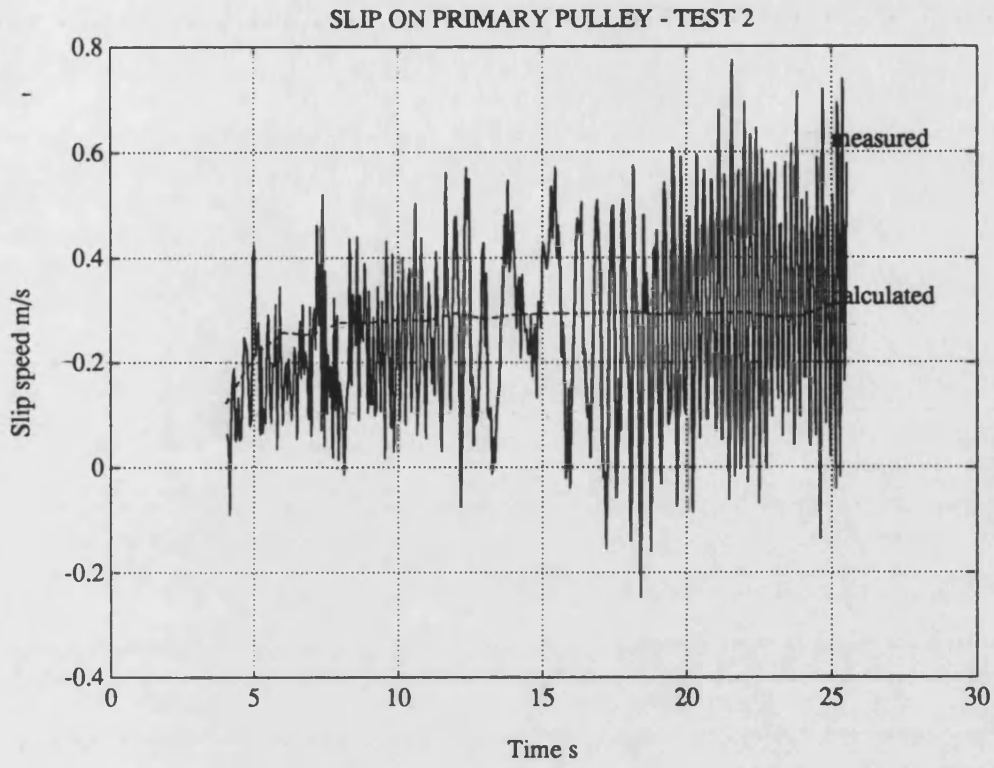

Figure 10.6 Test 2. Measured and calculated slips on the primary pulley

The third constant, the minimum film thickness t_{smin}, was not involved at this stage as the large torques being transferred produced large film thicknesses. The values obtained were:

$$\eta_{os} = 0.210 \text{ N s/m}^2 \qquad \alpha_s = 2.75 \times 10^{-8} \text{ m}^2/\text{N}$$

From the test data and with the viscous constants determined from the measured slips at 5 and 25 seconds, the slips on the primary pulley at intervals during the whole test can be calculated. They are shown plotted on top of the measured slips in figure 10.6. The calculated curve agrees with a mean line through the measured values very well. The measured slips on the secondary pulley can be determined similarly and, using the same viscous constants, the slips can also be calculated using the proposed model. These two curves are shown in figure 10.7. As the conditions in the secondary pulley are very different from those on the primary pulley, this gives a test of the validity of

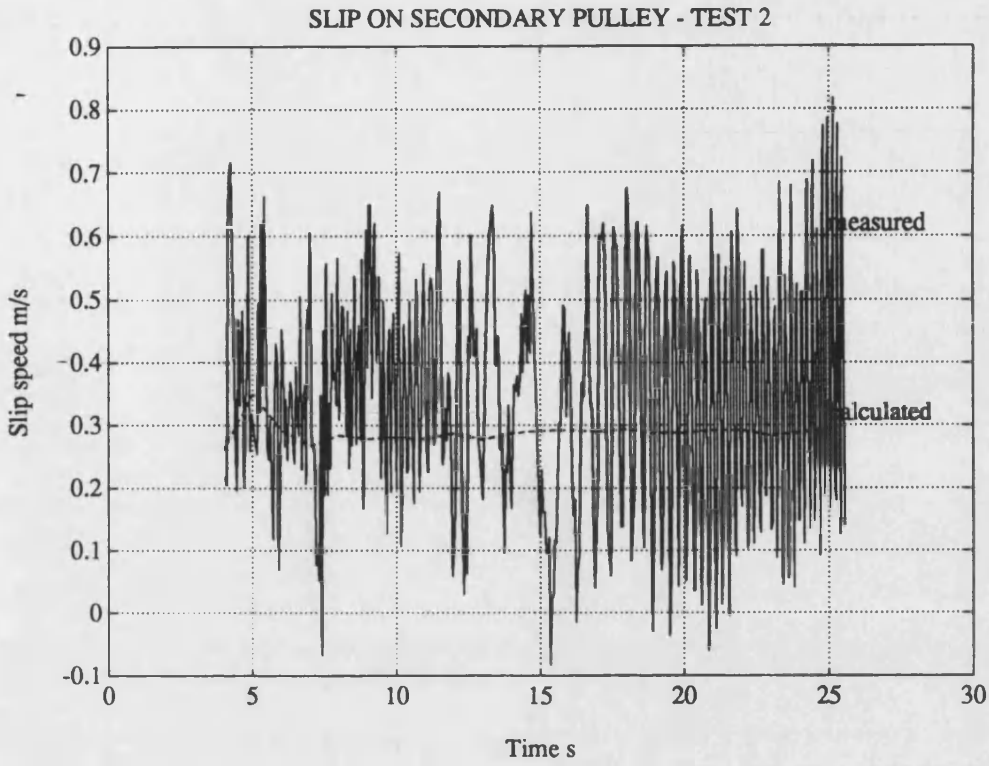

Figure 10.7 Test 2. Measured and calculated slips on the secondary pulley

the model and also of the accuracy of the measurements. The calculated curve is seen to be a little below the mean line of the measured values, perhaps 0.05 m/s below the mean value of about 0.35 m/s, but the two curves are very close. The two curves also show most of the same trends. The viscous model is seen to be very suitable and the measurements can be seen to be reliable.

With the two viscous constants determined, the quantities required for input to the computer model described in chapter 9 can be taken from the measured values at intervals during the test and used to determine other quantities. These calculated quantities can then be compared with the corresponding measured values in order to test the validity of the model. The following quantities shown plotted against time in

figure 10.2(a) and (b) were used as inputs to the computer model:

- Output shaft torque
- Output shaft speed
- Secondary pulley cylinder pressure
- Radius of the belt on the primary pulley

A further input was the radial velocity of the belt on the primary pulley deduced from the slope of the belt radius - time curve. The values of the quantities were calculated at one second intervals.

The most important result for validating the model is the overall slip - time curve. The values based on measurements are reproduced in figure 10.8 together with the calculated values. They show excellent agreement. Other quantities are compared as follows:

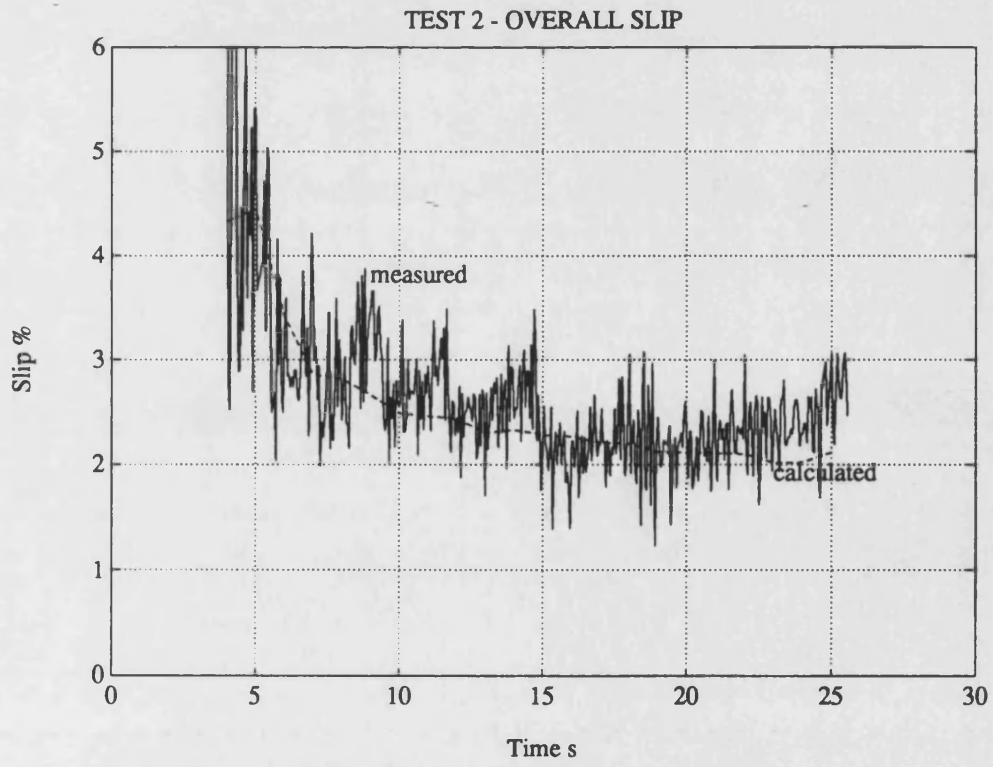

Figure 10.8 Test 2. Measured and calculated overall slips

Figure 10.9 Primary cylinder pressure

Figure 10.10 Torque input

Figure 10.11 Input shaft speed

The calculated primary pressure agrees well with the measured values towards the end of the test but is rather low at the start. This discrepancy can possibly be explained by the fact that the pressure was measured in the line leading to the cylinder. When the oil flow into the cylinder is high, as at the start of the test, the pressure drop in the line would give a high value for the measurement.

The calculated input torque agrees well with the measured values at the start of the test but gives high values towards the end, the error being about 5 N m in a measured value of 70 N m. No explanation can be found for this discrepancy.

The measured and calculated input shaft speeds agree well.

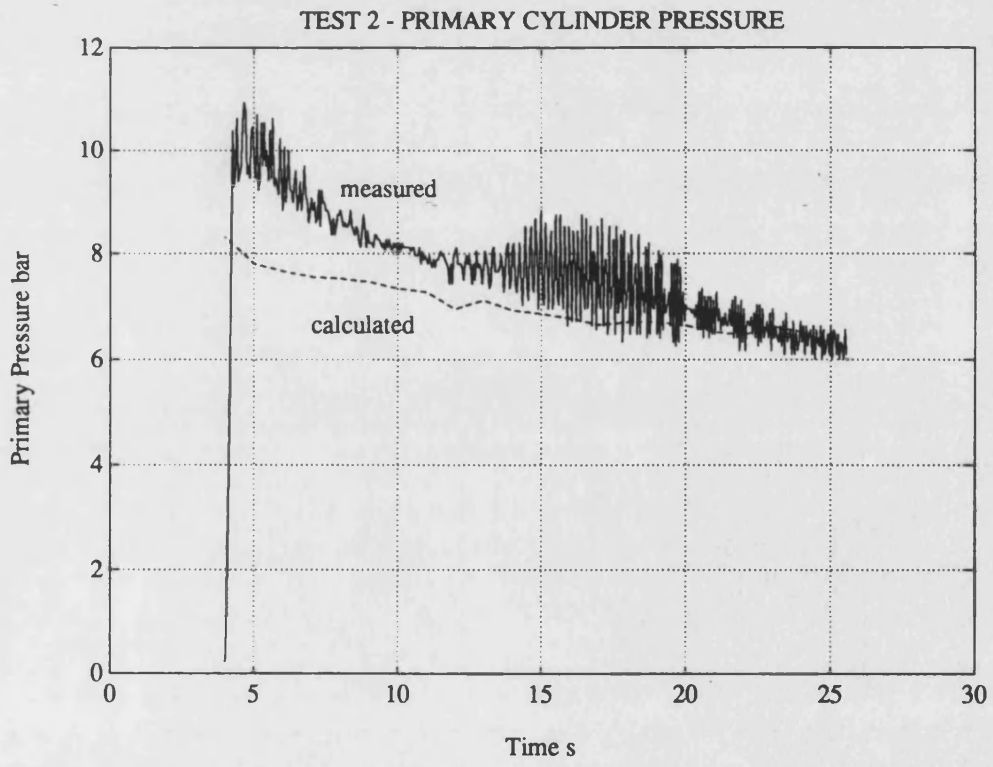

Figure 10.9 Test 2. Measured and calculated primary cylinder pressures

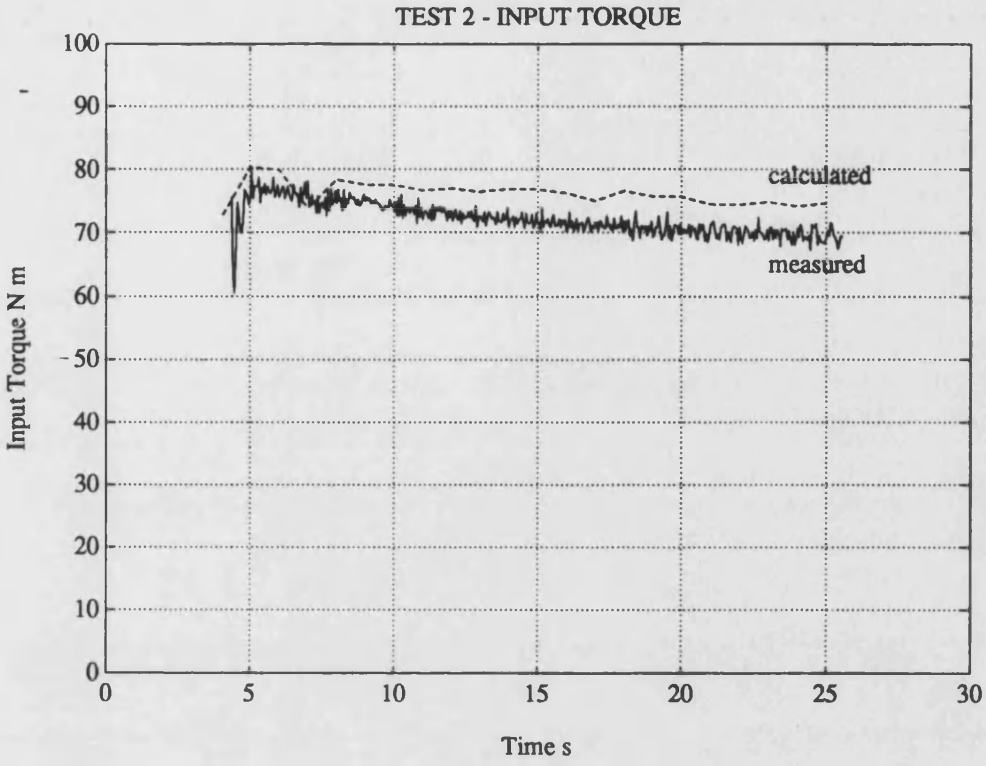

Figure 10.10 Test 2. Measured and calculated torque input

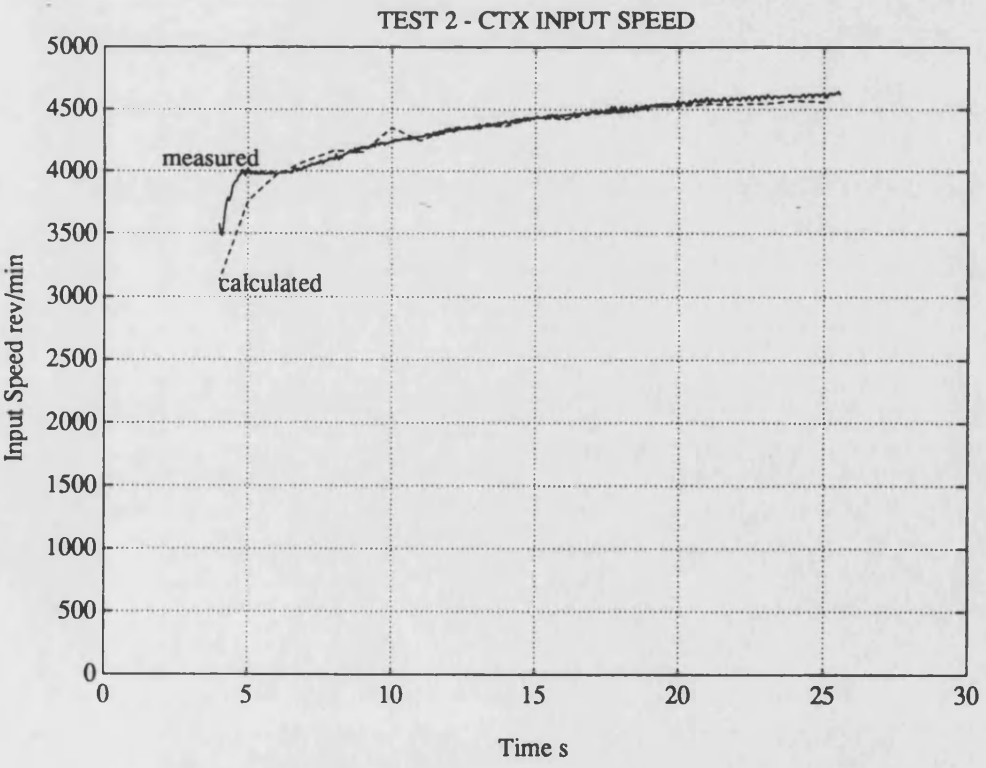

Figure 10.11 Test 2. Measured and calculated input shaft speeds

10.5 The Second set of tests, steady state tests using the standard control system

These tests were less important than the later, steady state tests in which the pulley radii were fixed but did provide data for the development of the transmission model while the rig was prepared for the later tests. They are used here as a further check on the validity of the viscous shear model and of the complete transmission model. In particular, the calculated primary pulley pressure can be compared with the steady state pressure measurement which will not contain any inaccuracy due to flow. In the later, fixed radius tests the primary pressure could not be measured as the moveable pulley half was resting on the shoulder or a spacer and the pressure was absent.

For this set of tests the dynamometer was used to fix the transmission output speed in a series of equally spaced values over the complete speed range. For each speed, five tests were run with input torques approximately equal to 20%, 40%, 60%, 80% and 100% of the maximum torque. These values were set by adjustment of the engine throttle. For each test the belt radii on the pulleys were determined by the standard control system and, after the conditions had been allowed to settle, all the measurements were collected a number of times and an average of each obtained. The results were sorted into five groups, A to E, in each of which the primary torque had an approximately constant value. Each group contains a series of fourteen sets of measurements in which the output speed was progressively increased over the whole range of speeds. As the output speed increased, the control system altered the pulley radii so that the primary radius went from minimum to maximum or, in the last group E, close to maximum. These results are in Appendix 4, Table 1.

The final computer model was applied to each set of measurements using as the inputs the measured values of output speed, output torque, secondary cylinder pressure and primary radius. The radial velocity on the primary pulley is zero in these steady state cases.

For each of the five groups of fixed input torque measurements, all the quantities considered are plotted against the speed of the transmission output shaft as follows:

Group A, 16 N m torque input. Figure 10.12

Group B, 32 N m torque input. Figure 10.13

Group C, 48 N m torque input. Figure 10.14

Group D, 64 N m torque input. Figure 10.15

Group E, maximum torque input. Figure 10.16

Each figure contains four graphs. In the first graph the two pulley radii are plotted for reference purposes. The second compares the measured and calculated primary pressures. The third compares the overall slips deduced from the measurements with the corresponding calculated values while the fourth similarly compares the overall mechanical efficiencies. Note that these mechanical efficiencies apply to the transmission in a completely standard condition.

The measured and calculated primary pressures show reasonable agreement especially for the lower input torques but with the higher torques there is a fairly large discrepancy with the low output speeds and good agreement at high speeds.

The overall slips agree well except for the first group with the small input torque, figure 10.12. Here the calculated slip is only about one third of the measured value.

The overall mechanical efficiencies agree remarkably well in all cases. It can be seen that the maximum efficiency is only about 86% when the input torque is a maximum

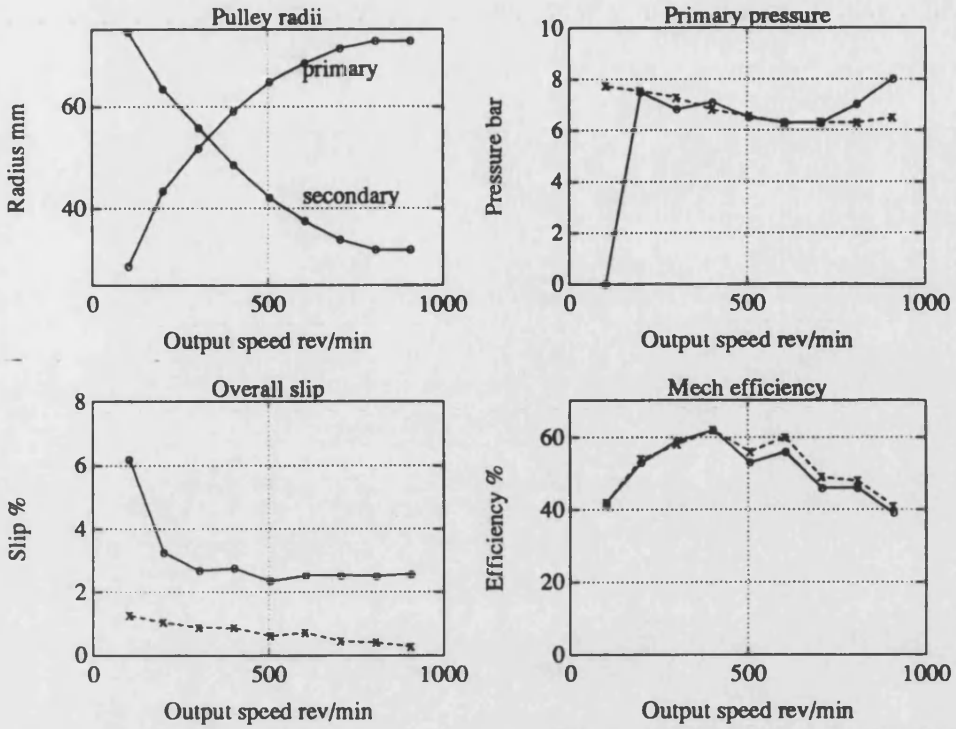

Figure 10.12 Measured (—) and calculated (---) steady state results with the standard control system, 16 N m input torque

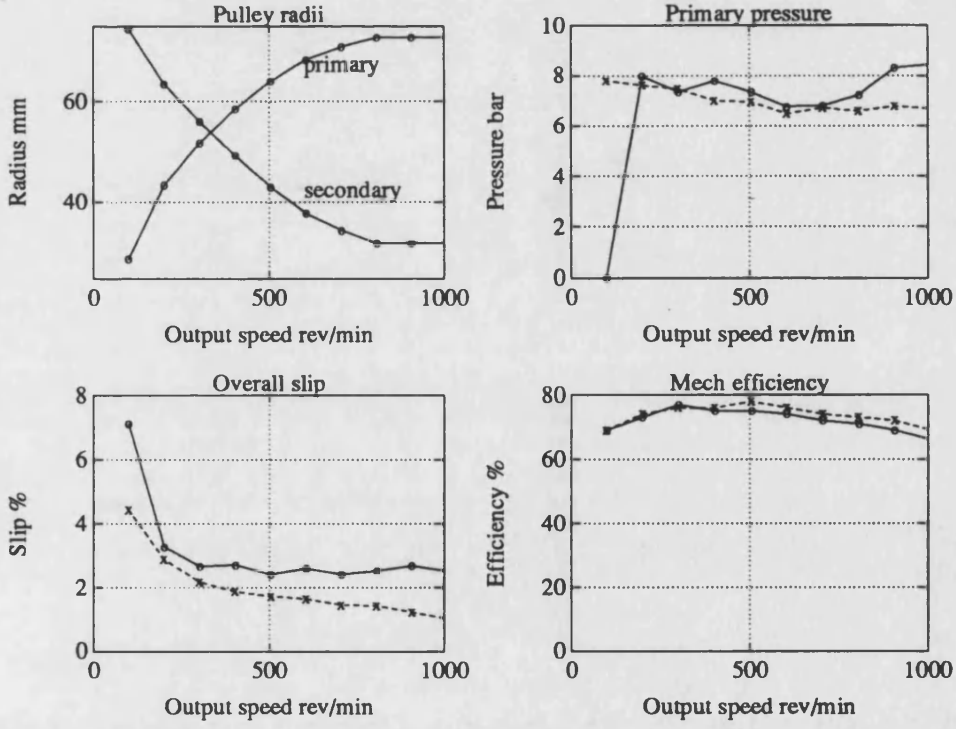

Figure 10.13 Measured (—) and calculated (---) steady state results with the standard control system, 32 N m input torque

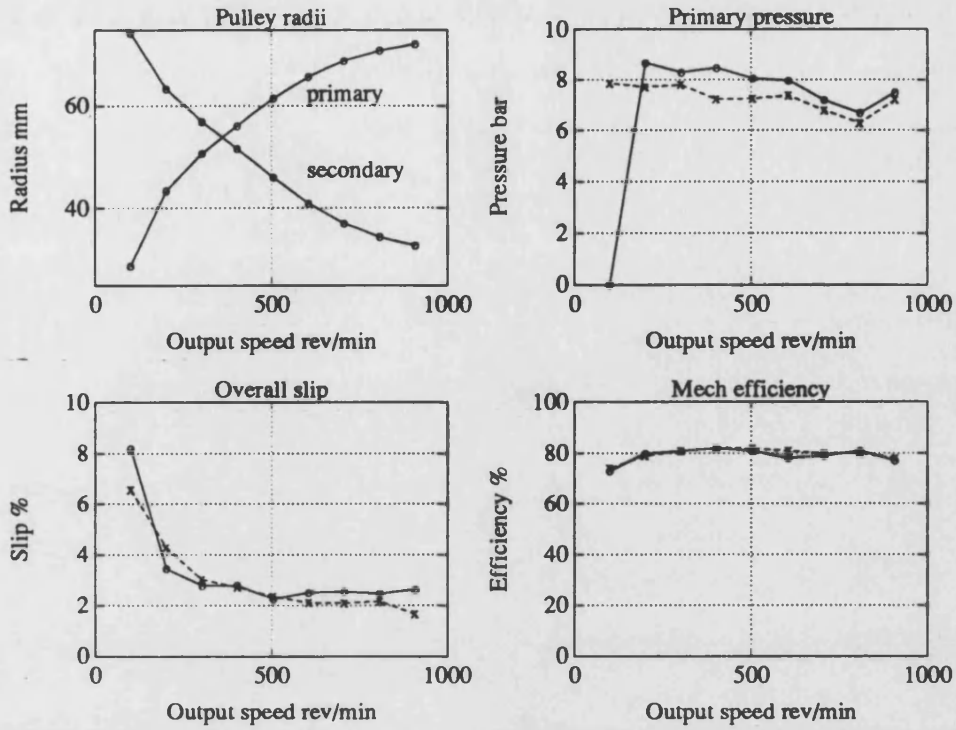

Figure 10.14 Measured (—) and calculated (---) steady state results with the standard control system, 48 N m input torque

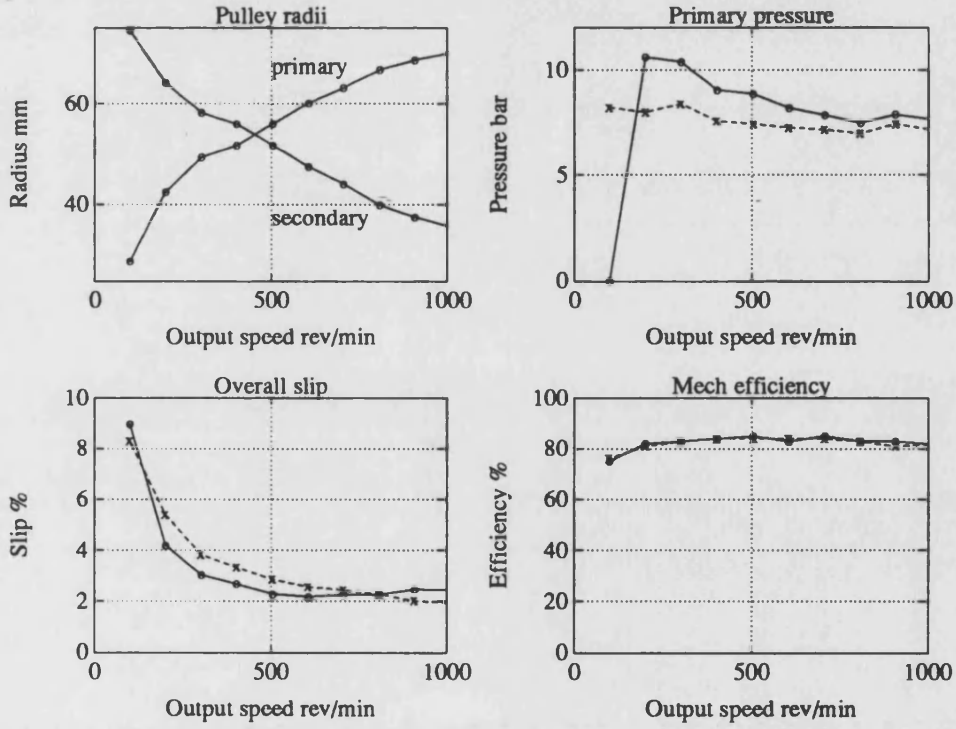

Figure 10.15 Measured (—) and calculated (---) steady state results with the standard control system, 64 N m input torque

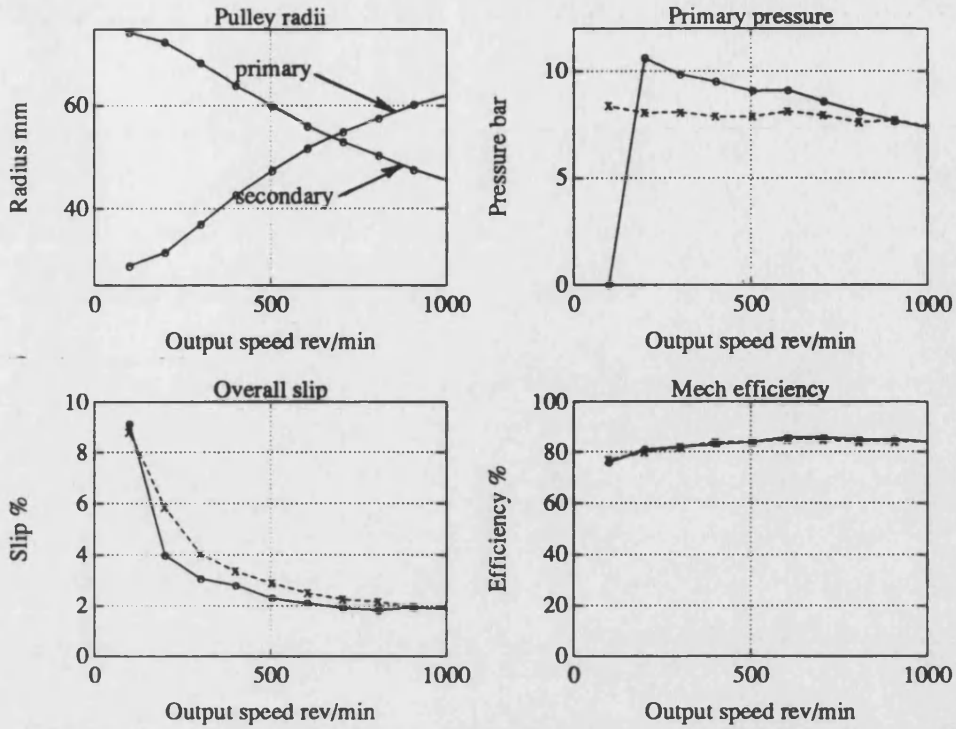

Figure 10.16 Measured (—) and calculated (---) steady state results with the standard control system, maximum input torque

and 85% when the input torque is 64 N m. With the lower input torques the efficiency is considerably reduced. These are very poor values but are believed to be correct. Even if the measured speeds are assumed to be in error by the maximum amount, see section 10.2, the maximum value of the efficiency is only increased to about 86.4%. The many losses present in the system have been identified and measured and are compatible with this result. The losses are fully discussed in section 10.8.

The input shaft speeds and torques calculated from the computer model are also compared with the measured values, the speeds in figure 10.17 and the torques in figure 10.18. Reasonably good agreement is obtained for the speeds except for the results with the low input torque which reflect the slip discrepancy in figure 10.12. The input torques show close agreement.

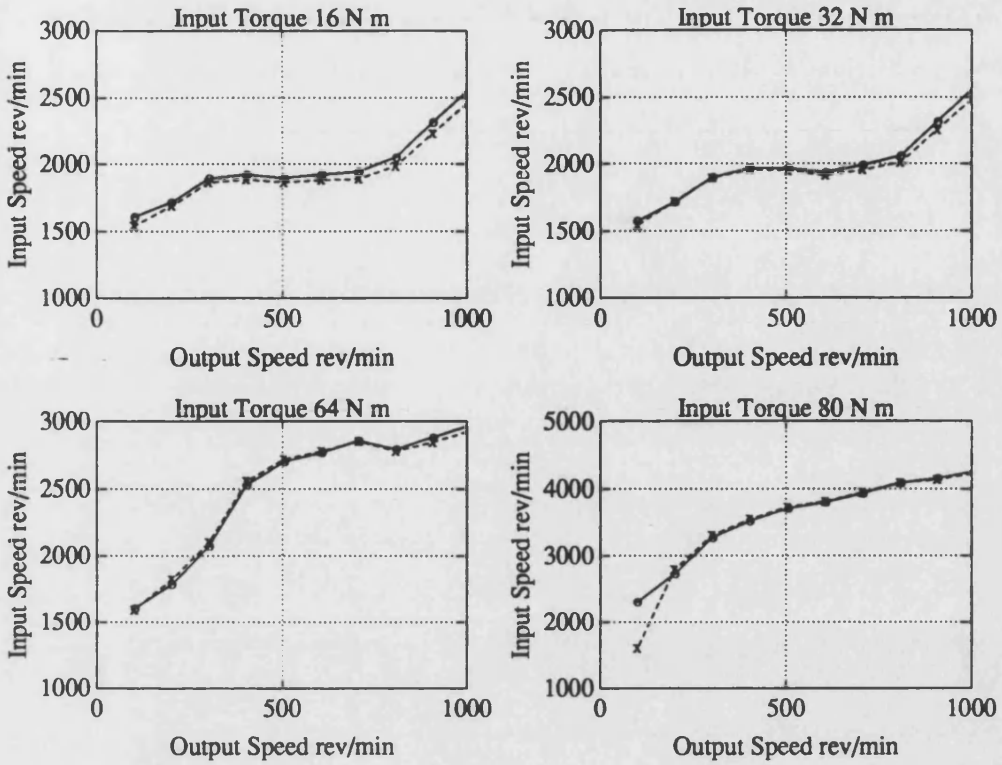

Figure 10.17 Measured (—) and calculated (---) input shaft speeds in steady state with the standard control system

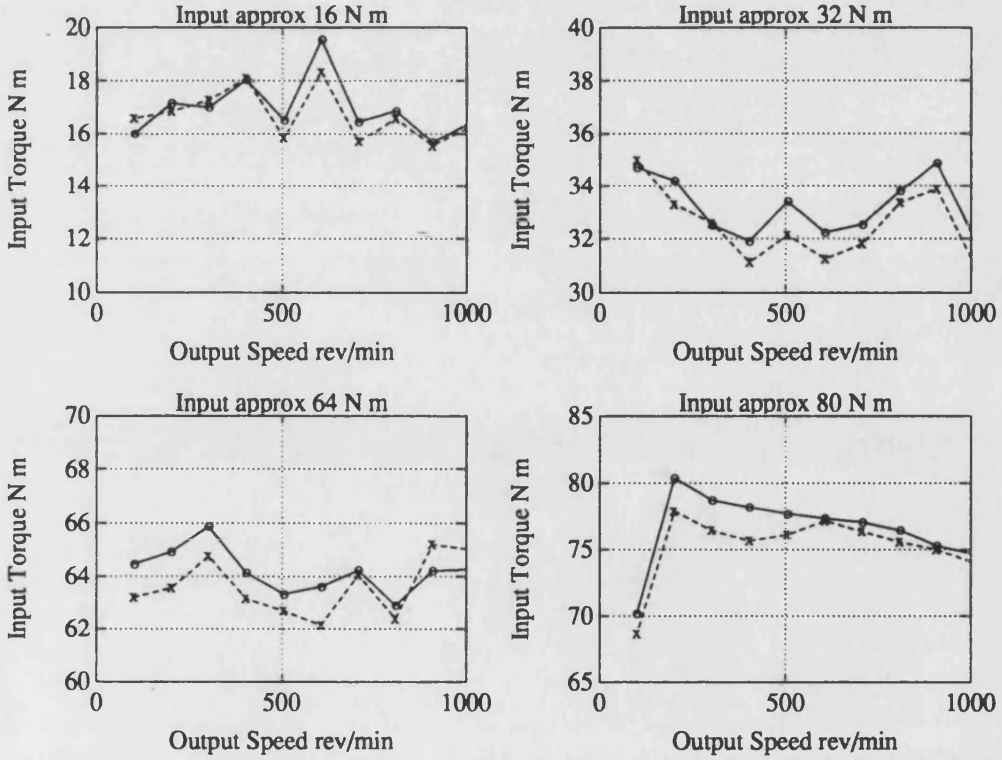

Figure 10.18 Measured (—) and calculated (---) input shaft torques in steady state with the standard control system

10.6 The Third set of tests, steady state tests with fixed radii and using an external control system to supply the required pressures

In this set of tests the radii were fixed by operating the transmission with zero primary pressure so that the moveable half of the primary pulley rested on a stop with a fixed pulley opening. The secondary pulley cylinder pressure was supplied from the external control system and could be set to any value required. The secondary pressure caused the belt to be tensioned in the normal way which, in turn, pressed the primary pulley half against its stop and the reaction from this took the place of the normal primary pressure. The primary stop was a shoulder on the pulley shaft which normally supports the pulley half when the transmission is in a low ratio. Various other radii were obtained by inserting one of a number of spacers between the pulley half and the shoulder.

1. The main tests were carried out in groups, namely V, W, X, Y and Z. The results are shown in Appendix 4, Tables 2 to 5 respectively, with group Y omitted. Each group contained the results for one set of fixed radii measurements. The values of the pulley radii for the groups are:

Group V	No spacer	R_p = 28.8 mm	R_s = 74.4 mm
Group W	Spacer 1	R_p = 39.2 mm	R_s = 67.1 mm
Group X	Spacer 2	R_p = 50.0 mm	R_s = 57.9 mm
Group Y	Spacer 3	As the time available for testing was limited, no measurements were taken in this group	
Group Z	Spacer 4	R_p = 70.1 mm	R_s = 35.5 mm

When changing a spacer between tests it was necessary to remove the transmission

from the rig, dismantle it, change the spacer, reassemble the transmission and replace it in the rig.

The measurements in each group were carried out with a series of transmission input speeds, a series of input torques and a series of secondary pressures. The external control system supplied a pressure to the clutch sufficient to prevent slip occurring in the clutch. The input speeds were maintained approximately constant at 1500, 3000 or 4500 rev/min by determining the appropriate output shaft speed and using the dynamometer constant speed facility. The external system supplied a constant pressure to the secondary pulley cylinder with values of 8, 16 or 24 bar with the addition of 6 bar to the two high ratio groups where lower pressures are appropriate. The series of input torques was obtained by adjustment of the engine throttle so that the full range was divided into five approximately equal parts with values of 16, 32, 48, 64 N m and full throttle.

These results were used to further investigate the viscous shear model by the comparison of overall slips determined from the measured values with slips calculated by use of the model. For some of the measurements it was found that the calculated oil film thickness between the segments and the pulley surface was extremely small, much less than could be achieved in reality because of the surface roughness that must be present. The calculated overall slip was then much less than the measured slip. This discrepancy was resolved by including a minimum film thickness, t_{smin}, in the model as explained in chapter 4. With this additional condition in the viscous shear model good agreement between measured and calculated slips was obtained. The value used was

$$t_{smin} = 110 \times 10^{-9} \text{ m.}$$

Graphs showing a comparison of the overall slips were plotted as follows. Each figure

is for a particular primary radius and shows three or four graphs in each of which the measured and calculated overall slips are plotted against the input torque for a particular secondary pressure.

Figure 10.19	No spacer	Primary radius = 28.8 mm
Figure 10.20	Spacer 1	Primary radius = 39.2 mm
Figure 10.21	Spacer 2	Primary radius = 50.0 mm
Figure 10.22	Spacer 4	Primary radius = 70.1 mm

When the results for the spacer 4 tests were inspected it was apparent that there was an error. Investigation of the radius measurements showed that the values of primary radius were too great. These values were corrected to make them compatible with the known belt length and to give overall slips with the same values as those from comparable tests in the first steady state series described in section 10.5. The graphs showing the slips in figure 10.22 then are obviously less reliable than the other results. The deduction of torque loss from these results would be little affected. Unfortunately no time was available for repeating these measurements as the test rig was required for another research project.

It can be seen that there is excellent agreement between the measured and calculated slips with the higher secondary pressures of 16 and 24 bar. With the lower pressures, both measured and calculated curves bend upwards as the torque is increased so that the slip becomes large. Both curves have the same form but the calculated curve is displaced to the left compared with the measured curve. This upward bend in the calculated curve to match the measured curve is seen as confirmation that the viscous model is correct although some adjustment of the empirical viscous constants would be needed to improve the fit.

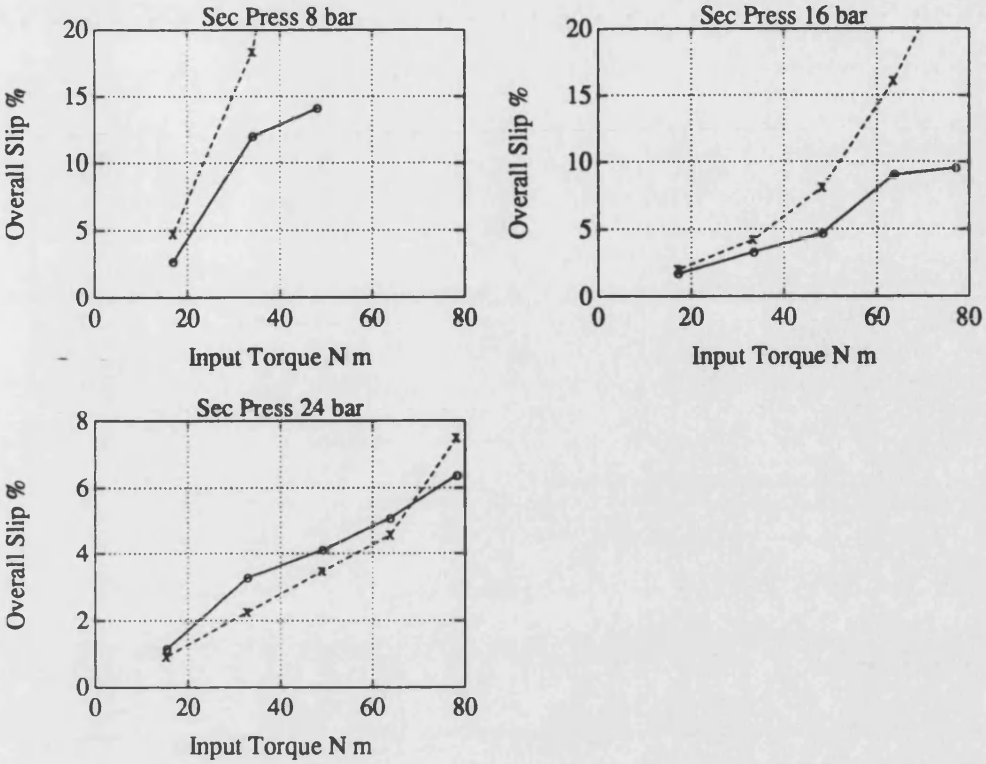

Figure 10.19 Measured (—) and calculated (---) overall slips plotted against input torque. Primary radius 28.8 mm, input shaft speed 3100 rev/min

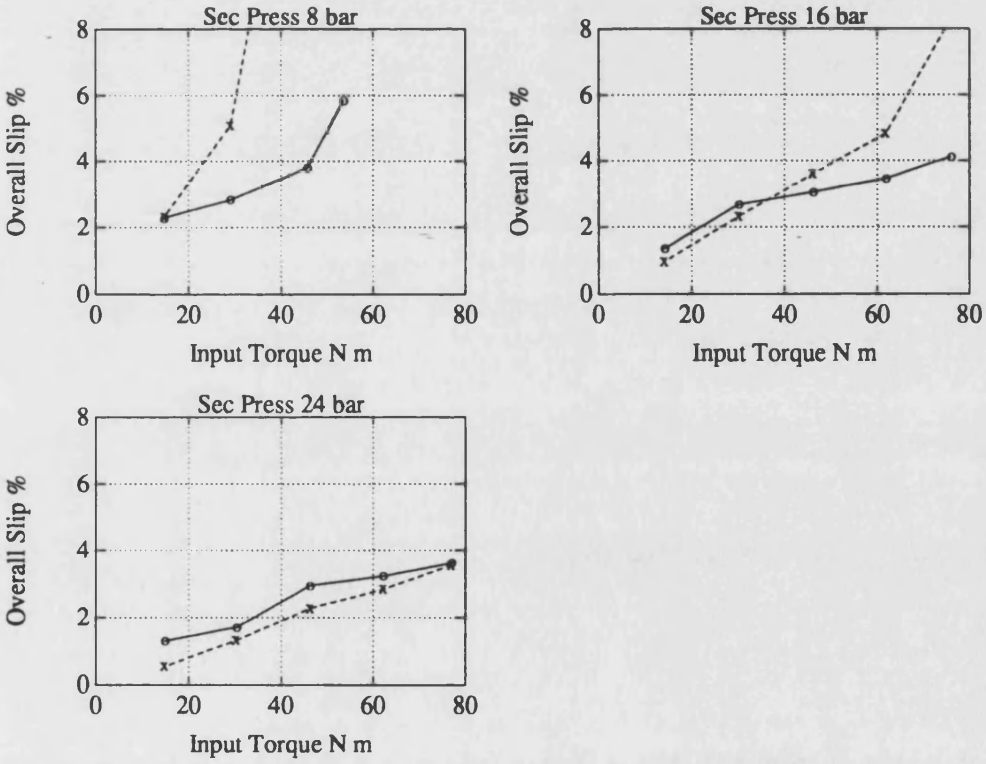

Figure 10.20 Measured (—) and calculated (---) overall slips plotted against input torque. Primary radius 39.2 mm, input shaft speed 2950 rev/min

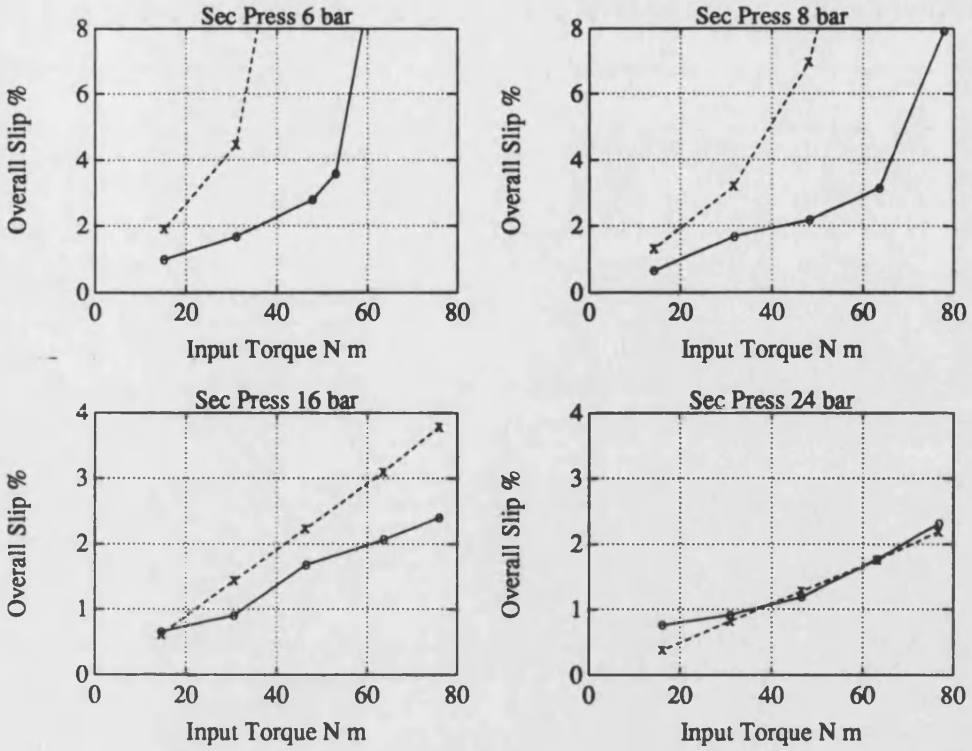

Figure 10.21 Measured (—) and calculated (---) overall slips plotted against input torque. Primary radius 50.0 mm, input shaft speed 2900 rev/min

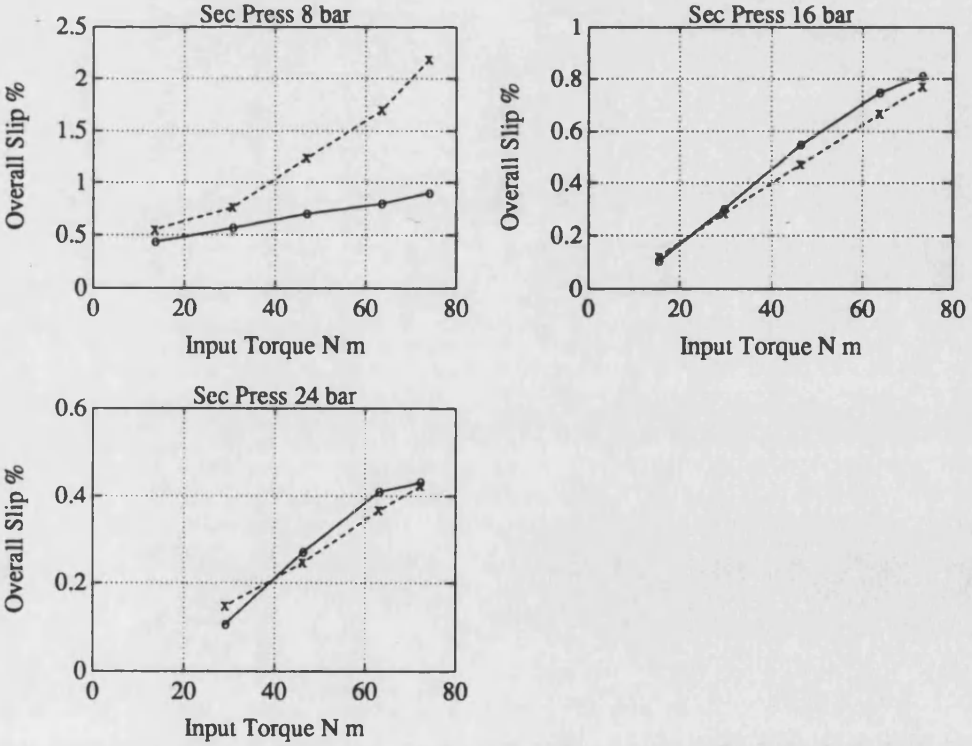

Figure 10.22 Measured (—) and calculated (---) overall slips plotted against input torque. Primary radius 70.1 mm, input shaft speed 4200 rev/min

2. Some further tests were carried out with fixed radii and using the external control system.

One set of tests was designed to resolve the issue of the effect of the magnitude of the total initial gap between the segments on the overall slip. These results are presented separately in chapter 8 and in Appendix 4, Tables 8 and 9.

Another set was to measure the torque loss on no-load and these results are presented in chapter 7 and in Appendix 4, Table 7. The main results in section 1 were used in the determination of the torque losses when on load.

The determination of the torque loss on no-load requires a knowledge of the losses along the input shaft. These losses were obtained by running the transmission with the belt removed and the torque input was measured at a number of input speeds set by adjustment of the engine throttle. As with all these tests, the pump was not fitted so

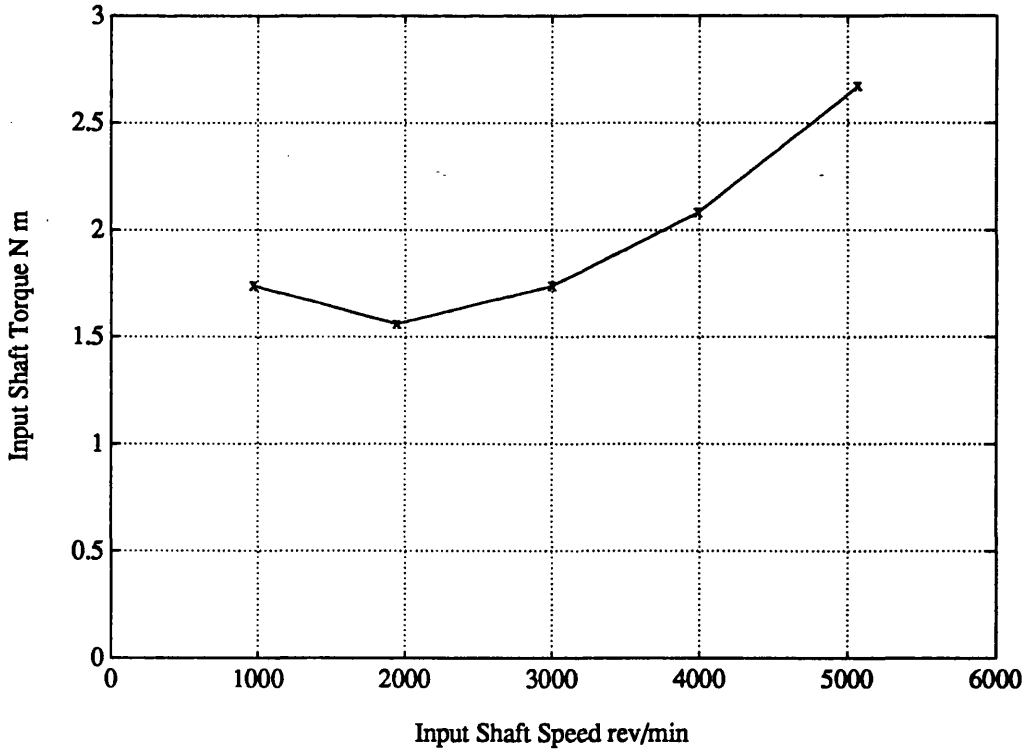

Figure 10.23 Variation of input shaft loss with input speed, no belt or pump

that the engine only has to overcome the shaft losses. It is important that the clutch is supplied with the normal operating pressure so the whole input shaft up to the pulley is running. The losses along the input shaft are plotted against input speed in figure 10.23. They appear to take the form of a constant loss with the addition of a term dependent on the square of the speed. In forward drive, the reverse clutch, a wet multi plate clutch, slips with a speed equal to the input speed but in the reverse direction and may be providing the majority of the second term. The values are listed in Appendix 4, Table 6.

10.7 Values of other quantities determined by use of the transmission model

The values of other quantities of importance in the transmission which were not measured were calculated from the model for a few operating conditions in order to give some idea of their behaviour.

The conditions chosen were a series of constant speeds over the whole range from very low up to the maximum for the car. It was assumed that the transmission was under the control of the standard control system. For a particular vehicle speed, the resistance to motion can be determined from the known road load relation and the required transmission output shaft speed and torque can be obtained. The belt radius on the primary pulley and the secondary pressure that would then be set by the control system can be determined by matching the output conditions with those in the measured results, interpolating as necessary, from the Second series of tests described in section 10.5, steady state tests with the standard control system. The following table shows the speed and torque required on the transmission output shaft for a series of

steady state speeds with the corresponding deduced values for the secondary pressure and the primary radius.

Vehicle speed	Vehicle resistance	Output shaft		Secondary pressure	Primary radius
		Speed	Torque		
km/h	N	rev/min	N m	bar	mm
14	132	136	37	20.8	34
28	154	273	43	14.4	52
42	190	409	53	12.0	59
56	240	546	67	10.8	67
70	305	682	85	9.5	68
84	384	819	108	8.5	71
98	478	955	134	9.4	70
112	586	1091	164	9.8	68
126	708	1228	198	9.9	67
140	845	1364	237	10.0	67

The values in the four right hand columns were used as inputs to the computer programme in order to evaluate the quantities required. The fifth input, the radial velocity of the belt on the primary pulley is zero in these steady state cases. Although these are calculated results, they are related to the measured steady state values described in section 10.5 as explained above and the comparison of measured and calculated quantities in that section showed the calculated values to be reliable.

The following quantities are shown plotted against vehicle speed in figure 10.24:

- input shaft speed

  input shaft torque

  primary radius, secondary radius

  belt speed, speed of inner band, speed of outer band

  segment compression, total band tension

  tension in inner band, tension in outer band

  secondary pressure, primary pressure

It can be seen that at the very low vehicle speeds the radii settings are kept at a low transmission ratio so that the input speed, i.e. the engine speed, is not uncomfortably low. The secondary pulley pressure is then high, presumably to keep the transmission in a state of readiness in case the driver suddenly calls for an acceleration. As the speed increases the secondary pressure is reduced while the primary pressure remains approximately constant causing the primary radius to increase. The speed reaches over 50 km/h before the radii get close to the overdrive ratio and the CVT is working efficiently. The total band tension is always substantially more than the segment compression so that a nett tensile load is maintained all round the belt with no chance of the problems that would develop if the two did become equal. The rise in band tension from a speed of about 85 km/h is largely due to the increase in the running speed of the belt. All the bands run faster than the belt segments, the difference being just discernable on the graph.

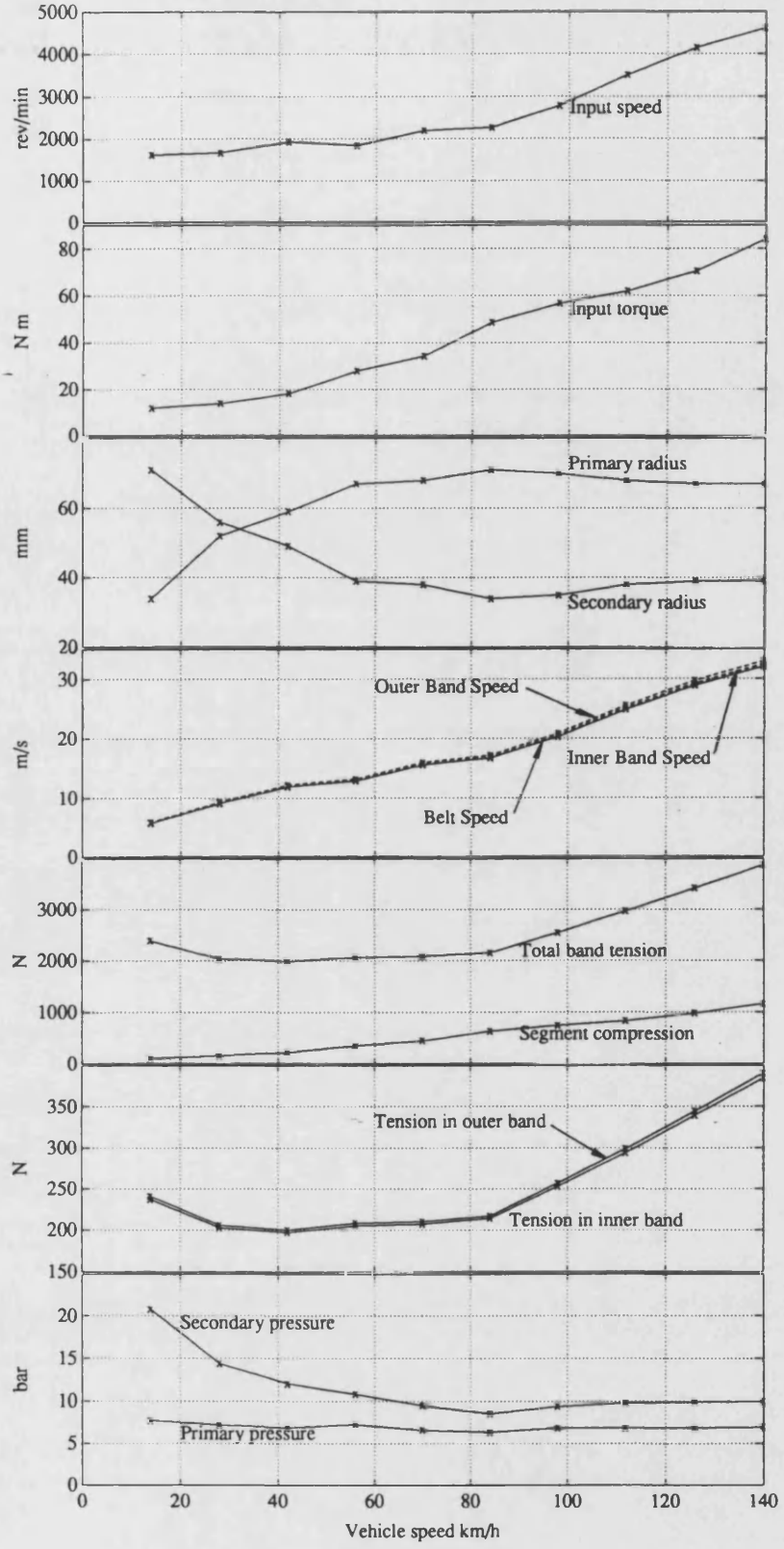

Figure 10.24 Variation in some transmission properties with vehicle speed in steady state using the standard control system

10.8 The magnitudes of losses in the transmission

Results from the calculations used to determine the quantities shown in figure 10.24, section 10.7, were used to evaluate the losses in the transmission. The input torque, T_i, was divided up as follows:

The useful input torque, T_{iu}, the part of the input torque used to supply the output from the transmission, was determined by multiplying the output torque by the ratio of output speed to input speed.

The pump loss, T_g, the torque required to drive the pressurising pump, was determined by use of equation 5.26 with the pump mechanical efficiency equal to 70%. This is quoted by Roovers [10.2] as the value at 30 bar and 3000 rev/min and is assumed to apply for all conditions.

The belt related torque loss, T_L, the torque required to continuously wedge the belt into and out of the pulleys, was determined from equation 7.5.

The loss in the final drive gears, T_{id}, was obtained by making the assumption that the mechanical efficiency of the final drive equals 98.5%. The input to the final drive from the secondary pulley is a torque T_s at a speed n_s. The output from the final drive to the drive shaft is a torque T_o at a speed n_o. If η_{md} is the mechanical efficiency of the final drive,

$$n_s T_s \eta_{md} = n_o T_o$$

The rate of energy loss

$$= n_s T_s - n_o T_o = n_o T_o \left(\frac{1}{\eta_{md}} - 1 \right)$$

If n_i is the speed of the input shaft, the torque on the input shaft required to supply this loss is

$$T_{id} = \frac{n_o T_o}{n_i}\left(\frac{1}{\eta_{md}} - 1\right) \qquad (10.3)$$

The loss along the input shaft, T_{is}, was obtained from the measured loss shown in figure 10.23.

The final loss, the loss due to slip in the belt-pulley system, T_{isl}, is the amount required to make up the difference between the torque input and the useful torque input.

Figure 10.25 shows how the overall mechanical efficiency varies with vehicle speed in steady state. These efficiency values do not agree with measured results given in Cuypers [10.3] and Hendriks [10.4] which both show values in the mid nineties per cent for all conditions except for those at very low torques. Unfortunately these papers give no details of the tests carried out. Roovers [10.2] does give some information on loss and efficiency but, once again, no details are given of the tests from which the information was obtained. He states that, over a vehicle speed range from 15 km/h up to the maximum, the belt and pump are responsible for a loss torque of 8 N m which agrees reasonably well with the sum of the Belt Torque Loss and the Pump Loss in figure 10.25. He also shows a graph of fuel consumption against vehicle speed in which the current CVT is compared with a 100% efficient CVT. Deducing the efficiency of the current CVT from this graph produces values close to those shown in figure 10.25 for the lower speeds but going up to approximately 88% at the

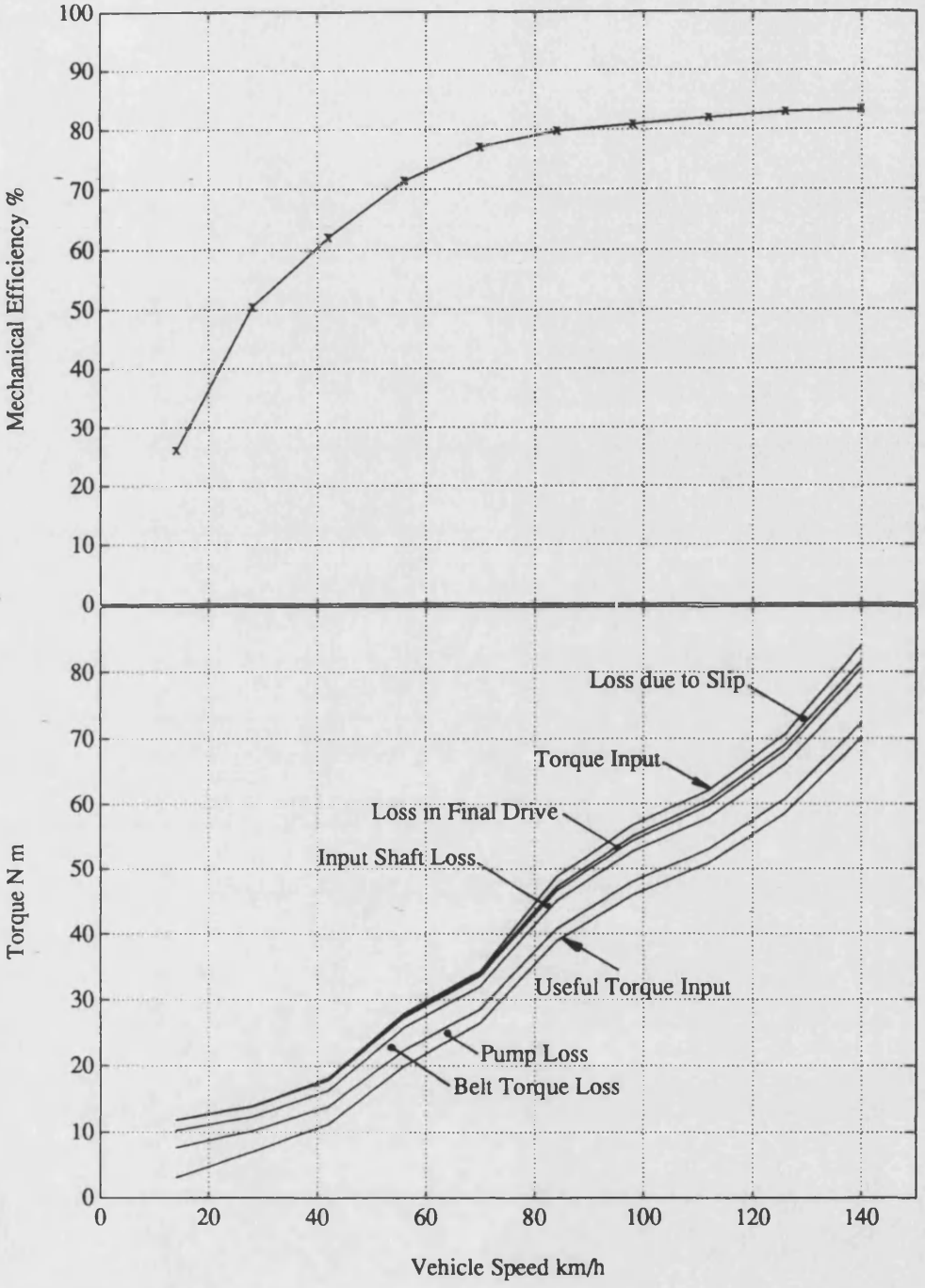

Figure 10.25 Variation of transmission mechanical efficiency with vehicle speed in steady state and the division of the input shaft torque into the useful torque and the various losses.

maximum speed.

Figure 10.25 also shows how the input torque is divided into useful torque and between the various losses. It shows a broad band of loss over the whole range of vehicle speeds and demonstrates the reasons for the very low mechanical efficiencies determined in section 10.5. The efficiencies are well below the efficiencies achieved by manual gearboxes for small cars which are in the range 92% to 95% for most input torques, van Dongen [10.5]. This explains why, as discussed in chapter 1, cars fitted with this CVT do not show an improvement in fuel economy over cars with conventional gearboxes. In order to show the details of these losses they are plotted separately against vehicle speed in figure 10.26.

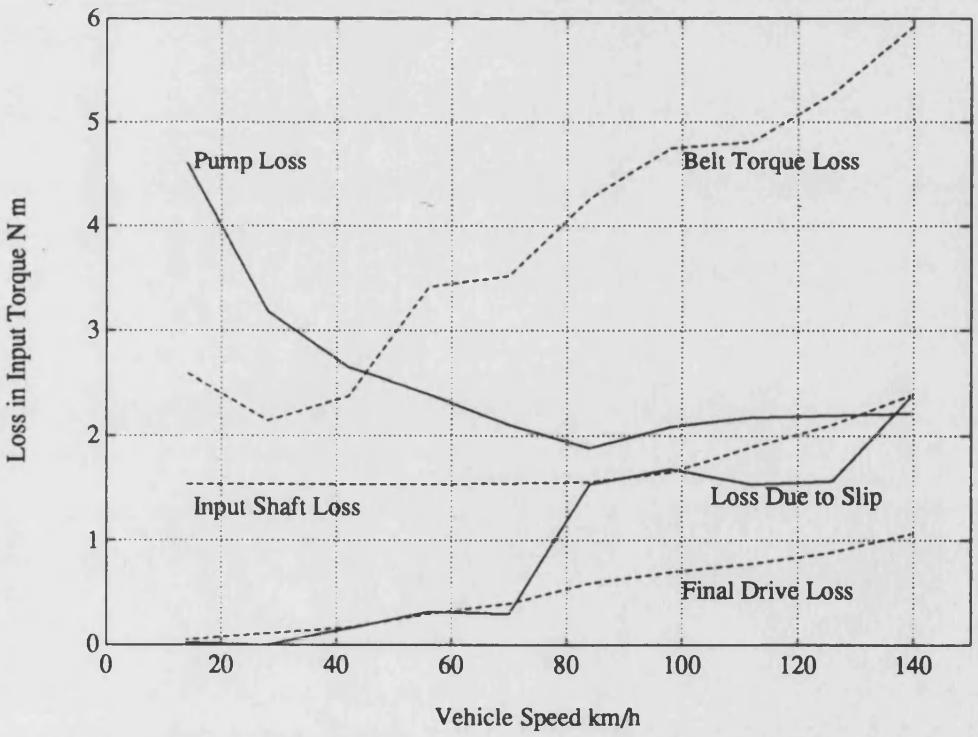

Figure 10.26 Variations in the various input torque losses with vehicle speed in steady state

The major loss is the belt torque loss. As was shown in chapter 7, this loss is large when the primary radius is large which occurs above approximately 55 km/h. The steady increase in the loss above that speed is brought about by the increase in band tension as the speeds rise. This loss is considered further in the discussion of results in chapter 11.

The other substantial loss is the pump loss. This depends on the secondary pressure and could be reduced if the pressure was reduced. This would also reduce the belt torque loss but would result in an increased loss due to slip. It is obvious that a controller which minimised the sum of these three inherent losses, as proposed by Guebeli et al [10.6], would be an advantage. The pump loss also depends on the oil flow rate, a reduction in this rate reducing the loss. The maximum flow rate is determined by the flow required to give an adequate rate of change of belt radii and this high flow is only required when the ratio is changing. A pump with a variable flow rate could reduce the loss at constant speed. This modification is being used in a new generation of transmissions by the manufacturer who uses a roller vane pump with two inlet and two outlet ports, Hendriks [10.4]. With the aid of a flow control valve, half the flow can be pumped round pressureless until it is required for a ratio change.

The loss along the input shaft is surprisingly large. It is probably mostly due to the drag of the reverse clutch the plates of which are running at the same speed as the input shaft relative to the stationary pressure plates. Although the clutch operating cylinder is not pressurised there will presumably be some viscous drag.

The final drive loss is applicable to all transmissions.

A pointer to the accuracy of these losses is in the loss due to slip. This was obtained by subtracting the sum of all the other losses from the known total loss. As the slips and the torques transferred both increase with speed it is to be expected that the loss would be very small at low speeds and increase approximately in proportion to the square of the speed. The loss obtained, although inevitably showing fluctuations, can be seen to agree with this form very closely. In particular, the loss at a speed of 20 km/h is very small. Errors in the other losses, unless they fortuitously cancelled each other, would tend to give a positive or a negative value here.

CHAPTER 11

Discussion of Results and Conclusions

11.1 The test rig

The test rig performed extremely well. It was designed to simulate the operation of a small car and the results showed that the accelerations and the maximum speed obtained were what would be expected for such a vehicle. This shows that the flywheel represented the vehicle inertia correctly and the road load used in the programme to control the dynamometer was also correct.

The instrumentation proved to be very effective. One important feature was the device used to measure the belt radius on the pulley. Without the radius measurements determination of the slips would have been very difficult and these were vital to the work. The assessment in section 10.2 showed that instrumentation errors were likely to be small.

11.2 The performance of the transmission with the standard control system

The acceleration and deceleration tests described in section 10.3 showed that the standard control system worked well. From the driveability point of view it would be very adequate with the drive take up from rest and the coming to rest being smooth, figures 10.1 and 10.5. It can be seen also that on coming to rest the transmission is

in a position to accept any acceleration demanded by the driver with the transmission in low ratio and the secondary pressure high. The performance, though, is rather unexciting, the acceleration and the maximum speed both being less than they might be because of the limited engine speed. The greatest engine speed recorded, at the start of Test 3, figure 10.3, is just over 4800 rev/min while during the acceleration in Test 2, figure 10.2, the engine speed starts at only 4000 rev/min and slowly builds to 4700 rev/min.

The response of the transmission to a required ratio change was found to be rapid. In figure 10.2 the change in primary radius closely follows the change in primary pressure while in other tests, not recorded, it was found that rapid throttle movement was closely followed by a ratio change.

The performance from the fuel efficiency point of view can be seen by reference to the results in sections 10.7 and 10.8 for a series of steady state speeds over the whole operating range. The table on the next page from the results plotted in figure 10.24 shows the required transmission input shaft speed and torque for a series of steady state vehicle speeds when the transmission is under the control of the standard control system.

The input shaft speed and torque are plotted on an engine map, a torque-speed diagram for the engine, to show the steady state running line, figure 11.1. Note that the reverse bend in the line at around 2000 rev/min engine speed is brought about by a relatively large change in the pulley radii. The wide open throttle torque line for the engine is shown together with the region of low specific fuel consumption (sfc) marked 'A'. Also shown on the engine map is an approximate running line typical of a small car with a 5-speed gearbox operating steadily in the fifth gear.

Vehicle speed	Input shaft speed	Input shaft torque
km/h	rev/min	N m
14	1619	11.91
28	1674	13.88
42	1929	18.13
56	1836	27.88
70	2193	34.30
84	2272	48.76
98	2787	56.78
112	3515	62.09
126	4148	70.64
140	4615	84.03

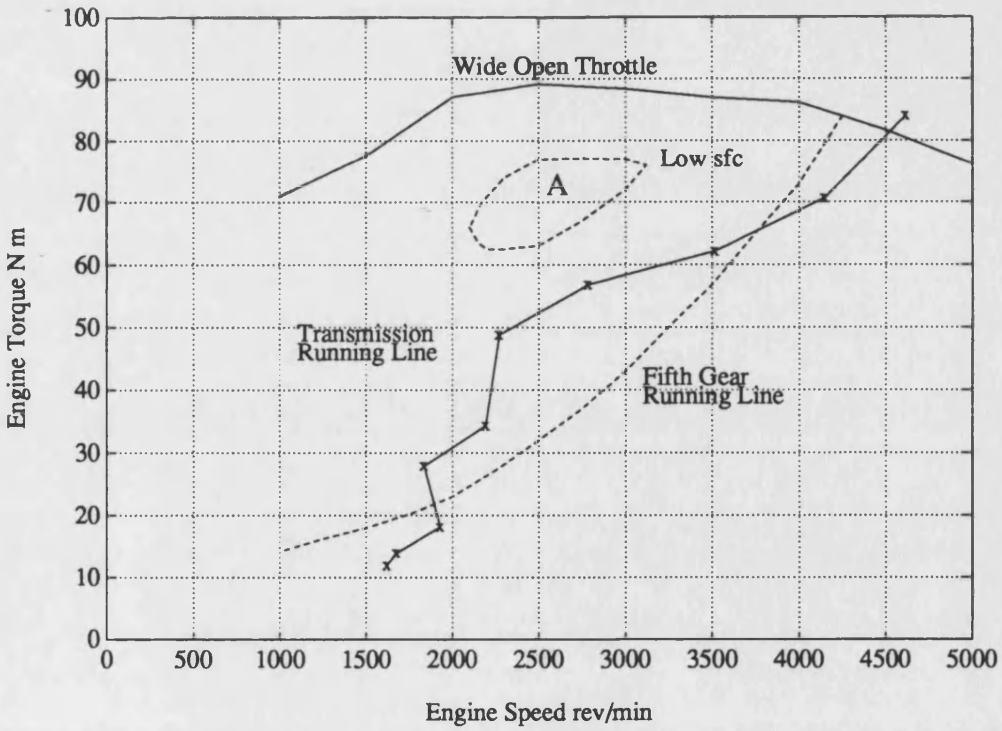

Figure 11.1 The engine map showing the steady state running lines for the transmission and for a car in fifth gear

The most efficient region for the engine to operate is around the area marked 'A' where the engine torque is high and the engine speed is low so that the power lost in internal friction in the engine is relatively small. It can be seen that the control system brings the transmission closer to this region than does the alternative fifth gear transmission over a large part of the operating range. However, the steeply rising part of the running line should be vertical and at as low an engine speed as possible consistent with comfortable running of the engine and the running line should pass much closer to the wide open throttle line, see figure 1.1. It is evident that there is still improvement to be gained if the control system moves the running line up to the region A. The running line achieved, above the 5th gear line for a considerable speed range, should be reflected in improved fuel economy but the poor mechanical efficiency, below 80% over this central part, manages to negate this. The efficiency of the normal fixed ratio gearbox is well into the nineties over this range [11.1]. However it can be seen that the control system is attempting to operate the transmission in the correct way for a CVT.

In comparison with a small car with an automatic gearbox and torque converter, a car fitted with this CVT should show some improvement in fuel economy. The mechanical efficiencies of both are very similar [11.1] but the CVT is able to run the engine in more efficient regions than can the automatic gearbox.

Methods of reducing the losses are considered later in this chapter.

11.3 Validation of the viscous shear model

The viscous model for the shear connection between the belt and the pulleys is based on elastohydrodynamic theory but does include a number of simplifying assumptions,

some of them perhaps rather crude, to enable the model to be easily used. Further work in this area could increase knowledge of the conditions in the contact and may result in changes to the design, for examples lubricant control and surface finish, which would improve the efficiency of operation. The present work suggests that some reduction in the first cost of the transmission could be made in that, if oil is present in the contact, the cost of the expensive treatment of the segment sides to eliminate the oil film [11.2] [11.3] can be saved by not using the treatment and leaving the segment sides flat. It is evident that with an oil film present and under elastohydrodynamic conditions the required shear stresses can be achieved.

The simplifying assumptions used in the viscous model are:

(a) That the pressure is uniform over the contact.

This will not be so in fact because of the inevitable discrepancies between the angles of the segment side and the pulley surface and also because of the roughened surface of the segment side after the special treatment. After some running it was noticed that the segment sides were becoming smooth as the roughened surface was worn away but the sides could not be bedding into the pulley surface as two pulleys are involved. If the effective contact is smaller than the area used in the model, the higher pressures would require the new empirical viscous relation to give higher viscosities with no overall change in the shear force. The only change would be in the line of action of the resultant force, a relatively small effect as the maximum change can only be in the region of 2 mm. The results from the transmission model would not be significantly altered by any refinement of this assumption.

(b) That the operating temperature in the contacts is a constant.

This assumption enables the viscosity to be put in terms of a simple relation similar

to the Barus Law with only two constants, η_{os} and α_s. It can only be justified by the fact that the model gives reasonable results in comparison with measured values. If the temperature does alter, as the conditions are confined to a small region, α_s will remain constant but η_{os} will vary, an increasing temperature reducing η_{os}. Thus the effect of increasing the temperature will be to increase the slip at the contact in order to transfer a given torque.

(c) That there is no oil starvation as the segment passes round a pulley.

It is considered likely that there will be plenty of oil available in front of the contact for the reasons stated in chapter 4. The calculations give oil film thicknesses compatible with the relative results of Collier and Goldsmith [11.4] from tests on a single segment with plenty of oil present and the calculated overall slips then agree reasonably well with measured slips over a wide range of conditions.

(d) That the model can be used in cases where there is considerable asperity contact

Once again this is justified by the fact that the viscous model continues to give reasonable agreement with measured results although in the low torque cases where asperity contact must be considerable the agreement is less good. The comparison of calculated drag results, including the use of a coefficient of friction with the part of the load taken by the asperities, with the measured results of Collier and Goldsmith [11.4] in chapter 4, section 4.9 shows better agreement than calculated results from the viscous model. However, this more complicated model was not used in calculations on the transmission because of the loss in simplicity.

The agreements between measured and calculated slips are reviewed as follows:

The Test 2 full throttle acceleration results were used to evaluate the two viscous constants, η_{os} and α_s. This was done by use of the slips on the primary pulley and,

although fitted at two points only, the measured and calculated curves showed the same form, figure 10.6. The secondary pulley where the conditions were very different from those in the primary pulley also produced reasonable agreement, figure 10.7, although the calculated slip values were a little low. The overall slips, figure 10.8, agreed very well.

The second set of tests, steady state cases, figures 10.12 to 10.16, produced excellent agreement for the overall slips with the larger input torques but poor agreement for the smaller torques where the asperity contact is probably considerable. With 16 N m input torque, about 20% of the maximum, the calculated slips are very low compared with the measured values while the results for 32 N m input are very much closer.

The third set of tests, also steady state, where the transmission was under the control of an external system enabling any desired secondary pressure to be set shows more interesting agreements, figures 10.19 to 10.22. These tests did show the necessity for including a minimum value of film thickness in the model. With the higher secondary pressures there is good agreement between measured and calculated values while with the lower pressures the agreement is not so good but, more interestingly and for some radii only, both curves show the same form, an increasing slope as the input torque is increased. These large and steady slips at the lower secondary pressures were not revealed in the second set of tests where the transmission was under the control of the standard control system which supplied a sufficient pressure to prevent excessive slip occurring.

The extent of the agreement between measured and calculated slips shows that over a large part of the operating envelope the simple, viscous model used is adequate. The decision to use it in every case is justified by its simplicity.

11.4 Validation of the transmission model

Apart from the slip, the only quantities measured during the tests which can be compared with calculated values from the model are:

Input shaft speed

Input shaft torque

Primary cylinder pressure.

The input speeds show good agreement, figure 10.11 for Test 2 and figure 10.17 for the first set of steady state tests, not surprising after the good agreements in the slips.

The agreement is less good for the input torques but the measured and calculated values are still reasonably close, figure 10.10 for Test 2 and figure 10.18 for the first set of steady state results. The Test 2 results, which are for an acceleration, show calculated values greater than the measured values with the discrepancy small at the start of the test and at its largest at the end where the acceleration is small and the transmission is operating close to steady state. In contrast, the steady state calculated values are, in general, less than the measured values. The steady state results closest to the results at the end of Test 2 are at the right hand end of the fourth graph in figure 10.18. No reason can be found to explain these contrasting results.

The calculated values for the primary pressure are rather disappointing, the biggest discrepancy being the error in the calculated value of approximately 20% at the start of Test 2 although the error does decrease to zero by the end of the test. It was suggested in chapter 10 that some or all of this error might be due to pressure loss in the line, the large flow into the cylinder giving a high measured pressure. However,

comparison of the Test 2 graph, figure 10.9, with that for the comparable steady state case with maximum input torque, figure 10.16, shows the same effect. In both these graphs the radii values from left to right are very similar as are the pulley pressures. It is interesting to determine what pressure changes are needed to produce the rapid change in belt configuration at the start of Test 2. Investigation of the measured results for Test 2 and for Steady state, group E shows that the differences in the pressure values are very small and difficult to determine accurately. Use of the computer model with the conditions the same as those near the start of Test 2 shows that the difference in the primary pressure required to alter conditions from steady state to those giving the radii changes shown is an increase of only 0.15 bar.

The steady state results, figures 10.12 to 10.16, show some reasonable agreement between measured and calculated values of primary pressure. In general the best agreement occurs with the lower input torques although both graphs for the two lowest torques, figures 10.12 and 10.13, show an increase in the measured pressure at the highest output speeds which is not matched by the calculated values. The medium input torque graph, figure 10.14, does show this increase in both measured and calculated values so that the model can match this effect at times. Both the graphs for the higher torques show the effect previously mentioned, low calculated values when the primary radius is small with good agreement when the radius is large.

Mechanical efficiencies determined from measured and calculated values are also shown in the steady state results, figures 10.12 to 10.16. In spite of small errors in the calculated input shaft speeds and torques, these show remarkable agreement and justify the use of calculated efficiencies in the work on losses in section 10.8.

Overall the extent of the agreement between the measured results and values calculated from the model for the few quantities that can be compared is a justification for the use of the model.

In simulation work, such as would be required in the development of a new control system, it is not necessary for all the detail included in the full model to be used. For instance the ten bands can be treated as one giving a large reduction in the number of equations required. A simplified model suitable for this work is given in Appendix number 2.

11.5 The effect of gaps between the segments

The effect of gaps on the slip was a problem for a long time during this work. Gerbert maintained that the large slips measured were due not to viscous shear but to the effect of gaps as explained in his paper [11.5]. However, he was not able to explain the slip which was measured on the secondary pulley. Some early tests to try and resolve this issue proved misleading. These repeated the second set of steady state tests with one segment removed from the belt and did show increased slips with this larger gap. Although doubts still remained, particularly on the exact location of the gaps, this effect was included in the transmission model on the assumption that the gaps occurred in the inlet sector of the primary pulley. The resulting calculated slips did show fair agreement with measured values. It was not until the very end of the work on the rig that a test was devised which did resolve this issue. The initial gap in the belt was increased slightly by grinding a thin layer off the face of a segment and this small increase did not result in extra slip. This showed that the gaps must be located in the straight length of the belt leaving the secondary pulley and enabled the

calculations described in Chapter 8 to be made with such good agreement with the measured values. With the standard belt it is not possible for the initial gap to affect the slip.

11.6 The belt related torque loss

The belt torque loss is dealt with in chapter 7 where it is shown that the loss can be large when the transmission is in an overdrive ratio, figures 7.3, 7.6 and 7.7. The actual magnitude of the loss when the transmission is in steady state under the control of the standard control system is shown in section 10.8, figures 10.25 and 10.26. In that section it is shown that the reason for the transmission not showing an improvement in fuel efficiency over conventional transmissions as it ought is because of the large losses which are detailed in figure 10.26. The belt torque loss is a substantial part of the total loss over the whole speed range and any reduction in it would result in improved economy.

One method of reducing the belt torque loss would be to reduce the secondary pulley clamping pressure. This is considered in relation to other losses as well in the next section. As this loss becomes large when the transmission is in an overdrive ratio with the primary radius large in relation to the secondary radius, another method would be to reconfigure the transmission to avoid this situation. Unfortunately the possible reconfigurations result in increased size of the transmission but careful design could keep it reasonably compact. It would be a price worth paying for a substantial increase in economy.

The most promising reconfiguration is to increase the maximum radius of the secondary pulley, with attendant increases in belt length, pulley centre distance and,

possibly, the primary pulley radius, so that the required ratio range can be achieved without the use of a small secondary radius. Another possibility is to prevent the secondary radius from becoming less than the primary radius and to obtain the required ratio range by the use of two belt-pulley systems in series, the output from the first being the input to the second. However, this is not likely to be useful as, even if the efficiency of each stage is considerably improved, the overall efficiency of the combination is bound to be low.

In order to assess the first reconfiguration, the same overall ratio range and minimum belt primary radius will be used but with a different final drive ratio in order to keep the ratio of engine speed to wheel speed the same. For the standard transmission, the low ratio is approximately 2.59:1 and the high ratio is 0.44:1 giving a ratio range of 5.89. The minimum radius of the belt on the primary pulley is 29 mm and the final drive ratio is 5.672:1.

One possibility is to have primary and secondary pulley diameters equal to 175 mm and 200 mm respectively compared with the 152 mm and 157 mm diameters of the standard pulleys. Other dimensions are:

Pulley centres distance 190 mm (155 mm standard)

Belt length 800 mm (648 mm standard)

Using the minimum primary radius of 29 mm in low ratio then gives the following radii if the same overall ratio range is to be achieved.

Low ratio: R_p = 29 mm R_s = 97 mm Ratio = 3.34:1

High ratio: R_p = 84 mm R_s = 48 mm Ratio = 0.57:1

Overall ratio range = 5.86

Required final drive ratio = 4.398:1

If a steady vehicle speed of 56 km/h is considered, calculation using the computer programme shows that the transmission with the standard control system operates with a belt torque loss equal to 3.89 N m. If the reconfigured transmission is operated at this speed with the same transmission ratio and with the secondary pressure adjusted to give the same band tension as in the standard case, the torque loss is 2.69 N m. This is a saving on the input torque of 1.20 N m when the total input is approximately 28 N m, a significant improvement. This revised torque loss was obtained using the same value of the constant K in the torque loss expression as in the standard case which is considered to be a reasonable assumption. If the calculations are repeated at 140 km/h the reduction in loss is from 6.61 N m in the standard case to 4.58 N m in the reconfigured case. These are significant improvements which can be obtained at the expense of a slightly larger transmission casing.

11.7 The losses in the system

The losses in input torque are shown plotted against vehicle speed in figure 10.26. Some of these losses can be reduced by redesigning the system:

The pump loss: A new generation of transmissions by the manufacturer uses a roller vane pump with two inlet and two outlet ports, Hendriks [11.3]. In steady state a flow control valve allows half the flow to be pumped round pressureless which would virtually halve the loss shown in the figure. The full flow is only required during a rapid ratio change.

The belt torque loss: It was shown in section 11.6 that this loss can be reduced by a reconfiguration of the belt-pulley system to avoid running the secondary pulley at a small radius.

Input shaft loss: This loss is larger than it ought to be, probably because of the drag in the reverse clutch. A redesign of the method of obtaining reverse drive should result in this loss being halved. The ECVT system which uses a magnetic powder clutch and employs two conventional synchromeshes for forward or reverse selection is used by some manufacturers, Sakai [11.6], and should have a smaller input loss.
Incorporation of all these design changes in the transmission would result in a significant reduction in the total loss and an improvement in fuel economy.

The use of an optimising control system as proposed by Guebeli et al [11.7] would result in the minimisation of the sum of the three inherent losses, the pump loss, the belt torque loss and the loss due to slip. Assuming that the same belt radii are set by the control system at the various vehicle speeds as in the standard case, these losses then depend only on the secondary pulley pressure. Using the transmission model, the secondary pressure giving the maximum mechanical efficiency can be determined for a particular vehicle speed. It was found that for all speeds there was a clearly defined pressure which gave a peak value for the efficiency.
Figure 11.2 shows the improvements in mechanical efficiency that are possible from this method of control. The optimum secondary pressure and corresponding efficiency are shown compared with the values obtained using the standard control system, all plotted against vehicle speed. The overall slips are also plotted in order to show the considerably greater slips that result from this optimisation. It is important that the nett force in a section of the belt is a tension, i.e. that the tensile force in the bands exceeds the compression in the segments. Although the optimum secondary pressures are much less than the standard pressures and the band tension is correspondingly

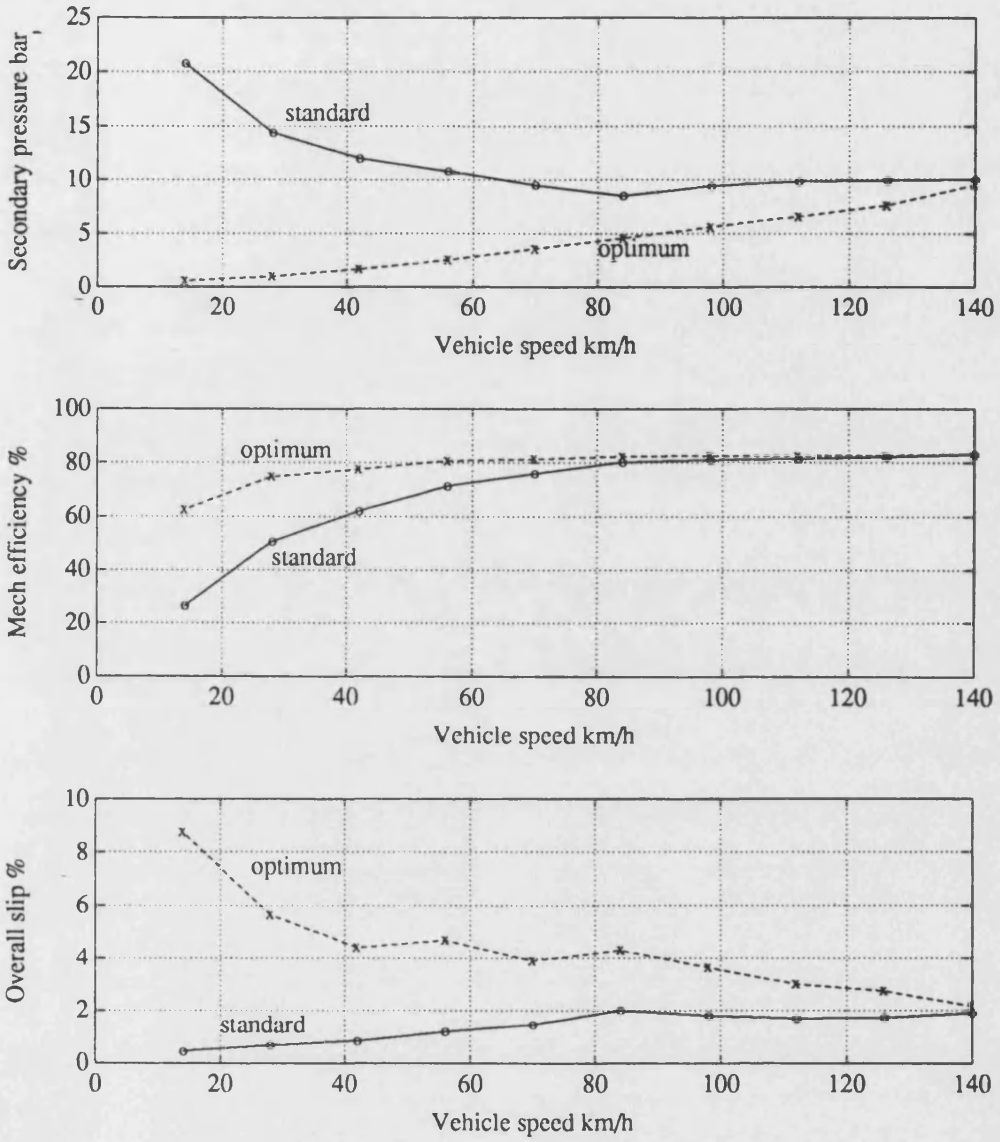

Figure 11.2 The improvements in mechanical efficiency obtainable by the use of an optimising control system

reduced, at all vehicle speeds the band tension is at least well over twice the segment compression.

If this optimisation is applied to the reconfiguration of the system considered in the last section even greater values of mechanical efficiency are obtained. For instance, at a steady speed of 56 km/h the standard transmission has an efficiency of 71.4%,

with the optimisation this becomes 80.8% while optimising the reconfigured transmission gives a value of approximately 84.0%. At the near maximum speed of 140 km/h the three values are, respectively, 83.2%, 85.3% and 85.9%.

These improvements in efficiency represent considerable reductions in fuel consumption. At 56 km/h for instance optimising the standard transmission gives a 12% improvement in fuel consumption while optimising the reconfigured transmission gives a 15% improvement. In particular, automobile operation in towns is carried out at speeds normally below 80 km/h so that big improvements in City Cycle performance can be expected. Note that these improvements do not include the effect of a variable flow pump or of a redesigned reverse clutch so that even better values are available.

Figure 11.2 does show that the optimised slips are much greater than the standard slips but above a speed of 40 km/h the slips do not exceed 4.5% and slips of this magnitude were measured at the start of the standard full throttle acceleration, Test 2, figure 10.2a. The higher slip speeds do result in thicker oil films being generated between the segment sides and the pulleys which would tend to protect the surfaces. It would be interesting to run a transmission for long periods with these slip values not only to confirm or otherwise that operating with these lower pressures is acceptable but also to verify that the improvements in efficiency are obtainable. Unfortunately the test rig has been handed on to another project and is not available for further tests. However, during the testing, the transmission was operated with high slips at times with no evident distress.

It is evident that with the low pressures proposed, if a full throttle acceleration is called for, the control system must be able to raise the pressures rapidly.

11.8 Conclusions

1. The simple viscous model based on elastohydrodynamic theory for the shear connection between the belt segments and the pulley surfaces is shown to well represent the measured slips for most of the operating conditions and to be adequate for the remainder. The Coulomb friction model used by earlier workers in the field is shown to be not suitable for representing the measured slips.

It is evident, though, that for some conditions, particularly when the transmission is lightly loaded, there must be considerable asperity contact between the surfaces. An extension of the model which included the effect of asperity contact did show better agreement with measured drag forces but was not used in the overall transmission model because of the loss in simplicity. Further work could be done to investigate the contact in order to increase understanding of the operation of the transmission.

2. The complete transmission model enables the operating conditions in the system to be determined for all cases and, where a property was measured, the corresponding calculated value is shown to give good agreement.

3. The problem of whether or not the total gap between the belt segments has an effect on the belt slip is resolved, it being shown that the gap in a normal belt has no effect.

4. The losses in the transmission are identified, in particular the three inherent losses: the pump loss, the belt torque loss and the loss due to slip. A semi-empirical theory is developed which enables the torque loss to be calculated and which gives good

agreement with measured values or values deduced from measurements.

5. The standard control system is shown to be good from the driveability point of view and does make the transmission follow a running line suitable for a continuously variable transmission and better than a corresponding 5 ratio gearbox in making the engine operate closer to the region where the engine torque is high and the engine speed is low. However, there is room for improvement by having a control system that pushes the running line further up on the engine map, figure 11.1.

6. The poor performance of the transmission from a fuel economy point of view is shown to be due to the large values of the losses for all operating conditions, the mechanical efficiency being very low. However, it is shown that very considerable improvements can be achieved, particularly for city operation, by the use of a control system that minimises the sum of the three inherent losses and allows the transmission to run with higher values of slip. Further improvements can be obtained by reconfiguring the transmission so that the secondary pulley is larger and does not need to run with the belt at a small radius. Further work is required on a transmission fitted with an optimising control system to show that these improvements are attainable and that the life of the transmission with the high slips is adequate. An increase in the flow of oil to the underside of the belt would be an advantage in these tests to ensure adequate oil is present in the contact between the belt and the pulleys.

REFERENCES

Chapter 1

1.1 Radtke, R.R. et al. Optimization of a continuously variable transmission with emission restraints. SAE 810107 1981.

1.2 Cuypers, M.H. Numerical evaluation of the torque capacities of mechanical drives, especially for continuously variable transmissions. ASME 80-C2/Det-120 1980.

1.3 Smith, M.J., Greenwood, C.J., Soar, G.B. A full-toroidal traction drive CVT - from theory into practice. Proc. I.Mech.E., Part C, 1992, 389/066.

1.4 Cuypers, M.H. Metal V-belt and V-chain traction drives. Proc. International Symposium on Advanced and Hybrid Vehicles, University of Strathclyde. 17-19 Sept, 1984.

1.5 Department of Energy, Office of Vehicle and Engine R & D. Advanced automotive transmission development status and research needs. August 1981.

1.6 Howard, G. The doubtful future of the CVT. Car Design and Technology. May 1992, page 44.

1.7 Van Doorne's Transmissie b v. Brochure on Company Profile and Product Range. VDT 05.92 1992.

1.8 Gerbert, G. Metal V-belt mechanics. ASME 84-DET-227 1984.

1.9 Becker, H.-J. Berechnung des Van Doorne cvt-schubgliederbandes. Proc. 1st Aachener Kolloquium, Fahrzeug- und Moterentechnik. Aachen, Oct 1987 page 457.

1.10 Sun, D.C. Performance analysis of a variable speed-ratio metal V-belt drive. ASME Journal of Mechanisms, Transmissions and Automation in design. Dec 1988 Vol 110 pp472-481.

1.11 Hendriks, E., ter Heegde, P., van Prooijen, T. Aspects of a metal pushing V-belt for automotive CVT application. SAE 881734 1988.

Chapter 2

2.1 Ford Motor Co. Continuously-variable transaxle for front wheel drive vehicles. Power International. Vol 33, No.389 p174.

2.2 Hahne, D. A continuously variable automatic transmission for small front wheel drive cars. Proc. I.Mech.E. Part C 2/84 1984.

Chapter 3

3.1 Hendriks, E., ter Heegde, P., van Prooijen, T. Aspects of a metal pushing V-belt for automotive CVT application. SAE 881734 1988.

3.2 Dowson, D. History of Tribology. Longman, 1979.

3.3 Gerbert, G. Metal V-belt mechanics. ASME 84-DET-227 1984.

3.4 Becker, H.-J. Berechnung des van Doorne cvt-schubgliederbandes. Proc. 1st Aachener Kolloquium, Fahrzeug- und Moterentechnik. Aachen, Oct 1987. p457.

3.5 Sun, D.C. Performance analysis of a variable speed-ratio metal V-belt drive. ASME Journal of Mechanisms, Transmissions and Automation in Design. Dec 1988, Vol 110 pp472-481.

3.6 Fujii, T., Kurokawa, T., Kanehara, S. Study on metal pushing V-belt type CVT. SAE International Congress and Exposition, Detroit, USA. March 1993.

Part 1: Relation between transmitting torque and pulley thrust. SAE 930666.

Part 2: Compression force between metal blocks and ring tension. SAE 930667.

3.7 Gerbert, G. Force and slip behaviour in V-belt drives. Acta Polytechnica Scandinavica. Mech Eng Series No.67, 1972.

3.8 Kim, H., Lee, J. Analysis of belt behaviour and slip characteristics for a metal V-belt CVT. MPT'91. Proc. JSME International Conference on Motion and Power Transmissions, Hiroshima, Nov 1991. pp394-399.

Chapter 4

4.1 Becker, H.-J. Berechnung des van Doorne cvt-schubgliederbandes. Proc. 1st Aachener Kolloquium, Fahrzeug- und Moterentechnik. Aachen. Oct 1987. p457.

4.2 Micklem, J.D., Longmore, D.K., Burrows, C.R. Modelling of the Van Doorne, metal V-belt, continuously variable transmission. MPT'91. Proc. JSME International Conference on Motion and Power Transmissions, Hiroshima, Nov 1991. pp400-404.

4.3 Guebeli, M., Micklem, J.D., Burrows, C.R. Maximum transmission efficiency of a steel belt continuously variable transmission. ASME Journal of Mechanical Design. Vol 115 No.4, 1993. pp1044-1048.

4.4 Collier, G.M., Goldsmith, A.A.J. Investigation of the lubricant film in a Ford CTX transmission. University of Bath Final Year Project. ME 11/93. 1993.

4.5 Johnson, K.L. One hundred years of Hertz contact. Proc. I.Mech.E. Vol 196, 1982. pp363-378.

4.6 Cameron, A. Basic Lubrication Theory. 3rd edition, 1981. Ellis Horwood.

4.7 Gohar, R. Elastohydrodynamics. 1988. Ellis Horwood.

4.8 Evans, C.R., Johnson, K.L. Rheological properties of elastohydrodynamic lubricants. Proc. I.Mech.E. Vol 200 Part C, 1986. pp303-312.

4.9 Johnson, K.L., Greenwood, J.A., Poon, S.Y. A simple theory of asperity contact in elastohydrodynamic lubrication. Wear. 19, 1972. pp91-108.

4.10 Kaneta, M. Effects of surface roughness in elastohydrodynamic lubrication. JSME International Journal. Series III, Vol 35, No.4, 1992 pp535-546

4.11 Karami, G., Evans, H.P., Snidle, R.W. Elastohydrodynamic lubrication of circumferentially finished rollers having sinusoidal roughness. Proc. I.Mech.E. Vol 201 Part C1 1987 pp29-36.

Chapter 5

5.1 -Kim, H., Lee, J. Analysis of belt behaviour and slip characteristics for a metal V-belt CVT. MPT'91. Proc. JSME International Conference on Motion and Power Transmissions. Hiroshima, Nov 1991. pp394-399.

5.2 Guebeli, M., Micklem, J.D., Burrows, C.R. Maximum transmission efficiency of a steel belt continuously variable transmission. ASME Journal of Mechanical Design. Vol 115 No.4 1993 pp1044-1048.

Chapter 6

6.1 Guebeli, M. A hydrostatic dynamometer for real-time engine testing Bath University Report No.083/1992.

6.2 Guebeli, M. Frequency to voltage converter. Bath University Report No.082/1992.

Chapter 7

7.1 Childs, T.H.C., Cowburn, D. Power transmission losses in V-belt drives. Proc. I.Mech.E. 1987 Vol 201, D1.
Part 1: paper 21/87. Part 2: paper 22/87.

7.2 Roovers, G. The CVT push belt: developments in efficiency and application range. 3rd European Automobile Engineers Co-operation Congress. Strasbourg, June 1991. EAEC No.91031.

7.3 Kim, H., Lee, J. Analysis of belt behaviour and slip characteristics for a metal V-belt CVT. MPT'91. Proc. JSME International Conference on Motion and Power Transmissions. Hiroshima, Nov 1991. pp394-399.

Chapter 8

8.1 - Gerbert, G. Metal V-belt mechanics. ASME 84-DET-227 1984.

Chapter 10

10.1 Becker, H.-J. Berechnung des van Doorne cvt-schubgliederbandes. Proc. 1st Aachener Kolloquium, Fahrzeug- und Moterentechnik. Aachen, Oct 1987 p457.

10.2 Roovers, G. The CVT push belt: developments in efficiency and application range. 3rd European Automobile Engineers Co-operation Congress. Strasbourg, June 1991. EAEC No.91031.

10.3 Cuypers, M.H. Metal V-belt and V-chain traction drives. International Symposium on Advanced and Hybrid vehicles. University of Strathclyde, 17-19 Sept 1984.

10.4 Hendriks, E. Qualitative and quantitative influence of a fully electronically controlled CVT on fuel economy and vehicle performance. SAE International Congress and Exposition, Detroit, USA. March 1993. SAE 930668.

10.5 van Dongen, L.A.M. Efficiency characteristics of manual and automatic passenger car transaxles. SAE 820741 1982.

10.6 Guebeli, M., Micklem, J.D., Burrows, C.R. Maximum transmission efficiency of a steel belt continuously variable transmission. ASME Journal of Mechanical Design. Vol 115 No.4 1993 pp1044-1048.

Chapter 11

11.1 - van Dongen, L.A.M. Efficiency characteristics of manual and automatic passenger car transaxles. SAE 820741. 1982.

11.2 Leibrand, N.J. Future developments in push belts for CVT application. Proc. I.Mech.E. Part C 1992 paper C389/212.

11.3 Hendriks, E., ter Heegde, P., van Prooijen, T. Aspects of a metal pushing V-belt for automotive CVT application. SAE 881734 1988.

11.4 Collier, G.M., Goldsmith, A.A.J. Investigation of the lubricant film in a Ford CTX transmission. University of Bath Final Year Project ME11/93.

11.5 Gerbert, G. Metal V-belt mechanics. ASME 84-DET-227 1984.

11.6 Sakai, Y. The 'ECVT' electro continuously variable transmission. SAE 880481 1988.

11.7 Guebeli, M., Micklem, J.D., Burrows, C.R. Maximum transmission efficiency of a steel belt continuously variable transmission. ASME Journal of Mechanical Design. Vol 115 No.4 1993 pp1044-1048.

APPENDIX 1

Papers Published with Synopses

Four papers were published during the course of this investigation.

The first was presented at the International Conference on Motion and Power Transmissions organised by the Japan Society of Mechanical Engineers and held in Hiroshima in November 1991. It proposed a viscous shear model for the segment-pulley contact after showing that a Coulomb friction model could not predict the measured slip.

The second paper was by Guebeli who used the transmission model with the viscous shear connection to show that the operation of the system could be optimised to give a maximum efficiency. It was presented at the 6th International Power Transmission and Gearing Conference organised by the American Society of mechanical Engineers and held in Phoenix, Arizona in September 1992 and was later published in the ASME Journal of Mechanical Design.

The third reported the findings on the Belt Torque Loss after this loss was found to be an important factor in the operation of the transmission. It was submited to The Institution of Mechanical Engineers and accepted for publication in Part D of the Proceedings in December 1993.

The fourth presented the model for the complete transmission. It was submitted to The

Institution of Mechanical Engineers and accepted for publication in Part C of the Proceedings in January 1994.

1. Micklem, J.D., Longmore, D.K., Burrows, C.R.

Modelling of the Van Doorne, Metal V-Belt, Continuously Variable Transmission.

Proceedings of The Japan Society of Mechanical Engineers International Conference on Motion and Power Transmissions. MPT'91. Hiroshima, November 23-26, 1991. Pages 400-404.

Synopsis: Previous papers on the Van Doorne, metal V-belt transmission are reviewed with regard to the slip in the system. All make use of a Coulomb friction model to describe the shear connection between the belt and the pulleys. It is shown that this model produces slip values which are very much less than the values obtained from measurements and that another more suitable model is required. A viscous friction model is proposed as an alternative. It is shown that the viscous model can predict the measured slips with good accuracy over a wide range of operating conditions except for conditions where the input torque is small. It is suggested that this discrepancy can be explained by an extra slip caused by gaps between the segments as they enter the primary pulley.

2. Guebeli, M., Micklem, J.D., Burrows, C.R.

Maximum Transmission Efficiency of a Steel belt Continuously Variable Transmission.

The American Society of Mechanical Engineers, Journal of Mechanical Design. Volume 115, number 4, December 1993, pages 1044-1048.

Synopsis: A mathematical model of the power transmission through a Van Doorne steel belt continuously variable transmission is developed. The approach is based on a simplified viscous oil shear stress model. This enables the determination of the power transmission loss resulting from shearing the oil film along the traction line. The power to maintain the necessary hydraulic clamping forces is taken into account to optimize the power transmission efficiency. The analytical solution is evaluated numerically and compared with experimental results. Variations in the hydraulic pump displacement that are determined by the required ratio adjustment dynamics show that with a sufficiently small pump, peak efficiencies exceeding 97 per cent are possible.

3. Micklem, J.D., Longmore, D.K., Burrows, C.R.

Belt Torque Loss in a Steel V-Belt Continuously Variable Transmission.

Proceedings of The Institution of Mechanical Engineers, Part D, volume 208, 1994.

Synopsis: To achieve the potential advantages to be gained by the use of a high ratio range, continuously variable transmission (CVT) in an automobile it is important that the system has a high efficiency and that any inherent loss mechanisms are fully understood.

This paper investigates the belt related torque loss in a steel V-belt CVT. Measurements show that the loss is dependent on the secondary pulley clamping force and on the belt configuration and these results are presented in the paper. A semi empirical model is proposed to explain the loss. The agreement between the measured results and the values calculated from the model is shown to be good.

It is also shown that when the system is in an overdrive ratio and a high efficiency

is particularly important the torque loss is large and the efficiency is severely limited, probably to less than 90 per cent.

4. Micklem, J.D., Longmore, D.K., Burrows, C.R.

Modelling of the Steel Pushing V-Belt Continuously Variable Transmission.

Proceedings of The Institution of Mechanical Engineers, Part C, volume 208, 1994.

Synopsis: The steel pushing V-belt continuously variable transmission (CVT) is now commercially available in the automobiles of a number of manufacturers but to date has not led to a significant reduction in fuel consumption. To develop its full potential it is necessary to have a good mathematical model of the system.

A number of models have been described in recent years but all make use of a Coulomb friction model for the shear connection between the belt and the pulleys. This paper proposes a friction model based on elastohydrodynamic theory. It is shown that there is good agreement between measured and calculated slip values for the transmission which justifies use of the model.

APPENDIX 2

A Simplified System Model

The model can be considerably simplified for use in simulation work where knowledge of detailed conditions is not required. Many of the details included in the complete system model, chapter 5, have only a small effect on the transmission. For instance the changes in the tension in bands 10 and 1 between adjacent stations which are expressed in equations 5.16 to 5.21 yield very small values in relation to the general level of tension when realistic values are entered in the equations. Similarly the changes in compression in the segments along the straight sections of the belt, equation 5.25, are equally small. The speeds of the individual bands, equation 5.5, are also not required. The viscous shear force applied by the inner band to the segment shoulder, force V in figure 5.4 and expressed by equation 5.11, is small in comparison with the shear force applied by the pulley surfaces to the segment sides and may be neglected. Hence the speed of the inner band is not required and equation 5.6 which gives the ratio v_1/v_s can also be neglected.

In order to reduce the computation time, the segment by segment treatment of the belt around the pulleys is also not necessary and can be replaced by an average condition.

The simplifications proposed are:

1. To treat the bands as a single band.
2. To assume a uniform mean pressure between the segments and a pulley and hence a uniform film thickness and viscosity for all the segments on the pulley.
3. To neglect the shear connection between segments and bands so that the band tension is uniform.

The equations required are then:

Belt kinematics

These are given by equations (5.1), (5.2), (5.3) and (5.4):

$$L = R_p\beta_p + R_s\beta_s + 2\sqrt{X^2 - (R_s - R_p)^2} \qquad \text{(A1)}$$

where

$$\beta_p = \pi - 2\alpha\,, \quad \beta_s = \pi + 2\alpha$$
$$\text{and} \quad \sin\alpha = \frac{R_s - R_p}{X} \qquad \text{(A2)}$$

$$v_{Rs} = -\,v_{Rp}\,\frac{\beta_p}{\beta_s} \qquad \text{(A3)}$$

Radial belt equation

Equation (5.13) can be integrated as a result of simplification 2 and becomes:

$$F = \frac{\beta}{2\tan\theta}\left[T_b - \frac{C_0 + C_\beta}{2} + \frac{\eta_s v_R 4acR}{st_s\cos^2\theta} - m_b v_s^2\right] \qquad \text{(A4)}$$

Longitudinal belt equations

As the conditions on the segments around a pulley are now uniform, equations (5.8) and (5.9) can be combined to give the torque contributed by a segment. This can be multiplied by the number of segments engaged to give the torque on the pulley.

$$T = \frac{4a\beta R}{s}\frac{\eta_s}{t_s}\left(n - \frac{v_s}{R}\right)\left(R^2c - Rc^2\cos\theta + \frac{c^3\cos^2\theta}{3}\right) \qquad \text{(A5)}$$

As the shear connection between bands and segments is being neglected

$$C_\beta - C_0 = \frac{T}{R} \qquad \text{(A6)}$$

Shear connection between segments and pulley

The normal load on the segment side/length of contact is given by equation (5.14). Assuming this is uniform around a pulley and neglecting the small effect of the radial velocity:

$$\frac{W_c}{L_c} = \frac{FS}{c\beta R\cos\theta} \tag{A7}$$

Equation (4.5):

$$R_c = R/\sin\theta \tag{A8}$$

Equation (4.3):

$$\frac{t_s}{R_c} = 1.90\left(\frac{\eta_o v_{sl}}{ER_c}\right)^{0.69}(E\alpha)^{0.56}\left(\frac{ER_cL_c}{W_c}\right)^{0.1} \tag{A9}$$

with the condition that t_s is not less than t_{smin}.

The width of the Hertzian contact, $2a$, is given by equation (4.1):

$$a = 1.52\left(\frac{W_cR_c}{L_cE}\right)^{1/2} \tag{A10}$$

The viscosity is given by equation (4.6):

$$\eta_s = \eta_{os}e^{\alpha_1 P_m} \tag{A11}$$

and the mean pressure by (5.15):

$$P_m = \frac{W_c}{L_c}\cdot\frac{1}{2a} \tag{A12}$$

Belt torque loss

The relations for the torque loss are given in equations (7.4), (7.6) and (7.7):

Determine the factors k_p and k_s from

$$R\sqrt{1 - k^2} = K \tag{A13}$$

The torque transferred in the secondary pulley is then the output torque plus T_{Ls} where

$$T_{Ls} = \frac{T_b R_s}{k_s}(1 - k_s^2) \tag{A14}$$

The torque input to the primary pulley is increased by T_{Lp} where

$$T_{Lp} = \frac{T_b R_p}{k_p}(1 - k_p^2) \tag{A15}$$

Torque required to drive the pressurising pump, T_g

The pump torque is given by equation (5.26) and is added to the input torque

$$T_g = \frac{2V_p(F_s - F_{sp})}{\eta_{mp}\pi^2(D_{s1}^2 - D_{s2}^2)} \tag{A16}$$

Comparison with experimental results

In order to demonstrate that these simplified equations give reliable results, they were used to determine the Overall Slip, the Primary Cylinder Pressure and the Input Torque using the values from Test 2, figure 10.2(a) and (b), listed in section 10.4. The calculated values are compared with the measured values in figure A2.1. It can be seen that the agreement is good and little different from the results obtained with the full model, figures 10.8, 10.9 and 10.10.

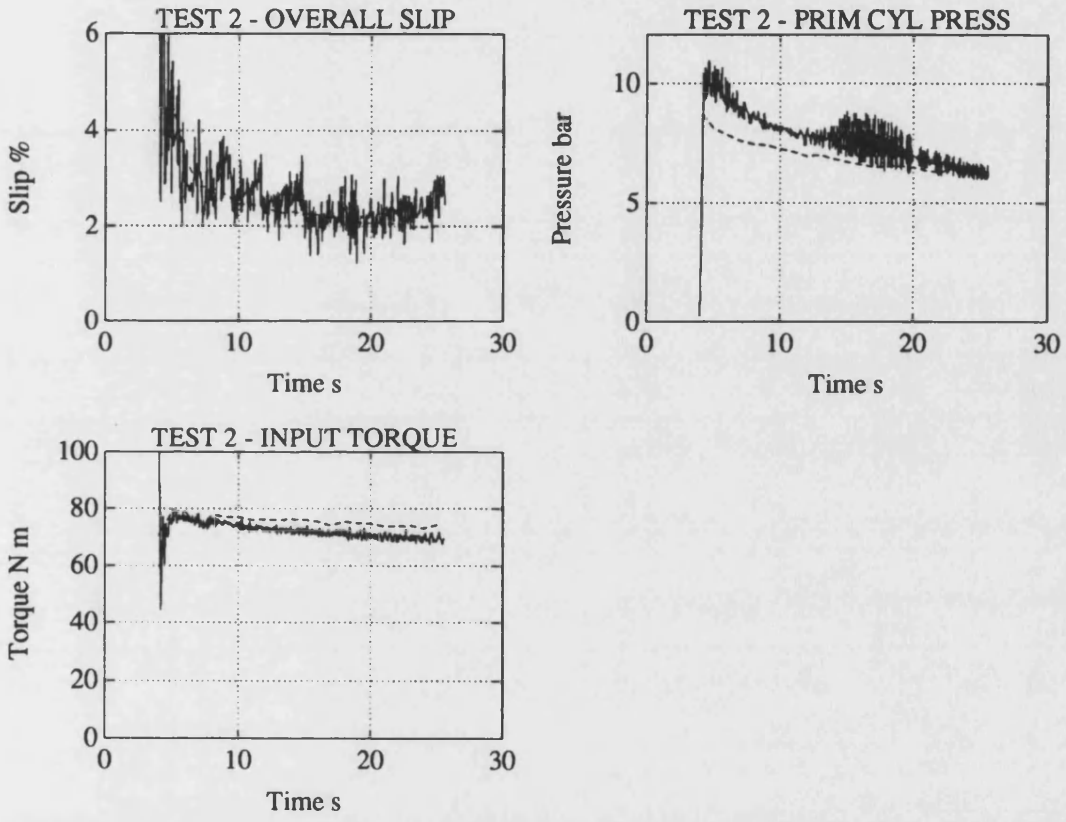

Figure A2.1 Comparison of results from the simplified model (---) with measured values (—) from Test 2

APPENDIX 3

The Computer Programmes

A possible sequence of calculations using the equations for the transmission model is shown in chapter 9. This sequence was used to construct a computer programme called BELTOPX.BAS written in BASIC. When the programme is run, the computer requests the input of the values of the five input parameters, the computation is carried out and the important calculated quantities are displayed on the screen. This programme was progressively modified during the course of the investigation as, for examples, the emphasis on the choice of input parameters changed from transmission output shaft to input shaft and back again; the inclusion of the effect of gaps between the segments was required; the inclusion of belt torque loss was required; the viscous shear model for the segment pulley contact was changed from empirical to elastohydrodynamic; the calculations around a pulley were changed from an average treatment of the segments to a segment by segment calculation. The final programme, BELTOP14, which embodies all the effects determined in the course of the research is listed below.

The values of the dimensions, etc, for the transmission tested which were used in the programmes are listed on the following page.

Pulley centres distance, X, 155 mm

Belt length, L, 648.6 mm

Thickness of a band, t_b, 0.191 mm

Distance of segment shoulder above rocking edge, x, 1.20 mm

Segment thickness, s, 2.184 mm

Length of segment side, c, 4.60 mm

Half the pulley wedge angle, θ, 11°

Total width of the two band packs, w, 17.52 mm

Mass per unit length of a band, m, 0.0262 kg/m

Mass of a segment, m_s, 0.00294 kg

Final drive speed ratio, R_d, 5.672

Modulus of elasticity, E, 207 GN/m^2

Basic viscosity of the oil, η_o, 0.0068 N s/m^2

Viscosity pressure coefficient, α, 1.403 x 10^{-8} m^2/N

Empirical values for the elastohydrodynamic contact:

Basic viscosity, η_{os}, 0.210 N s/m^2

Viscosity pressure coefficient, α_s, 2.75 x 10^{-8} m^2/N

Minimum film thickness, t_{smin}, 110 x 10^{-9} m

Assumed oil film thicknesses:

Between bands, t_f, 0.5 x 10^{-6} m

Between inner band and segment shoulder, t_{fl}, 0.8 x 10^{-6} m

Assumed mechanical efficiencies:

Final drive, η_{md}, 98.5%

Oil pump, η_{mp}, 70.0%

Outer and inner secondary pulley cylinder diameters,

D_{s2}, 120.5 mm; D_{s1}, 45 mm

Outer and inner primary pulley cylinder diameters,

D_{p2}, 166 mm; D_{p1}, 45 mm

Force exerted by the spring in the sec. pulley cylinder, F_{sp}, 750 N

Volumetric flow rate of oil through the pump, V_p, 9.72 cm^3/rev

The listing of the final programme, BELTOP14, is on the following pages.

```
10 DIM V(11),Y(11),T1(11),VSLS(20),STSG(20),VSLP(20),CP1(20)
20 READ C,L,TB,X,S,CS,TH,E,TF,TF1,E0,ALF,W,M,MS,RD
30 DATA 0.155,0.6486,0.000191,0.0012,0.002184,0.0046,0.192,207E9
40 DATA 0.0000005,0.0000008,0.0068,1.403E-8,0.01752,0.0262,0.00294,5.672
50 READ E0S,ALFS,EMD,EMP,TSMN
60 DATA 0.210,2.75E-8,0.985,0.70,110E-9
70 PRINT "TYPE IN VALUES OF:-"
80 PRINT "OUTPUT SHAFT SPEED rev/min"
90 PRINT "OUTPUT TORQUE N m"
100 PRINT "SEC PULLEY CYLINDER PRESSURE bar"
110 PRINT "BELT RADIUS ON PRIMARY PULLEY m"
120 PRINT "RADIAL VELOCITY OF BELT ON PRIMARY PULLEY m/s"
130 INPUT NOUT,TOUT,PS,RP,VRP
140 NS=NOUT*RD*.10472
150 TS=-TOUT/RD/EMD
160 FS=(PS+.765)*981.4
200 REM DETERMINE RS AND ANGLES OF LAP
210 RS=.0026/RP
220 SINA=(RS-RP)/C
230 A=ATN(SINA/(1-SINA^2)^.5)
240 L1=RP*(3.14159-2*A)+RS*(3.14159+2*A)+2*(C^2-(RS-RP)^2)^.5
250 IF L1-L>.001 THEN 330
260 IF L1-L<0 THEN 350
270 RS=RS-.00001
280 SINA=(RS-RP)/C
290 A=ATN(SINA/(1-SINA^2)^.5)
300 L2=RP*(3.14159-2*A)+RS*(3.14159+2*A)+2*(C^2-(RS-RP)^2)^.5
310 IF L2-L>.0001 THEN 270
320 GOTO 370
330 RS=RS-.0002
340 GOTO 220
350 RS=RS+.0002
360 GOTO 220
370 BP=3.14159-2*A
380 BS=3.14159+2*A
390 VRS=-VRP*BP/BS
400 Z=L-RP*BP-RS*BS
450 REM DETERMINE BAND SPEEDS IN TERMS OF VS
460 Z3=RP*BP*(RP+X)/(RP+X+TB/2)
470 Z4=RS*BS*(RS+X)/(RS+X+TB/2)
480 V(1)=(L+6.2832*X)/(Z3+Z+Z4)
490 SVNS=V(1)^2
500 FOR N=2 TO 10
510 Z5=(RP+X+(N-1)*TB)^2*BP/(RP+X+(N-1.5)*TB)
520 Z6=(RS+X+(N-1)*TB)^2*BS/(RS+X+(N-1.5)*TB)
530 Z7=(RP+X+(N-1)*TB)^2*BP/(RP+X+(N-.5)*TB)
540 Z8=(RS+X+(N-1)*TB)^2*BS/(RS+X+(N-.5)*TB)
550 V(N)=V(N-1)*(Z5+Z+Z6)/(Z7+Z+Z8)
560 SVNS=SVNS+V(N)^2
570 NEXT N
630 TB1=2*TAN(TH)*FS/BS-TS/RS/2+(NS*RS)^2*(MS/S+M*SVNS)
700 REM DETERMINE BELT SPEED
710 ISYN=0
720 FOR N=1 TO 10
730 Y(N)=L+6.2832*(X+(N-.5)*TB)
740 ISYN=ISYN+1/Y(N)
750 NEXT N
760 Z1=RS^2*CS-RS*CS^2*COS(TH)+CS^3*(COS(TH))^2/3
770 Z2=2*RS*CS-CS^2*COS(TH)
780 YS=RS-2*Z1/Z2
790 M1=INT(RS*BS/S)
800 CT=1
805 VSLS(1)=.1
810 VS=(NS+VSLS(CT)/(RS-YS))*RS
820 CP=0
822 KP=(1-(.006/RP)^2)^.5
824 KS=(1-(.006/RS)^2)^.5
826 TLS=TB1*RS/KS*(1-KS^2)+TS*(1/KS-1)
828 TLP=TB1*RP*KP*(1/KP^2-1)+TS*RP/RS*(1-KP)
```

```
830 STSG(CT)=0
840 FS1=0
850 FOR N=1 TO M1
860 WPLS=(TB1-CP-VS^2*(MS/S+M*SVNS))*S/(2*CS*RS*SIN(TH))
870 RFS=5.24*RS
880 AS=(2.317*WPLS*RFS/E)^.5
890 PSM=WPLS/2/AS
900 C10=E0*VSLS(CT)/E/RFS
910 C11=E*RFS/WPLS
920 TSS=1.93*C10^.69*(E*ALF)^.56*C11^.1*RFS
930 IF TSS<TSMN THEN 950
940 GOTO 951
950 TSS=TSMN
951 IF N=1 THEN 953
952 GOTO 954
953 TSS3=TSS
954 IF N=M1 THEN 956
955 GOTO 960
956 TSS2=TSS
960 ESS=E0S*EXP(ALFS*PSM)
970 WS=2*ESS/TSS*(NS-VS/RS)*AS*(2*RS*CS-CS*CS*COS(TH))
980 DC=-WS*(1-YS/RS)
990 CP=CP+DC
1000 TSG=WS*(RS-YS)
1010 STSG(CT)=STSG(CT)+TSG
1020 C20=ESS*VRS*4*AS*CS*RS/(S*TSS*COS(TH)*COS(TH))
1030 DFSG=(TB1-CP+C20-VS^2*(MS/S+M*SVNS))*S/(2*RS*TAN(TH))
1040 FS1=FS1+DFSG
1050 NEXT N
1060 IF ABS(FS-FS1)<40 THEN 1090
1070 TB1=TB1*FS/FS1
1080 GOTO 820
1090 IF ABS((TS-TLS)-STSG(CT))<.2 THEN 1115
1092 IF CT>1 THEN 1100
1094 VSLS(2)=VSLS(1)*(TS-TLS)/STSG(1)
1096 CT=2
1098 GOTO 810
1100 CT=CT+1
1102 X10=(TS-TLS)*(VSLS(CT-2)-VSLS(CT-1))
1103 X11=VSLS(CT-1)*STSG(CT-2)-VSLS(CT-2)*STSG(CT-1)
1104 X12=STSG(CT-2)-STSG(CT-1)
1105 VSLS(CT)=(X10+X11)/X12
1110 GOTO 810
1115 VSLS=VSLS(CT)
1120 FOR N=1 TO 10
1130 V(N)=V(N)*VS
1140 NEXT N
1150 T1(1)=TB1/Y(1)/ISYN
1160 FOR N=2 TO 10
1170 T1(N)=T1(1)*Y(1)/Y(N)
1175 NEXT N
1180 C2=CP
1300 REM DETERMINE CONDITIONS AT THE PRIMARY PULLEY
1310 M2=INT(RP*BP/S)
1320 Z11=RP^2*CS-RP*CS^2*COS(TH)+CS^3*(COS(TH))^2/3
1330 Z12=2*RP*CS-CS^2*COS(TH)
1340 YP=RP-2*Z11/Z12
1350 VSLP(1)=.2
1355 CT=1
1360 NP=VSLP(CT)/(RP-YP)+VS/RP
1370 CP1(CT)=C2
1380 STSG1=0
1390 FP1=0
1400 FOR N=1 TO M2
1410 WPLP=(TB1-CP1(CT)-VS^2*(MS/S+M*SVNS))*S/(2*CS*RP*SIN(TH))
1420 RFP=5.24*RP
1430 AP=(2.317*WPLP*RFP/E)^.5
1440 PPM=WPLP/2/AP
```

```
1450 C12=E0*VSLP(CT)/E/RFP
1460 C13=E*RFP/WPLP
1470 TSP=1.93*C12^.69*(E*ALF)^.56*C13^.1*RFP
1480 IF TSP<TSMN THEN 1500
1490 GOTO 1501
1500 TSP=TSMN
1501 IF N=1 THEN 1503
1502 GOTO 1504
1503 TSP1=TSP
1504 IF N=M2 THEN 1506
1505 GOTO 1510
1506 TSP4=TSP
1510 ESP=E0S*EXP(ALFS*PPM)
1520 WP=2*ESP/TSP*VSLP(CT)/(RP-YP)*AP*(2*RP*CS-CS*CS*COS(TH))
1530 DC1=-WP*(1-YP/RP)
1540 CP1(CT)=CP1(CT)+DC1
1550 TSG1=WP*(RP-YP)
1560 STSG1=STSG1+TSG1
1570 C21=ESP*VRP*4*AP*CS*RP/(S*TSP*COS(TH)*COS(TH))
1580 DFSG1=(TB1-CP1(CT)+C21-VS^2*(MS/S+M*SVNS))*S/(2*RP*TAN(TH))
1590 FP1=FP1+DFSG1
1600 NEXT N
1610 IF ABS(CP1(CT))<10 THEN 1640
1614 IF CT>1 THEN 1624
1616 VSLP(2)=VSLP(1)*C2/(C2-CP1(1))
1618 CT=2
1620 GOTO 1360
1624 CT=CT+1
1626 X13=VSLP(CT-2)*CP1(CT-1)-VSLP(CT-1)*CP1(CT-2)
1628 X14=CP1(CT-1)-CP1(CT-2)
1630 VSLP(CT)=X13/X14
1635 GOTO 1360
1640 TP=STSG1
1650 FP=FP1
1660 PP=FP/2005.2
1670 TG=.1547*PS/EMP
1680 TC=.005*NP
1690 TI=TP+TLP+TG+TC
1700 NI=NP*9.549
1710 SL=(-NS*RS/(NP*RP)+1)*100
1720 EFF=TOUT*NOUT/(TI*NI)
1900 REM PRINT OUT OF RESULTS
1901 PRINT
1902 PRINT
1903 PRINT
1904 PRINT"TSS3 =";TSS3;TAB(30);"TSS2 =";TSS2
1905 PRINT"TSP1 =";TSP1;TAB(30);"TSP4 =";TSP4
1910 PRINT "RP =";RP;TAB(20);"RS =";RS;TAB(40);"BP =";BP;TAB(60);"BS =";BS
1920 PRINT "VRP =";VRP;TAB(20);"VRS =";VRS
1930 PRINT "VS =";VS;TAB(40);"V1 =";V(1);TAB(60);"V2 =";V(2)
1940 PRINT "V3 =";V(3);TAB(20);"V4 =";V(4);TAB(40);"V5 =";V(5);TAB(60);
1941 PRINT "V6 =";V(6)
1950 PRINT "V7 =";V(7);TAB(20);"V8 =";V(8);TAB(40);"V9 =";V(9);
1951 PRINT TAB(60);"V10 =";V(10)
1960 PRINT "C2 =";C2;TAB(40);"ST1 =";TB1
1970 PRINT "T1,1 =";T1(1);TAB(20);"T1,2 =";T1(2);TAB(40);"T1,3 =";T1(3);
1971 PRINT TAB(60);"T1,4 =";T1(4)
1980 PRINT "T1,5 =";T1(5);TAB(20);"T1,6 =";T1(6);TAB(40);"T1,7 =";T1(7);
1981 PRINT TAB(60);"T1,8 =";T1(8)
1990 PRINT "T1,9 =";T1(9);TAB(20);"T1,10 =";T1(10)
1995 PRINT "VSLS =";VSLS
1996 PRINT "VSLP =";VSLP(CT)
2000 PRINT "FS =";FS;TAB(20);"FP =";FP
2010 PRINT "Nin =";NI;TAB(20);"Nout =";NOUT
2020 PRINT "TG =";TG;TAB(20);"TC =";TC;TAB(40);"TP =";TP
2021 PRINT "TI =";TI;TAB(20);"TO =";TOUT
2030 PRINT "PP =";PP;TAB(20);"PS =";PS
2040 PRINT "SLIP =";SL;"%";TAB(20);"EFF =";EFF
2050 END
```

A typical print out of results is shown below. It is for the case where:

- Output shaft speed = 900 rev/min

  Output shaft torque = 250 N m

  Secondary pulley cylinder pressure = 8 bar

  Belt radius on primary pulley = 65 mm

  Radial velocity of belt on primary pulley = 0

```
TSS3 = 1.1E-07                TSS2 = 1.166389E-07
TSP1 = 2.145727E-07           TSP4 = 1.960487E-07
RP = .065          RS = 4.169002E-02   BP = 3.44351     BS = 2.839671
VRP = 0            VRS = 0
VS = 22.70182                          V1 = 22.98648    V2 = 23.02848
V3 = 23.07049      V4 = 23.11249       V5 = 23.1545     V6 = 23.1965
V7 = 23.2385       V8 = 23.28051       V9 = 23.32251    V10 = 23.36452
C2 = 1121.615                          ST1 = 2704.858
T1,1 = 272.7026    T1,2 = 272.2052     T1,3 = 271.7095  T1,4 = 271.2157
T1,5 = 270.7237    T1,6 = 270.2335     T1,7 = 269.745   T1,8 = 269.2584
T1,9 = 268.7734    T1,10 = 268.2902
VSLS = .3933325
VSLP = .6838388
FS = 8601.972      FP = 10731.78
Nin = 3439.283     Nout = 900
TG = 1.768         TC = 1.80086        TP = 72.5457
TI = 77.32119      TO = 250
PP = 5.351973      PS = 8
SLIP = 4.804379 %  EFF = .846089
```

APPENDIX 4

Tables of Results

The First set of tests

Results from these tests are not tabulated here because of the quantity of data involved. However, all the values are plotted in figures 10.1 to 10.11.

The Second set of tests

This set is represented by Table 1 which shows the repeat results after the inclusion of the Primary Pulley Speed. This speed was included after the discovery of a very high slip in a few high torque cases, see results D1 and E1, in order to discover whether the slip was in the belt system or the clutch, the latter being the case. The results are for steady state conditions with the transmission under the control of the standard control system. Each test is for a fixed output shaft speed set by the dynamometer and a fixed input shaft torque set by adjustment of the engine throttle. The set is divided into five groups, A, B, C, D and E, each with a uniform input shaft torque and containing the results for fourteen output shaft speeds.

The Third set of tests

This set is of steady state tests with fixed pulley radii obtained by the use of spacers

to set the primary radius. It is divided into a number of groups, each with a particular spacer fixing the radii and with the transmission under the control of an external system supplying the pressures, and is represented by a number of Tables as follows: For the main tests, results from Groups V, W, X and Z are listed in Tables 2 to 5 respectively, no results being taken in Group Y. The results in each Group are divided into subgroups with approximately uniform input shaft torques and show tests for low, medium and high input shaft speeds with a range of secondary pressures. Some lines of results are missing when the test was aborted because the transmission was slipping badly.

Table 6 shows the results for the measurement of the input shaft loss when the transmission was run without a belt.

Table 7 shows results for the transmission running with the output shaft disconnected in order to determine the belt torque loss on no-load. It is divided into four groups, a, b, c and d, each for a fixed radius set by a particular spacer.

Table 8 shows the results for a repeat of the Group V tests, Table 2, but with an increased gap between segments obtained by removing a segment from the belt.

Table 9 shows the reults for a repeat of the Group W tests, Table 3, but with an increased gap obtained by grinding 0.40 mm off the face of one segment.

Table 1 **Steady state results with the transmission under the control of the standard control system. 13 June 1991.**

		Engine Speed [rpm]	Prim. Pulley Speed [rpm]	Sec. Pulley Speed [rpm]	Belt Speed [m/s]	Prim. Torque [Nm]	Sec. Torque [Nm]	Prim. Radius [mm]	Sec. Radius [mm]	Prim. Press. [bar]	Sec. Press. [bar]	Clutch Press. [bar]	Throttle Angle [deg]	Belt Slip. [%]	CTX Efficency
A	1	1611.35	1624.04	588.44	4.77	15.99	18.74	28.80	74.55	0.01	22.52	2.68	7.18	6.21	0.43
	2	1720.53	1725.96	1140.53	7.77	17.16	13.74	43.35	63.47	7.50	17.48	2.84	7.76	3.26	0.53
	3	1895.19	1897.03	1712.03	10.21	16.99	11.14	51.88	55.89	6.83	14.65	3.00	8.42	2.68	0.59
	4	1923.54	1927.92	2281.42	11.81	18.05	9.42	59.10	48.57	7.12	11.99	3.06	8.83	2.76	0.62
	5	1899.23	1909.12	2868.05	12.80	16.51	5.87	64.81	42.12	6.51	10.32	3.09	8.32	2.35	0.54
	6	1923.60	1933.29	3437.05	13.67	19.57	6.13	68.52	37.57	6.31	9.15	3.13	9.12	2.53	0.56
	7	1946.49	1955.39	4013.77	14.38	16.44	3.71	71.36	33.88	6.30	8.62	3.11	8.51	2.54	0.47
	8	2054.12	2061.76	4585.92	15.48	16.86	3.49	72.83	31.92	7.03	8.33	3.15	9.08	2.51	0.46
	9	2314.51	2316.53	5152.32	17.42	15.65	2.77	72.82	31.90	8.03	8.60	3.29	9.75	2.56	0.39
	10	2568.82	2574.68	5727.00	19.33	16.40	2.62	72.82	31.94	8.18	8.47	3.50	10.85	2.43	0.36
	11	2824.05	2832.52	6301.97	21.25	17.53	2.04	72.81	31.95	8.10	8.29	3.62	12.22	2.36	0.26
	12	3087.52	3088.09	6876.44	23.23	17.24	2.56	72.80	31.91	7.43	7.68	3.76	13.11	2.39	0.33
	13	3348.71	3353.29	7443.12	25.17	18.00	2.92	72.78	32.00	8.01	8.26	3.94	14.37	2.40	0.36
	14	3608.81	3605.32	8015.04	27.10	18.18	2.98	72.77	31.96	6.97	7.30	4.06	15.29	2.38	0.36
B	1	1575.51	1585.96	569.23	4.62	34.70	66.27	28.80	74.54	0.01	22.69	2.75	10.75	7.11	0.69
		1718.41	1727.28	1141.74	7.74	34.21	37.69	43.55	63.44	7.97	17.57	2.98	11.35	3.28	0.73
		1901.11	1904.78	1712.62	10.22	32.52	27.71	51.71	55.96	7.33	14.95	3.21	11.84	2.66	0.77
		1968.34	1976.47	2284.87	11.95	31.91	20.61	56.48	49.22	7.78	12.28	3.28	12.06	2.71	0.75
		1967.34	1972.27	2865.80	13.13	33.40	17.28	64.04	43.01	7.33	11.06	3.32	12.36	2.41	0.75
		1936.87	1948.70	3436.54	13.75	32.24	13.49	68.37	37.76	6.76	9.49	3.34	12.14	2.60	0.74
		1991.85	1995.98	4012.18	14.64	32.55	11.60	70.93	34.43	6.80	9.13	3.35	12.29	2.41	0.72
		2059.59	2062.72	4563.23	15.51	33.80	10.83	72.79	31.94	7.22	8.56	3.38	12.98	2.52	0.71
		2316.80	2324.60	5151.82	17.44	34.87	10.83	72.80	31.97	8.30	8.87	3.58	14.65	2.68	0.69
		2576.32	2578.95	5727.57	19.36	32.04	9.47	72.79	31.95	8.43	8.76	3.75	14.99	2.51	0.66
		2833.61	2836.57	6300.13	21.29	32.19	9.25	72.79	31.96	8.35	8.55	3.89	16.24	2.48	0.64
		3091.31	3095.51	6868.01	23.22	33.78	9.67	72.78	31.99	7.65	7.82	3.96	17.92	2.48	0.64
		3350.95	3357.07	7444.61	25.21	33.73	9.77	72.75	32.01	8.20	8.49	4.13	18.94	2.42	0.64
	14	3615.79	3613.84	8014.90	27.15	32.45	9.27	72.75	32.00	7.18	7.48	4.26	19.54	2.43	0.63
C	1	1592.00	1599.24	567.36	4.64	49.15	101.44	28.80	74.53	0.00	22.89	2.83	14.40	8.19	0.74
		1717.10	1726.97	1140.63	7.74	49.53	59.97	43.38	63.40	8.67	17.85	3.07	15.32	3.46	0.80
		1974.65	1982.85	1713.05	10.39	48.07	45.34	50.64	56.99	8.36	16.02	3.45	16.57	2.77	0.82
		2155.28	2158.01	2281.97	12.54	47.99	37.17	56.16	51.63	8.47	13.26	3.61	17.61	2.79	0.82
		2187.36	2190.24	2865.21	13.96	47.70	29.61	61.50	45.96	8.08	12.07	3.66	17.73	2.25	0.81
		2181.06	2189.97	3434.83	14.90	49.62	24.73	65.84	40.92	7.98	11.23	3.69	18.33	2.51	0.78
		2197.89	2206.31	4010.03	15.72	47.03	20.56	68.99	36.99	7.20	9.39	3.65	17.59	2.55	0.80
		2271.87	2274.24	4582.95	16.70	47.93	19.16	70.99	34.36	6.68	8.50	3.73	18.18	2.47	0.81
		2390.62	2393.10	5151.18	17.85	48.87	17.39	72.26	32.69	7.51	9.04	3.83	19.15	2.63	0.77
		2582.81	2584.43	5727.14	19.41	49.59	17.22	72.76	32.00	8.23	8.96	3.97	20.50	2.53	0.77
		2842.31	2842.73	6301.62	21.35	48.44	17.17	72.76	32.00	8.39	8.74	4.11	21.69	2.49	0.79
		3099.41	3100.35	6875.45	23.30	49.35	17.32	72.75	32.00	7.82	8.11	4.21	23.83	2.46	0.78
		3365.29	3364.84	7443.47	25.25	50.06	17.07	72.73	32.06	8.48	8.76	4.41	25.98	2.48	0.75
	14	3620.81	3623.66	8011.85	27.19	49.41	16.56	72.73	32.09	7.44	7.75	4.56	27.37	2.44	0.74

Table 1(continued).

	Engine Speed [rpm]	Prim. Pulley Speed [rpm]	Sec. Pulley [rpm]	Belt Speed [m/s]	Prim. Torque [Nm]	Sec. Torque [Nm]	Prim. Radius [mm]	Sec. Radius [mm]	Prim. Press. [bar]	Sec. Press. [bar]	Clutch Press. [bar]	Throttle Angle [deg]	Belt Slip [%]	CTX Efficncy
D	2183.29	1601.43	563.29	4.66	64.45	138.15	28.80	74.53	-0.02	23.92	3.09	26.39	0.97	0.55
	1784.02	1794.60	1140.19	7.86	64.91	83.83	42.53	64.13	10.60	18.92	3.39	23.79	4.20	0.83
	2076.45	2084.42	1712.52	10.63	65.86	66.83	49.33	58.22	10.37	17.46	3.76	26.11	3.03	0.84
	2531.29	2537.21	2281.17	13.59	64.13	60.12	51.72	55.99	9.05	15.18	4.24	29.45	2.68	0.84
	2698.65	2705.02	2864.17	15.70	63.32	50.70	56.07	51.74	8.87	13.75	4.42	30.24	2.28	0.85
	2770.39	2775.15	3434.13	17.26	63.60	42.83	60.11	47.52	8.18	12.44	4.45	31.14	2.18	0.83
	2858.29	2863.09	4005.53	18.70	64.23	38.84	63.15	44.12	7.86	11.49	4.58	33.06	2.25	0.85
	2794.43	2800.61	4582.38	19.31	62.89	31.88	66.72	39.86	7.49	10.37	4.51	30.92	2.26	0.83
	2884.54	2886.04	5150.26	20.47	64.20	29.73	68.61	37.50	7.88	10.62	4.61	33.01	2.47	0.83
	2975.00	2980.39	5725.23	21.57	64.26	27.57	70.09	35.60	7.66	9.86	4.61	34.50	2.44	0.83
	3076.27	3079.73	6300.34	22.66	66.09	26.32	71.30	34.00	7.11	8.66	4.67	36.33	2.44	0.82
	3121.09	3123.23	6864.60	23.41	65.64	23.80	72.64	32.19	7.38	8.58	4.69	36.94	2.59	0.80
	3374.02	3371.44	7443.61	25.31	64.82	23.27	72.69	32.12	8.45	9.09	4.72	38.59	2.45	0.79
	3635.66	3628.84	8010.78	27.24	65.43	23.20	72.69	32.15	7.85	8.23	4.98	41.04	2.36	0.78
E	2296.77	1607.47	564.50	4.64	70.18	151.82	28.80	74.52	0.01	24.34	3.13	32.86	9.14	0.53
	2738.89	2733.41	1136.28	8.90	80.36	156.35	31.43	72.60	10.63	23.20	4.78	83.58	3.98	0.81
	3275.59	3270.26	1710.54	12.53	78.72	123.90	36.99	68.54	9.83	20.93	5.01	90.11	3.07	0.82
	3525.90	3522.90	2279.27	15.55	78.19	100.21	42.62	64.04	9.50	18.69	5.17	90.11	2.80	0.83
	3714.04	3708.64	2864.16	18.20	77.70	84.96	47.40	59.97	9.05	17.01	5.21	90.11	2.29	0.84
	3807.00	3800.89	3433.28	20.35	77.34	73.83	51.70	56.03	9.10	16.25	5.27	90.11	2.10	0.86
	3938.40	3934.61	4006.38	22.41	77.07	64.79	54.91	52.91	8.55	15.00	5.32	90.11	1.90	0.86
	4088.96	4085.10	4580.68	24.35	76.45	57.78	57.48	50.33	8.07	13.62	5.28	90.11	1.81	0.85
	4157.25	4152.00	5150.12	25.88	75.19	51.44	60.13	47.54	7.64	13.03	5.42	90.11	1.93	0.85
	4260.23	4256.51	5723.60	27.39	74.38	46.70	62.12	45.34	7.32	12.16	5.47	90.11	1.85	0.84
	4356.15	4353.00	6298.92	28.78	73.41	42.10	63.88	43.30	6.93	11.31	5.51	90.11	1.91	0.83
	4431.79	4429.09	6860.27	30.03	72.20	40.01	65.49	41.36	6.63	10.56	5.56	90.11	2.03	0.86
	4466.99	4463.73	7441.20	30.92	71.60	35.29	67.15	39.33	6.46	9.85	5.58	90.11	2.13	0.82
	4611.04	4606.50	8012.91	32.38	69.72	32.67	68.01	38.28	6.12	9.20	6.02	90.11	2.09	0.81

Table 2 **Group V, steady state results with the transmission under external control. No spacer, R_p = 29 mm approx. 24 June 1992.**

	Engine Speed [rpm]	Prim. Pulley Speed [rpm]	Sec. Pulley [rpm]	Belt Speed [m/s]	Prim. Torque [Nm]	Sec. Torque [Nm]	Prim. Radius [mm]	Sec. Radius [mm]	Prim. Press. [bar]	Sec. Press. [bar]	Clutch Press. [bar]	Throttle Angle [deg]	Belt Slip [%]	CTX Efficncy
	1477.00	1482.74	568.17	4.23	15.81	33.86	28.94	74.38	1.23	7.93	5.64	6.42	1.53	0.82
	2990.62	2991.28	1132.93	8.60	16.88	35.80	28.93	74.35	1.02	8.10	5.37	12.27	2.67	0.80
	4344.39	4342.89	1699.41	12.87	17.67	34.88	29.69	73.83	0.84	7.65	5.10	17.30	2.70	0.77
	1463.87	1468.18	567.52	4.31	16.64	34.19	28.89	74.38	1.10	16.15	5.54	6.54	0.47	0.80
16 Nm	2973.83	2973.91	1132.84	8.71	17.19	35.29	28.83	74.41	0.96	15.92	5.34	12.33	1.69	0.78
	4461.15	4459.98	1699.09	13.10	15.68	29.96	28.81	74.39	0.79	16.08	5.07	17.09	1.63	0.73
	1464.35	1468.16	567.18	4.33	17.65	34.47	28.85	74.38	1.02	24.01	5.45	6.71	0.40	0.76
	2958.20	2958.65	1133.06	8.73	15.30	29.19	28.81	74.38	0.87	24.27	5.22	11.83	1.14	0.73
	4461.23	4460.37	1699.44	——	16.31	29.43	28.81	74.39	0.72	24.19	4.98	17.29	1.63	0.69
	1499.17	1502.18	567.35	4.14	32.95	76.45	28.93	74.34	1.22	7.93	5.63	9.87	2.96	0.88
	3306.51	3305.78	1133.04	8.65	34.08	78.23	28.94	74.32	1.03	8.08	5.37	18.59	11.97	0.79
	4561.49	4559.74	1699.65	12.92	32.99	71.47	29.64	73.84	0.83	8.14	5.10	24.52	7.14	0.81
	1490.00	1494.11	567.42	4.29	32.55	73.80	28.90	74.37	1.08	16.17	5.53	9.75	2.28	0.86
32 Nm	3023.79	3024.13	1132.97	8.70	33.40	75.81	28.83	74.40	0.95	15.92	5.32	17.13	3.31	0.85
	4572.83	4570.52	1699.72	13.05	31.96	70.78	28.81	74.39	0.78	16.05	5.06	24.11	3.99	0.82
	1493.76	1497.23	566.92	4.32	33.45	73.85	28.83	74.42	1.01	24.00	5.43	9.96	2.27	0.84
	3025.26	3025.17	1132.89	8.75	32.82	72.48	28.81	74.43	0.86	24.31	5.20	17.06	3.27	0.83
	4564.99	4563.25	1700.24	——	33.07	71.73	28.81	74.40	0.72	24.27	4.97	24.53	3.78	0.81
	1743.36	1748.15	567.44	4.17	47.28	111.76	28.97	74.27	1.22	7.94	5.63	14.66	16.78	0.77
	3386.33	3385.39	1133.17	8.72	48.03	113.37	28.94	74.29	1.02	8.08	5.37	24.78	14.07	0.79
	4467.44	4466.25	1699.03	12.84	48.07	104.21	30.44	73.34	0.84	8.14	5.10	33.18	8.33	0.82
	1499.35	1502.99	566.90	4.30	47.83	111.74	28.90	74.36	1.08	16.19	5.52	13.43	2.95	0.88
48 Nm	3064.99	3065.42	1132.52	8.71	48.25	112.98	28.83	74.38	0.94	15.96	5.32	22.84	4.68	0.87
	4674.78	4672.82	1699.46	13.14	48.35	111.55	28.81	74.37	0.78	16.04	5.04	34.75	6.12	0.84
	1501.42	1504.26	567.57	4.33	48.30	111.04	28.86	74.40	1.01	23.98	5.42	13.53	2.73	0.87
	3053.48	3053.32	1133.71	8.74	49.07	113.55	28.81	74.41	0.85	24.33	5.19	23.23	4.11	0.86
	4601.47	4599.65	1699.65	——	48.17	109.61	28.81	74.39	0.71	24.27	4.96	33.87	4.60	0.84
	1948.07	1952.10	567.26	4.53	63.15	150.59	28.97	74.25	1.20	7.94	5.61	23.58	25.53	0.69
	4327.69	4326.19	1699.44	12.83	63.07	131.03	31.88	72.39	0.83	8.15	5.10	45.95	10.79	0.82
	1517.66	1522.49	567.91	4.31	64.27	152.73	28.88	74.34	1.07	16.19	5.51	24.77	4.00	0.89
64 Nm	3206.32	3205.73	1132.30	8.72	63.58	151.41	28.86	74.36	0.93	15.98	5.30	36.18	9.00	0.84
	4897.95	4895.72	1699.52	0.02	56.94	132.75	28.81	74.37	0.76	16.13	5.02	47.01	10.40	0.81
	1510.80	1513.71	567.81	4.34	66.21	155.34	28.85	74.37	0.99	23.97	5.41	27.06	3.31	0.88
	3082.02	3082.30	1133.19	8.76	63.77	150.31	28.81	74.39	0.84	24.32	5.18	34.85	5.08	0.87
	4711.77	4709.61	1699.91	——	63.28	147.28	28.81	74.37	0.70	24.27	4.94	56.15	6.83	0.84
	1565.20	1569.24	567.50	4.32	72.96	174.41	28.85	74.33	1.05	16.21	5.49	88.80	6.83	0.87
	3225.75	3225.73	1133.08	8.74	77.19	185.35	28.87	74.35	0.92	16.00	5.29	89.93	9.53	0.84
W.O.T.														
	1512.12	1515.82	567.63	4.33	72.05	169.99	28.85	74.37	0.99	23.96	5.40	88.82	3.47	0.89
	3122.82	3122.69	1132.56	8.78	78.16	185.90	28.81	74.38	0.84	24.31	5.17	89.89	6.37	0.86

Table 3 **Group W, steady state results with the transmission under external control. Spacer 1, R_p = 39 mm approx. 21 July 1992.**

	Engine Speed	Prim. Pulley Speed	Sec. Pulley	Prim. Torque	Sec. Torque	Prim. Radius	Sec. Radius	Prim. Press.	Sec. Press.	Clutch Press.	Throttle Angle	Belt Slip	CTX Efficncy
	[rpm]	[rpm]	[rpm]	[Nm]	[Nm]	[mm]	[mm]	[bar]	[bar]	[bar]	[deg]	[%]	
	1448.82	1455.33	833.07	13.65	18.09	39.25	67.06	1.50	7.87	4.95	6.05	2.19	0.77
	2923.58	2927.55	1674.80	14.73	19.35	39.26	67.06	1.40	8.00	4.85	11.86	2.28	0.76
	4404.94	4406.96	2514.70	13.41	16.06	39.26	67.05	1.36	7.95	4.76	16.44	2.56	0.69
	1434.87	1441.66	832.60	15.45	19.72	39.22	67.07	1.45	16.80	4.94	6.35	1.24	0.75
16 Nm	2900.86	2904.46	1674.97	14.12	17.08	39.22	67.08	1.36	16.12	4.85	11.49	1.35	0.71
	4358.67	4361.37	2515.11	14.21	15.95	39.21	67.06	1.30	16.00	4.73	16.48	1.38	0.65
	1436.43	1442.37	832.39	13.68	14.89	39.19	67.09	1.39	24.36	4.88	6.39	1.19	0.64
	2902.20	2906.30	1674.71	14.80	16.32	39.18	67.11	1.33	24.05	4.78	11.64	1.30	0.64
	4364.81	4367.63	2515.02	13.35	12.66	39.17	67.11	1.26	24.06	4.66	16.38	1.35	0.55
	1459.15	1464.76	832.96	30.43	46.03	39.24	67.05	1.50	7.88	4.95	9.32	2.83	0.87
	2940.82	2944.20	1674.35	29.08	43.24	39.24	67.05	1.41	7.99	4.86	15.98	2.83	0.86
	4448.37	4450.34	2514.79	30.51	44.57	39.24	67.03	1.36	7.95	4.76	22.91	3.47	0.83
	1454.95	1461.15	832.19	29.80	43.51	39.19	67.15	1.43	16.78	4.93	9.43	2.43	0.84
32 Nm	2944.22	2947.42	1674.15	30.17	43.74	39.19	67.15	1.35	16.15	4.85	16.30	2.67	0.83
	4425.14	4427.70	2515.11	30.94	43.58	39.18	67.14	1.30	15.98	4.71	22.89	2.66	0.81
	1440.43	1446.12	832.39	30.89	43.79	39.17	67.12	1.39	24.40	4.87	9.59	1.37	0.83
	2917.54	2921.21	1674.56	30.41	42.82	39.17	67.16	1.32	24.11	4.77	16.23	1.70	0.82
	4377.59	4379.57	2515.09	30.64	41.51	39.16	67.14	1.25	23.99	4.65	22.62	1.54	0.79
	1463.28	1473.20	832.81	45.99	71.88	39.22	67.02	1.50	7.87	4.96	12.81	3.40	0.90
	2971.27	2974.69	1674.71	45.66	70.77	39.23	67.03	1.42	7.95	4.87	21.61	3.80	0.88
	4541.67	4543.77	2515.11	45.75	69.74	39.22	67.02	1.36	7.95	4.76	32.16	5.43	0.85
	1465.22	1470.02	832.58	47.81	73.33	39.18	67.14	1.43	16.78	4.93	13.41	2.94	0.88
48 Nm	2955.59	2959.72	1674.47	46.10	70.19	39.18	67.14	1.35	16.13	4.84	21.65	3.05	0.87
	4444.14	4446.51	2515.11	46.17	69.24	39.17	67.13	1.29	15.99	4.71	31.98	3.07	0.86
	1463.65	1469.63	832.37	46.06	67.14	39.14	67.21	1.38	24.48	4.87	13.01	2.75	0.84
	2959.32	2963.39	1674.67	46.27	68.82	39.14	67.22	1.31	24.04	4.76	21.71	2.94	0.85
	4446.79	4449.27	2514.79	46.95	68.97	39.13	67.22	1.24	23.87	4.63	32.55	2.90	0.84
	1535.33	1538.36	833.29	63.37	100.35	39.23	66.99	1.51	7.86	4.97	22.11	7.50	0.87
	3036.01	3039.92	1675.07	53.50	83.93	39.23	67.03	1.43	7.96	4.87	26.30	5.84	0.87
	1467.64	1476.60	832.77	61.82	96.01	39.17	67.13	1.43	16.82	4.93	21.77	3.35	0.89
64 Nm	2969.49	2973.19	1674.75	61.79	94.36	39.17	67.13	1.35	16.05	4.84	32.28	3.46	0.87
	4485.01	4487.59	2515.32	62.03	95.86	39.16	67.12	1.28	16.02	4.70	50.19	3.91	0.88
	1468.66	1477.26	832.37	62.29	95.72	39.13	67.21	1.35	23.97	4.81	24.71	3.22	0.88
	2969.93	2973.45	1674.92	62.13	95.56	39.13	67.22	1.31	24.11	4.76	33.08	3.23	0.88
	4467.54	4469.97	2515.32	62.84	95.36	39.12	67.23	1.23	24.00	4.63	50.92	3.30	0.86
	1472.03	1480.12	832.39	70.63	110.94	39.17	67.12	1.43	16.84	4.93	88.82	3.62	0.90
	2990.06	2994.13	1675.14	76.03	123.36	39.16	67.11	1.35	16.04	4.83	89.81	4.12	0.92
	4519.52	4521.98	2515.34	69.31	107.76	39.15	67.12	1.29	16.00	4.70	89.77	4.63	0.87
W.O.T.	1478.69	1480.32	832.88	71.14	110.38	39.13	67.21	1.33	23.93	4.81	88.92	3.36	0.88
	2981.69	2985.40	1674.71	76.98	121.89	39.12	67.22	1.31	24.05	4.75	89.83	3.62	0.90
	4475.44	4477.88	2515.49	70.05	107.29	39.12	67.22	1.23	23.97	4.63	89.75	3.47	0.87

Table 4 **Group X, steady state results with the transmission under external control. Spacer 2, R_p = 50 mm approx. 14 July 1992.**

	Engine Speed [rpm]	Prim. Pulley Speed [rpm]	Sec. Pulley [rpm]	Prim. Torque [Nm]	Sec. Torque [Nm]	Prim. Radius [mm]	Sec. Radius [mm]	Prim. Press. [bar]	Sec. Press. [bar]	Clutch Press. [bar]	Throttle Angle [deg]	Belt Slip [%]	CTX Efficncy
	1422.56	1425.88	1228.90	14.58	12.88	50.03	57.80	1.61	5.96	4.71	6.19	0.43	0.77
	2870.94	2871.00	2459.74	15.19	13.39	50.04	57.83	1.59	5.97	4.71	11.64	0.99	0.76
	3849.68	3847.36	3694.40	15.77	11.53	53.20	54.83	1.57	5.92	4.58	15.44	1.04	0.71
	1423.18	1427.41	1228.75	14.86	13.27	50.02	57.84	1.62	6.14	4.78	6.25	0.46	0.78
	2864.23	2864.00	2460.49	14.15	12.17	50.02	57.84	1.59	6.10	4.72	11.36	0.66	0.75
	4297.34	4294.02	3694.51	15.62	11.96	50.11	57.76	1.59	6.17	4.65	16.76	0.83	0.67
16 N m	1427.96	1431.15	1228.85	16.23	13.92	49.95	57.94	1.55	16.20	4.75	6.44	0.41	0.75
	2873.27	2872.88	2460.32	14.61	11.88	49.95	57.95	1.53	16.09	4.69	11.50	0.66	0.70
	4324.43	4320.85	3694.42	14.99	10.48	49.95	57.96	1.50	16.48	4.60	16.60	0.80	0.60
	1433.36	1437.01	1228.94	14.81	11.20	49.90	58.04	1.51	24.20	4.69	6.26	0.54	0.65
	2882.91	2882.63	2459.98	16.09	11.92	49.90	58.03	1.48	24.21	4.62	11.85	0.76	0.64
	4339.52	4336.30	3694.51	14.18	8.53	49.90	58.06	1.43	24.15	4.51	16.42	0.86	0.52
	1433.29	1436.65	1228.83	30.47	30.77	50.08	57.80	1.61	5.96	4.69	9.21	1.20	0.87
	2893.50	2893.21	2460.22	31.07	31.32	50.02	57.84	1.61	5.97	4.72	16.08	1.68	0.87
	4251.77	4248.16	3693.91	29.55	27.96	50.71	57.22	1.67	5.87	4.66	21.47	1.89	0.83
	1439.32	1442.90	1228.62	32.24	33.00	50.00	57.89	1.62	6.15	4.78	9.53	1.41	0.88
	2897.44	2897.07	2460.32	31.74	32.08	50.00	57.89	1.59	6.13	4.71	16.29	1.68	0.87
	4363.59	4359.57	3694.79	32.00	30.94	49.99	57.90	1.56	6.18	4.64	22.92	1.84	0.83
32 N m	1432.56	1436.27	1228.92	31.92	31.70	49.95	57.95	1.55	16.20	4.74	9.43	0.73	0.86
	2881.92	2881.28	2460.15	30.62	30.06	49.94	57.96	1.52	16.10	4.68	15.96	0.91	0.85
	4338.26	4333.89	3694.19	32.06	29.63	49.96	57.97	1.49	16.50	4.60	22.79	1.09	0.80
	1436.57	1440.10	1228.71	30.66	29.24	49.90	58.05	1.50	24.19	4.68	9.28	0.75	0.82
	2889.97	2888.67	2460.19	31.00	28.85	49.90	58.04	1.47	24.21	4.61	16.00	0.92	0.80
	4350.46	4347.02	3694.06	31.55	28.31	49.90	58.07	1.43	24.14	4.50	22.82	1.11	0.77
	1443.42	1446.51	1228.79	46.92	49.42	50.04	57.81	1.63	5.96	4.77	12.84	1.87	0.91
	2927.23	2926.46	2460.15	47.87	50.48	50.02	57.84	1.61	5.95	4.72	21.88	2.80	0.90
	4320.10	4316.03	3694.83	47.37	48.14	50.54	57.34	1.57	5.91	4.66	31.17	2.89	0.88
	1441.00	1444.67	1229.00	46.33	48.68	50.03	57.86	1.62	6.15	4.78	12.64	1.62	0.91
	2913.67	2913.54	2460.41	48.22	50.93	49.98	57.89	1.59	6.12	4.72	22.00	2.19	0.90
	4392.03	4388.16	3694.53	47.40	48.72	49.96	57.91	1.55	6.21	4.64	31.92	2.41	0.87
48 N m	1449.13	1452.54	1228.83	49.13	50.89	49.92	58.03	1.54	16.18	4.74	13.46	1.67	0.89
	2910.12	2909.34	2460.47	46.43	47.95	49.92	58.04	1.51	16.12	4.68	21.22	1.68	0.88
	4372.37	4368.49	3694.53	45.94	46.09	49.92	58.03	1.48	16.51	4.59	30.75	1.68	0.86
	1440.71	1443.99	1228.83	47.77	48.64	49.89	58.06	1.50	24.19	4.67	13.08	0.96	0.88
	2899.43	2899.15	2460.73	46.64	46.64	49.88	58.07	1.46	24.21	4.60	21.14	1.19	0.86
	4361.63	4358.18	3694.23	48.31	47.26	49.88	58.09	1.42	24.14	4.50	32.06	1.28	0.84

Table 4(continued).

	Engine Speed	Prim. Pulley Speed	Sec. Pulley	Prim. Torque	Sec. Torque	Prim. Radius	Sec. Radius	Prim. Press.	Sec. Press.	Clutch Press.	Throttle Angle	Belt Slip	CTX Efficncy
	[rpm]	[rpm]	[rpm]	[Nm]	[Nm]	[mm]	[mm]	[bar]	[bar]	[bar]	[deg]	[%]	
	2953.04	2952.27	2460.34	53.01	56.36	50.01	57.85	1.61	5.98	4.74	24.64	3.59	0.89
	1450.46	1453.49	1229.30	64.24	68.65	50.00	57.86	1.62	8.15	4.78	26.42	2.12	0.91
	2944.76	2944.77	2461.37	63.62	68.58	49.96	57.88	1.58	8.09	4.72	34.65	3.16	0.91
	4434.92	4430.79	3694.49	63.17	66.52	49.94	57.90	1.55	8.20	4.64	49.11	3.34	0.89
64 Nm	1454.41	1457.77	1229.28	64.21	68.16	49.90	58.03	1.54	16.18	4.73	26.86	1.93	0.91
	2915.78	2914.95	2454.75	63.61	68.35	49.90	58.04	1.51	16.14	4.67	33.52	2.06	0.91
	4392.30	4388.22	3694.62	62.75	65.29	49.90	58.06	1.48	16.54	4.58	47.18	2.05	0.88
	1454.79	1458.54	1229.15	64.67	67.77	49.86	58.14	1.49	24.18	4.66	26.72	1.72	0.89
	2919.57	2919.42	2460.19	63.21	65.81	49.86	58.13	1.47	24.19	4.60	33.40	1.77	0.89
	4379.47	4375.65	3694.04	63.81	65.21	49.85	58.12	1.42	24.12	4.50	49.32	1.58	0.87
	1466.89	1460.87	1228.64	70.34	76.99	49.98	57.85	1.62	8.14	4.78	89.19	2.65	0.93
	3097.36	3096.33	2460.79	77.96	84.65	49.93	57.86	1.59	8.09	4.71	89.95	7.91	0.87
	4521.38	4517.41	3694.10	70.26	74.79	49.93	57.89	1.55	8.19	4.63	89.94	5.20	0.88
	1456.41	1459.52	1228.96	70.72	75.90	49.89	58.03	1.54	16.21	4.73	89.93	2.06	0.91
W.O.T.	2931.92	2932.28	2459.85	75.93	83.41	49.89	58.04	1.51	16.18	4.67	89.95	2.40	0.95
	4401.49	4397.64	3694.36	72.14	75.94	49.89	58.05	1.47	16.54	4.58	89.93	2.25	0.89
	1461.47	1462.35	1228.77	71.07	75.42	49.85	58.16	1.49	24.15	4.66	88.93	1.97	0.90
	2939.31	2939.34	2460.62	76.90	82.98	49.85	58.17	1.46	24.21	4.60	89.96	2.31	0.91
	4394.37	4390.60	3694.08	71.97	74.79	49.85	58.15	1.42	24.13	4.50	89.94	1.86	0.88

Table 5 **Group Z, steady state results with the transmission under external control. Spacer 4, R_p = 71 mm approx. 16 July 1992.**

	Engine Speed	Prim. Pulley Speed	Sec. Pulley	Prim. Torque	Sec. Torque	Prim. Radius	Sec. Radius	Prim. Press.	Sec. Press.	Clutch Press.	Throttle Angle	Belt Slip	CTX Efficncy
	[rpm]	[rpm]	[rpm]	[Nm]	[Nm]	[mm]	[mm]	[bar]	[bar]	[bar]	[deg]	[%]	
	1359.27	1364.30	2790.21	15.75	4.32	71.32	34.22	1.59	5.91	5.04	6.00	1.87	0.57
	2735.06	2737.20	5589.79	15.38	3.61	71.29	34.30	1.55	6.02	4.98	11.25	1.74	0.48
	1364.37	1369.07	2790.01	13.33	3.16	71.27	34.30	1.57	8.04	5.05	5.64	1.93	0.49
	2746.24	2749.18	5590.37	14.74	3.10	71.24	34.40	1.52	8.08	4.97	11.12	1.82	0.43
	4165.68	4165.66	8397.82	13.59	1.09	71.14	34.58	1.41	7.96	4.79	15.70	2.00	0.16
16 Nm	1386.46	1391.04	2789.89	15.44	2.99	71.12	34.68	1.52	16.05	5.04	6.08	2.20	0.39
	2792.04	2794.18	5589.77	13.19	1.14	71.09	34.80	1.48	16.20	4.95	10.87	2.07	0.17
	4249.17	4249.41	8399.98	15.48	0.54	70.94	35.05	1.37	16.37	4.78	16.52	2.33	0.07
	1411.15	1415.20	2789.74	14.79	0.72	70.97	35.12	1.48	24.29	4.96	6.09	2.46	0.10
	2846.40	2848.37	5590.54	14.72	-0.13	70.94	35.27	1.43	24.06	4.86	11.41	2.43	-0.02
	4296.18	4295.30	8324.29	13.94	-2.69	70.76	35.55	1.30	24.24	4.68	16.10	2.63	-0.38

Table 5(continued).

	Engine Speed [rpm]	Prim. Pulley Speed [rpm]	Sec. Pulley [rpm]	Prim. Torque [Nm]	Sec. Torque [Nm]	Prim. Radius [mm]	Sec. Radius [mm]	Prim. Press. [bar]	Sec. Press. [bar]	Clutch Press. [bar]	Throttle Angle [deg]	Belt Slip [%]	CTX Efficncy
	1362.88	1367.51	2790.03	29.71	10.93	71.29	34.25	1.60	5.92	5.05	8.59	1.98	0.76
	2743.54	2745.34	5590.20	31.39	11.24	71.26	34.34	1.55	6.02	4.99	15.65	1.87	0.74
	1368.68	1373.50	2789.67	31.79	11.72	71.24	34.35	1.47	8.05	5.04	9.04	2.07	0.76
	2754.74	2756.75	5590.20	31.46	11.01	71.22	34.44	1.53	8.08	4.97	15.81	1.93	0.72
	4177.42	4177.82	8398.08	30.64	9.32	71.11	34.63	1.42	7.96	4.80	21.55	2.11	0.62
32 Nm	1393.04	1396.89	2790.06	34.79	11.99	71.10	34.76	1.53	16.07	5.03	9.67	2.36	0.70
	2803.22	2805.66	5588.94	30.46	9.25	71.08	34.88	1.47	16.21	4.94	15.65	2.25	0.61
	4261.38	4261.19	8399.62	29.80	7.29	70.92	35.12	1.37	16.37	4.77	21.55	2.39	0.49
	1414.90	1419.19	2789.54	29.72	7.79	70.95	35.18	1.47	24.28	4.95	8.88	2.53	0.52
	2854.48	2856.52	5589.49	29.78	7.05	70.92	35.34	1.42	24.06	4.86	15.64	2.49	0.47
	4349.95	4349.38	8399.92	29.11	5.37	70.73	35.63	1.31	24.24	4.67	21.86	2.72	0.36
	1365.90	1370.51	2789.61	46.54	18.83	71.26	34.27	1.47	5.92	5.05	12.23	2.12	0.83
	2749.62	2752.03	5590.18	46.27	18.45	71.24	34.37	1.54	6.01	4.99	20.35	1.99	0.82
	1371.08	1375.74	2789.46	47.66	19.35	71.22	34.37	1.57	8.06	5.04	12.55	2.15	0.83
	2760.80	2763.80	5590.20	46.50	18.25	71.20	34.48	1.51	8.08	4.96	20.44	2.05	0.80
	4190.30	4190.10	8401.33	46.91	17.07	71.09	34.67	1.41	7.95	4.79	30.00	2.22	0.74
48 Nm	1393.06	1398.80	2789.80	46.25	17.39	71.08	34.79	1.53	16.07	5.03	12.10	2.38	0.76
	2811.16	2813.13	5590.37	45.98	16.75	71.06	34.93	1.46	16.21	4.94	20.47	2.32	0.73
	4275.64	4275.46	8397.35	46.41	15.52	70.90	35.19	1.35	16.36	4.77	30.15	2.52	0.66
	1420.21	1424.15	2789.76	47.56	16.38	70.92	35.25	1.46	24.28	4.94	12.68	2.63	0.68
	2861.92	2865.45	5589.75	46.57	15.15	70.89	35.41	1.41	24.07	4.84	20.92	2.55	0.64
	4361.35	4360.59	8398.31	46.20	13.35	70.71	35.69	1.29	24.12	4.66	30.71	2.79	0.56
	1369.14	1374.63	2789.93	64.60	27.52	71.23	34.27	1.59	5.92	5.06	24.07	2.35	0.88
	2756.52	2759.09	5589.49	62.66	25.71	71.21	34.38	1.55	6.05	4.99	31.40	2.19	0.84
	1374.38	1378.72	2789.82	64.12	26.97	71.20	34.39	1.57	8.06	5.04	25.30	2.27	0.86
	2767.39	2769.39	5590.05	62.52	26.24	71.18	34.49	1.52	8.02	4.96	30.52	2.19	0.86
	4200.93	4201.45	8402.74	63.56	25.19	71.06	34.70	1.42	7.95	4.80	45.48	2.33	0.80
64 Nm	1396.98	1401.23	2789.61	63.63	25.90	71.06	34.82	1.52	16.06	5.02	25.56	2.43	0.82
	2817.75	2819.71	5591.04	62.79	24.74	71.04	34.97	1.48	16.24	4.94	31.38	2.40	0.79
	4290.04	4289.52	8398.57	63.01	23.70	70.88	35.25	1.36	16.33	4.76	46.63	2.63	0.73
	1423.35	1427.81	2789.93	63.87	24.24	70.90	35.31	1.46	24.27	4.94	24.26	2.68	0.75
	2872.49	2874.23	5590.29	62.27	22.93	70.86	35.47	1.40	24.05	4.84	31.81	2.65	0.72
	4375.21	4374.62	8400.65	63.07	21.81	70.68	35.76	1.28	24.14	4.65	47.56	2.85	0.67
	1376.12	1379.92	2789.63	72.25	31.23	71.18	34.39	1.57	8.04	5.04	89.92	2.32	0.89
	2775.41	2777.69	5591.08	70.84	33.43	71.15	34.50	1.51	8.12	4.96	89.90	2.40	0.86
	4206.06	4205.40	8398.27	73.92	30.35	71.05	34.72	1.40	7.94	4.79	89.81	2.41	0.83
	1399.29	1403.29	2789.46	70.43	30.00	71.04	34.85	1.37	16.07	5.02	89.83	2.50	0.86
W.O.T.	2820.59	2824.46	5590.86	77.49	32.88	71.01	34.98	1.47	16.23	4.93	89.91	2.49	0.85
	4295.43	4296.84	8400.39	73.40	28.56	70.86	35.27	1.35	16.34	4.75	89.81	2.69	0.77
	1425.93	1430.09	2790.01	71.16	28.21	70.88	35.34	1.46	24.27	4.93	89.91	2.74	0.78
	2880.35	2882.04	5591.68	76.35	31.17	70.84	35.52	1.40	24.04	4.83	89.85	2.70	0.80
	4379.18	4378.30	8398.83	72.20	26.28	70.66	35.78	1.28	24.15	4.65	89.79	2.88	0.70

Table 6 Steady state results with no belt installed and the pump disabled so that the input shaft losses can be measured. 2 July 1992.

Engine Speed	Prim. Torque	Prim. Press.	Sec. Press.	Clutch. Press.	Throttle Angle
[rpm]	[Nm]	[bar]	[bar]	[bar]	[deg]
968.93	1.74	1.59	15.67	4.50	3.83
1943.03	1.56	1.59	15.69	4.49	5.81
3005.23	1.74	1.59	15.69	4.47	9.33
3991.99	2.08	1.59	15.68	4.44	12.70
5071.27	2.67	1.57	15.69	4.38	16.41
1941.29	1.41	1.59	15.71	6.01	5.31
3758.15	1.99	1.59	15.71	5.96	11.25
2102.36	1.46	1.65	7.98	6.04	5.61
2095.28	1.37	1.57	28.35	6.00	5.63
3916.64	1.96	1.54	28.17	5.92	11.51
3985.42	1.87	1.64	8.24	6.03	11.51

Table 7 Steady state results with the output shaft disconnected so that the transmission is on no-load.

Table 7a No spacer, R_p = 29 mm approx. 25 June 1992.

Engine Speed	Prim. Torque	Prim. Radius	Sec. Radius	Prim. Press.	Sec. Press.	Clutch. Press.	Throttle Angle
[rpm]	[Nm]	[mm]	[mm]	[bar]	[bar]	[bar]	[deg]
983.47	3.15	28.92	74.43	1.27	15.75	3.68	3.69
2096.11	2.95	28.92	74.45	1.26	15.72	3.66	6.05
2970.53	3.25	28.92	74.45	1.26	15.70	3.63	8.81
4193.95	3.67	28.93	74.44	1.25	15.73	3.58	12.64
4975.01	3.99	28.94	74.44	1.23	15.73	3.57	15.35
2034.93	3.06	28.90	74.45	1.21	18.01	2.99	5.73
2077.81	3.10	28.90	74.44	1.19	17.99	5.64	5.83
2136.59	2.24	28.94	74.40	1.31	8.75	3.71	5.78
1982.30	4.24	28.88	74.49	1.19	27.41	3.63	5.82

Table 7b Spacer 1, R_p = 39 mm approx. 21 July 1992.

Engine Speed	Prim. Torque	Prim. Radius	Sec. Radius	Prim. Press.	Sec. Press.	Clutch. Press.	Throttle Angle
[rpm]	[Nm]	[mm]	[mm]	[bar]	[bar]	[bar]	[deg]
839.41	3.23	39.31	67.06	1.57	7.96	5.02	3.40
920.71	4.04	39.26	67.09	1.51	16.19	4.92	3.41
875.04	4.78	39.23	67.12	1.46	24.04	4.97	3.34
2993.40	3.12	39.32	67.07	1.58	7.95	5.00	9.78
3013.66	4.11	39.26	67.13	1.51	16.18	4.96	9.73
3054.45	5.00	39.22	67.17	1.45	23.98	4.92	9.87
4987.45	4.33	41.72	65.19	0.94	8.03	4.84	17.16
4937.34	4.89	39.30	67.14	1.49	16.17	4.88	16.84
4922.28	5.85	39.25	67.19	1.44	24.01	4.85	16.85

Table 7c Spacer 2, R_p = 50 mm approx. 14 July 1992.

Engine Speed	Prim. Torque	Prim. Radius	Sec. Radius	Prim. Press.	Sec. Press.	Clutch. Press.	Throttle Angle
[rpm]	[Nm]	[mm]	[mm]	[bar]	[bar]	[bar]	[deg]
986.45	2.94	50.04	57.85	1.33	8.00	4.18	3.68
930.45	3.43	49.98	57.95	1.25	16.23	4.11	3.69
892.64	4.94	49.92	58.06	1.22	24.25	4.13	3.69
3027.03	3.43	50.06	57.85	1.51	8.04	4.55	9.05
3009.72	4.28	49.99	57.96	1.46	16.00	4.58	9.09
3066.00	5.48	49.94	58.06	1.45	24.17	4.55	9.77
5015.67	5.15	53.42	54.75	1.18	8.11	4.57	16.71
4909.63	5.47	50.03	57.99	1.56	16.08	4.57	16.69
5041.61	6.83	49.97	58.12	1.46	24.32	4.53	17.17

Table 7d **Spacer 4, R_p = 71 mm approx. 16 July 1992.**

Engine Speed	Prim. Torque	Prim. Radius	Sec. Radius	Prim. Press.	Sec. Press.	Clutch. Press.	Throttle Angle
[rpm]	[Nm]	[mm]	[mm]	[bar]	[bar]	[bar]	[deg]
864.51	5.47	71.33	34.28	1.49	7.90	4.94	3.72
899.30	7.43	71.16	34.67	1.47	16.18	4.96	4.16
1000.64	11.14	71.01	35.06	1.44	24.17	4.91	4.91
2000.06	5.81	71.31	34.35	1.50	8.06	4.94	6.93
2039.95	8.24	71.14	34.74	1.48	16.32	4.84	7.58
2034.91	11.59	71.01	35.14	1.44	24.10	4.90	8.28
3073.97	6.74	71.27	34.42	1.58	8.08	5.01	10.56
3034.91	9.31	71.14	34.81	1.54	15.91	5.02	11.07
3053.78	13.26	71.00	35.27	1.48	24.02	4.95	12.09

Table 8 **A repeat of the Group V tests, Table 2, with an increased gap in the belt obtained by removing one segment. 3 July 1992.**

	Engine Speed [rpm]	Prim. Pulley Speed [rpm]	Sec. Pulley [rpm]	Prim. Torque [Nm]	Sec. Torque [Nm]	Prim. Radius [mm]	Sec. Radius [mm]	Prim. Press. [bar]	Sec. Press. [bar]	Clutch Press. [bar]	Throttle Angle [deg]	Belt Slip [%]	CTX Efficncy
	1504.43	1509.16	557.55	15.01	31.76	28.86	74.42	1.56	8.09	5.01	6.63	4.75	0.78
	3094.65	3095.40	1123.32	16.24	33.57	28.93	74.38	1.53	8.00	4.94	12.85	6.68	0.75
	4385.97	4384.61	1690.03	16.76	31.35	30.20	73.63	1.43	8.32	4.82	17.34	6.02	0.72
	1512.27	1516.23	557.64	17.04	35.45	28.82	74.45	1.51	16.20	4.99	7.07	4.99	0.77
16 Nm	3063.49	3065.11	1124.17	16.36	32.73	28.83	74.44	1.48	16.36	4.91	12.73	5.30	0.73
	4679.53	4677.66	1690.42	17.50	33.73	28.82	74.43	1.42	16.06	4.81	18.66	6.67	0.70
	1463.46	1468.08	557.18	15.89	30.24	28.82	74.42	1.44	24.27	4.90	6.59	1.98	0.72
	2957.85	2959.33	1123.63	16.50	31.22	28.82	74.43	1.43	24.07	4.86	12.33	1.93	0.72
	4456.14	4454.62	1689.61	16.68	29.81	28.81	74.42	1.38	24.17	4.77	17.59	2.03	0.68
	1579.30	1582.41	558.57	32.13	74.54	28.87	74.38	1.57	8.09	5.02	10.25	9.06	0.82
	3355.24	3356.10	1123.56	22.12	48.38	28.89	74.39	1.53	8.00	4.94	15.84	13.79	0.73
	4454.74	4453.17	1690.07	32.07	67.60	30.12	73.64	1.46	8.33	4.83	23.57	7.21	0.80
	1517.52	1521.34	557.79	32.93	75.01	28.81	74.43	1.51	16.24	4.97	10.14	5.29	0.83
32 Nm	3103.46	3104.68	1123.50	31.48	70.70	28.82	74.42	1.47	16.38	4.91	17.18	6.56	0.81
	4802.29	4800.06	1689.83	31.69	69.29	28.82	74.42	1.40	16.06	4.80	25.40	9.09	0.77
	1523.43	1528.36	557.92	33.40	74.53	28.81	74.46	1.43	24.28	4.90	10.25	5.66	0.81
	3096.21	3097.07	1123.97	32.48	71.25	28.81	74.46	1.42	24.09	4.83	17.38	6.21	0.80
	4727.59	4725.48	1689.98	32.00	67.58	28.81	74.46	1.37	24.19	4.75	25.25	7.57	0.76
	1781.34	1787.60	557.59	39.12	91.79	28.87	74.37	1.57	8.08	5.02	13.04	19.65	0.73
	4362.89	4361.21	1690.50	41.86	88.33	30.90	73.14	1.48	8.29	4.85	28.46	8.25	0.82
	1522.26	1527.16	557.66	48.59	114.29	28.81	74.41	1.50	16.26	4.96	13.90	5.69	0.86
48 Nm	3282.25	3283.01	1123.86	48.95	115.10	28.82	74.40	1.48	16.40	4.90	24.74	11.63	0.80
	4889.50	4887.11	1690.89	37.82	84.52	28.82	74.42	1.41	16.06	4.79	29.50	10.67	0.77
	1522.82	1533.36	557.38	47.63	110.05	28.81	74.44	1.43	24.24	4.89	13.61	6.08	0.84
	3138.98	3139.93	1123.48	49.62	114.43	28.81	74.44	1.41	24.05	4.82	24.24	7.55	0.83
	4840.59	4838.63	1690.18	48.18	108.37	28.81	74.46	1.36	24.21	4.73	36.36	9.73	0.79
	1531.48	1534.79	557.51	63.34	151.14	28.81	74.39	1.49	16.29	4.96	25.68	6.21	0.87
	3255.16	3255.17	1122.98	62.92	149.36	28.83	74.40	1.47	16.34	4.89	37.24	10.98	0.82
64 Nm	1533.52	1539.91	556.95	65.02	153.28	28.81	74.42	1.43	24.21	4.88	27.01	6.58	0.85
	3239.25	3240.21	1123.50	63.38	149.10	28.81	74.43	1.41	24.02	4.82	37.08	10.43	0.82
	4939.30	4936.81	1690.93	61.56	141.57	28.81	74.46	1.35	24.15	4.72	61.64	11.48	0.79
W.O.T.	1540.09	1545.32	557.14	72.49	172.01	28.81	74.41	1.42	24.24	4.87	88.87	6.88	0.86

Table 9 **A repeat of the Group W tests, Table 3, with an increased gap obtained by grinding 0.40 mm off the face of a one segment. 23 July 1992.**

	Engine Speed [rpm]	Prim. Pulley Speed [rpm]	Sec. Pulley [rpm]	Prim. Torque [Nm]	Sec. Torque [Nm]	Prim. Radius [mm]	Sec. Radius [mm]	Prim. Press. [bar]	Sec. Press. [bar]	Clutch Press. [bar]	Throttle Angle [deg]	Belt Slip [%]	CTX Efficncy
	1461.74	1466.01	846.74	16.57	22.73	39.28	67.08	1.61	7.88	5.07	6.65	2.35	0.79
	2941.31	2944.64	1697.34	15.57	20.37	39.28	67.06	1.59	8.08	5.02	11.97	2.58	0.75
	4434.65	4436.28	2546.07	15.34	18.94	39.30	67.07	1.56	8.10	4.93	16.96	3.03	0.71
16 N m	1438.55	1444.02	846.59	14.64	18.27	39.25	67.08	1.55	15.87	5.03	6.24	0.80	0.73
	2901.89	2904.68	1697.51	15.72	19.71	39.26	67.10	1.53	16.28	4.98	11.88	1.11	0.73
	4358.45	4360.08	2546.55	16.24	18.83	39.25	67.10	1.49	16.18	4.89	17.05	1.16	0.68
	1439.61	1445.47	846.38	15.63	17.99	39.21	67.11	1.50	24.23	4.98	6.41	0.78	0.67
	2903.51	2906.65	1697.42	15.53	17.31	39.21	67.12	1.47	24.26	4.92	11.81	1.04	0.65
	4362.86	4364.62	2546.79	15.85	16.63	39.21	67.13	1.43	24.29	4.83	16.92	1.09	0.61
	1466.60	1476.45	846.07	32.56	49.05	39.26	67.06	1.61	7.88	5.07	9.74	3.09	0.86
	2964.66	2967.96	1697.49	31.42	47.07	39.26	67.05	1.59	8.07	5.02	16.50	3.30	0.86
	4484.79	4485.84	2546.37	31.82	46.31	39.27	67.05	1.55	8.10	4.93	23.51	4.05	0.83
	1468.69	1473.55	846.20	31.70	45.53	39.22	67.15	1.54	15.90	4.91	9.57	2.65	0.82
32 N m	2956.29	2959.57	1697.66	32.44	47.32	39.22	67.18	1.52	16.32	4.97	16.65	2.74	0.84
	4440.91	4442.12	2546.83	31.10	44.02	39.22	67.16	1.48	16.15	4.88	22.90	2.80	0.81
	1452.49	1458.46	846.12	32.23	45.68	39.20	67.17	1.49	24.18	4.97	9.64	1.58	0.82
	2915.48	2918.92	1696.97	32.73	46.21	39.20	67.15	1.46	24.26	4.91	16.60	1.41	0.82
	4376.76	4377.80	2546.66	32.31	43.98	39.19	67.16	1.42	24.25	4.82	23.09	1.32	0.79
	1478.93	1483.37	846.22	48.10	75.09	39.24	67.04	1.61	7.88	5.07	13.31	3.52	0.89
	3044.85	3047.36	1697.75	47.76	74.21	39.25	67.04	1.59	8.06	4.98	22.66	5.79	0.87
	4714.58	4714.99	2546.89	48.58	73.78	39.30	67.01	1.54	8.09	4.92	35.42	8.82	0.82
	1477.63	1481.53	846.25	48.07	73.48	39.21	67.14	1.54	15.94	5.02	13.28	3.15	0.87
48 N m	2970.45	2973.35	1697.38	47.50	72.51	39.21	67.17	1.52	16.27	4.96	21.99	3.20	0.87
	4468.67	4469.88	2546.87	47.89	72.18	39.20	67.15	1.48	16.16	4.88	33.02	3.38	0.86
	1478.49	1481.86	846.51	47.05	69.97	39.17	67.23	1.48	24.14	4.96	13.01	2.94	0.85
	2970.59	2973.96	1697.14	47.38	70.57	39.17	67.24	1.46	24.22	4.91	21.91	3.03	0.85
	4462.44	4464.13	2546.70	47.69	69.09	39.17	67.24	1.42	24.30	4.81	32.75	3.04	0.83
	1495.70	1500.37	846.46	57.90	91.28	39.27	67.01	1.61	7.87	5.07	19.39	4.68	0.89
	3268.65	3271.02	1697.90	57.28	89.63	39.29	67.03	1.59	8.06	5.01	30.98	12.33	0.81
	4691.50	4692.17	2546.40	56.28	85.33	39.71	66.70	1.53	8.10	4.92	44.23	9.75	0.82
	1483.83	1488.60	846.70	65.73	102.88	39.19	67.13	1.54	15.93	5.02	27.93	3.55	0.89
64 N m	2986.86	2989.77	1697.29	63.47	98.83	39.20	67.15	1.52	16.30	4.96	34.40	3.73	0.88
	4530.11	4531.42	2546.98	63.55	97.87	39.19	67.15	1.48	16.18	4.87	52.27	4.66	0.87
	1482.34	1488.17	846.74	64.06	98.16	39.16	67.22	1.48	24.13	4.96	25.98	3.31	0.87
	2983.98	2986.83	1697.81	63.65	97.11	39.16	67.24	1.46	24.26	4.90	34.40	3.38	0.87
	4484.08	4485.74	2546.70	62.87	95.27	39.16	67.24	1.41	24.23	4.80	50.04	3.50	0.86
	1486.59	1491.70	846.81	72.78	115.20	39.19	67.12	1.54	15.91	5.01	88.87	3.74	0.90
	3008.06	3012.33	1697.84	77.66	125.21	39.19	67.13	1.51	16.27	4.96	89.96	4.42	0.91
	4546.26	4547.87	2546.63	69.82	108.44	39.19	67.14	1.47	16.17	4.87	89.91	5.02	0.87
W.O.T.	1492.17	1491.19	847.05	72.33	113.79	39.15	67.22	1.48	24.15	4.96	88.87	3.46	0.89
	2995.87	3000.02	1697.97	75.67	123.55	39.16	67.23	1.45	24.34	4.90	89.96	3.80	0.92
	4494.00	4495.06	2546.68	70.88	108.65	39.16	67.24	1.41	24.22	4.80	89.91	3.69	0.87